Analytical and Experimental Study of Fluid Friction and Heat Transfer in Low Reynolds Number Flow Heat Exchangers

by

Yuri Stephan Muzychka

A thesis
presented to the University of Waterloo
in fulfilment of the
thesis requirement for the degree of

Doctor of Philosophy
in
Mechanical Engineering

Waterloo, Ontario, Canada, 1999

The University of Waterloo requires the signatures of all persons using or photocopying this thesis. Please sign below, and give address and date.

Abstract

Analysis of fluid friction and heat transfer in low Reynolds number flow heat exchangers is undertaken. Three configurations typically utilized in compact heat exchangers are examined. These are: the plain non-circular duct of constant cross-sectional area, the offset or interrupted strip fin, and the turbulator strip. Analytical models for each of these geometries are developed by combining asymptotic solutions using simple non-linear superposition.

Models for predicting the friction factor - Reynolds number product, fRe, and Nusselt number, Nu, in non-circular ducts for hydrodynamically fully developed flow (HFDF), hydrodynamically developing flow (HDF), thermally fully developed flow (TFDF), thermally developing flow (TDF), and simultaneously developing flow (SDF) are developed. Thermal and hydrodynamic entrance models are developed by combining the asymptotic solutions for small and large values of the dimensionless duct length. Through the use of a novel characteristic length, the square root of the cross-sectional flow area, scatter in the dimensionless data for fully developed laminar flows is considerably reduced. Most numerical and analytical data are predicted within $\pm$ 10% for HFDF and TFDF, $\pm$ 12% for HDF and TDF, and $\pm$ 15% for SDF for most non-circular ducts.

Simple analytic models for predicting the Fanning friction factor, f, and Colburn j factor of two common enhancement devices, the offset strip fin and the turbulator strip are developed from fundamental solutions of fluid dynamics and heat transfer. Models for the offset strip fin are valid over the full range of Reynolds numbers for rectangular and other non-circular sub-channel cross-sections. Model predictions for the offset strip fin agree with published experimental data within $\pm$ 20%. Models for the turbulator strip are valid over the full Reynolds number range for both straight and curved turbulator profiles. Model predictions for the turbulator strip agree with new experimental data to within $\pm$ 20%.

Finally, a detailed experimental study of the thermal and hydraulic characteristics of turbulator strips is undertaken. Simple design correlations are presented along with a performance evaluations of each device using the constant mass flow rate and constant pumping power criteria.

Acknowledgements

This work would not have been possible without the support and contributions of many people.

First, I owe great thanks to my supervisor Dr. M.M. Yovanovich for providing me with the opportunity to pursue this work and granting me the freedom to pursue my own ideas. Thanks to my examining committee, Dr. G. Davidson, Dr. M. Renksizbulut, Dr. W. Lennox, and Dr. A.E. Bergles for their comments and suggestions. Special thanks to Long Manufacturing Inc. for providing the financial assistance and in particular Tom Lemczyk for recognizing the need for new ideas.

Thanks to Alan Hodgson and Marius Van Reenen for their technical assistance and to Phil Morley for his valuable contributions to the design and development of the experimental apparatus. Thanks to everybody at the Microelectronics Heat Transfer Laboratory, especially Rick Culham, Pete Teertstra, and Mirko Stevanović.

Finally, thanks to my family for supporting me through this long journey, especially my wife Julie, who had to endure the endless days and weeks of frustration, this would not have been possible without you.

For My Parents

Contents

List of Tables

List of Figures

Nomenclature

Roman Symbols

A	=	flow area, m^2
A_1, A_2, A_3, A_4	=	arbitrary constants
a	=	major axis of ellipse or rectangle, m
b	=	minor axis of ellipse of rectangle, m
c	=	radial and/or linear dimension, m
C	=	empirical constant
C_o	=	Kozeny coefficient
C_D	=	drag coefficient
C_c	=	cold capacity rate, W/K
C_f	=	skin friction coefficient, $\equiv \overline{\tau}/(\frac{1}{2}\rho\overline{w}^2)$
C_h	=	hot capacity rate, W/K
C_p	=	heat capacity, J/kgK
C_r	=	capacity rate ratio
C_1, C_2, C_3, C_4, C_5	=	constants
D	=	diameter of circular duct, m
D_h	=	hydraulic diameter of plain channel, $\equiv 4A/P$
d^*	=	dimensionless diameter ratio, $\equiv D_h/D_{max}$
d_h	=	hydraulic diameter of enhanced channel, $\equiv 4V_{free}/A_{wet}$
$\mathbf{E}(\cdot)$	=	complete elliptic integral second kind
e	=	eccentricity, m
e^*	=	dimensionless eccentricity, $\equiv e/(r_o - r_i)$
f	=	friction factor $\equiv \overline{\tau}/(\frac{1}{2}\rho\overline{w}^2)$
$g(\epsilon)$	=	shape function
Gz	=	Graetz number, $\equiv \pi/4z^*$
H	=	channel or fin height, m
h	=	heat transfer coefficient, W/m^2K
j	=	Colburn factor, $\equiv St_{\mathcal{L}}Pr^{2/3}$
K_e, Kc	=	expansion/contraction loss coefficient
K_{eff}	=	effective loss coefficient

K, K_∞	=	incremental pressure drop factor
K_1, K_2	=	empirical constants
k	=	thermal conductivity, W/mK
k_o	=	Kozeny constant, ≈ 2.5
L	=	length of channel, m
L_e	=	tortuous or effective flow length, m
L_f	=	interrupted fin length, m
L^+	=	dimensionless hydrodynamic entrance length,$\equiv L/\mathcal{L}Re_\mathcal{L}$
L^*	=	dimensionless thermal entrance length,$\equiv L/\mathcal{L}Re_\mathcal{L}Pr$
l_1, l_2	=	characteristic dimensions of non-circular duct, m
m	=	area mismatch parameter, $\equiv A_{D_h}/A$, Ch. 3
	=	Falkner-Skan wedge parameter, Ch. 3
	=	correlation parameter, Ch. 6
$\dot{m}$	=	mass flow rate, kg/s
N	=	number of sides of polygons
n	=	correlation parameter, Ch. 3,4
	=	hyperellipse shape parameter, Ch. 1
	=	inward directed normal, Ch. 2
$Nu_\mathcal{L}$	=	Nusselt number, $\equiv h\mathcal{L}/k$
P	=	perimeter, m
$\dot{P}$	=	pumping power,W
p	=	pressure, Pa
	=	correlation parameter, Ch.6
$Po_\mathcal{L}$	=	Poiseuille number, $\equiv \frac{\tau_w \mathcal{L}}{\mu \overline{w}}$
Pr	=	Prandtl number, $\equiv \nu/\alpha$
p^*	=	dimensionless pressure, $\equiv p/(\frac{1}{2}\rho\overline{w}^2)$
q	=	heat flux, W/m^2
	=	correlation parameter, Ch. 6
Q	=	heat transfer, W
Q	=	volumetric flow rate, m^3/s
r	=	radius, m
R_c, R_h	=	fluid resistance, K/W
$Re_\mathcal{L}$	=	Reynolds number, $\equiv \overline{w}\mathcal{L}/\nu$
r^*	=	dimensionless radius ratio, $\equiv r_i/r_o$
s	=	arc length, m
	=	fin spacing, m
S_o	=	effective fin length, m
St	=	Stanton number $\equiv Nu/(RePr)$
t	=	fin thickness, m
T	=	temperature, K
T_m	=	bulk temperature, K
T_w	=	wall temperature, K
U	=	overall heat transfer coefficient, W/m^2K

U_∞	=	free stream velocity, m/s
u, v, w	=	velocity components, m/s
V	=	volume, m^3
$\vec{V}$	=	velocity vector, m/s
w	=	axial velocity, m/s
$\overline{w}$	=	average velocity, m/s
W	=	width of channel, m
	=	fin width, m
X	=	chord length, m
x, y, z	=	cartesian coordinates, m
z	=	axial coordinate, m
$z^*_{\mathcal{L}}$	=	dimensionless axial position for thermally developing flows, $\equiv z/\mathcal{L}Re_{\mathcal{L}}Pr$
$z^+_{\mathcal{L}}$	=	dimensionless axial position for hydrodynamically developing flows, $\equiv z/\mathcal{L}Re_{\mathcal{L}}$

Subscripts

app	=	apparent
b	=	bare, boundary
C	=	circular
c	=	circumscribed, cold, contraction, core, critical
cf	=	creeping flow
cp	=	constant property
d_h, D_h	=	based upon hydraulic diameter
e	=	enhanced, entrance, expansion, effective
eff	=	effective
f	=	fin
fd	=	fully developed
FP	=	flat plate
h	=	hot
$H, H1$	=	based upon isoflux condition
hy	=	hydrodynamic
i	=	inscribed, inner, in, initial
lam	=	laminar
m	=	mean, mixed or bulk value
NC	=	non-circular
o	=	outer
P	=	based upon perimeter
PS	=	plane stagnation
T	=	based upon isothermal condition
th	=	thermal
tur	=	turbulent
w	=	wall

x = local value
z = local value
∞ = fully developed limit
$\mathcal{L}$ = based upon arbitrary length $\mathcal{L}$
$\sqrt{A}$ = based upon square root of area

Superscripts

C = circular
E = elliptical
O = circular duct limit
P = polygonal
R = rectangular
$\overline{(\cdot)}$ = denotes average value of $(\cdot)$
$*$ = denotes dimensionless quantity
$+$ = denotes dimensionless quantity

Greek Symbols

α = thermal diffusivity, m^2/s
β = aspect ratio, $\equiv \sqrt{A_i/A_o}$
= Falkner-Skan wedge parameter
ϵ = aspect ratio, $\equiv b/a$
ϵ = effectiveness, $\equiv q/q_{max}$
η = efficiency
γ = symmetry parameter
κ = bypass fraction
λ = wavelength, m
μ = dynamic viscosity, Ns/m^2
ν = kinematic viscosity, m^2/s
ϕ = angular measurement, rad
= shape function, Ch.3
ψ = shape function
ρ = fluid density, kg/m^3
σ = frontal area ratio,$\equiv \frac{A_{free}}{A_{front}}$
τ = wall shear stress, N/m^2
θ = fin angle, rad
θ = temperature excess, $T - T_b$, K

Acronyms

AER = area enhancement ratio
ERR = entrance reduction ratio
FAR = fin area ratio

$HFDF$	=	hydrodynamically fully developed flow
HDF	=	hydrodynamically developing flow
HPD	=	high pressure direction
$LMTD$	=	log mean temperature difference
LPD	=	low pressure direction
NTU	=	number of transfer units
OSF	=	offset strip fin
TDF	=	thermally developing flow
$TFDF$	=	thermally fully developed flow
UWF	=	uniform wall flux
UWT	=	uniform wall temperature

Chapter 1

Motivation and Scope

1.1 Introduction

This thesis is concerned with the development of models for predicting the heat transfer and pressure drop characteristics in compact heat exchangers. Most compact heat exchangers take advantage of surface enhancements for augmenting heat transfer. Common augmentation devices include continuous plate fins, offset or interrupted strip fins, turbulator strips, and corrugated ribs. Past research in this area has largely been numerical and/or experimental in nature. Correlations based upon numerical and experimental data have been developed, but are limited to a small number of configurations and/or range of parameters.

Presently, there are only a few general models and correlations which enable the prediction of heat transfer and fluid flow characteristics in plain ducts and a limited number of enhanced channels. Thus, extensive Handbooks (Rohsenow et al. (1985a, 1985b, 1998), Kakac et al. (1987)) and specialized texts (Shah and London (1978), Kays and London (1984), Webb (1995)) containing data and correlations for many geometries are frequently required. The development of models that are applicable to families of similar geometries and enhancement devices provides greater flexibility in the design of heat exchangers.

A novel approach in the design and optimization of heat exchangers that is rapidly gaining popularity is the method of entropy generation minimization (EGM), Bejan (1996). This approach to design addresses the irreversibilities in heat exchangers which result from heat transfer and fluid friction. EGM analysis usually begins with a simple thermodynamic expression for the rate of entropy generation $\dot{S}'_{gen}$ per unit length (Bejan, 1996):

$$\dot{S}'_{gen} = \frac{q'\Delta T}{T^2} + \frac{\dot{m}}{\rho T}\left(-\frac{dp}{dx}\right) \geq 0 \tag{1.1}$$

Introduction of the Colburn j factor (heat transfer) and Fanning friction factor f (fluid friction) usually results in expressions having the form

$$\dot{S}_{gen} = \frac{q^2 D_h Pr^{2/3}}{4 L T^2 \dot{m} c_p j} + \frac{2 L \dot{m}^3 f}{\rho^2 T D_h A^2} \tag{1.2}$$

where L is the passage length, q is the heat transfer rate, $\dot{m}$ is the mass flow rate, c_p is the heat capacity of the working fluid, ρ is the density of the working fluid, Pr is the fluid Prandtl number of the working fluid, D_h is the hydraulic diameter of the duct or channel, and T is the absolute temperature of the thermal reservoir or surroundings. Equation (1.2) illustrates the competing effects of heat transfer and fluid friction irreversibilities. A thermodynamic optimum exists such that $d\dot{S}/dx_i = 0$ where x_i is the parameter to be optimized.

In most heat exchanger design problems the working fluid, heat transfer rate, and mass flow rate are usually known. If the passage geometry or enhancement device are also specified, then the design problem is simply reduced to finding the optimum size given other constraints. However, if the optimization is one of determining the ideal passage or enhancement configuration, then accurate knowledge of the heat transfer j and fluid friction f characteristics as a function of geometry is essential. This can only be achieved by means of general models that encompass a broad range of parameters.

Presently, there is lack of simple geometrically based models which enable the prediction of heat transfer and fluid friction characteristics in non-circular plain and/or enhanced channels. The aim of the present work is to develop models for three distinct families of heat transfer surfaces utilized in the design of heat exchangers, namely, the plain duct of non-circular cross-section, the offset or interrupted strip fin, and the turbulator strip.

1.2 Research Objectives

The motivation for this work was provided by DANA Corporation - Long Manufacturing Division, of Oakville, Ontario, a manufacturer of OEM and after market automotive heat exchangers. Long Manufacturing presently supplies the automotive industry with many types of automotive engine and transmission oil coolers and radiators. Recent studies conducted by the Advanced Engineering Group of Long Manufacturing (Lemczyk, (1992, 1994)) have indicated that there is a lack of understanding of the mechanisms controlling the fluid flow and heat transfer in low speed or low Reynolds number flow heat exchangers with thermal enhancement devices such as turbulator strips and offset strip fins. Of particular interest to Long Manufacturing is the development of new models that will predict the fluid friction and heat transfer characteristics in compact heat exchanger cores with and without thermal enhancement devices. These models would supplement the current predictive capability at Long Manufacturing during various stages in the design of new heat exchangers.

Presently, Long Manufacturing relies heavily on costly numerical modelling and experimental measurements to optimize the design of typical automotive heat exchangers. New models that predict the fluid friction and heat transfer characteristics in heat exchanger cores must be developed. These models will help minimize the design time and help reduce costs through a reduction of prototyping and experimentation at the various design stages.

Long Manufacturing (Lemczyk, 1994) have outlined several research objectives which would benefit the development of compact heat exchangers. These are:

- Definition of characteristic length for arbitrary duct shapes which would lead to better correlation of laminar flow heat transfer and pressure drop data
- Development of new models and/or correlations for predicting heat transfer and pressure drop in ducts of arbitrary shape
- Obtain new experimental data to supplement the development of theoretical models for thermal enhancement devices
- Theoretical modeling of enhanced surface geometries such as turbulators, continuous plate fins, and offset strip fins

In the fluid flow and heat transfer literature, the tradition of using the hydraulic diameter of a non-circular duct as a characteristic length usually results in large discrepancies, on the order of ± 50 percent, in laminar flow data for non-circular ducts. Kakac and Liu (1997). In the case of turbulent flow. it is well established that use of the hydraulic diameter yields better correlation of data in non-circular ducts, on the order of $\pm 10 - \pm 15$ percent, Kakac and Liu (1997). As part of the model development for plain ducts and channels a more appropriate length scale has to be chosen which reduces the discrepancies in the laminar flow data. This new length scale will be chosen based upon the results of dimensional analysis on an arbitrary shaped duct.

In most compact heat exchanger applications, passage lengths are usually short. In these instances, entrance effects significantly increase the pressure drop and heat transfer. A limited number of correlations are available which predict these characteristics, however, a more general correlation or model is required which is applicable

to many common passage shapes found in heat exchangers. These models need to be developed for various flow conditions and thermal boundary conditions.

For many automotive heat exchangers, size is one of the most important constraints. Most automotive oil coolers take advantage of numerous thermal enhancement devices. These devices are often utilized to enhance the heat transfer characteristics usually at the expense of the fluid friction. Few models are presently available for these devices, most of which are empirically based. New models which are analytically based would allow accurate prediction of the heat transfer and fluid friction characteristics as a function of many geometric parameters.

Finally, in order to validate models for flows in complex enhanced channels, experimental data is required. Unfortunately, very little information is available in the open literature for certain enhancement devices typically found in automotive heat exchangers. This lack of data is attributed to many enhancement devices being proprietary technology. As a result, performance characteristics for many enhanced surface technologies are not reported in product, trade or research journals. As part of this research program, a database of experimental data is being created for many of the devices which have been developed by Long Manufacturing in order to validate the proposed models for these devices.

1.3 Problem Statement

Heat transfer and pressure drop in compact heat exchangers have been examined by numerous researchers in the past. The most important solutions and data have been reviewed in several Handbooks (Kays and Perkins (1985), Shah and Bhatti (1987), Bergles (1998), Webb (1987)) and advanced texts (Shah and London (1978), Kays and London (1984), Webb (1994), Shah (1998)). This particular class of heat transfer problem has many variations, thus researchers have been developing new solutions and conducting experiments for many common configurations. Typically, research has

been divided into plain and enhanced channels and laminar and turbulent flows. This has led to an abundance of solutions and data in all of these areas which ultimately overwhelm designers of compact heat exchangers.

Figure 1.1 shows a typical automotive oil cooler manufactured by Long Manufacturing. In most applications, engine or transmission oil is the internal fluid with air or liquid coolant as the external fluid. Typical operating conditions are summarized in Table 1.1. Each channel contains an enhancement device which is typically referred to as a plate fin. Variations of the plate fin include the offset strip fin (OSF) and turbulator strip (or turbulizer). Such devices are often employed to enhance heat transfer in each channel by providing increased surface area and/or increasing the heat transfer coefficient by interrupting the development of thermal and hydrodynamic boundary layers. However, the penalty of increasing the surface area or obstructing the flow is an increase in pressure drop. Due to size and rating constraints imposed by the automotive industry, these devices must be optimized to provide maximum heat transfer at reasonable pressure drops and/or mass flow rates.

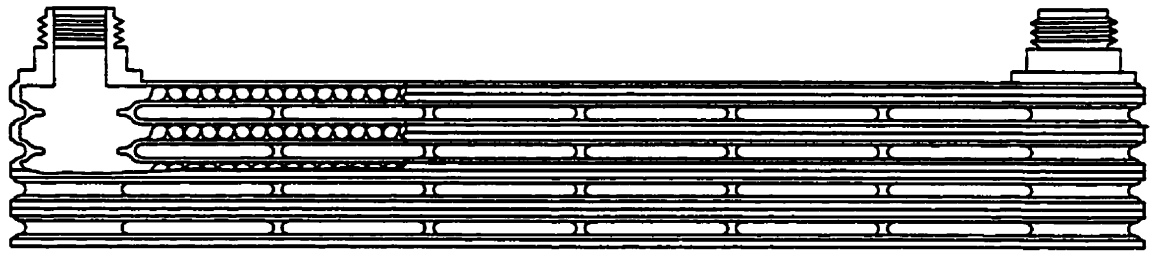

Fig. 1.1 - Typical Automotive Oil Cooler.

Several typical compact heat exchanger surfaces are shown in Fig. 1.2. These geometries utilize either plate fins, offset strip fins, louvered fins, or perforated fins (Shah and Webb, 1983). The latter four geometries are designed to provide increased heat transfer by promoting the development of new thermal and hydrodynamic boundary

layers at each fin surface in addition to providing increased surface area. In many applications plate fin arrangements such as the offset strip fin may function in two orientations. These orientations are the low pressure direction (LPD) where the fluid flows parallel to the fin surfaces and the high pressure direction (HPD) where the fluid impinges on the fin surface, (refer to Fig. 1.3). In the latter case the plate fin is often referred to as a turbulator, even though boundary layers are predominantly laminar.

Table 1.1
Typical Operating Conditions of Automotive Heat Exchangers (Lemczyk, 1995)

Hot Fluids	Engine, Transmission, and Power Steering Oils
Coolants	Water, Ethylene Glycol, and Air
Operating Temperatures	$90\,°C \leq$ Hot Fluids $\leq 140\,°C$ $20\,°C \leq$ Coolants $\leq 105\,°C$
Flow Rates	$2 \times 10^{-5} \leq$ Hot Fluids $(m^3/s) \leq 2 \times 10^{-2}$ $4 \times 10^{-5} \leq$ Coolants $(m^3/s) \leq 1.5 \times 10^{-2}$ $2 \leq$ Air $(m/s) \leq 20$
Prandtl Number	$0.7 \leq Pr \leq 500$
Reynolds Number	$1 \leq Re_{d_h} \leq 10000$

In many practical applications, the plate fin and offset strip fins have a wide range of geometrical parameters. Some common configurations include triangular, square, sinusoidal, rectangular, and trapezoidal. Many of the models which have been developed do not address all of the geometrical considerations or have only been developed for the rectangular geometry. In addition, no correlations have been found which predict the heat transfer and pressure drop characteristics in the HPD flow orientation of offset strip fin or turbulator devices. In Chapter 6, models will be developed which address the various geometric configurations, i.e. shape and orientation in flow field.

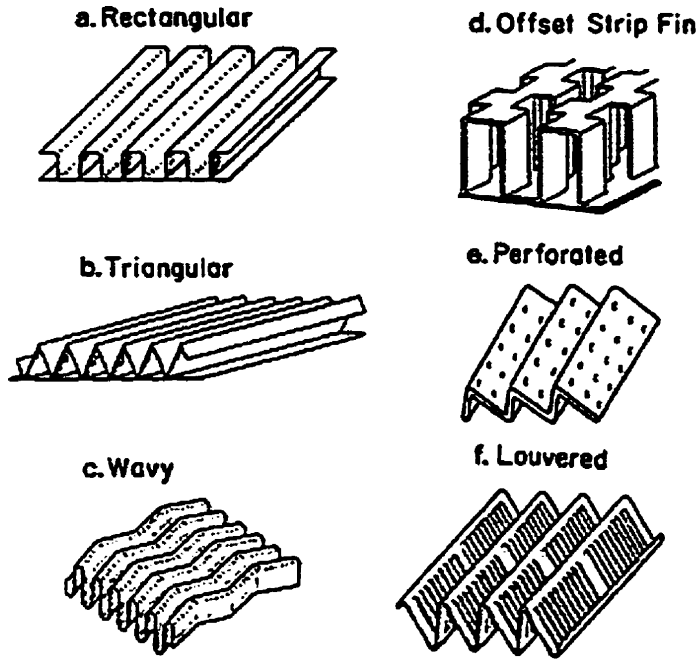

Fig. 1.2 - Typical Compact Heat Exchanger Surfaces.

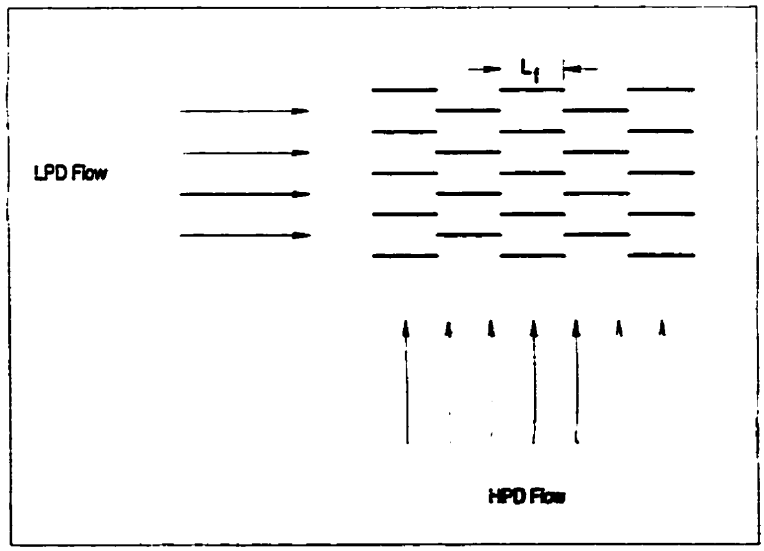

Fig. 1.3 - LPD and HPD Flow Arrangements.

1.3.1 Flow Conditions

The design parameters for many automotive heat exchangers prescribe low Reynolds number flow. In these cases the flow regime may be classified as laminar if $Re_{D_h} \leq 2000$ for plain surface ducts, where $Re_{D_h} = \overline{w} D_h / \nu$. In other instances, a complex laminar type flow may be produced when there are internal surface enhancements which interrupt the thermal and hydrodynamic boundary layer development and increase heat transfer. In such cases laminar flow at the fin surface may be achieved for Reynolds numbers as high as $Re_{D_h} \leq 10000$, while the main flow may be turbulent (Shah and Webb, 1983). In most practical applications the Re_{D_h} rarely exceeds 10000 (Shah and Webb, 1983).

1.3.2 Thermal Boundary Conditions

A large number of thermal boundary conditions for duct flow problems have been addressed in the heat transfer literature. The two most commonly addressed conditions are the uniform wall temperature (UWT) condition denoted by the subscript (T) and the uniform wall flux (UWF) condition denoted by subscript (H). Several variations of these two boundary conditions exist and are discussed in detail in Shah and London (1974, 1978). For certain geometries, the (H) condition is also denoted as $(H1)$ and $(H2)$. These conditions deal with how peripheral variations in temperature and heat flux are dealt with in two dimensional cross-sections. For the special case of the circular duct, circular annular duct and parallel plate geometry these conditions are both equivalent to the (H) condition.

The $H1$ condition is representative of ducts and surfaces which have a high thermal conductivity. Peripheral variations in temperature are small or negligible for the $H1$ condition. The $H2$ condition is representative of ducts and surfaces which are composed of low thermal conductivity materials. In these applications the temperature varies peripherally for the non-circular geometries. Most compact heat exchangers

are constructed with high thermal conductivity materials such as aluminum, copper, steel, and brass. For this work it will be sufficient to examine only the (T), (H) and $(H1)$ boundary conditions.

In applications where enhancement devices are utilized, the boundary condition is usually assumed to be that of uniform wall temperature. Experimental data for many enhancement devices are usually obtained with this boundary condition. In two fluid heat exchangers the assumption of uniform wall temperature is quite reasonable. However, in many single fluid applications such as electronics power supply cooling, experimental data may not accurately reflect the uniform wall flux condition which is more likely.

1.3.3 Heat Exchanger Geometries

The number of duct geometries which have been studied in the heat transfer literature is too large to examine each in detail. Only the most common and practical duct geometries will be considered for this work. Most of these geometries are found in various plate fin arrangements. Three classifications of plain duct geometries have been considered for this work. These are singly connected ducts or ducts whose flow area is enclosed only by a single contour (refer to Figs. 1.4 and 1.5), multiply connected ducts such as annular regions with circular and non-circular contours (refer to Fig. 1.6), and ducts with internal surface enhancements such as plate fins, offset strip fins, and turbulator strips (see Fig. 1.2).

Singly connected ducts which have received the most attention are the circular, rectangular, elliptical, triangular, and regular polygonal ducts. Another geometry which has received a lot of attention is the infinite parallel plate channel which is a special case of the rectangular duct and circular annular duct. Other ducts such as the sine duct and variations of the rectangular duct such as the rhombic duct, stadium, and modified stadium ducts will also be examined. Figures 1.4 and 1.5 illustrate the most common singly connected geometries of interest.

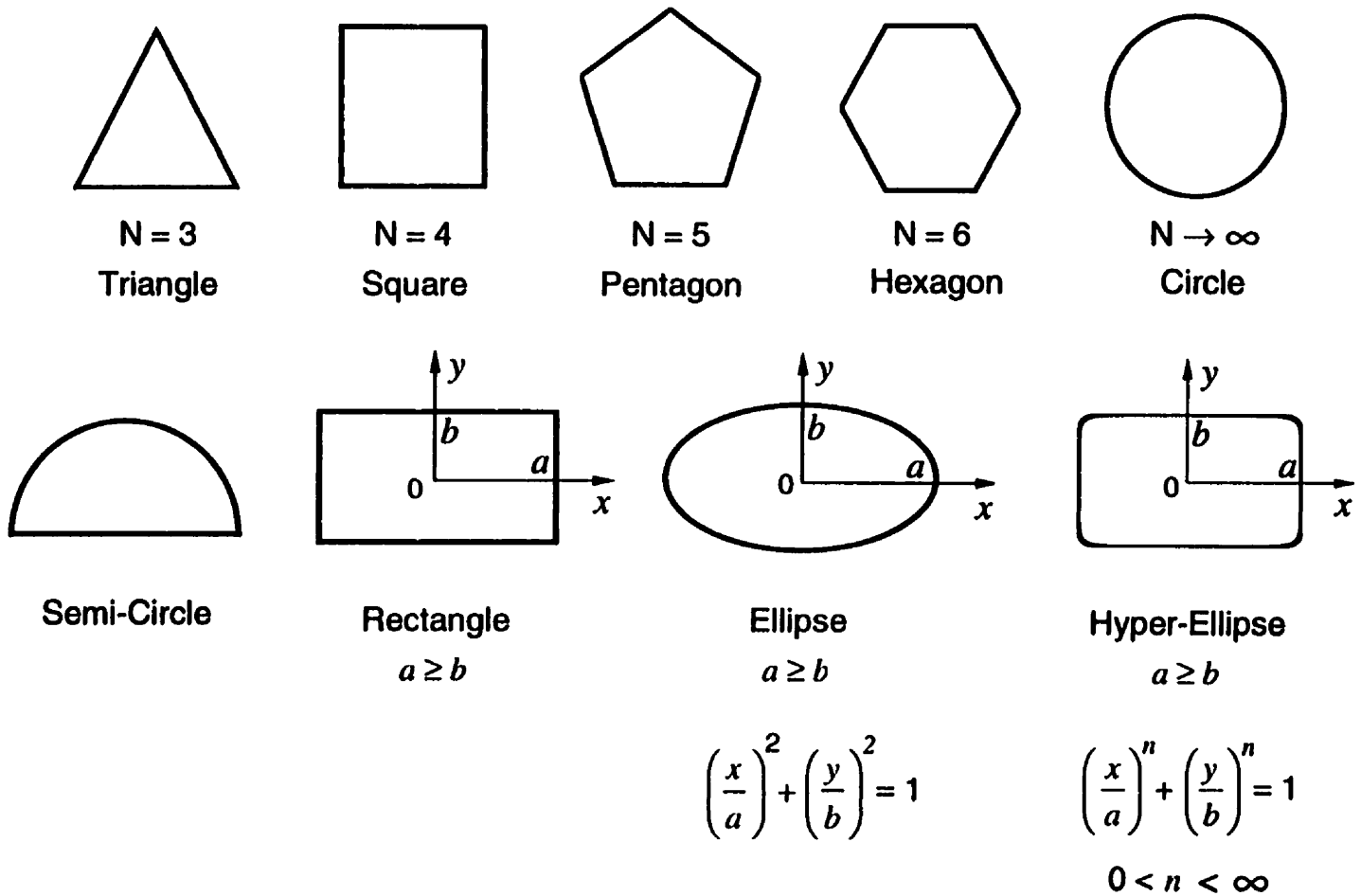

Fig. 1.4 - Common Singly Connected Duct Geometries.

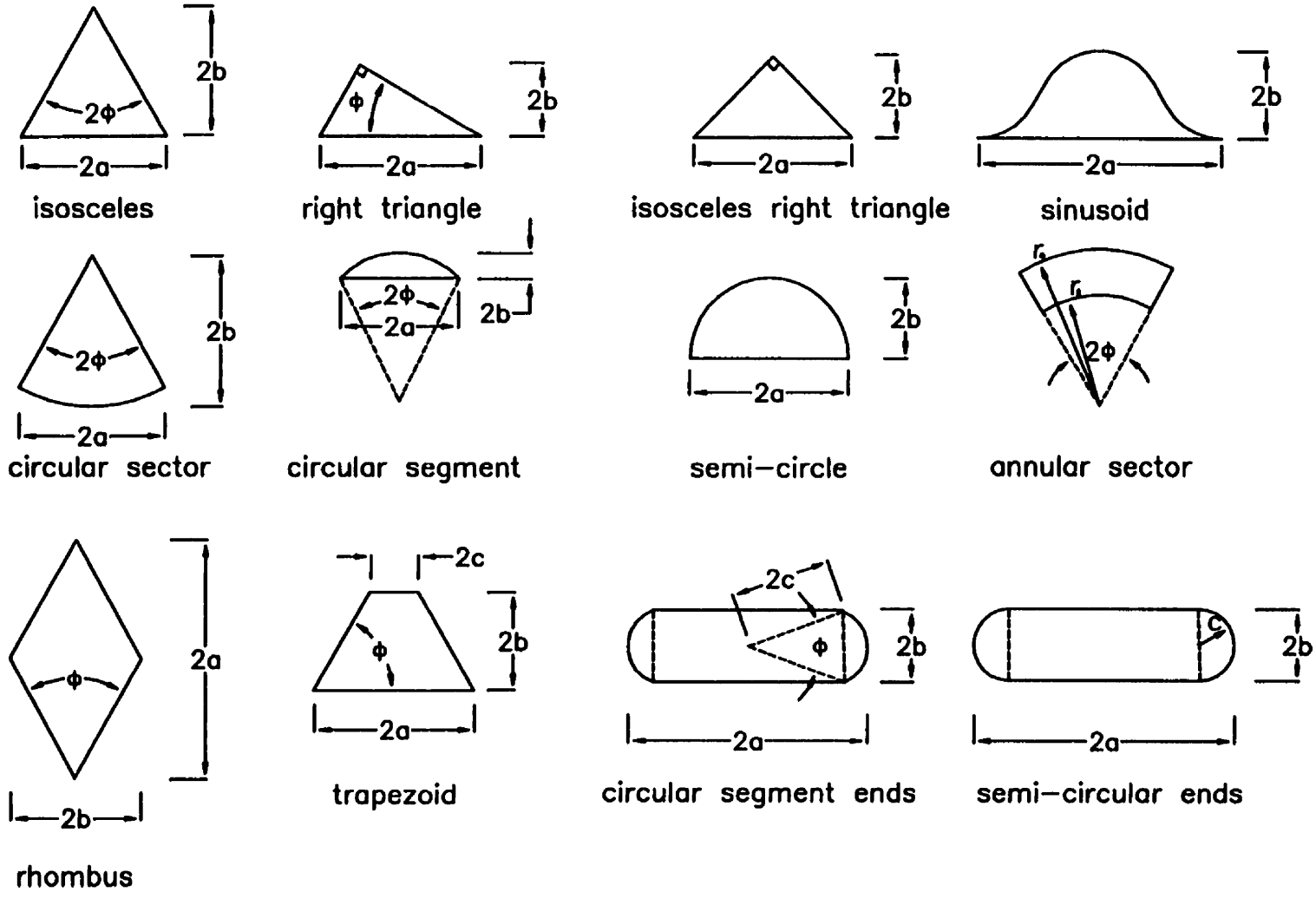

Fig. 1.5 - Other Singly Connected Duct Geometries.

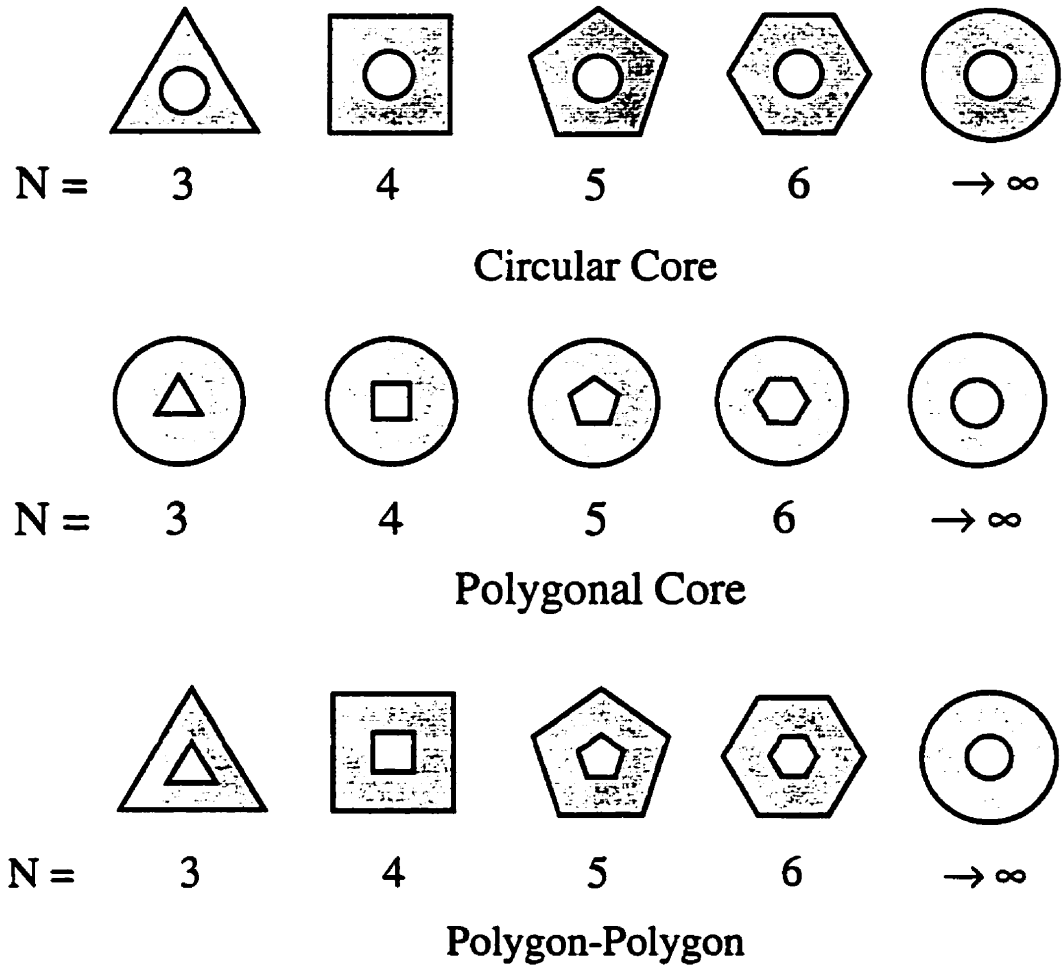

Fig. 1.6 - Common Doubly Connected Duct Geometries.

The simplest multiply connected region is the concentric circular annular duct. Several variations of the circular annular duct exist, namely, the polygonal duct with circular core, the circular duct with polygonal core, and the most general case where both ducts are polygonal and concentric, (refer to Fig. 1.6). Of these three variations, only the first two have been examined in the literature (Shah and London, 1978).

Finally, in most compact heat exchanger designs, flow channels contain modifications such as fins, twisted tapes, turbulator strips, or corrugated ribs. This class of geometries has currently received the least attention from the point of view of modeling. Much of the work for this class of geometries has been numerical and/or experimental. Enhancement devices of interest are the continuous plate fin, offset strip fin, and turbulator strips. Many of these devices are shown in Fig. 1.2.

1.4 Outline of Thesis

The remainder of the thesis is organized as follows. Chapter 2 will summarize the governing equations and dimensionless groups for many of the problems addressed in this thesis. Chapter 3 reviews the currently available models and correlations. Chapter 4 presents the development of models for many common plain ducts utilized in compact heat exchangers. Chapter 5 outlines the procedures for obtaining experimental data for the enhancement devices being examined in this thesis. Chapter 6 presents the development of enhanced surface models and provides comparisons with experimental data. Chapter 7 summarizes the findings and suggests areas which need further examination.

Chapter 2

Governing Equations and Dimensionless Groups

2.1 Introduction

The basic governing equations for laminar forced convection heat transfer are given below in vector notation. These equations are for the most general case, governing the simultaneous development of fluid velocity and temperature distributions. Traditionally, the following simplifications are generally imposed upon the governing equations, namely:

- steady incompressible flow
- constant fluid properties
- no body forces, $\vec{g} = 0$
- negligible axial conduction
- negligible viscous dissipation

The continuity, momentum, and energy equations are:

$$\nabla \cdot \vec{V} = 0 \tag{2.1}$$

$$(\vec{V} \cdot \nabla)\vec{V} = -\frac{1}{\rho}\nabla p + \nu \nabla^2 \vec{V} \tag{2.2}$$

$$(\vec{V} \cdot \nabla)T = \alpha \nabla^2 T \tag{2.3}$$

In later sections, the fluid flow and heat transfer problems are discussed in more detail for specific flow conditions and geometries related to heat exchanger design. The governing equations are subject to the following boundary and inlet conditions.

At the duct wall or surface, the fluid is subject to the no slip condition:

$$\vec{V}_w = 0 \tag{2.4}$$

and one of the following thermal boundary conditions:

$$\begin{cases} q_{wall} = k\left.\dfrac{\partial T}{\partial n}\right|_w, & \textbf{UWF} \\ T_{wall} = T_w, & \textbf{UWT} \end{cases} \tag{2.5}$$

Finally, a uniform inlet velocity

$$V_{in} = w_i \tag{2.6}$$

and uniform inlet temperature

$$T_{in} = T_i \tag{2.7}$$

are usually prescribed.

2.2 Reduced Equations for Duct Flow

Several laminar flow problems are encountered in the design of heat exchangers. The simplest of these arises when the velocity and temperature profiles are fully developed. In certain applications the velocity distribution may be developing if the duct is not much longer than the hydrodynamic entrance length. In this case, the pressure drop will be much higher than the case where the velocity distribution is fully developed in a longer duct. In other applications, especially when dealing with highly viscous fluids such as oils, the velocity profile develops more quickly than the temperature profile and may be considered to be fully developed in a region when the thermal boundary layer begins developing. Such problems are often referred to as Graetz problems or thermal entrance problems. Finally, the most general case (and difficult to analyze) occurs when both the velocity and temperature profiles develop together. This problem is generally referred to as the combined entrance problem or simultaneously developing flow. Both the hydrodynamic and thermal entrance problems are examined in this thesis.

2.2.1 Fluid Friction

The hydrodynamic duct flow problem being considered is shown in Fig. 2.1. Initially the fluid enters the duct with a uniform velocity. A hydrodynamic boundary layer begins to form as fluid particles near the duct wall decelerate, while in the core region fluid particles accelerate to maintain continuity of the flow field. Further downstream the boundary layer continues to grow until it eventually coalesces and the flow becomes fully developed.

In cartesian coordinates the governing equations for the hydrodynamic entrance problem are the continuity equation

$$\frac{\partial u}{\partial x} + \frac{\partial v}{\partial y} + \frac{\partial w}{\partial z} = 0 \tag{2.8}$$

and momentum equation in the direction of the flow,

$$u\frac{\partial w}{\partial x} + v\frac{\partial w}{\partial y} + w\frac{\partial w}{\partial z} = -\frac{1}{\rho}\frac{dp}{dz} + \nu\left(\frac{\partial^2 w}{\partial x^2} + \frac{\partial^2 w}{\partial y^2}\right) \tag{2.9}$$

The single momentum equation in the flow direction results from the following boundary layer idealizations, $w >> u, v$, and $\mu(\partial^2 w/\partial z^2)$, $(\partial p/\partial x)$, and $(\partial p/\partial y)$ negligible, and $(\partial w/\partial x), (\partial w/\partial y) >> (\partial w/\partial z), (\partial u/\partial x_i), (\partial v/\partial x_i)$, where x_i is used to denote the three cartesian coordinates x, y, z for $i = 1, 2, 3$.

The pressure gradient term may be written as

$$-\frac{1}{\rho}\frac{dp}{dz} = w_c\frac{dw_c}{dz} \tag{2.10}$$

where $w_c = w_c(z)$ is the velocity of the accelerating core. The above equations are subject to the no slip condition $(u, v, w)_{wall} = 0$, the boundedness condition $w(x, y, z) \neq \infty$, and the inlet condition $w(x, y, 0) = w_i$.

Due to the non-linear terms in Eq. (2.9) solutions for hydrodynamically developing flows are generally more difficult to obtain than fully developed flows. Developing flows require simultaneous solution to both the continuity, Eq. (2.8), and the momentum, Eq. (2.9), equations given above. Despite this difficulty, analytic and approximate analytical solutions for developing laminar flows have been obtained for the circular duct (Langhaar, 1942), rectangular duct (Miller and Han, 1971), elliptical duct (Bhatti, 1983), parallel plates (Schlichting, 1979) and circular annular duct (Sparrow and Lin, 1964). Solutions for many other geometries have also been obtained numerically and are discussed in Shah and London (1978) and Shah and Bhatti (1987).

For fully developed flow in a duct of arbitrary cross-section, the Navier-Stokes equations reduce to the momentum equation in the flow direction. The resulting equation

is the Poisson equation in one or two dimensions depending upon the cross-sectional geometry. In this case, the source term is the constant pressure gradient along the length of the duct.

In cartesian coordinates the governing equation for fully developed laminar flow in a constant cross-sectional area duct is

$$\frac{\partial^2 w}{\partial x^2} + \frac{\partial^2 w}{\partial y^2} = \frac{1}{\mu}\frac{dp}{dz} \tag{2.11}$$

which represents a balance between the pressure and viscous forces. Equation (2.11) is subject to the no slip condition $w(x,y) = 0$ at the wall of the duct and to the boundedness $w(x,y) \neq \infty$ condition within the duct cross-section.

Solutions for many of the different duct geometries shown in Figs. 1.4-1.6 have been obtained using various analytical and numerical methods and are discussed in Shah and London (1978) and Shah and Bhatti (1987). Numerical and analytical results are often presented in terms of the dimensionless friction factor. The Fanning friction factor is defined as

$$f = \frac{\overline{\tau}_w}{\frac{1}{2}\rho\,\overline{w}^2} \tag{2.12}$$

which is usually written in terms of the Reynolds number as follows

$$f Re_{\mathcal{L}} = 2\,\frac{\overline{\tau}_w\,\mathcal{L}}{\mu\,\overline{w}} \tag{2.13}$$

where $\mathcal{L}$ is a characteristic length scale of the duct cross-section, usually chosen to be the hydraulic diameter $D_h = 4A/P$, where A is the cross-sectional area and P is the perimeter. The average wall shear stress $\overline{\tau}_w$ may be written in terms of the pressure gradient by performing a force balance on an arbitrary slug of fluid. This results in:

$$\overline{\tau}_w = -\frac{A}{P}\frac{dp}{dz} \tag{2.14}$$

A general form of the friction factor Reynolds group in terms of the solution for the velocity distribution is

$$fRe_{\mathcal{L}} = 2\mathcal{L}\frac{\frac{1}{P}\oint \left.\frac{\partial w}{\partial n}\right|_w ds}{\frac{1}{A}\iint_A w\, dA} \tag{2.15}$$

where $\left.\frac{\partial w}{\partial n}\right|_s$ represents the velocity gradient at the duct wall with respect to an inward directed normal and ds is the differential of arc length.

If the flow is developing, an apparent friction factor (Shah and London, 1978) which accounts for the wall shear and increase in momentum in the inviscid core can be defined as

$$f_{app}Re_{\mathcal{L}}(z^+) = fRe_{\mathcal{L}} + \frac{K(z^+)}{4z^+} = \frac{\Delta p^*}{4z^+} \tag{2.16}$$

where the incremental pressure drop $K(z^+)$ is defined as the difference between the total pressure drop in the duct and the pressure drop if the flow were fully developed at every point along the duct, or

$$K(z^+) = \Delta p^* - \left(-\frac{dp^*}{dz^+}\right)_{fd} z^+ \tag{2.17}$$

where $\Delta p^* = \frac{p_i - p_z}{\frac{1}{2}\rho\overline{w}^2}$, $z^+ = \frac{z/\mathcal{L}}{Re_{\mathcal{L}}}$ is the dimensionless duct length and $\mathcal{L}$ is an arbitrary length scale usually chosen to be the hydraulic diameter, $D_h = 4A/P$.

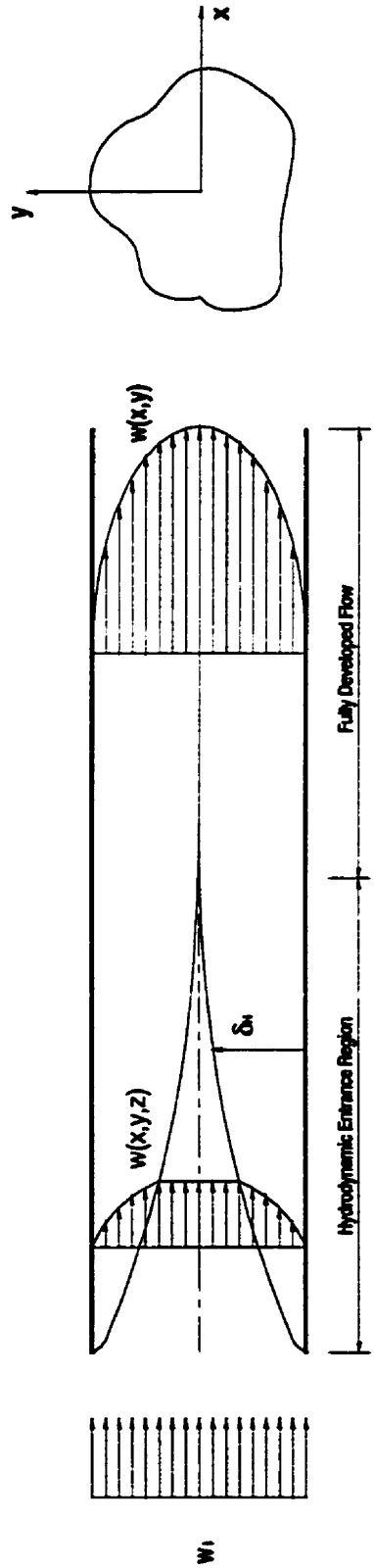

Fig. 2.1 - Hydrodynamic Entrance Problem.

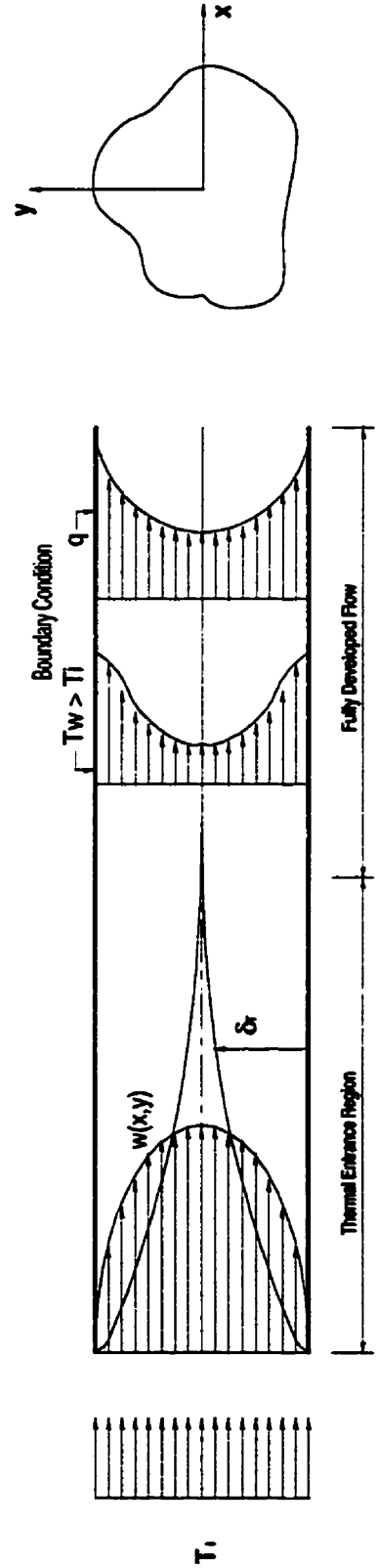

Fig. 2.2 - Thermal Entrance Problem.

2.2.2 Heat Transfer

Forced convection heat transfer problems in ducts may be classified as either thermally developing or thermally fully developed. The first case may be further divided depending upon whether the velocity profile is developing or fully developed. Simultaneous development of velocity and temperature profiles is the most difficult problem to analyze. Most solutions to this type of problem have been obtained using numerical methods. The second type of thermally developing flow occurs when the velocity profile is established, (refer to Fig. 2.2). This type of problem is easier to solve and is often referred to as the Graetz problem or Graetz-Nusselt problem, Shah and London (1978) . Finally, for the case of fully developed flow, both velocity and temperature profiles are fully developed. This is the case for very long flow passages. Both fully developed and thermally developing flows will be examined.

When both the hydrodynamic and thermal boundary layers develop simultaneously, the energy equation in cartesian co-ordinates takes the following form:

$$u\frac{\partial T}{\partial x} + v\frac{\partial T}{\partial y} + w\frac{\partial T}{\partial z} = \alpha\left(\frac{\partial^2 T}{\partial x^2} + \frac{\partial^2 T}{\partial y^2}\right) \tag{2.18}$$

where the effects of axial conduction and viscous dissipation have been ignored.

In addition to the energy equation, the continuity, Eq. (2.8), and momentum, Eq. (2.9), equations must be solved. To date, few solutions to this combined set of equations have been obtained.

If the hydrodynamic boundary layer is fully developed or develops at a much faster rate than the thermal boundary layer, the energy equation for thermally developing laminar flow becomes:

$$\frac{\partial^2 T}{\partial x^2} + \frac{\partial^2 T}{\partial y^2} = \frac{w}{\alpha}\frac{\partial T}{\partial z} \tag{2.19}$$

where $w = w(x, y)$ is the fully developed velocity profile which may be obtained from the solution to Eq. (2.11).

Equations (2.18) and (2.19) are subject to the inlet condition

$$T(x, y, 0) = T_i \tag{2.20}$$

and one of the following boundary conditions

$$\begin{cases} q_{wall} = k\left.\dfrac{\partial T}{\partial n}\right|_w, & \textbf{UWF} \\ T_{wall} = T_w, & \textbf{UWT} \end{cases} \tag{2.21}$$

in addition to the boundedness condition, $T(x, y, z) \neq \infty$, at any point within the duct cross-section.

When the flow becomes thermally fully developed the energy equation may be written in terms of the mixing cup temperature $T_m(z)$, (Kays and Crawford, 1993)

$$\frac{\partial^2 T}{\partial x^2} + \frac{\partial^2 T}{\partial y^2} = \frac{w}{\alpha}\frac{dT_m}{dz} \tag{2.22}$$

for the uniform wall flux (UWF) case, and

$$\frac{\partial^2 T}{\partial x^2} + \frac{\partial^2 T}{\partial y^2} = \frac{w}{\alpha}\left(\frac{T_w - T}{T_w - T_m}\right)\frac{dT_m}{dz} \tag{2.23}$$

for the uniform wall temperature (UWT) case, where

$$T_m(z) = \frac{1}{\overline{w}A}\iint_A wT\,dA \tag{2.24}$$

A general dimensionless heat transfer coefficient or Nusselt number may be defined as

$$Nu_{\mathcal{L}} = \frac{\bar{q}_w(z)\,\mathcal{L}}{k\,(\overline{T}_w(z) - T_m(z))} = \frac{h\mathcal{L}}{k} \tag{2.25}$$

where $T_m(z)$ is the mixing cup fluid temperature, $\overline{T}_w(z)$ is the average wall temperature, and $\bar{q}_w(z)$ is the average wall heat flux at any point along the duct.

In terms of the solutions to Eqs. (2.18,2.19,2.22, and 2.23), the Nusselt number, $Nu_{\mathcal{L}}$, may be defined as follows

$$Nu_{\mathcal{L}} = \mathcal{L}\,\frac{\frac{1}{P}\oint -\left.\frac{\partial T}{\partial n}\right|_w ds}{\frac{1}{P}\oint T_w\,ds - \frac{1}{\overline{w}\,A}\iint_A w\,T\,dA} \tag{2.26}$$

where $\left.\frac{\partial T}{\partial n}\right|_w$ represents the temperature gradient at the duct wall with respect to an inward directed normal, ds is the differential of arc length, $\mathcal{L}$ is an arbitrary characteristic length scale to be determined later, A is the cross-sectional area and P is the wetted perimeter of the duct. Traditionally, $\mathcal{L} = 4A/P$, the hydraulic diameter of the duct. If the flow is thermally developing, an additional parameter, the dimensionless duct length defined as

$$z^* = \frac{z}{\mathcal{L}Re_{\mathcal{L}}Pr} \tag{2.27}$$

arises in the solution, as does the Prandtl number in the case of the combined entrance problem. Finally, the local Nusselt number is related to the average Nusselt number through

$$\overline{Nu} = \frac{1}{z}\int_0^z Nu(z)dz \tag{2.28}$$

Solution to this problem for thermally fully developed flow in a circular duct is discussed in most basic heat transfer texts (Incropera and DeWitt (1990), Bejan (1993)) and all advanced level texts (Burmeister (1993), Kays and Crawford (1993), Bejan (1995)). Equation (2.19) may be solved analytically for the circular duct and parallel plate channel, however, the solution requires the evaluation of hypergeometric functions (Newman (1973), Lauwerier (1951)). Sellars, Tribus, and Klein (1956) developed approximate mathematical relations for the eigenvalues and eigenfunctions for the general solution to the circular duct. Leveque (Drew (1931), Newman (1973), Bird et al. (1960)) obtained an asymptotic solution in the entrance region of a circular duct where the thermal boundary layer is thin. A general form of the Leveque solution for non-circular ducts was later proposed by Shah and London (1978) and is discussed in Chapter 3.

For non-circular ducts, a full numerical solution to Eq. (2.19) is required. Numerical solutions have been found for many non-circular ducts and data are compiled in Shah and London (1978) and Shah and Bhatti (1987). Finally, if both hydrodynamic and thermal boundary layers are developing, Eq. (2.18) is generally solved numerically using approximate solutions for the velocity distribution, or a full numerical solution may be obtained for both the hydrodynamic and thermal boundary layers. The Karman-Pohlhausen integral method has also been used to obtain approximate solutions in the combined entrance region, Sparrow (1955).

2.2.3 Hydrodynamic and Thermal Entrance Lengths

Knowledge of the extent of the hydrodynamic and thermal boundary layer development is important if the appropriate model or correlation is to be applied to a particular problem. Approximate expressions have been adopted in the heat transfer

literature which determine the extent of boundary layer development. These approximate expressions are given below, Burmeister (1993).

The length of hydrodynamic boundary layer development in straight ducts of constant cross-sectional area is usually determined by the approximate expression given below:

$$L_{hy} \approx 0.05 D_h Re_{D_h} \tag{2.29}$$

The above expression approximately defines the point where the centerline velocity is $0.99\, w_{max}$, Shah and London (1978). The length of thermal boundary layer development in straight ducts of constant cross-sectional area is usually determined by the approximate expression given below:

$$L_{th} \approx 0.05 D_h Re_{D_h} Pr \tag{2.30}$$

The above expression approximately defines the point where the local Nusselt number is $1.05\, Nu_{fd}$, Shah and London (1978). In Chapter 4, new expressions are developed for predicting the length of entrance region or the point along the duct beyond which the friction factor or Nusselt number no longer changes with increasing duct length.

2.3 Enhanced Surfaces

A typical turbulator in either LPD or HPD flow (refer to Fig. 1.3) will experience heat transfer and friction on flat or curved surfaces in several orientations. If a surface is inclined, the effects of longitudinal pressure gradient need to be considered in the analysis. Furthermore, heat transfer coefficients are generally higher on inclined surfaces due to stagnation effects. Examinaton of the general wedge type flow provides some indication of the effects that turbulator fin angle and fin width have on the

overall performance. In addition, these effects will be incorporated into a model to be developed later for the turbulator and OSF enhancement devices.

2.3.1 Laminar Boundary Layer Equations

Fundamental solutions for laminar boundary layer flow over wedge type geometries (refer to Fig. 2.3) are available in all advanced texts on convective heat transfer (Bejan (1995), Burmeister (1993), Cebeci and Bradshaw (1984), Eckert and Drake (1972)) and boundary layer theory (Churchill (1987), Schlichting (1979), White (1991)). In cartesian coordinates the governing equations for laminar boundary layer flow over a wedge are:

$$\frac{\partial u}{\partial x} + \frac{\partial v}{\partial y} = 0 \tag{2.31}$$

$$u\frac{\partial u}{\partial x} + v\frac{\partial u}{\partial y} = -\frac{1}{\rho}\frac{dp}{dx} + \nu\frac{\partial^2 u}{\partial y^2} \tag{2.32}$$

$$u\frac{\partial T}{\partial x} + v\frac{\partial T}{\partial y} = \alpha\frac{\partial^2 T}{\partial y^2} \tag{2.33}$$

The pressure gradient term in Eq. (2.32) may be written as

$$-\frac{1}{\rho}\frac{dp}{dx} = U_\infty \frac{dU_\infty}{dx} \tag{2.34}$$

where $U_\infty = Cx^m$, $m = \dfrac{\beta}{2-\beta}$, $2\phi = \beta\pi$ is the wedge angle, and C is a constant. Equations (2.31-2.34) are valid for external flows. Application to bodies in confined flows assumes that boundary layers formed on the body surfaces are thin relative to the channel spacing.

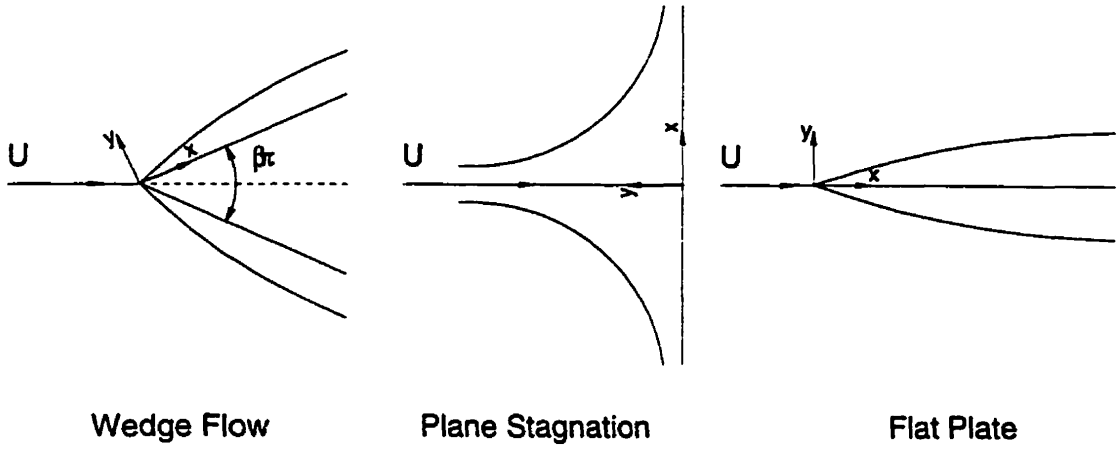

Fig. 2.3 - Flow Over a Wedge.

2.3.2 Dimensionless Groups

Experimental data for enhanced surfaces are usually presented in terms of the Fanning friction factor f and Colburn j factor. The Fanning friction factor for an enhanced surface may be defined as:

$$f = \frac{\overline{\tau}_w}{\frac{1}{2}\rho\overline{w}^2} \tag{2.35}$$

The average shear stress $\overline{\tau}_w$ may be written in terms of the pressure gradient by performing a force balance on a control volume within the enhanced channel. This results in:

$$\overline{\tau}_w = -\frac{V_{free}}{A_{wet}}\frac{dp}{dz} \tag{2.36}$$

where V_{free} is the volume of free space and A_{wet} is the total wetted surface area. This leads to the three dimensional equivalent of the hydraulic diameter defined as $d_h = 4V_{free}/A_{wet}$, Churchill (1987).

The friction factor then becomes

$$f = \frac{\frac{V_{free}}{A_{wet}}\left(-\frac{dp}{dz}\right)}{\frac{1}{2}\rho\overline{w}^2} = \frac{\frac{d_h}{4}\left(-\frac{dp}{dz}\right)}{\frac{1}{2}\rho\overline{w}^2} \tag{2.37}$$

Data may also be presented in terms of the friction factor Reynolds group fRe.

Heat transfer data are usually presented in terms of the Colburn j - factor (Shah and London, 1978), which is related to the Nusselt number by the following relation

$$j = St\,Pr^{2/3} = \frac{Nu}{Re\,Pr^{1/3}} \tag{2.38}$$

or may presented in terms of

$$jRe = \frac{Nu}{Pr^{1/3}} \tag{2.39}$$

which is analogous to fRe.

Traditionally, results for enhanced geometries are presented in terms of the friction factor - f and the Colburn - j factor, whereas results for plain ducts are presented in terms of the fRe number and Nu number.

2.4 Solution Methods

Before concluding this review of the governing equations, a brief discussion of the various solution methods which have been applied to obtain the numerous analytic, approximate analytic and numerical results is appropriate, in order to better understand the need for approximate models.

A variety of techniques have been applied in obtaining solutions. The most common are Fourier methods such as separation of variables or eigenfunction expansions. These methods have been successfully applied in obtaining solutions to fully developed flows for a wide range of geometries and to thermally developing flows for a limited number of geometries. Other methods for fully developed flows include least squares or point matching methods and conformal transformations. A number of approximate methods have also been applied to the hydrodynamic entrance problem. These include linearization methods and the Karman-Pohlhausen integral method. Finally, for the most complex problem involving the simultaneous development of hydrodynamic and thermal boundary layers, either full numerical or semi-numerical solutions have been applied in obtaining solutions.

Application of the various solution techniques has lead to an abundance of data for the problems discussed in this Chapter. A summary of the most important solutions and data is provided in Chapter 3. A comprehensive review of the state of the art in predictive techniques for many duct shapes and enhancement devices is also provided.

Chapter 3

Literature Review

3.1 Introduction

This Chapter presents a review of the state of the art in predictive models for both plain non-circular ducts and enhanced channels containing offset strip fins and turbulator devices. The heat transfer and fluid flow literature is rich with analytical, experimental and numerical results. Only the most practical and general models are reviewed, first beginning with laminar flow in straight non-circular ducts and then proceeding to enhanced channels.

Fully developed laminar fluid flow and heat transfer in circular ducts is discussed in all basic fluid mechanics texts, e.g. White (1986) and heat transfer texts e.g. Bejan (1993), Incropera and DeWitt (1990). The hydrodynamic problem has been treated in more detail in advanced fluid mechanics texts e.g. Churchill (1987), Knudsen and Katz (1958), Schlichting (1979), and White (1992), while the associated thermal problem is discussed in virtually all convective heat transfer texts e.g. Bejan (1995), Burmeister (1993), and Kays and Crawford (1993). The results presented in these references are usually for the most common duct configurations encountered in heat transfer and fluid flow problems, namely, the parallel plate channel, circular duct, rectangular duct, and circular annular duct geometries. These geometries have

received the most attention as a result of their extensive use in heat exchanger applications. The solutions for these geometries for most flow conditions are analytical or approximate analytical in nature.

Many other common and less common geometries have been examined in the fluid mechanics and heat transfer literature. A comprehensive review of this problem was compiled by Shah and London (1978), while shorter reviews have appeared in numerous Handbooks e.g. Kays and Perkins (1985), Shah and Bhatti (1987), and Ebadian and Dong (1998). At least forty different geometries have been analyzed using a variety of analytical and numerical techniques for various thermal boundary conditions for both developing and fully developed laminar flows. A summary of the available data and solutions for the most common duct shapes is provided in Table 3.1.

Analysis of thermal enhancement devices has been predominantly experimental. However, a small number of numerical studies have also been published (Sparrow et al. (1977), Patankar et al. (1977), Patankar (1990)). A comprehensive review of thermal enhancement techniques was compiled by Webb (1987, 1994) and by Kalinin and Dreitser (1998) while shorter reviews have been written by Shah (1982), Shah and Webb (1983), and Webb (1995).

Despite all of the research which has been conducted, one area which has been overlooked is the development of simple models which accurately predict the heat transfer and pressure drop in plain ducts of any cross-sectional shape and in geometries containing thermal enhancement devices. Presently, only a few studies are available which approximate the heat transfer and pressure drop factors in plain ducts and a limited number of enhanced surface geometries. The relevant past research in the area of modelling of plain ducts and enhanced channels is discussed in the sections which follow.

Table 3.1

Summary of Plain Duct Solutions

Geometry	fRe_{fd}	$f_{app}Re(z^+)$	UWT Nu_{fd}	UWT $Nu(z^*)$	UWF Nu_{fd}	UWF $Nu(z^*)$
			Singly Connected			
Circular	√	√	√	√	√	√
Parallel Plate	√	√	√	√	√	√
Rectangular	√	√	√	√	√	√
Square	√	√	√	√	√	√
Elliptic	√	√	√	√	√	√
Polygonal $N \geq 3$	√	√	√	√	√	√
Equilateral Triangle	√	√	√	√	√	√
Isosceles Triangle	√	√	√	√	√	√
Isosceles Right Triangle	√	√	√	√	√	√
Right Triangle	√	×	×	×	√	×
Semi-Circle	√	√	×	×	√	√
Circular Sector	√	√	√	×	√	×
Circular Segment	√	×	×	×	√	×
Annular Sector	√	×	√	×	√	×
Stadium	√	×	×	×	√	×
Modified Stadium	√	×	×	×	√	×
Rhombic	√	×	×	×	√	×
Trapezoidal	√	×	×	×	√	×
Sinusoidal	√	×	√	×	√	×
Cusps	√	×	×	×	×	×
			Doubly Connected			
Concentric Annular	√	√	√	√	√	√
Eccentric Annular	√	√	×	×	√	√
Polygonal Annular	√	×	×	×	√	×

√ - Data Available

× - No Data Available

3.2 Plain Duct Models

A review of the available literature has shown that only a few general approaches to predicting the heat transfer and friction characteristics in plain ducts or channels have been proposed. These models vary from relatively simple expressions to complex sets of equations. Many of the models are generalized correlations which are based upon the work of earlier researches.

3.2.1 Friction Factor

The apparent friction factor in a circular or non-circular duct may be computed from the following expressions (Shah and London (1978), Shah and Bhatti (1987))

$$f_{app}Re = \begin{cases} \dfrac{3.44}{\sqrt{z^+}}, & z^+ < 0.001 \quad \text{(a)} \\ (fRe)_{fd} + \dfrac{K_\infty}{4z^+}, & z^+ > 0.05 \quad \text{(b)} \end{cases} \tag{3.1}$$

where K_∞ is the value of the incremental pressure drop when the flow becomes fully developed. The solutions for $f_{app}Re$ given above are only valid for very short ducts or very long ducts. To establish the complete $f_{app}Re$ relationship, knowledge of the incremental pressure drop $K(z^+)$ is necessary.

A number of models have been proposed to simplify the analysis for a duct in the transition region ($0.001 < z^+ < 0.05$). These models are based upon the early work of Bender (1969). Bender (1969) combined the result of Shapiro et al. (1954), Eq. (3.1a), with the result for the "long" duct, Eq. (3.1b), to provide a model which is valid over the entire length of a circular duct. Shah (1978) later extended the model of Bender (1969) to predict results for the equilateral triangle, the circular annulus, the rectangular duct, and parallel plate channel geometries. Shah (1978) achieved this by generalizing the form of the model of Bender (1969), and tabulating coefficients for each particular case. The model proposed by Shah (1978) is

$$f_{app}Re_{D_h} = \frac{3.44}{\sqrt{z^+}} + \frac{(fRe)_{fd} + K_\infty/4z^+ - 3.44/\sqrt{z^+}}{1 + C/(z^+)^2} \tag{3.2}$$

where $(fRe)_{fd}$ is the fully developed value of the friction factor Reynolds number group, K_∞ is the value of the incremental pressure drop in the fully developed region, and C is a correlation coefficient. The value of C in the above model varies considerably for each geometry analyzed by Shah (1978), thus limiting its extension to other geometries. Values for C computed by Shah (1978) vary by a factor of ten. Thus $(fRe)_{fd}$ and K_∞ are not sufficient for predicting the results for other duct cross-sections.

Recently, Yilmaz (1990) proposed a more general model of Shah (1978). Rather than tabulating coefficients, Yilmaz (1990) developed expressions for the fully developed friction factor $(fRe)_{fd}$, incremental pressure drop K_∞, and the coefficient C which appear in the Shah (1978) extension of the Bender (1969) model. The model of Yilmaz (1990) takes the following form:

$$f_{app}Re_{D_h} = \frac{3.44}{\sqrt{z^+}} + \frac{16\psi + K/4z^+ - 3.44/\sqrt{z^+}}{1 + 0.98 \times 10^{-4}K^{3.14}/(z^+)^2} \tag{3.3}$$

where

$$\psi = 1 + \frac{(\psi_\infty - 1)}{1 + 0.33d^{*2.25}/(m-1)} \tag{3.4}$$

and

$$\psi_\infty = \frac{3}{8}d^{*2}(3 - d^*) \tag{3.5}$$

are shape factors relating the non-circular duct to a circular duct.

The incremental pressure drop for the arbitrary geometry is obtained from

$$K = \frac{1.33}{1 + (1.33/K_\infty - 1)/[1 + 0.74d^{*2}/(m-1)]} \tag{3.6}$$

where

$$K_\infty = \frac{12}{5}(3 - d^*)^2 \left[\frac{9}{7}\left(\frac{3-d^*}{7-3d^*}\right) - \frac{1}{5-2d^*}\right] \tag{3.7}$$

with $m = A/A_{D_h}$, $d^* = D_h/D_{max}$, where A_{D_h} is the area based upon the hydraulic diameter, $A_{D_h} = \pi D_h^2/4$, and D_{max} is the diameter of the maximum inscribed circle.

This model is more general than that of Shah (1978) but quite complex. Despite its complexity, the model of Yilmaz (1990) is accurate over the entire range of the entrance and fully developed regions for many duct cross-sections. The primary drawback of the simple model proposed by Shah (1978) is the requirement of tabulated coefficients and parameters for each geometry, i.e. $(fRe)_{fd}$, K_∞, and C, thus limiting interpolation for geometries such as the rectangular duct whose solution varies with aspect ratio. In the case of the model developed by Yilmaz (1990), interpolation is no longer a problem, however this is achieved at the cost of simplicity. Although the model of Yilmaz (1990) is only a function of two geometry specific parameters, m and d^*, there may be some difficulty in determining D_{max} for certain duct shapes.

3.2.2 Nusselt Number

Models for predicting heat transfer in circular and non-circular ducts have also been developed. The earliest of these was a model developed by Hausen (see Rohsenow and Choi, 1961) for the Graetz problem in a circular duct. This model is given below in a generalized form proposed by Kays (see Rohsenow and Choi, 1961)

$$Nu = Nu_\infty + \frac{K_1/z^*}{1 + K_2/(z^*)^n} \tag{3.8}$$

where Nu_∞ is the fully developed Nusselt number in a circular duct and K_1, K_2, and n are correlation coefficients whose values all depend upon the boundary condition UWT or UWF.

Later, simple models were proposed by Churchill and Ozoe (1973a,b) as part of the development of a more general model for simultaneously developing flow in a circular duct. Churchill and Ozoe (1973a,b) combined the asymptotic solution of Leveque (Knudsen and Katz (1958), Bird et al., (1960), and Newman (1973)) for the thermal entrance region with the fully developed asymptote in the following forms:

$$\frac{Nu_{z,T} + 1.7}{5.357} = \left[1 + (123.5z^*)^{-8/9}\right]^{3/8} \tag{3.9}$$

for the UWT condition, and

$$\frac{Nu_{z,H} + 1}{5.364} = \left[1 + (70.0z^*)^{-10/9}\right]^{3/10} \tag{3.10}$$

for the UWF condition.

In the thermal entrance region of non-circular ducts, Shah and London (1978) proposed the following model

$$Nu = C_1 C_2 \left(\frac{fRe}{z^*}\right)^{\frac{1}{3}} \tag{3.11}$$

where the constant C_1 determines whether the Nusselt number is an average or local value and the constant C_2 determines whether the boundary condition is UWT or UWF. This result is a generalized Leveque type solution in which the velocity gradient

Table 3.2

Relationships for Yilmaz and Cihan (1993, 1995) Models

Isothermal (UWT)	Isoflux (UWF)
$Nu_m = Nu_\infty \left\{ 1 + 4.212 \frac{\Psi\Phi^3}{z^* Nu_\infty} - 0.8 \left(\frac{\Psi\Phi^3}{z^* Nu_\infty} \right)^{2/3} \right\}^{1/3}$	$Nu_z = Nu_\infty \left\{ 1 + 2.212 \frac{\Psi\Phi^3}{z^* Nu_\infty} - 0.76 \left(\frac{\Psi\Phi^3}{z^* Nu_\infty} \right)^{2/3} \right\}^{1/3}$
$\Phi = 1 + \frac{\frac{3(d^*/2)^{7/8}}{1+d^*} - 1}{1 + \frac{0.25}{m-1}}$	$\Phi = 1 + \frac{\frac{3(d^*/2)^{2/3}}{1+d^*} - 1}{1 + \frac{0.4}{m-1}}$
$\Psi = 1 + \frac{\psi_\infty - 1}{1 + 0.33 \frac{d^{*2.25}}{m-1}}$	$\Psi = 1 + \frac{\psi_\infty - 1}{1 + 0.33 \frac{d^{*2.25}}{m-1}}$
$\psi_\infty = \frac{3}{8} d^{*2} (3 - d^*)$	$\psi_\infty = \frac{3}{8} d^{*2} (3 - d^*)$
$Nu_\infty = 3.657 \left(1 + \frac{\phi_\infty - 1}{1 + \frac{1}{m-1}} + \Delta\phi \right)$	$Nu_\infty = 4.364 \left(1 + \frac{\phi_\infty - 1}{1 + \frac{0.6}{m-1}} \right)$
$\phi_\infty = 0.5155 \frac{(d^*)^2}{3 - d^*}$	$\phi_\infty = 1.4153 \frac{7/3 - d^*}{(3/d^* - 1)^2}$
$\Delta\phi = \Delta\phi_{max} \frac{0.95(m-1)^{0.5}}{1 + 0.038(m-1)^3}$	-
$\Delta\phi_{max} = \frac{7 \times 10^{-3} d^{*8}}{(1 + 10 d^{*-28})(1 + 64 \times 10^{-8} d^{*28})^{0.5}}$	-

at the duct wall is written in terms of the fRe product. This model is valid only for very short ducts.

Recently, Yilmaz and Cihan (1993, 1995) developed a series of equations to predict the heat transfer characteristics in non-circular ducts over the entire thermal entrance region. Yilmaz and Cihan (1993, 1995) developed correlations for predicting the fully developed Nusselt number for the UWT and the UWF conditions and combined these results with a generalized Leveque type solution for the entrance to provide a model which is valid over the entire duct length. These correlating equations accurately predict the Nusselt numbers for most non-circular duct geometries, however they are rather cumbersome for engineering calculations, (see Table 3.2).

The primary drawback of the correlations developed by Yilmaz and Cihan (1993, 1995) is that they require a substantial number of expressions to be evaluated before obtaining the final results. Despite this additional work, these models predict the Nusselt numbers accurately with a maximum error of ± 10 percent and a root mean square (RMS) error typically less than 5 percent. These models like that of Yilmaz (1990) are intended primarily for singly connected ducts, however, Yilmaz (1990) and Yilmaz and Cihan (1993, 1995) also applied them to model doubly connected ducts with a maximum error of approximately ± 20 percent. Finally, the models developed by Yilmaz and Cihan (1993, 1995) were developed for the average Nusselt number for UWT condition and local Nusselt number for UWF condition. No reasons are given for this difference.

In the combined entrance region where both hydrodynamic and thermal boundary layers develop simultaneously, Churchill and Ozoe (1973a,b) developed the following expressions:

$$\frac{Nu_{z,T}+1.7}{5.357[1+(Gz/97)^{8/9}]^{3/8}} = \left[1+\left(\frac{Gz/71}{[1+(Pr/0.0468)^{2/3}]^{1/2}[1+(Gz/97)^{8/9}]^{3/4}}\right)^{4/3}\right]^{3/8} \tag{3.12}$$

for the UWT condition, and

$$\frac{Nu_{z,H}+1}{5.364[1+(Gz/55)^{10/3}]^{3/10}} = \left[1+\left(\frac{Gz/28.8}{[1+(Pr/0.0207)^{2/3}]^{1/2}[1+(Gz/55)^{10/9}]^{3/5}}\right)^{5/3}\right]^{3/10} \tag{3.13}$$

for the UWF condition, where $Gz = \frac{\pi}{4\,z^*}$ is the Graetz number. These models were developed using the asymptotic correlation method of Churchill and Usagi (1972) and are valid for all Prandtl numbers $0 < Pr < \infty$, but are only valid for the circular duct.

For the case of a parallel plate channel, Stephan (1959) correlated numerical results in the following way:

$$Nu_{m,T} = 7.55 + \frac{0.024(z^*)^{-1.14}}{1+0.0358Pr^{0.17}(z^*)^{-0.64}} \tag{3.14}$$

which is valid for $0.1 < Pr < 1000$. Shah and Bhatti (1987) obtained the following expression for the local Nusselt number from the correlation developed by Stephan (1959)

$$Nu_{z,T} = 7.55 + \frac{0.024(z^*)^{-1.14}(0.0179Pr^{0.17}(z^*)^{-0.64}-0.14)}{(1+0.0358Pr^{0.17}(z^*)^{-0.64})^2} \tag{3.15}$$

Finally, Sparrow (1955) used the Karman-Pohlhausen integral method to obtain the following approximate analytical expression for the Nusselt number

$$Nu_{m,T} = \frac{0.664\sqrt{1/z^*}}{Pr^{1/6}} \left(1 + 6.27 \left(\frac{Pr}{1/z^*}\right)^{4/9}\right)^{1/2} \tag{3.16}$$

which is valid for $Pr > 2$ and $z^* < 0.01$.

Only a limited set of numerical data are available for the combined entrance region. In addition to numerical data for the circular duct and the parallel plate channel for a range of Prandtl numbers, a small set of data for the rectangular and triangle ducts exists for $Pr = 0.72$. All of the available data and models for the combined entrance region were reviewed by Kakac and Yener (1981).

3.2.3 Limitations of Present Models

The models reviewed in the previous sections represent the current state of the art for internal flow problems. A number of limitations exist for each of the general models presented earlier. They are discussed below.

The model of Shah (1978) is the simplest and most accurate for predicting apparent friction factors over the entire range of dimensionless duct lengths. However, it is limited to the circular duct. square duct. equilateral triangular duct. parallel plate channel, and selected cases of the rectangular and circular annular ducts. In addition to the limited number of geometries, it also requires tabulated coefficients for each specific case. The model developed by Yilmaz (1990) overcomes the limitations of the model of Shah (1978), however, it does so at the cost of simplicity. Both models are based upon the combination of the "short" duct and "long duct" solutions using the approach proposed by Bender (1969). In this approach the incremental pressure drop factor K_∞ is required in the "long duct" solution. As a result of the complex correlating equations for K developed by Yilmaz (1990), the simple physical behaviour of the hydrodynamic entrance problem is lost. It is apparent from the available data, that smooth transition occurs from the solution obtained by Shapiro et al. (1954)

for the entrance region, to that of fully developed flow. Since the solution obtained by Shapiro et al. (1954) accounts for the increase in momentum of the accelerating core, use of the term K_∞ in a hydrodynamic entrance model such as that proposed by Bender (1969) is redundant.

The models of Yilmaz and Cihan (1993, 1995) are the only general models which predict the heat transfer characteristics in non-circular ducts for thermally developing flow conditions. The limitations of these models are threefold. First, they are exceedingly complex, consisting of series of correlating equations which relate the characteristic behaviour of non-circular ducts to the circular duct. Second, the model for the UWT condition is developed only for average value of the Nusselt number, while the model for the UWF condition is developed for the local Nusselt number. Finally, the apparent simple behaviour of thermally developing flow data is lost as a result of the complex series of correlating equations.

In the combined entrance region, no models are presently available which may be used to predict the results for non-circular ducts. Only the circular duct and parallel plate channel have been modeled over a wide range of Prandtl numbers and dimensionless duct lengths. Finally, for fully developed flows, the only models available for predicting the friction factor Reynolds number product fRe and the Nusselt number Nu in non-circular ducts are the correlating equations proposed by Yilmaz (1990) and Yilmaz and Cihan (1993, 1995).

3.3 Enhanced Duct Models

Many enhancement devices have been analyzed numerically and experimentally. The most practical and economical means of enhancing heat transfer in compact heat exchangers are discussed in the recent text by Webb (1994). This comprehensive review of the literature has compiled the most important experimental and numerical results, along with many empirical models derived from these results. What appears

to be lacking in the field of enhanced heat transfer are general models based on physical principles. One reason for the lack of models derived from fundamentals is the disagreement between predicted results and experimental results which is usually attributed to manufacturing related issues (burred edges) and flow related assumptions (laminar wakes).

3.3.1 Offset Strip Fins

Manglik and Bergles (1990, 1995) provide an extensive summary of the past experimental, numerical, and analytical work involving offset strip fins. Only a few models for the offset strip fin arrangement are analytically based. The simplest of these models was first proposed by Kays (Kays and Crawford, 1993). This model treats the fin as a flat plate and does not consider the effect of the channel walls.

Kays (Kays and Crawford, 1993) proposed the following simple model based upon forced convection over a flat plate:

$$f = \frac{1.328}{\sqrt{Re_{L_f}}} + \frac{t C_D}{2L_f} \tag{3.17}$$

and

$$j = \frac{0.664}{\sqrt{Re_{L_f}}} \tag{3.18}$$

where $C_D \approx 0.88$ is the drag coefficient for a flat plate normal to the direction of flow, based upon the potential flow solution and L_f is the length of the fin. These models only consider heat transfer and friction from the fin surfaces and do not consider the contributions from the channel walls. Eqs. (3.17,3.18) are only valid in the laminar region and were proposed for comparative purposes only.

Wieting (1975) developed multiple regression correlations based upon data from 23 offset strip fin configurations. Wieting (1975) presented correlations for both the laminar and turbulent regions and also developed correlations for the critical Reynolds number. The correlations for the laminar and turbulent regions are presented below:

Laminar $Re_{D_h} \leq 1000$

$$f = 7.661(L_f/D_h)^{-0.384}(s/H)^{-0.092}Re_{D_h}^{-0.712} \tag{3.19}$$

and

$$j = 0.483(L_f/D_h)^{-0.162}(s/H)^{-0.184}Re_{D_h}^{-0.536} \tag{3.20}$$

Turbulent $Re_{D_h} \geq 2000$

$$f = 1.136(L_f/D_h)^{-0.781}(t/D_h)^{0.534}Re_{D_h}^{-0.198} \tag{3.21}$$

and

$$j = 0.242(L_f/D_h)^{-0.322}(t/D_h)^{0.089}Re_{D_h}^{-0.368} \tag{3.22}$$

The critical Reynolds numbers for the intersection of the laminar and turbulent asymptotes for the f and j factors are:

$$Re^*_{D_h,f} = 41(L_f/D_h)^{0.772}(s/H)^{-0.179}(t/D_h)^{-1.04} \tag{3.23}$$

and

$$Re^*_{D_h,j} = 61.9(L_f/D_h)^{0.952}(s/H)^{-1.1}(t/D_h)^{-0.53} \tag{3.24}$$

Joshi and Webb (1987) developed an analytic model for the rectangular offset-strip fin geometries. The equations for laminar and turbulent flow conditions are:

$$\eta Nu = \frac{1-\gamma}{(1+\alpha+\delta)^2}\left(\frac{1+\delta}{1+\alpha+\delta}\eta_f Nu_f + \frac{\alpha}{1+\alpha+\delta}Nu_e\right) \tag{3.25}$$

and

$$f = \frac{1-\gamma}{(1-\gamma)(1+\alpha+\delta)}\left(f_p + \alpha f_e + \frac{tC_D}{2L_f}\right) \tag{3.26}$$

where $\gamma = t/s$, $\alpha = s/H$, and $\delta = t/L_f$ are dimensionless parameters based upon the fin spacing s, fin length L_f, fin thickness t, and channel height H. η is the overall surface efficiency and η_f is the fin efficiency. The remaining parameters are presented in Table 3.3 for the laminar and turbulent regions.

Table 3.3

Equations for Joshi and Webb (1987) Model†

Term		Equation
Laminar Wake Region		
Nu_f	=	$F_{h,\alpha}[24.2 - 3690L_s^+ + 37\times10^4(L_s^+)^2]$
Nu_e	=	$7.45 - 16.9\alpha + 22.1\alpha^2 - 9.75\alpha^3$
f_f	=	$F_{f,\alpha}[65.5 - 11.63\times10^3 L_s^+ + 13.38\times10^5(L_s^+)^2]/Re_s$
f_e	=	$(23.94 - 30.05\alpha + 32.37\alpha^2 - 12.08\alpha^3)/Re_{sh}$
C_D	=	0.88
Turbulent Wake Region		
Nu_f	=	$0.36Re_{D_h}^{0.067}Pr^{1/3}(L_f/D_h)^{-0.174}$
Nu_e	=	$0.023Re_{D_h}^{0.8}Pr^{1/3}$
f_f	=	$15.33Re_{D_h} - 0.785(L_f/D_h)^{-0.324}$
f_e	=	$0.079Re_{sh}^{-0.25}$
C_D	=	0.88

† From Webb (1994)

The parameters $F_{h,\alpha}$, $F_{f,\alpha}$ are defined graphically in Joshi and Webb (1987) and Webb (1994), and $L_s^+ = L_f/(2sRe_s)$ is the dimensionless fin length. The model of Joshi and Webb (1987) also contains three different definitions of the Reynolds number.

In addition to developing an analytic model, Joshi and Webb (1987) also present multiple regression correlations for the laminar and turbulent regions. The correlations for the laminar and turbulent regions are:

Laminar $Re_{D_h} \leq Re^*_{D_h}$

$$f = 8.12(L_f/D_h)^{-0.41}(s/H)^{-0.02}Re_{D_h}^{-0.74} \tag{3.27}$$

and

$$j = 0.53(L_f/D_h)^{-0.15}(s/H)^{-0.14}Re_{D_h}^{-0.5} \tag{3.28}$$

Turbulent $Re_{D_h} \geq Re^*_{D_h} + 1000$

$$f = 1.12(L_f/D_h)^{-0.65}(t/D_h)^{0.17}Re_{D_h}^{-0.36} \tag{3.29}$$

and

$$j = 0.21(L_f/D_h)^{-0.24}(t/D_h)^{0.02}Re_{D_h}^{-0.40} \tag{3.30}$$

The value of the critical Reynolds number $Re^*_{D_h}$ is determined from the following expression

$$Re^*_{D_h} = 257\left(\frac{L_f}{s}\right)^{1.23}\left(\frac{t}{L_f}\right)^{0.58}\left(\frac{D_h}{(t + 1.238L_f/\sqrt{Re_{L_f}})}\right) \tag{3.31}$$

Manglik and Bergles (1990) also developed correlations based upon multiple regression analysis of available data. Their correlations differ from those of Wieting (1975) and Joshi and Webb (1987) in the definition of the hydraulic diameter. Correlations for the laminar and turbulent regions are:

Laminar $Re_{D_h} \leq Re^*_{D_h}$

$$f = 9.624(s/H)^{-0.186}(t/L_f)^{0.305}(t/s)^{-0.266}Re_{D_h}^{-0.742} \tag{3.32}$$

and

$$j = 0.652(s/H)^{-0.154}(t/L_f)^{0.150}(t/s)^{-0.068}Re_{D_h}^{-0.540} \tag{3.33}$$

Turbulent $Re_{D_h} \geq Re^*_{D_h} + 1000$

$$f = 1.870(s/H)^{-0.094}(t/L_f)^{0.682}(t/s)^{-0.242}Re_{D_h}^{-0.299} \tag{3.34}$$

and

$$j = 0.244(s/H)^{-0.104}(t/L_f)^{0.196}(t/s)^{-0.173}Re_{D_h}^{-0.406} \tag{3.35}$$

The value of the critical Reynolds number $Re^*_{D_h}$ is defined by the expression developed by Joshi and Webb (1987), given earlier.

Table 3.4

Definitions of Hydraulic Diameter for Offset Strip Fin Models

Model	Definition of D_h
Wieting (1975)	$\frac{2sH}{s+H}$
Joshi and Webb (1987)	$\frac{2(s-t)HL_f}{sL_f+HL_f+tH}$
Manglik and Bergles (1990)	$\frac{4sHL_f}{2(sL_f+HL_f+tH)+ts}$

In addition, Manglik and Bergles (1990) also combined the laminar and turbulent asymptotes using the method of Churchill and Usagi (1972) to provide a correlation

which is valid in the transition region. The resulting correlations which include the transition region are:

$$f = 9.624(s/H)^{-0.186}(t/L_f)^{0.305}(t/s)^{-0.266}Re_{D_h}^{-0.742} \\ [1 + 7.669 \times 10^{-8}(s/H)^{0.92}(t/L_f)^{3.77}(t/s)^{0.236}Re_{D_h}^{4.43}]^{0.1} \tag{3.36}$$

and

$$j = 0.652(s/H)^{-0.154}(t/L_f)^{0.150}(t/s)^{-0.068}Re_{D_h}^{-0.540} \\ [1 + 5.63 \times 10^{-5}(s/H)^{0.51}(t/L_f)^{0.46}(t/s)^{-0.106}Re_{D_h}^{1.34}]^{0.1} \tag{3.37}$$

In all of the above correlations a different definition for D_h has been chosen. A summary of these definitions is given in Table 3.4.

3.3.2 Turbulator Strips

In many of the reviews on enhanced heat transfer (Webb (1994), Kalinin and Dreitser (1998)) an abundance of data is available for many common enhancements such as rib turbulators, internally finned tubes and channels, louvered fins, and offset strip fins. Many automotive heat exchangers employ turbulator strips and other enhanced heat transfer technology as a means of enhancing heat transfer. However, as discussed by Webb (1994) most of the enhanced heat transfer surfaces employed by the automotive industry are considered proprietary technology, and details of the heat transfer and fluid friction characteristics are not published.

As a result of the lack of published data, no models are readily available in the open literature. As part of this work, new experimental data will be obtained for a number of turbulator strip configurations. This new data will be used in conjunction with the analytical model development in addition to providing useful empirical correlations.

Patankar et al. (1977) used numerical methods to solve the two dimensional configuration shown in Fig. 1.3 for the HPD configuration and Sparrow et al. (1977) used the same approach to solve the LPD configuration. However, these configurations assumed a large channel height such that three dimensional effects were not present. Later Kelkar and Patankar (1985) solved the three dimensional LPD configuration and found a significant reduction in the enhancement characteristics compared with the two dimensional case.

The data of Patankar et al. (1977) for the HPD configuration having fins of width L_f and spacing L_f in both parallel and transverse directions have been digitized and correlated by the following expressions:

$$f = 2.31 \left(Re_{L_f}\right)^{0.1} \tag{3.38}$$

for the friction factor, and

$$j_R = 0.294 \left(Re_{L_f}\right)^{-0.3013} \tag{3.39}$$

and

$$j_F = 2.814 \left(Re_{L_f}\right)^{-0.5642} \tag{3.40}$$

and

$$j_A = 1.246 \left(Re_{L_f}\right)^{-0.4753} \tag{3.41}$$

for the Colburn j factor, where the subscripts F, R, and A represent the front, rear and average values for the obstruction, respectively, and $Re_{L_f} = \overline{w} L_f / \nu$. The Reynolds number range is limited to $200 < Re < 2000$.

In their study, Patankar et al. (1977) reported that extremely high velocities, on the order of four times the average flow velocity, were encountered in the stream of fluid which by-passed the recirculation zone. Since this result is based upon a two

dimensional system, the effect of the channel height H, would be to reduce the overall enhancement. Thus, based upon the work of Patankar et al. (1977), Eq. (3.41) is likely the theoretical maximum value for the Colburn j factor for transverse flow through the array. Finally, the friction factor is approximately independent of the Reynolds number, indicating that almost all of the pressure drop is due to form drag.

3.3.3 Limitations of Present Models

The models reviewed in the previous sections represent the current state of the art for predicting friction and heat transfer characteristics in the offset strip fin arrays. A number of limitations exist for each of the models presented earlier. They are discussed below.

A primary disadvantage of the multiple regression models developed by Wieting (1975), Joshi and Webb (1987), and Manglik and Bergles (1990), is that they are based upon experimental data for 21 OSF configurations found in Kays and London (1984). Since the regression models are based on actual experimental data, they are only valid in the Reynolds number range typical of the experiments $200 < Re < 10000$. Analysis of the laminar flow correlations reveals that at low Reynolds numbers, $Re \rightarrow 0$, the f and j factors are proportional to $1/Re^{0.75}$ and $1/Re^{0.5}$, which are incorrect. At very low Reynolds numbers, the characteristics of the flow in an OSF array are similar to that of fully developed laminar flow in ducts which is proportional to $1/Re$.

With the exception of the correlations developed by Manglik and Bergles (1990,1995), none of the regression models are valid in the transition region. It will be shown later in Chapter 6 that the model of Manglik and Bergles (1990,1995) will under predict the data for $Re < 200$ and $Re > 10000$. If a new configuration does not fall within the range of parameters for which these models were developed, considerable uncertainty in the results must be expected. All of the correlations developed assume that the micro-channels formed by the interrupted fin are rectangular. However, in

many applications the shape is not necessarily rectangular. If an offset fin array is developed from other shapes such as a triangular, sinusoidal, and trapezoidal cross-sections, then these correlations are not applicable.

The analytical model developed by Joshi and Webb (1987) overcomes some of the limitations of the regression correlations. However, the Joshi and Webb (1987) model is very complex and requires several parameters which are presented graphically. Although the model should represent the correct behaviour for very small and very large values of the Reynolds number, the model is unable to predict the data which fall in the transition region. Finally, in their development, Joshi and Webb (1987) assume that the boundary layers on the fin walls do not affect the boundary layers on the channel walls. However, at low Reynolds number where boundary layers are thick, this assumption is incorrect. Joshi and Webb (1987) treat the fin surfaces as boundary layer flow and the channel walls as fully developed flow. As a result, the correct low Reynolds number behaviour is captured in the model, but the essential physics of the flow is not.

In applications involving turbulator strips, the only available data are the correlations derived from the numerical study of Patankar et al. (1977). These results are valid over a moderate range of Reynolds numbers, however, they are only valid for flows which are two dimensional. In most practical applications, the flow is three dimensional and the effect of the channel walls is to reduce the overall enhancement.

3.4 Summary

This chapter reviewed the pertinent data, models, and correlations for both plain ducts and enhanced geometries which are considered in this work. In the next Chapter, the development of models for plain ducts is presented along with comparisons with the data and models reviewed in this Chapter.

Chapter 4

Modelling and Analysis: Plain Ducts

4.1 Introduction

This chapter examines the laminar flow heat transfer and friction characteristics of many plain duct geometries. Five fundamental problems will be examined. These are: hydrodynamically fully developed flow (HFDF), hydrodynamically developing flow (HDF), thermally fully developed flow (TFDF), thermally developing flow (TDF), and simultaneously developing flow (SDF), (refer to Fig. 4.1). The analysis presented in this Chapter results in simple models which predict the friction factors and Nusselt numbers for many duct geometries for developing and fully developed flows. First, the approach to modelling heat transfer and fluid friction for laminar flows is presented. Following this, the details of model development for fully developed and developing flows are presented.

4.2 Approach to Modelling

In this section the approach to modelling internal laminar flow problems is presented. First, the important characteristics of each of the five fundamental internal flow prob-

lems are discussed. Then a discussion on the superposition of asympotic solutions is presented. Finally, a detailed analysis and discussion on the selection of a new characteristic length for non-dimensionalizing the heat transfer and fluid friction data is presented.

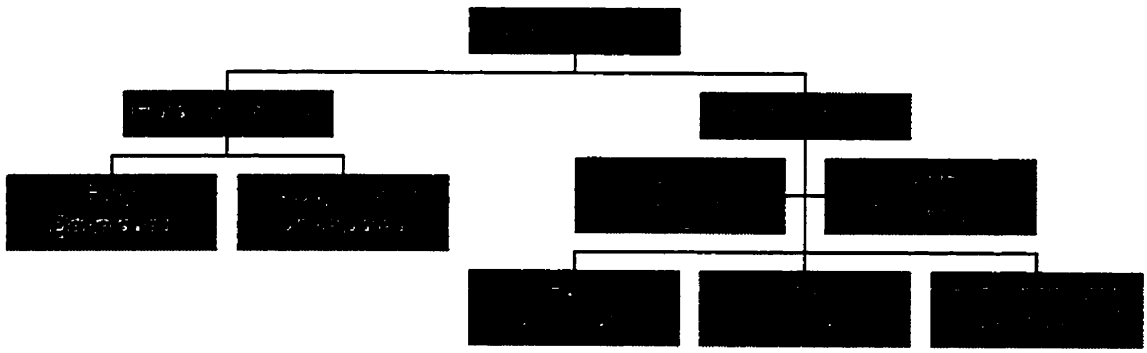

Fig. 4.1 - Summary of Internal Flow Problems.

4.2.1 Characteristics of Internal Flow Problems

Examination of results for each of the laminar flow problems provides valuable insight regarding the approach to modelling the characteristics in straight non-circular ducts. Figures 4.2-4.4 illustrate the typical behaviour exhibited by most of the available analytic solutions and numerical data.

Beginning first with the hydrodynamic problem, Fig. 4.2 illustrates the behaviour of the apparent friction factor as a function of the dimensionless duct length, z^+. In the entrance region of all ducts regardless of shape, the results are identical to that for the circular duct. This behaviour is characterized by the following expression:

$$f_{app}Re = \frac{3.44}{\sqrt{z^+}} \tag{4.1}$$

which was obtained by Shapiro et al. (1954).

However, as the flow becomes fully developed, the effect of duct shape becomes more prominent. Eventually, all of the fully developed flow results approach a constant value at large values of z^+. This constant is a strong function of shape and geometry of the duct:

$$fRe = A_1 \tag{4.2}$$

where A_1 depends upon the shape of the duct. For most common duct shapes $12 < A_1 < 24$, Shah and London (1978).

If the velocity distribution is fully developed and the temperature distribution is allowed to develop, similar behaviour is observed in the thermal entrance region. Figure 4.3 illustrates the typical behaviour of the thermal entrance problem with fully developed velocity distribution. In the thermal entrance region, the results do not vary significantly, but are still weak functions of the shape and geometry of the duct and the thermal boundary condition imposed at the duct wall. This behaviour is characterized by the following approximate analytical expression first attributed to Leveque (Drew, 1931):

$$Nu = A_2 \left(\frac{fRe}{z^*} \right)^{1/3} \tag{4.3}$$

where A_2 depends upon the thermal boundary condition at the duct wall. The Leveque approximation is valid where the thermal boundary layer develops in the region near the wall where the velocity profile may be assumed to be linear. The weak effect of duct geometry in the entrance region is due to the presence of the friction factor Reynolds number group, fRe, in the above expression, which is representative of the average velocity gradient at the duct wall. The typical range of the fRe group is $6.5 < fRe_{D_h} < 24$. However, for most common shapes this range is $12 < fRe_{D_h} < 24$, Shah and London (1978). This results in $2.29 < fRe^{1/3} < 2.88$, which illustrates the weak dependency of the thermal entrance region on shape and geometry.

As the flow becomes thermally fully developed the results approach a constant value. This constant is a strong function of shape and geometry of the duct as well as the type of thermal boundary condition imposed at the duct wall:

$$Nu = A_3 \tag{4.4}$$

where A_3 depends upon both the duct shape and the thermal boundary condition. For most duct geometries, $1.5 < A_3 < 8.23$, Shah and London (1978).

Finally, if both hydrodynamic and thermal boundary layers develop simultaneously, the results are strong functions of the fluid Prandtl number. Figure 4.4 illustrates the dependency of the Nusselt number on Prandtl number. In the combined entrance region the behaviour for very small values of z^* may be adequately modelled by:

$$Nu = \frac{A_4}{\sqrt{z^*}\, Pr^{1/6}} \tag{4.5}$$

where the constant A_4 depends upon the thermal boundary condition at the duct wall. As the hydrodynamic and thermal boundary layers become fully developed, results for non-circular geometries tend to the constant A_3.

The smooth transition from small values of (z^+, z^*) to large values of (z^+, z^*) suggests that a simple model may easily be developed by combining the asymptotic behaviour in some manner. In the next section a procedure for combining these asymptotic results is discussed.

4.2.2 Superposition of Asymptotic Solutions

The proposed models for hydrodynamically developing flow and thermally developing flow take the form:

$$y(z) = [y_{z\to 0}^n + y_{z\to\infty}^n]^{1/n} \tag{4.6}$$

where $y_{z\to 0}$ and $y_{z\to\infty}$ are asymptotic solutions for small and large values of the

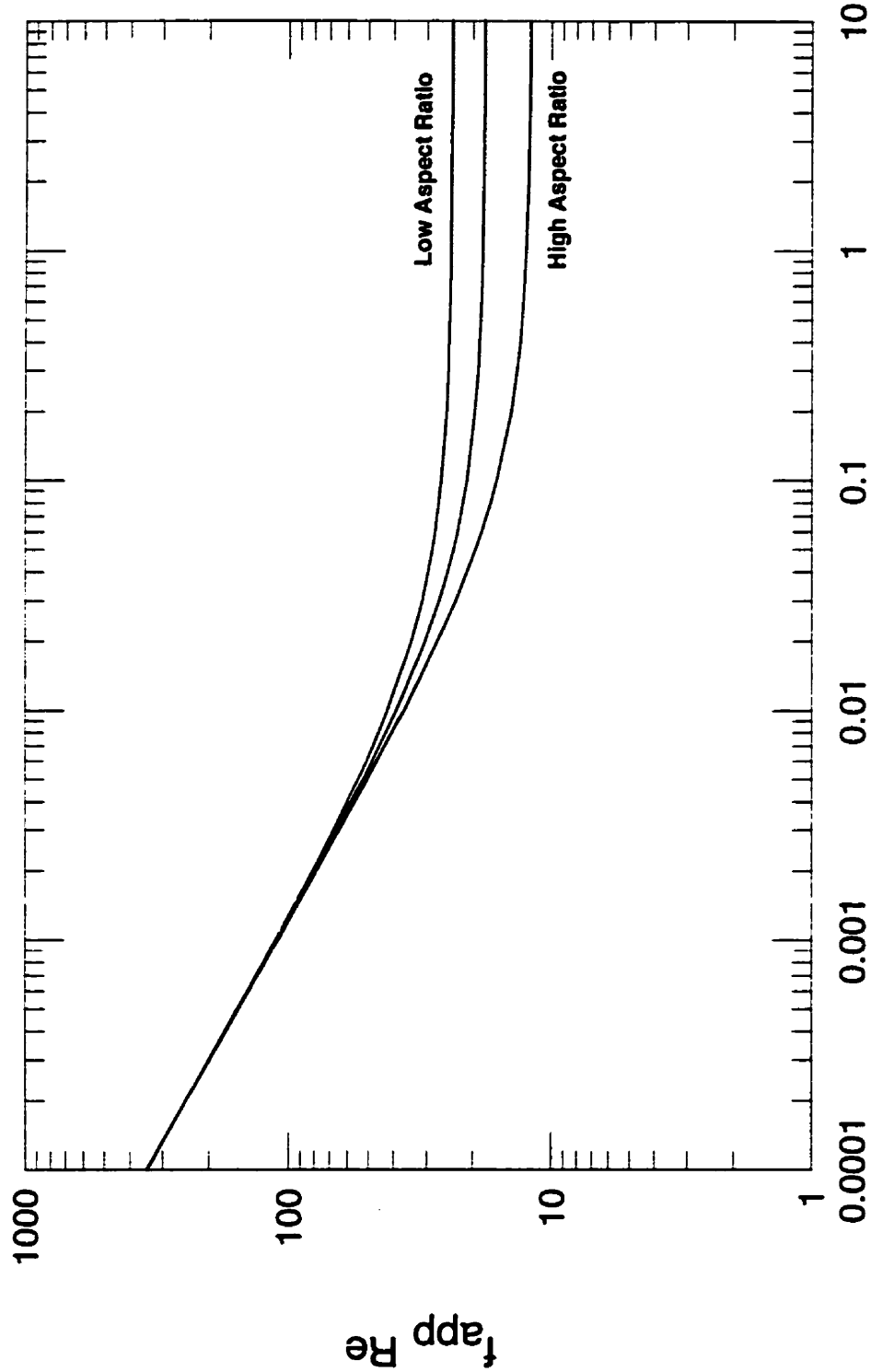

Fig. 4.2 - Characteristics of Friction Factor Group $f_{app}Re$.

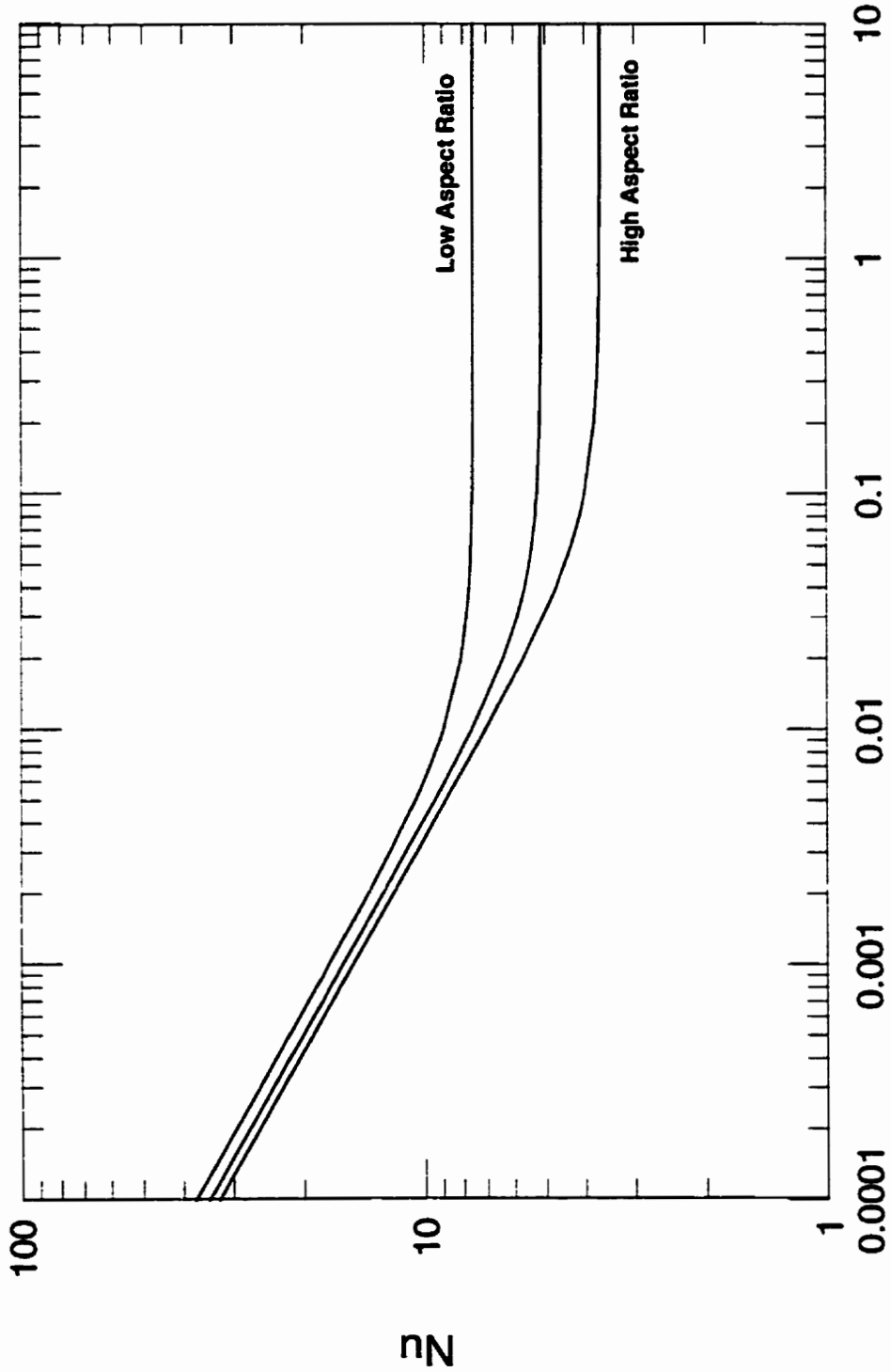

Fig. 4.3 - Characteristics of Thermally Developing Flow.

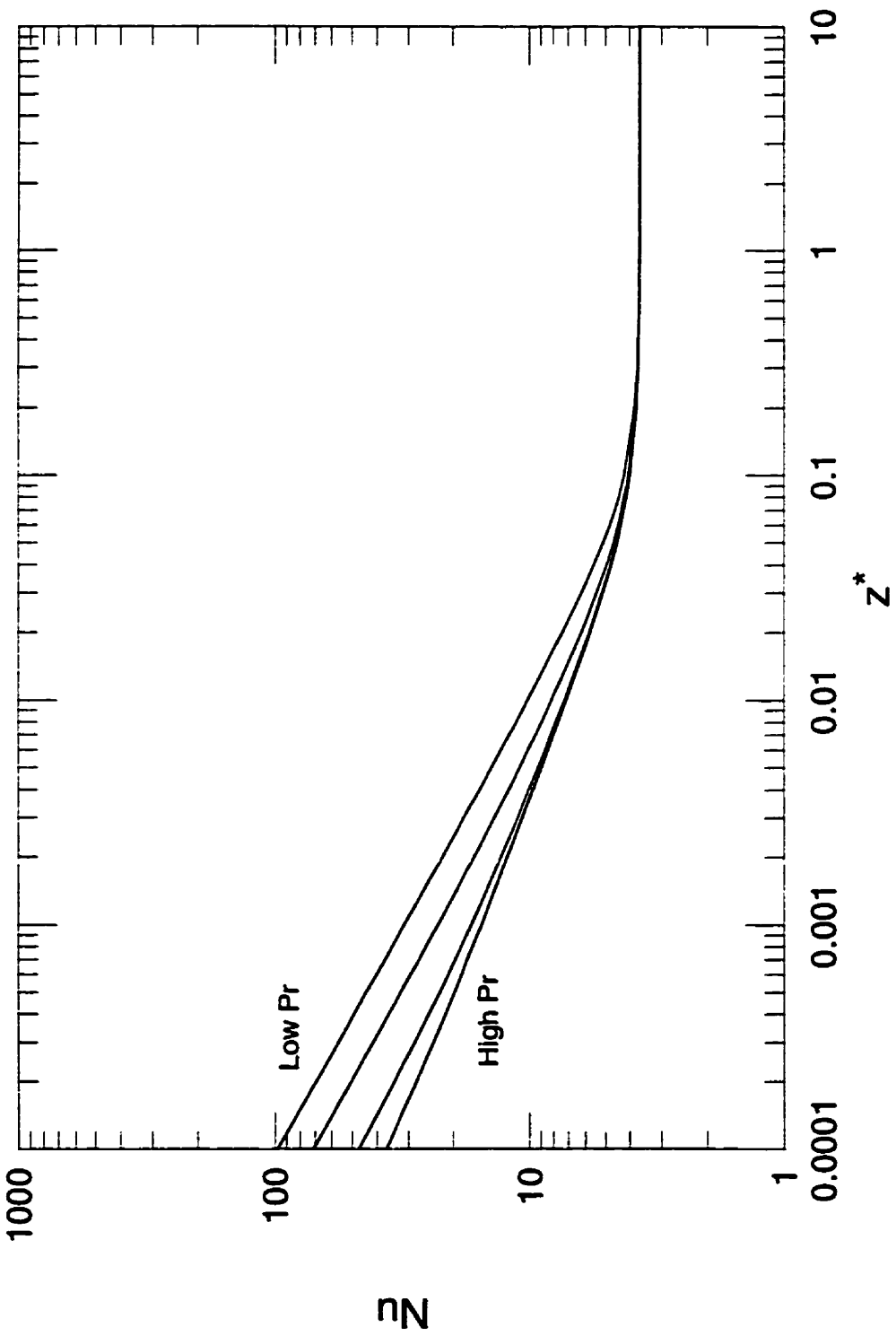

Fig. 4.4 - Characteristics of Simultaneously Developing Flow.

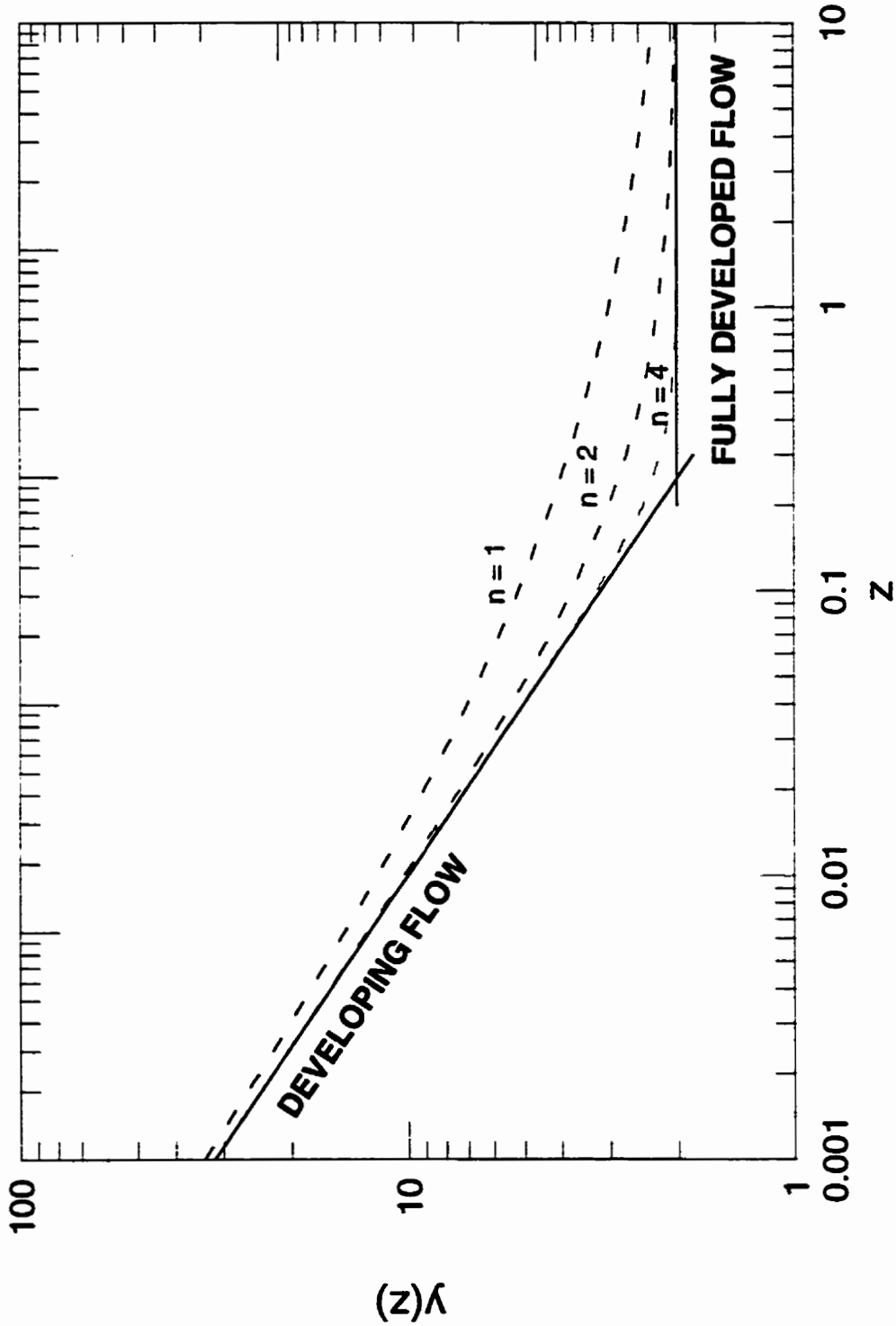

Fig. 4.5 - Superposition of Asymptotic Solutions.

independent variable z and n is the fitting or "blending" parameter. This method of combining asymptotic solutions is discussed in detail by Churchill and Usagi (1972). This approach assumes that smooth transition exists between the two asymptotes.

The effect of the parameter n in Eq. (4.6) is shown in Fig. 4.5. It is clear that the value of n is only important in the transition region. The results for large and small values of the independent parameter z, remain unchanged. The parameter n may be chosen using a number of methods as discussed by Churchill and Usagi (1972). In this Chapter, n is chosen as the value which minimizes the root mean square (RMS) difference between the model predictions and the available data. If n is a weak function of the shape, geometry, or thermal boundary condition, a single value may be chosen which best represents all of the available data for non-circular ducts.

This approach has been quite successful in developing models for predicting forced convection from flat plates and in circular ducts for a wide range of Prandtl numbers (Churchill and Ozoe, 1973a,b), natural convection (Raithby and Hollands, 1998), transient conduction from isothermal convex bodies (Yovanovich et al., 1995), and pressure drop in channels containing periodic cuboid shaped obstructions (Teertstra et al. 1998).

4.2.3 Characteristic Length

In the previous section the characteristics of laminar internal flow problems were discussed. It was shown that the results for non-circular geometries are strong functions of geometry for fully developed flows. It is desirable to eliminate or reduce the effects of geometry such that the general trends for all duct shapes may be easily modelled. This may be achieved by examining the characteristic length scale which is used to non-dimensionalize the heat transfer and fluid flow data.

Based on the geometry of a non-circular duct, three immediately obvious choices for a characteristic length are:

- Perimeter, $\mathcal{L} = P$
- Square Root of Area, $\mathcal{L} = \sqrt{A}$
- Hydraulic Radius, $\mathcal{L} = A/P$

In the heat transfer and fluid flow literature the convention is to use the hydraulic diameter $4A/P$, or hydraulic radius A/P. This characteristic length arises naturally from a simple control volume balance on an arbitrarily shaped straight duct. Figure 4.6 illustrates the possible relationships between a non-circular duct and the equivalent circular duct using the area and/or perimeter to define an effective duct diameter. It is clear that the definitions given above are proportional to the various effective diameters proposed in Fig. 4.6. In Appendix A, dimensional analysis using the buckingham Π theorem was undertaken for fully developed flow. It was shown that only the perimeter or the square root of the flow area result as possible choices for the characteristic length. However, an additional parameter $P/\sqrt{A}$ arose in the analysis. The significance of this parameter is discussed shortly.

Several less obvious choices for a characteristic length may also be chosen. These definitions may be obtained from characteristic dimensions, l_1 and l_2, of the duct cross-sectional geometry, i.e. the semi-axes of an ellipse or rectangle and the height and base of a triangle. These lengths may be combined in the following manner:

- Arithmetic Mean, $\mathcal{L} = \dfrac{l_1 + l_2}{2}$
- Geometric Mean, $\mathcal{L} = \sqrt{l_1 l_2}$
- Harmonic Mean, $\mathcal{L} = \dfrac{2 l_1 l_2}{l_1 + l_2}$
- Quadratic Mean, $\mathcal{L} = \sqrt{l_1^2 + l_2^2}$

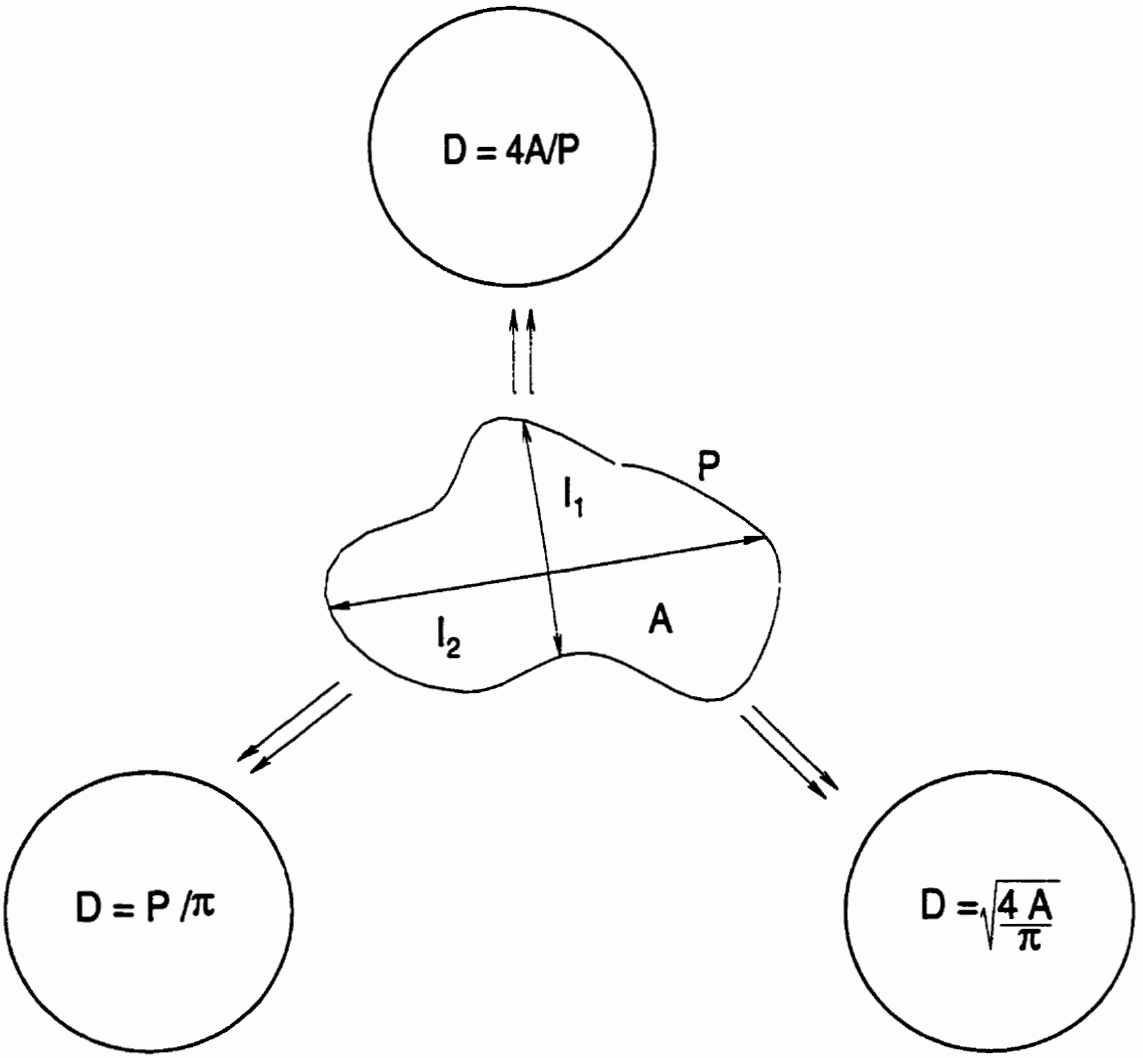

Fig. 4.6 - Equivalent Duct Diameters.

Examination of the two lists of possible choices reveals that the $\mathcal{L} = P$, $\mathcal{L} = \sqrt{A}$, and $\mathcal{L} = A/P$ are proportional to the arithmetic mean, geometric mean, and harmonic mean, respectively, of the characteristic dimensions l_1 and l_2.

All three possibilities for $\mathcal{L}$ given above have a number of potential flaws. First, the perimeter and area are not definable for a parallel plate channel. This is not a problem for singly or doubly connected regions having finite area and perimeter. This aspect does not pose a problem for the definition of the hydraulic diameter. However, a number of deficiencies in the hydraulic diameter concept should be addressed, namely, that the hydraulically equivalent circular area and perimeter based upon the hydraulic diameter are not the same as the true area and perimeter of the non-circular duct. This mismatch in area and perimeter is the probable cause in the mismatch of dimensionless laminar flow data. Finally, the hydraulic diameter concept produces results which are in contradiction of correct physical behaviour. In a number of cases where a duct shape varies with aspect ratio, the dimensionless results decrease with decreasing aspect ratio, which is contradictory to observation that fluid friction and heat transfer generally increase with a decrease in aspect ratio.

All three length scales have been examined. It was observed that $\mathcal{L} = P$ and $\mathcal{L} = \sqrt{A}$ succeeded in bringing the dimensionless results closer together for similar ducts, i.e. rectangular and elliptical or polygonal. In both cases, better correlation of the laminar flow data was achieved versus the duct aspect ratio. For low aspect ratio ducts, $\mathcal{L} = P$ provided better correlation than $\mathcal{L} = \sqrt{A}$. For high aspect ratio ducts such as the polygonal ducts, $\mathcal{L} = \sqrt{A}$ provided better correlation than $\mathcal{L} = P$. Overall, $\mathcal{L} = \sqrt{A}$ was found to be more effective at collapsing the data over a wide range of duct aspect ratios.

It may also be argued on physical grounds that the square root of the flow area is essentially the same as preserving the duct area or maintaining a constant mass flow rate. That is

$$(\rho\overline{w}A)_C = (\rho\overline{w}A)_{NC} \tag{4.7}$$

Now if both the circular and non-circular ducts have the same mass velocity $G = \rho\overline{w}$ then,

$$A_C = A_{NC} \tag{4.8}$$

and the effective circular diameter becomes

$$D_{eff} = \sqrt{\frac{4A_{NC}}{\pi}} \tag{4.9}$$

In other words, the characteristic length $\mathcal{L} = \sqrt{A} \propto D_{eff}$.

As an example, consider the square duct. If the the effective diameter is based upon preserving the perimeter, a 27.3 percent increase in cross-sectional area is observed. If the effective diameter is based upon preserving the cross-sectional area, an 11.4 percent decrease in perimeter is observed. Finally, when the effective diameter is based upon the hydraulic diameter, there is a 21.5 percent reduction in area and perimeter. It appears then, that preserving the cross-sectional area results in an equivalent duct which is geometrically similar to the original non-circular duct. These concepts are essentially the same when the duct area and perimeter vary with duct aspect ratio, except that an additional constraint, the preservation of the aspect ratio is also imposed.

Finally, the characteristic length should also be representative of a direction parallel to a vector normal to the duct wall. Since this length changes around the perimeter of many ducts, $\mathcal{L} = \sqrt{A}$ appears to represent the geometric mean value. Consider the rectangular and elliptic cross-sections having semi-axes of length a and b. The square root of the cross-sectional area for each duct gives $\sqrt{4ab}$ and $\sqrt{\pi ab}$ for the rectangle and ellipse, respectively. Both a and b are directions normal to the duct wall.

In the sections which follow, it will be shown that the characteristic length, $\mathcal{L} = \sqrt{A}$, is more effective than the hydraulic diameter for correlating laminar flow data. As a result, simple models will be developed for HFDF, HDF, TFDF, TDF, and SDF which are valid for many duct shapes. The solutions for several singly and doubly-connected domains are re-analyzed using the characteristic length $\mathcal{L} = \sqrt{A}$. Data for the different ducts summarized in Table 3.1 will be re-scaled according to the following definitions:

$$fRe_{\sqrt{A}} = fRe_{D_h}\left(\frac{P}{4\sqrt{A}}\right) \tag{4.10}$$

and

$$Nu_{\sqrt{A}} = Nu_{D_h}\left(\frac{P}{4\sqrt{A}}\right) \tag{4.11}$$

If the flow is developing, the dimensionless duct lengths for the thermal and hydrodynamic problems are also re-scaled for consistency:

$$z^+_{\sqrt{A}} = \frac{z}{D_h Re_{D_h}}\left(\frac{P}{4\sqrt{A}}\right)^{-2} \tag{4.12}$$

and

$$z^*_{\sqrt{A}} = \frac{z}{D_h Re_{D_h} Pr}\left(\frac{P}{4\sqrt{A}}\right)^{-2} \tag{4.13}$$

Finally, it may be seen that the parameter $P/\sqrt{A}$ which appeared in the dimensional analysis given in Appendix A, is essentially a geometric scaling parameter. This parameter also arose in the models developed by Yilmaz (1990) and Yilmaz and Cihan (1993, 1995), i.e. $A/A_{D_h} = \frac{1}{4\pi}(P/\sqrt{A})^2$.

4.3 Fully Developed Flow

In this section the fully developed flow friction factor Reynolds number group fRe and the fully developed flow Nusselt number Nu are examined. Using the results of the preceding section, it is shown that better correlation of the numerical data is achieved when the characteristic length is chosen to be $\mathcal{L} = \sqrt{A}$. A simple model will be developed for the fRe group based upon the solution for the elliptic duct. It will also be shown that the Nusselt number may be modelled in terms of the fRe group.

4.3.1 Friction Factor

The results for the friction factor Reynolds number group, fRe, are first analyzed for the simplest and most common duct shapes, the regular polygons, and the rectangular and elliptic cross-sections. The fRe results for polygonal shapes are presented in Table 4.1 for the characteristic lengths $\mathcal{L} = 4A/P$ and $\mathcal{L} = \sqrt{A}$. Also presented in Table 4.1 is the ratio of the fRe result of the polygon to the fRe result of the circular duct for each case. It is clear from the last column of Table 4.1, that when $\mathcal{L} = \sqrt{A}$ is used, there is very little difference between the regular polygons and the circular duct results. When the hydraulic diameter is used as a characteristic length, the results for all of the regular polygons are within 16.7 percent of the value for the circular duct, as shown in the third column of Table 4.1. However, when the characteristic length is $\mathcal{L} = \sqrt{A}$, all of the results for the regular polygons are within 7.1 percent of the value for the circular duct. The largest difference occurs with the triangular duct. When $N \geq 4$ the difference becomes negligible, reducing to less than 0.12 percent.

Figure 4.7 presents the results for the rectangular duct and elliptic duct. The results for two other geometries, namely the circular duct with diametrically opposed flat sides (Cheng and Jamil, 1970), also referred to as the modified stadium duct, and the rectangular duct with semi-circular ends (Zarling, 1976), also referred to as the stadium duct, are also presented in Figs. 4.7. The fRe_{D_h} results for these four ge-

ometries vary substantially with the aspect ratio b/a, which is a ratio of the minor and major axes. When the results are replotted in Fig. 4.8 according to Eq. (4.10), the results for these four geometries have virtually collapsed onto one another. Numerical values for the elliptic and rectangular geometries are presented in Table 4.2 for both definitions of the characteristic length $\mathcal{L} = D_h$ and $\mathcal{L} = \sqrt{A}$. Also presented in Table 4.2 are the ratios of fRe results for the rectangular duct and fRe results for the elliptic duct at corresponding aspect ratios. It may be seen from the last column of Table 4.2, that $\mathcal{L} = \sqrt{A}$ appears to be more appropriate than $\mathcal{L} = D_h$ over the entire range of $\epsilon = b/a$. It is easily seen that the results for the rectangular duct and elliptic duct differ by less than 7 percent when the characteristic length is $\mathcal{L} = \sqrt{A}$, whereas if the characteristic length is the hydraulic diameter, the results differ by as much as 31 percent.

Table 4.1

fRe Results for Polygonal Geometries

(Cheng (1966), Shih (1967))

N	fRe_{D_h}	$\left(\frac{fRe^P}{fRe^C}\right)_{D_h}$	$fRe_{\sqrt{A}}$	$\left(\frac{fRe^P}{fRe^C}\right)_{\sqrt{A}}$
3	13.33	0.833	15.19	1.071
4	14.23	0.889	14.23	1.004
5	14.73	0.921	14.04	0.990
6	15.05	0.941	14.01	0.988
7	15.31	0.957	14.05	0.991
8	15.41	0.963	14.03	0.989
9	15.52	0.970	14.04	0.990
10	15.60	0.975	14.06	0.992
20	15.88	0.993	14.13	0.996
∞	16	1.000	14.18	1.000

Table 4.2

fRe Results for Elliptical and Rectangular Geometries

Shah and London (1978)

	fRe_{D_h}			$fRe_{\sqrt{A}}$		
b/a	Rectangular	Elliptical	$\left(\frac{fRe^R}{fRe^E}\right)_{D_h}$	Rectangular	Elliptical	$\left(\frac{fRe^R}{fRe^E}\right)_{\sqrt{A}}$
0.01	23.67	19.73	1.200	119.56	111.35	1.074
0.05	22.48	19.60	1.147	52.77	49.69	1.062
0.10	21.17	19.31	1.096	36.82	35.01	1.052
0.20	19.07	18.60	1.025	25.59	24.65	1.038
0.30	17.51	17.90	0.978	20.78	20.21	1.028
0.40	16.37	17.29	0.947	18.12	17.75	1.021
0.50	15.55	16.82	0.924	16.49	16.26	1.014
0.60	14.98	16.48	0.909	15.47	15.32	1.010
0.70	14.61	16.24	0.900	14.84	14.74	1.007
0.80	14.38	16.10	0.893	14.47	14.40	1.005
0.90	14.26	16.02	0.890	14.28	14.23	1.004
1.00	14.23	16.00	0.889	14.23	14.18	1.004

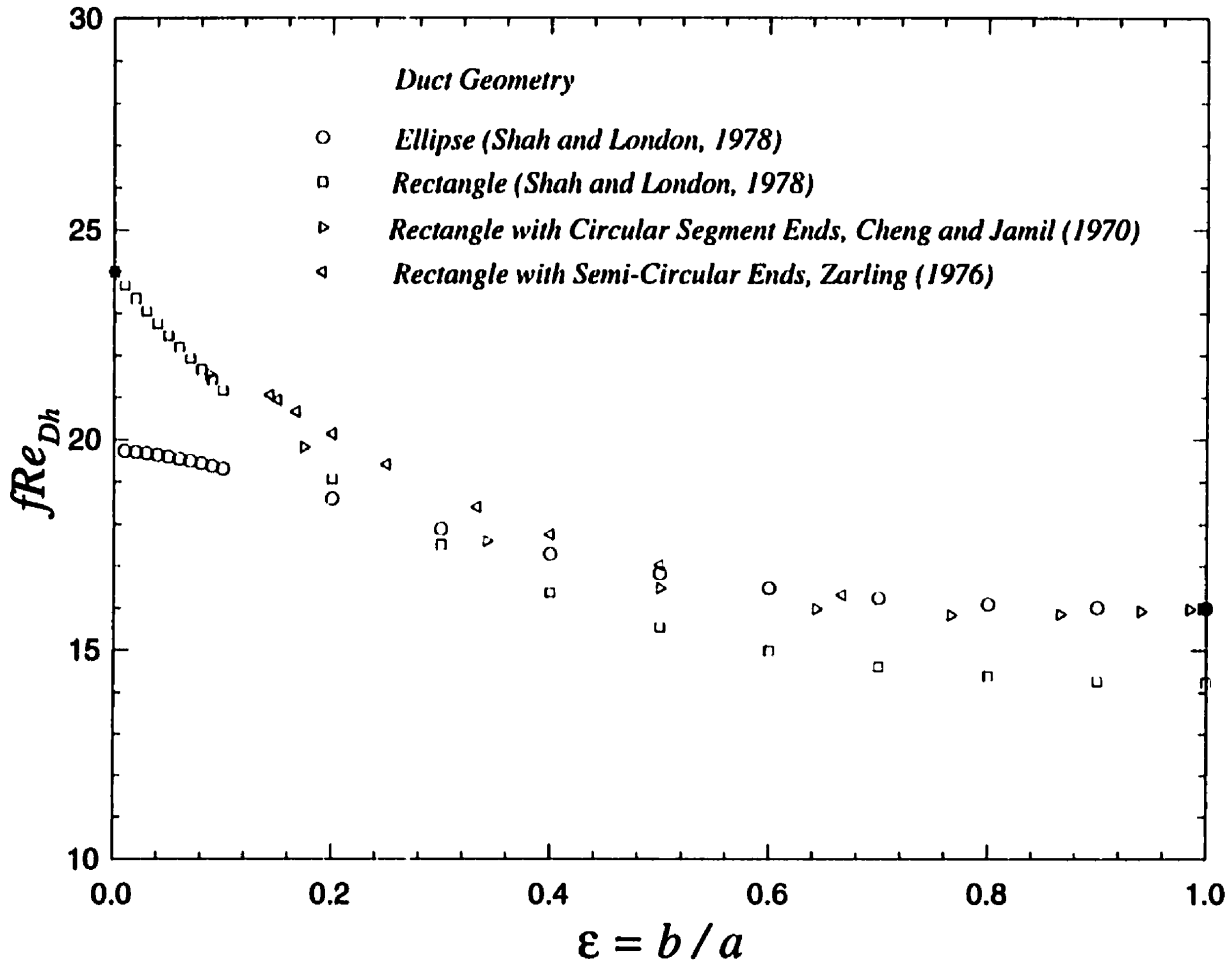

Fig. 4.7 - fRe_{D_h} for Common Singly-Connected Geometries.

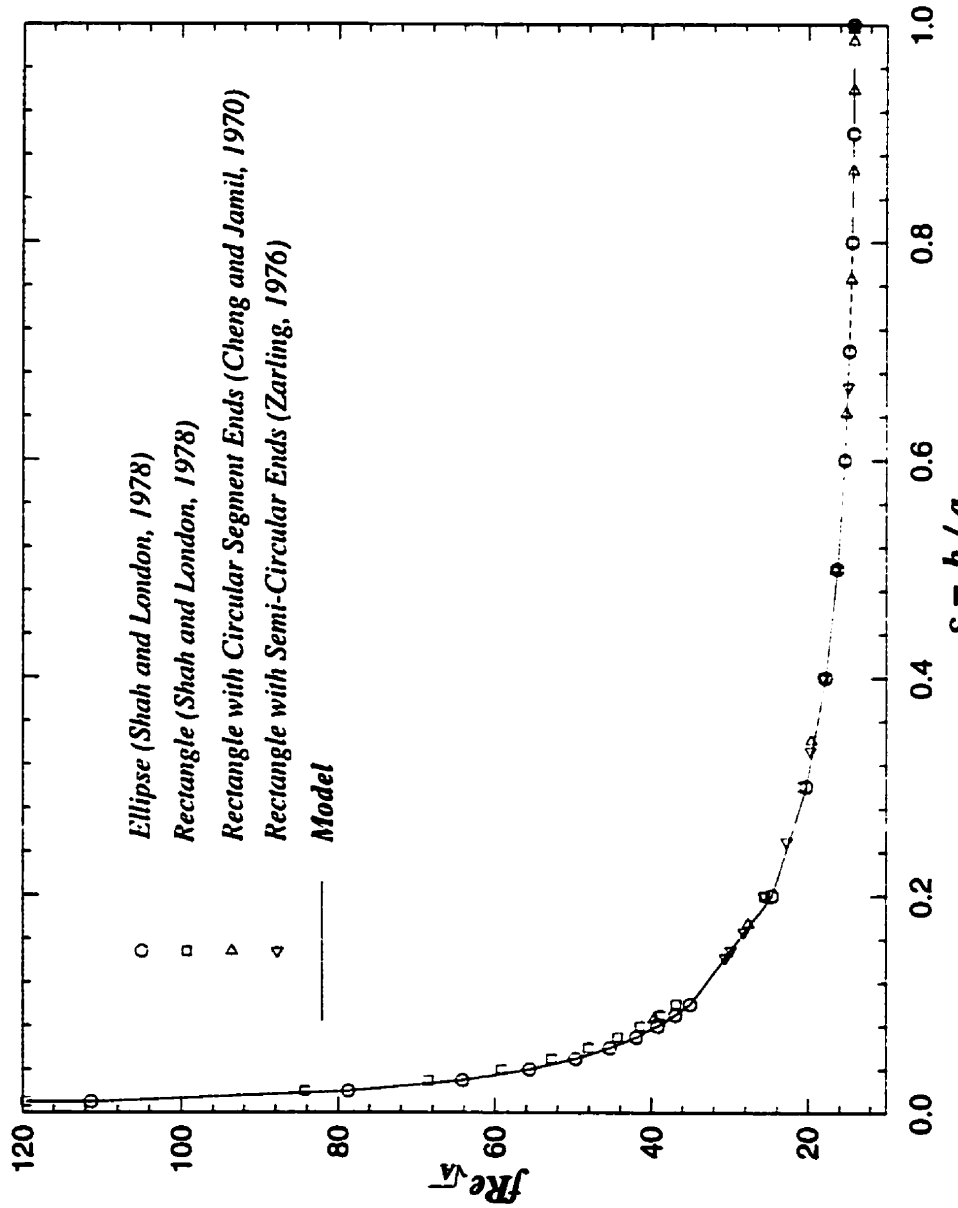

Fig. 4.8 - $fRe_{\sqrt{A}}$ for Common Singly-Connected Geometries.

As $\epsilon \rightarrow 0$, the ratio of the results for the rectangular and elliptic ducts in the last column of Table 4.2 tend toward 7.6 percent. Finally, the parallel plate channel geometry for which $\mathcal{L} = \sqrt{A}$ is undefined, may be adequately modelled as a rectangular duct of aspect ratio $\epsilon = 0.01$. Thus, it is sufficient for modelling purposes to limit the range of duct aspect ratio to $0.01 < \epsilon < 1$.

All of the results in Fig. 4.8 may be approximated by the solution for the elliptical duct. The elliptical duct was chosen to model all of the results because it has a closed form solution, whereas the rectangular duct requires a series solution to describe the velocity distribution. The expression which accurately models the data in Fig. 4.8 is

$$fRe_{\sqrt{A}} = 8\sqrt{\pi}\left(\frac{\pi}{4}\frac{(1+\epsilon^2)}{\sqrt{\epsilon}\,\mathbf{E}(\sqrt{1-\epsilon^2})}\right) \tag{4.14}$$

where $\mathbf{E}(\cdot)$ is the complete elliptic integral of the second kind and $0.01 < \epsilon = \frac{b}{a} \leq 1$ is the aspect ratio of the duct. To eliminate the problem of evaluating the elliptic integral, an approximate expression was developed for the shape function $g(\epsilon)$ defined as

$$g(\epsilon) = \left(\frac{\pi}{4}\frac{1+\epsilon^2}{\sqrt{\epsilon}\mathbf{E}(\sqrt{1-\epsilon^2})}\right) \tag{4.15}$$

such that

$$fRe_{\sqrt{A}} = 8\sqrt{\pi}g(\epsilon) \tag{4.16}$$

The shape function $g(\epsilon)$ may be accurately computed with the expression:

$$g(\epsilon) \approx \left[(1/0.92)^{1-\epsilon}(\sqrt{\epsilon} - \epsilon^{3/2}) + \epsilon\right]^{-1} \tag{4.17}$$

Equation (4.17) is valid over the range $0.01 \leq \epsilon \leq 1$ with an RMS error of 0.70 percent and a maximum error less than ± 2 percent. The function $g(\epsilon)$ accounts for the effects of geometry on the friction factor in the elliptic duct. Later it will be shown that this function may also be used to model the effects of geometry on the Nusselt number.

Comparisons of the proposed model for other singly-connected ducts are presented in Figs. 4.9 and 4.10 and in Table 4.3. The fRe results are shown for both $\mathcal{L} = 4A/P$ and $\mathcal{L} = \sqrt{A}$. The additional geometries of interest are the isosceles triangle (Shah, 1975), right triangle (Sparrow and Haji-Sheikh, 1965), circular sector (Eckert and Irvine, 1956), circular segment (Sparrow and Haji-Sheikh, 1966), sinusoid (Shah, 1975), rhombus (Shah, 1975), various cusp shapes (Shih (1967), Ratkowsky and Epstein (1968), Gunn and Darling (1963)) and the circular annular sector (Shah and London, 1978).

Table 4.3

fRe for Various Cusps

Geometry	fRe_{D_h}	$fRe_{\sqrt{A}}$
Square Corner Cusp	7.06	13.60
Triangular Corner Cusp	7.80	13.10
Side Cusp	6.50	12.75
3 Sided Cusp	6.50	12.72
4 Sided Cusp	6.61	11.20
Circular Duct	16.00	14.18

All of the results are plotted versus an aspect ratio ϵ, which is defined as the ratio of the maximum width and height of each geometry with the constraint that $0 < \epsilon \leq 1$. The aspect ratio may be interpreted as a measure of the slenderness of the duct. From a physical standpoint, the more slender a duct is, the higher the friction factor Reynolds number group. Definitions of the aspect ratio used for reducing the data

are summarized in Table 4.4. If the duct is doubly connected such as the annulus or eccentric annulus, the aspect ratio was taken to be the ratio of the maximum duct spacing and the average duct perimeter.

Table 4.4
Definitions of Aspect Ratio
Used in Data Plots

Geometry	Aspect Ratio
Regular Polygons	$\epsilon = 1$
Singly-Connected‡	$\epsilon = \frac{b}{a}$
Trapezoid	$\epsilon = \frac{2b}{a+c}$
Annular Sector	$\epsilon = \frac{1-r^*}{(1+r^*)\Phi}$
Doubly-Connected	$\beta = \sqrt{\frac{A_i}{A_o}}$
Circular Annulus	$\epsilon = \frac{(1-r^*)}{\pi(1+r^*)}$
Eccentric Annulus	$\epsilon = \frac{(1+e^*)(1-r^*)}{\pi(1+r^*)}$

‡ All except annular sector and trapezoid.

The numerical results for these other geometries do not display any clear trend versus the aspect ratio ϵ in Fig. 4.8. Some geometries show an increase in fRe_{D_h} with decreasing ϵ, while others decrease with decreasing ϵ. When the results are presented in terms of $fRe_{\sqrt{A}}$ as shown in Fig. 4.9 the trend is quite clear, all geometries have $fRe_{\sqrt{A}}$ which increase with a decrease in ϵ. The results for these other geometries are predicted reasonably well by Eq. (4.14) for geometries having corner angles greater than 15 degrees. At angles less than 15 degrees, the effect of small corner angles

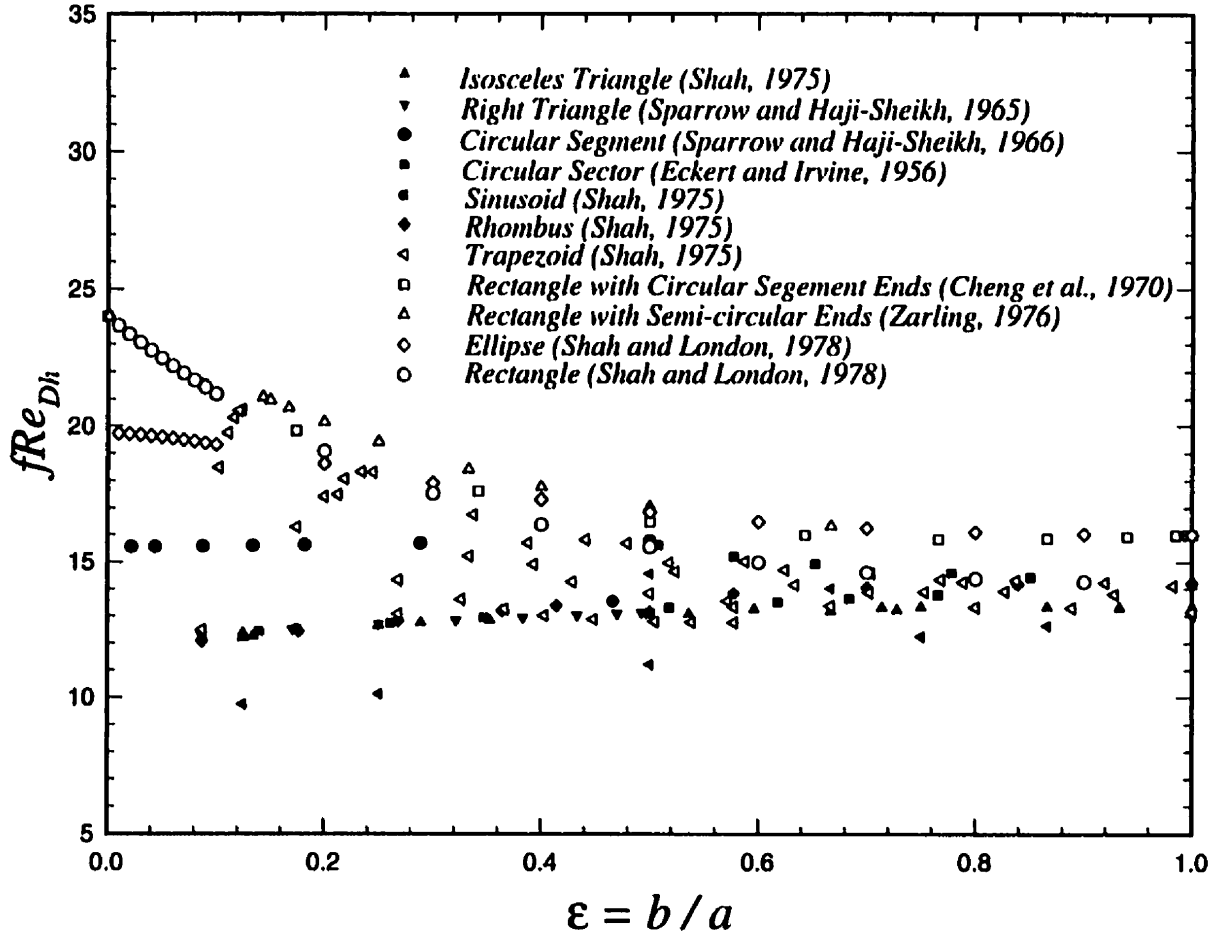

Fig. 4.9 - fRe_{D_h} for All Singly-Connected Geometries.

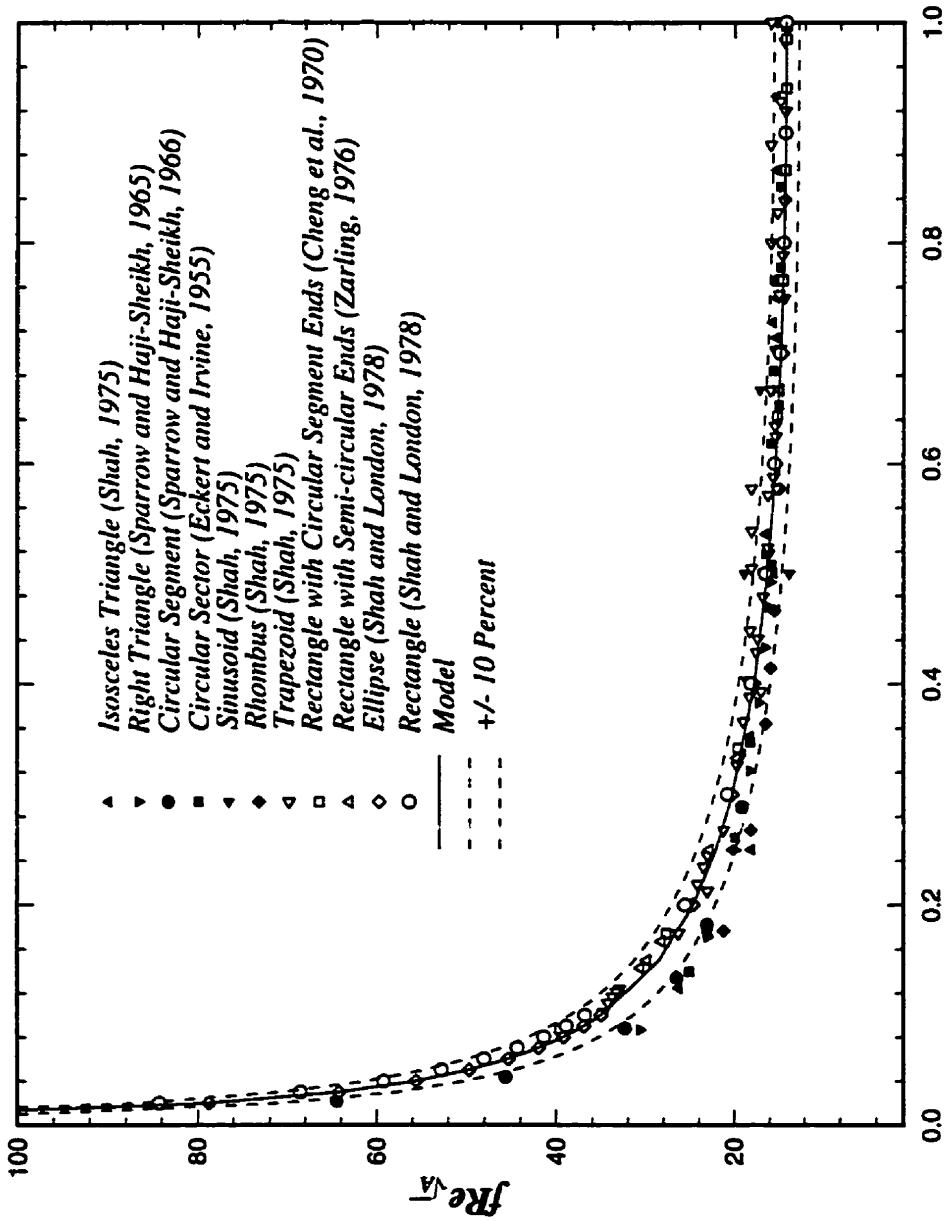

Fig. 4.10 - $fRe_{\sqrt{A}}$ for All Singly-Connected Geometries.

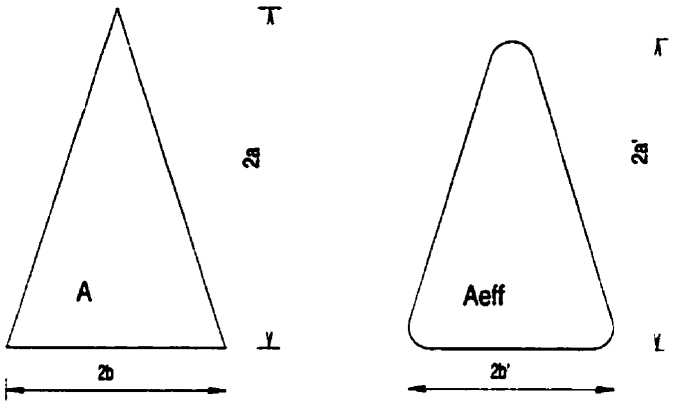

Fig. 4.11 - Effective Duct Shape.

becomes prominent and the results are no longer predicted by Eq. (4.14). If an effective aspect ratio is defined which excludes the stagnant zone in the corner regions (see Fig. 4.10), then the results for these duct shapes would be in better agreement with Eq. (4.14). However, most data are predicted by Eq. (4.14) to within ±10 percent as shown in Fig. 4.10, for all of the geometries analyzed provided that $\theta_c >$ 15°. Finally, to further illustrate, the effectiveness of the characteristic length $\mathcal{L} = \sqrt{A}$, a comparison of various cusp shapes, which result in tube bundle applications is presented in Table 4.3. The results for the most common cusp shapes have fRe values which are much closer to that of a circular duct.

The results for the circular annular sector are presented separately in Figs. 4.12 and 4.13. For this geometry the aspect ratio is defined as the ratio of the spacing of the annular sector $(r_o - r_i)$ to the average arc length $(r_o + r_i)\Phi$ such that $0 < \epsilon < 1$. As the value of $r^* = r_i/r_o \rightarrow 0$, the annular sector becomes a circular sector and the definition of the aspect ratio is no longer appropriate. This explains why some of the data points in Fig. 4.13 diverge from the predictions of Eq. (4.14). However, as the value of $r^* = r_i/r_o \rightarrow 1$ the annular sector becomes a curved rectangular geometry and the definition of aspect ratio is compatible with that of the rectangular geometry. For comparative purposes, the results for the circular sector are plotted along with

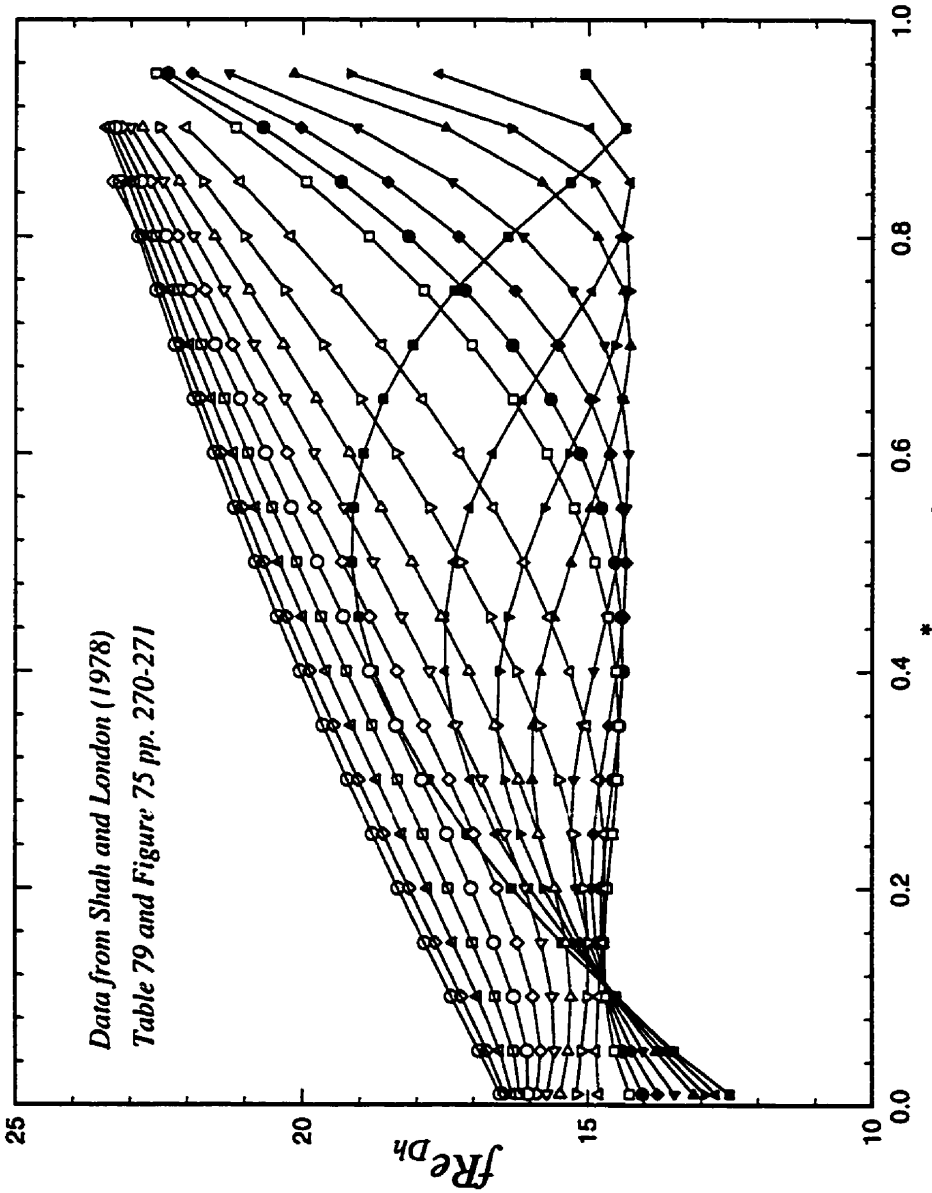

Fig. 4.12 - fRe_{D_h} for Annular Sector.

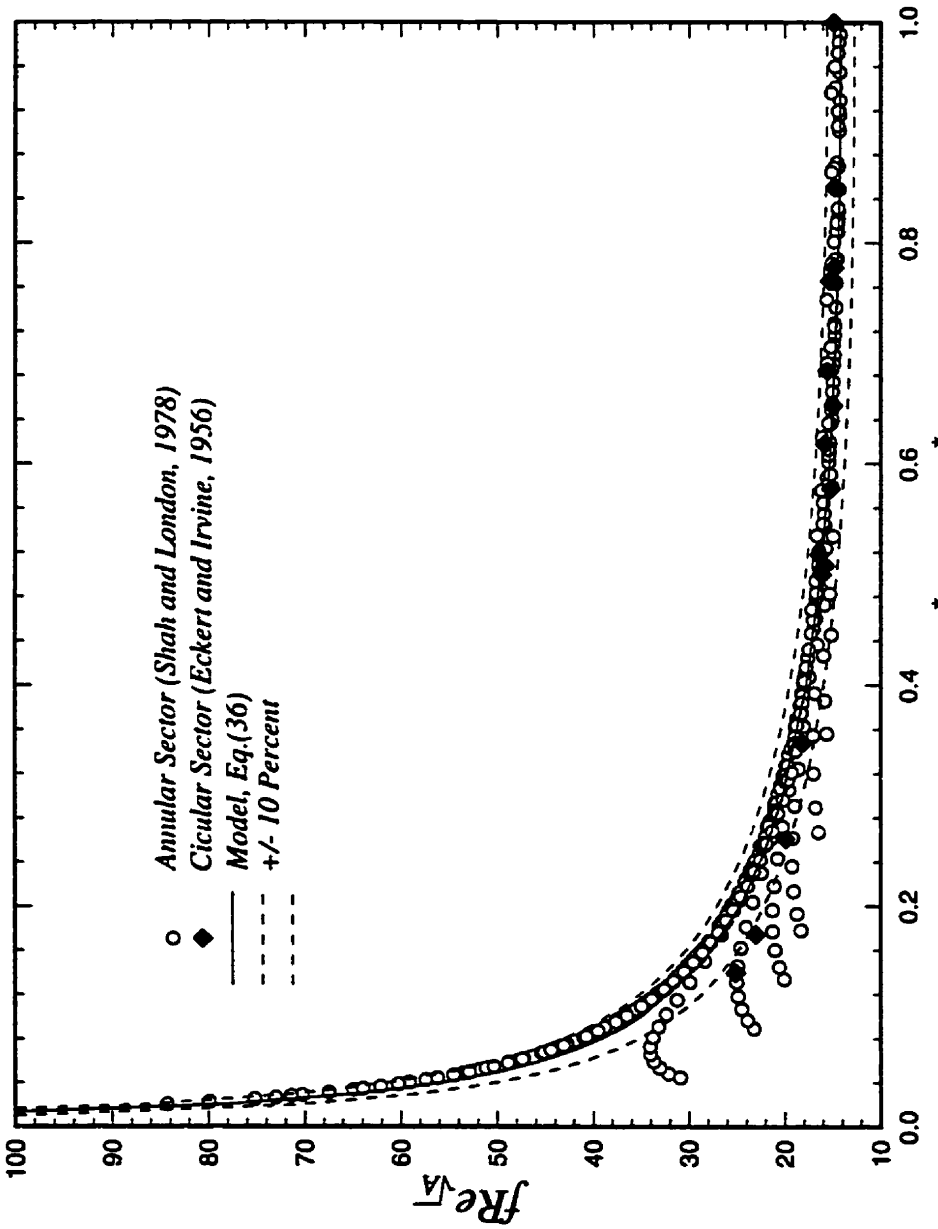

Fig. 4.13 - $fRe_{\sqrt{A}}$ for Annular Sector.

the results for the annular sector in Fig. 4.13 when the aspect ratio is taken to be ratio of the maximum height and width. It should also be noted that the results for the circular sector also fall short of the prediction due to the effect of the small apex angle which was discussed earlier. These comparisons illustrate the importance of the definition of aspect ratio. At small values of ϵ which correspond to small values of r^*, the definition of the aspect ratio needs to be modified to the ratio of the radius and chord length of the sector as shown in Fig. 1.5.

Another useful group of geometries are the polygonal annular ducts. Several variations are possible. They may be circular-polygonal, polygonal-circular, or a combination of similar polygons which are concentric. Only the first two of these cases were examined in the literature by Ratkowsky and Epstein (1968) and Hagan and Ratkowsky (1968). The results are plotted in Fig. 4.14 for the case of a circular boundary with a polygonal core and a polygonal boundary with circular core. At first sight, these appear to be very different geometries. However, if the fRe results are based upon the square root of the flow area, $\sqrt{A_o - A_i}$, and a more suitable aspect ratio defined as $\beta = \sqrt{A_i/A_o}$, the results are identical to the results predicted by the solution for the circular annular geometry for a wide range of β as shown in Fig. 4.15. The solution for the circular annular geometry is given by

$$fRe_{\sqrt{A}} = 8\sqrt{\pi}\left[\frac{(1-\beta)\sqrt{1-\beta^2}}{1+\beta^2-\dfrac{1-\beta^2}{\ln(1/\beta)}}\right] \tag{4.18}$$

where $\beta = \sqrt{A_i/A_o}$, which reduces to $\beta = r_i/r_o = r^*$ for the circular annulus.

As the inner boundary approaches the outer boundary several smaller regions are formed. At this point the domain is no longer doubly-connected, but is now composed of several singly-connected areas in parallel. Thus the definitions of flow area and aspect ratio are no longer valid in this region. The area should now be based upon

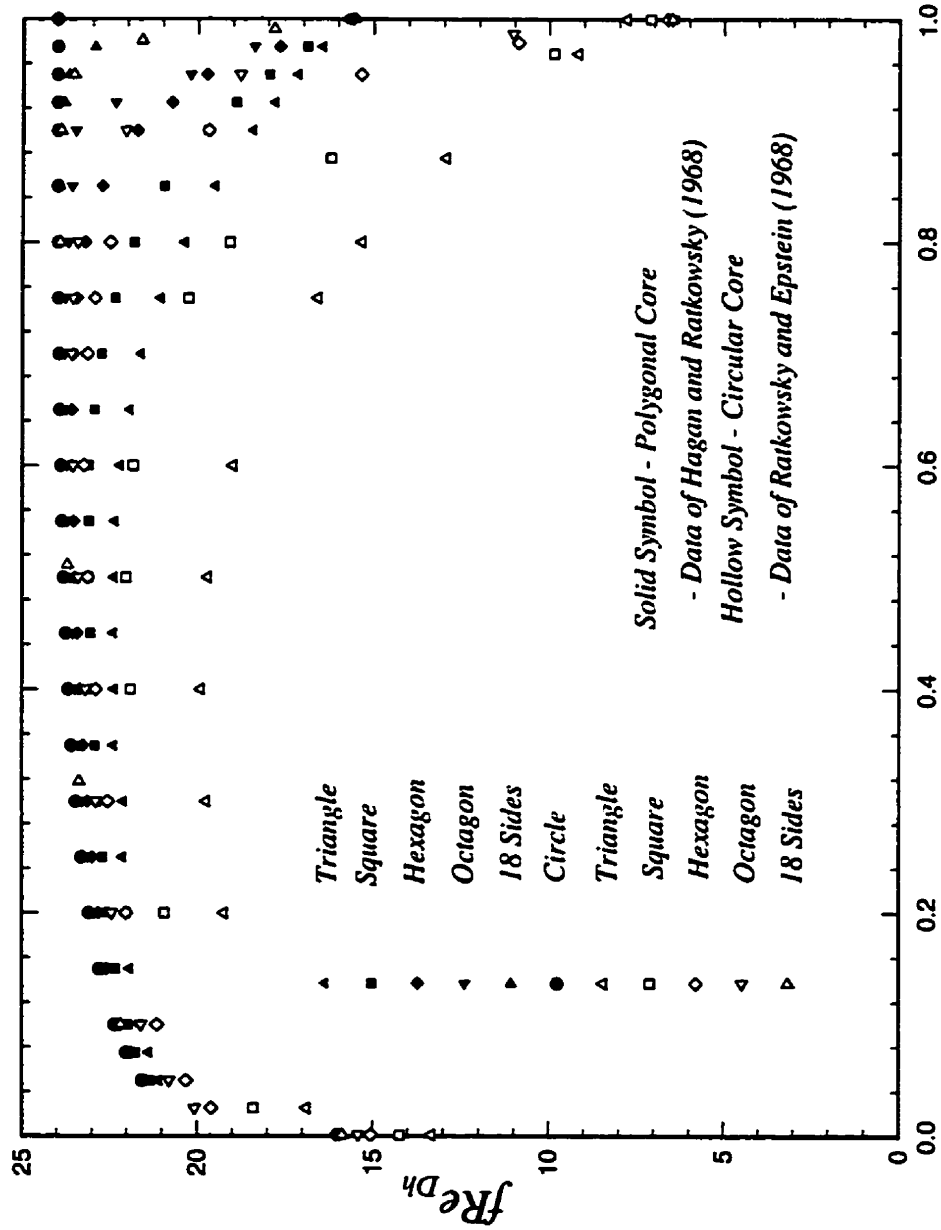

Fig. 4.14 - fRe_{D_h} for Doubly-Connected Geometries.

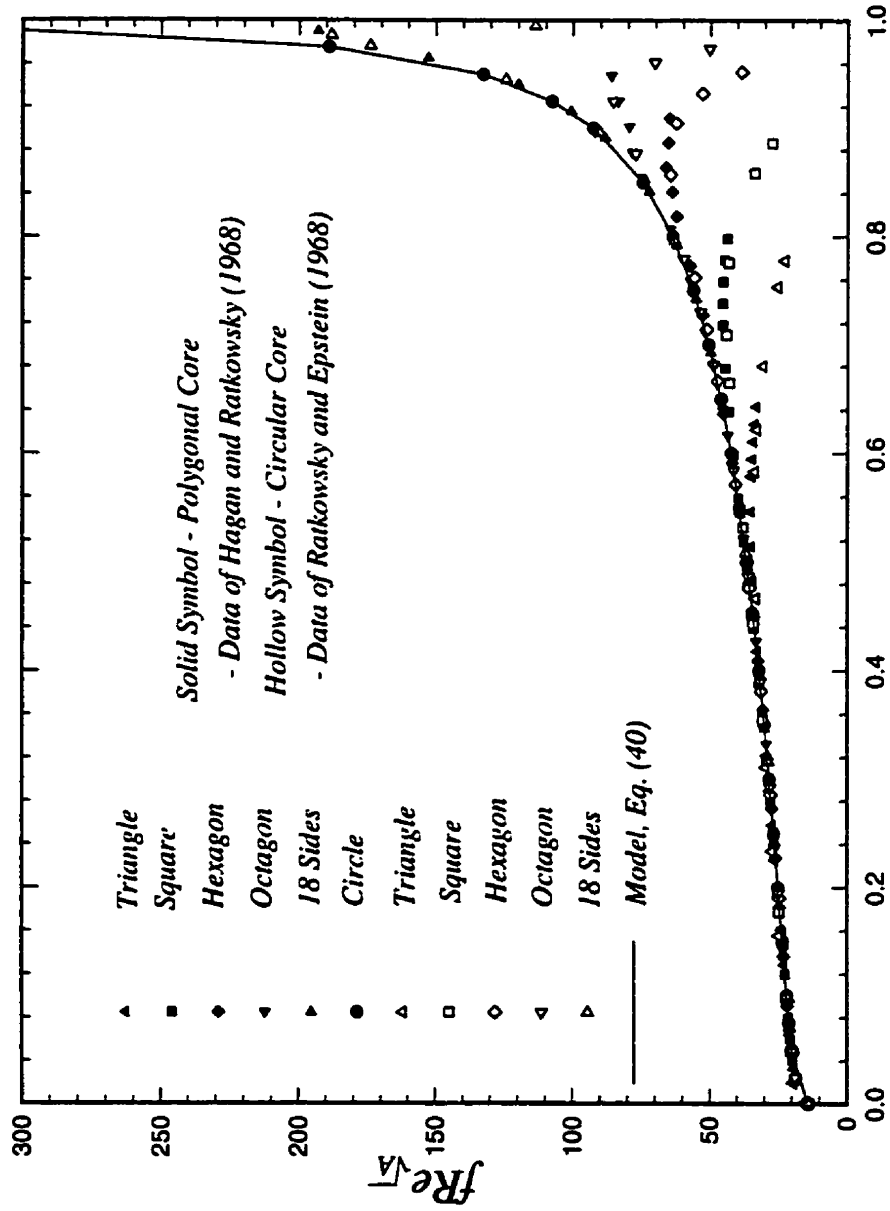

Fig. 4.15 - $fRe_{\sqrt{A}}$ for Doubly-Connected Geometries.

the area of the singly-connected domain and the aspect ratio defined in terms of this new geometry. It is for these reasons that the results diverge from the solution of the circular annular region in Fig. 4.15. The $fRe_{\sqrt{A}}$ results may also be predicted from the expression for the singly-connected regions, Eq. (4.14), using the definition of aspect ratio ϵ from Table 4.4 for the circular annulus with $r^* = \beta$.

For most practical applications the value of β is such that the numerical values of the $fRe_{\sqrt{A}}$ may be accurately computed from the solution for the circular annulus. Table 4.5 summarizes the critical values (when data diverge) and maximum values (when boundaries touch) of $\beta = \sqrt{A_i/A_o}$ for the data of Ratkowsky and Epstein (1968) and Hagan and Ratkowsky (1968).

Finally, it may be reasonable to expect the results for concentric homologous polygons. i.e. triangle-triangle, square-square, (see Fig. 1.6), to behave approximately as a concentric circular annulus for the entire range of $\beta = \sqrt{A_i/A_o}$.

Table 4.5

Critical and Maximum Values of $\beta = \sqrt{A_i/A_o}$

N	Critical Values	Maximum Values	
		Polygonal Core	Circular Core
3	0.52	0.643	0.778
4	0.68	0.798	0.886
6	0.80	0.910	0.952
8	0.88	0.949	0.974
18	0.96	0.990	0.995
∞	1.000	1.000	1.000

4.3.2 Nusselt Number

The approach applied in the previous section not only simplifies the results for the fRe group, but may also be used to non-dimensionalize the Nusselt numbers for various flow conditions and thermal boundary conditions.

Table 4.6 compares the Nusselt number for both slug and fully developed flows for both the (UWT) and (UWF) boundary conditions. The Nu_{D_h} results of many polygonal ducts were obtained from Shah and London (1978) and Bejan (1993). These data are from the work of Cheng (1966, 1969), Shih (1967), and Asako et al. (1988). The results for $Nu_{\sqrt{A}}$ for each flow condition and thermal boundary condition approximately reduce to a single constant for the duct geometries presented. The differences between the triangular duct ($N = 3$) and the circular duct ($N = \infty$) are 13.9 percent and 9.1 percent for the UWT and UWF boundary conditions, respectively, for the fully developed flow condition. These differences reduce to 8.0 percent and 6.5 percent for the square duct. When the characteristic length is the hydraulic diameter, the relative differences between the circular duct and the triangular duct are 32.5 percent and 28.7 percent for the UWT and UWF boundary conditions, respectively, for the fully developed flow condition.

These differences are much less for the slug flow condition since the uniform velocity distribution includes the corners, whereas for fully developed flow the effect of sharp corners is more pronounced. The relative differences between the circular duct and the square duct are 0.28 percent and 3.5 percent for the UWF and UWT, respectively, when $\mathcal{L} = \sqrt{A}$.

The results given in Table 4.6 are for the polygonal duct geometries. To extend this analysis to geometries which have varying aspect ratios, the rectangular duct, elliptical duct, and some miscellaneous geometries of elongated shape are also examined. Figures 4.16 and 4.17 compare the data for the rectangular duct obtained from Shah and London (1978), the elliptical duct obtained from Ebadian et al. (1986), and some

miscellaneous ducts from Shah and London (1978) when the characteristic length is $\mathcal{L} = \sqrt{A}$. When the results are based upon the square root of cross-sectional area two distinct bounds are formed for the Nusselt number. The lower bound consists of all duct shapes which have corner angles less than 90 degrees, while the upper bound consists of all ducts with rounded corners and/or right angled corners.

Table 4.6

Nusselt Numbers for Slug and Fully Developed Flow (FDF) for Regular Polygons

		Isoflux		Isothermal	
	Geometry	**FDF**†	**Slug**‡	**FDF**†	**Slug**‡
Nu_{D_h}	Triangle	3.11	-	2.47	-
	Square	3.61	7.08	2.98	4.93
	Hexagon	4.00	7.53	3.35‡	5.38
	Octagon	4.21	7.69	3.47‡	5.53
	Circular	4.36	7.96	3.66	5.77
$Nu_{\sqrt{A}}$	Triangle	3.51	-	2.79	-
	Square	3.61	7.08	2.98	4.93
	Hexagon	3.74	7.01	3.12	5.01
	Octagon	3.83	7.00	3.16	5.03
	Circular	3.86	7.06	3.24	5.11

† Data of Shih (1967) and Cheng (1966, 1969)

‡ Data of Asako et al. (1988)

A model has been developed which accurately predicts the data for the elliptic duct by comparing the solution of the friction factor of Eq. (4.14) with the data for the Nusselt numbers of Ebadian et al. (1986). The shape function $g(\epsilon)$ which accounts for aspect ratio effects in the friction factor-Reynolds number group may also be used to obtain a model for the Nusselt number in elliptic ducts. Multiplying the shape function by the Nusselt number for the circular duct gives

$$Nu_{\sqrt{A}} = Nu^0_{\sqrt{A}} \left(\frac{\pi}{4} \frac{1+\epsilon^2}{\sqrt{\epsilon}\mathbf{E}(\sqrt{1-\epsilon^2})} \right) = Nu^0_{\sqrt{A}}\, g(\epsilon) \tag{4.19}$$

where $Nu^0_{\sqrt{A}}$ is equal to 3.24 for the (UWT) boundary condition and 3.86 for the (UWF) boundary condition. This simple expression predicts the data of Ebadian et al. (1986) with an RMS error of 3.78 percent for the isothermal boundary condition and 4.70 percent for the isoflux boundary condition.

The Nusselt number for thermally fully developed flow in other non-circular ducts may be approximated by the following relation

$$Nu_{\sqrt{A}} = Nu^0_{\sqrt{A}} \left(\frac{fRe_{\sqrt{A}}}{8\sqrt{\pi}\epsilon^{\gamma}} \right) \tag{4.20}$$

The parameter γ is chosen based upon the geometry. Values for γ which define the upper and lower bounds in Figs. 4.16 and 4.17 are fixed at $\gamma = 1/10$ and $\gamma = -3/10$. respectively. Data for many geometries (Shah and London, 1978) are shown in Figs. 4.16 and 4.17 with the bounds determined by Eq. (4.20). It is clear that using the square root of the cross-sectional flow area reduces the variation in results of similar geometries. Almost all of the available data are predicted within $\pm$ 10 percent by Eq. (4.20), with the exception of the circular segment duct.

Finally, data for the doubly connected regions shown in Fig. 1.6 are compared with the proposed model, Eq. (4.20), in Fig. 4.18. The $fRe_{\sqrt{A}}$ in Eq. (4.20) may be computed using the expression for the singly-connected regions, Eq. (4.14). The appropriate definition of aspect ratio, ϵ, is given in Table 4.4 for the circular annulus with $r^* = \beta = \sqrt{A_i/A_o}$. Overall agreement between the model and the data is within $\pm$15 percent.

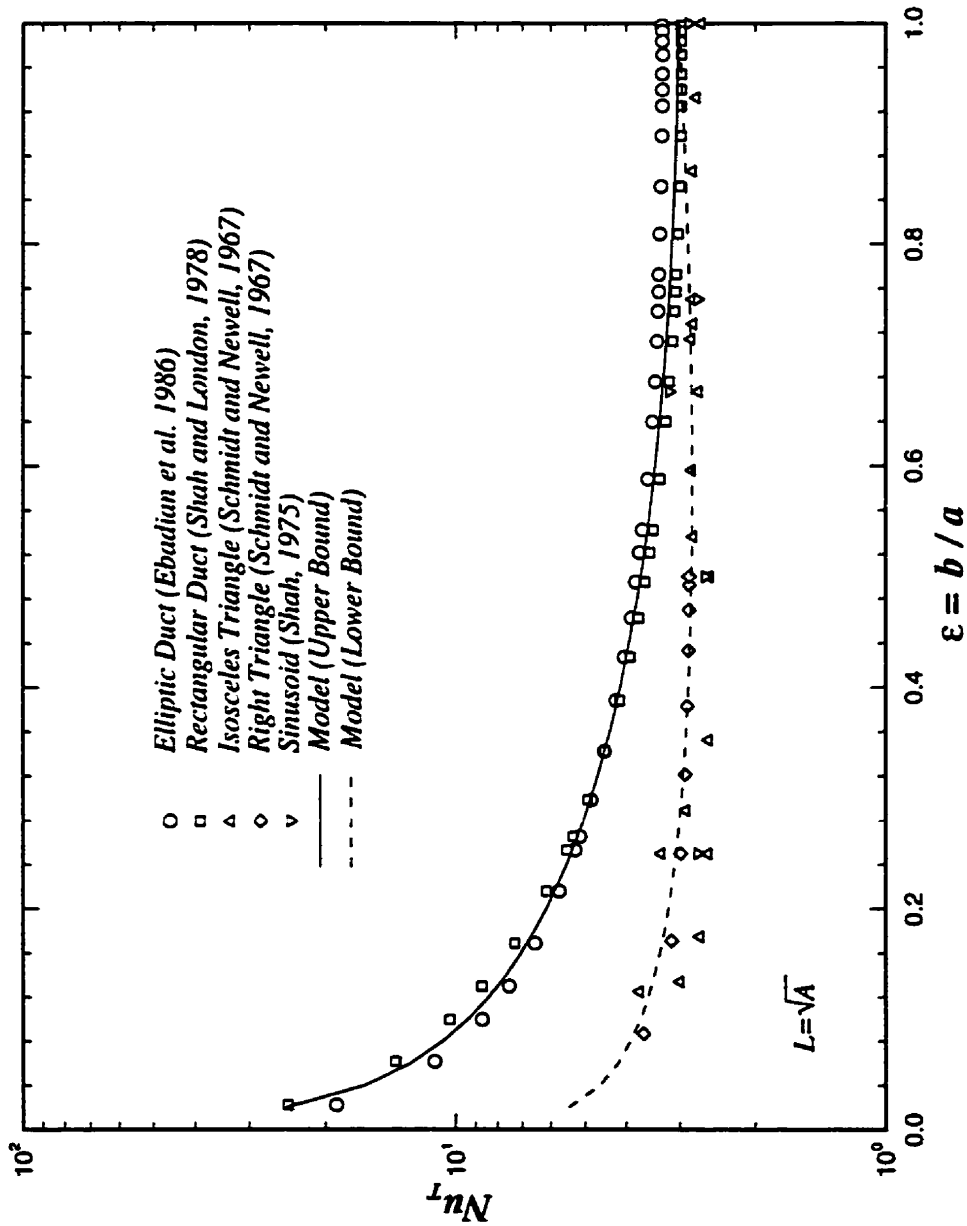

Fig. 4.16 - Fully Developed Flow Nu_T.

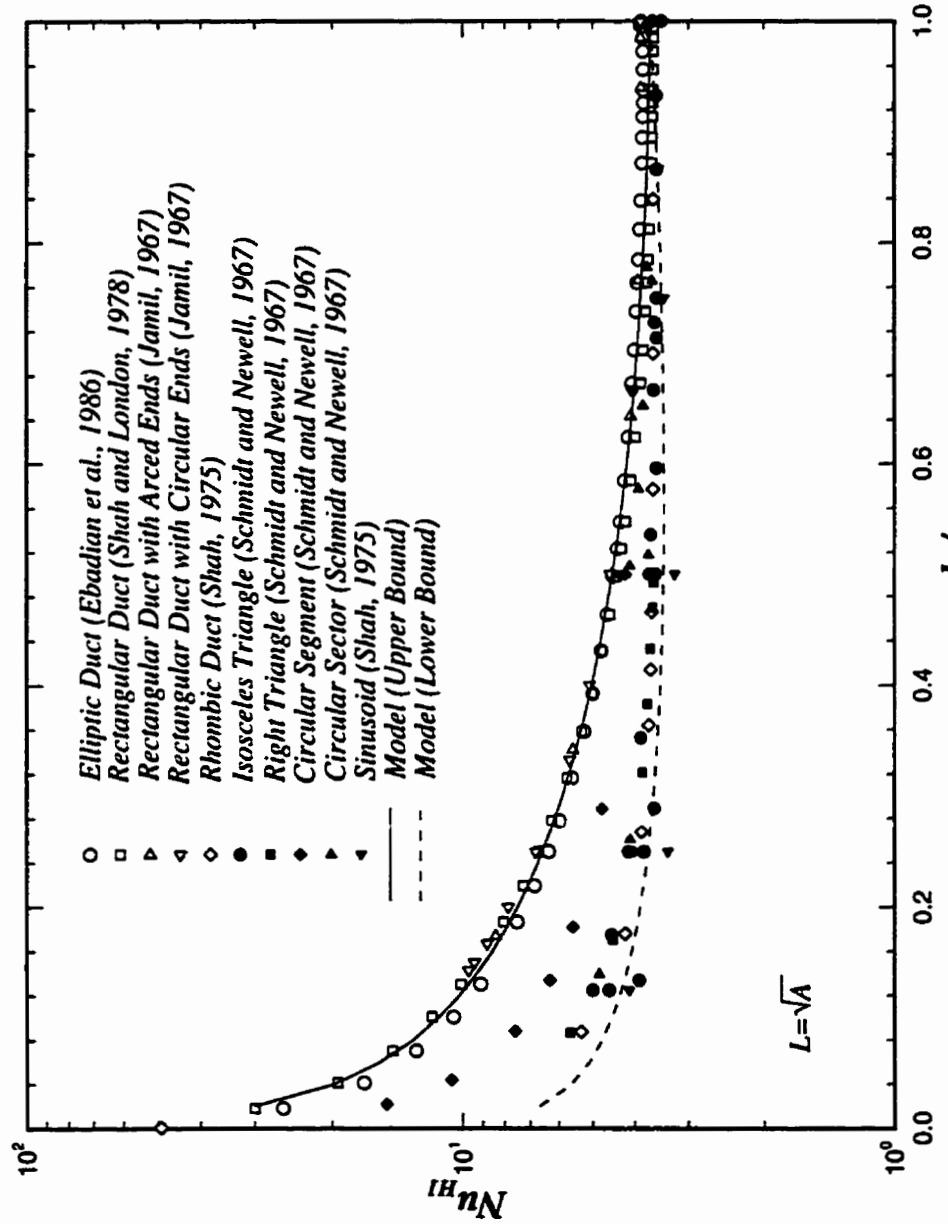

Fig. 4.17 - Fully Developed Flow Nu_{HI}.

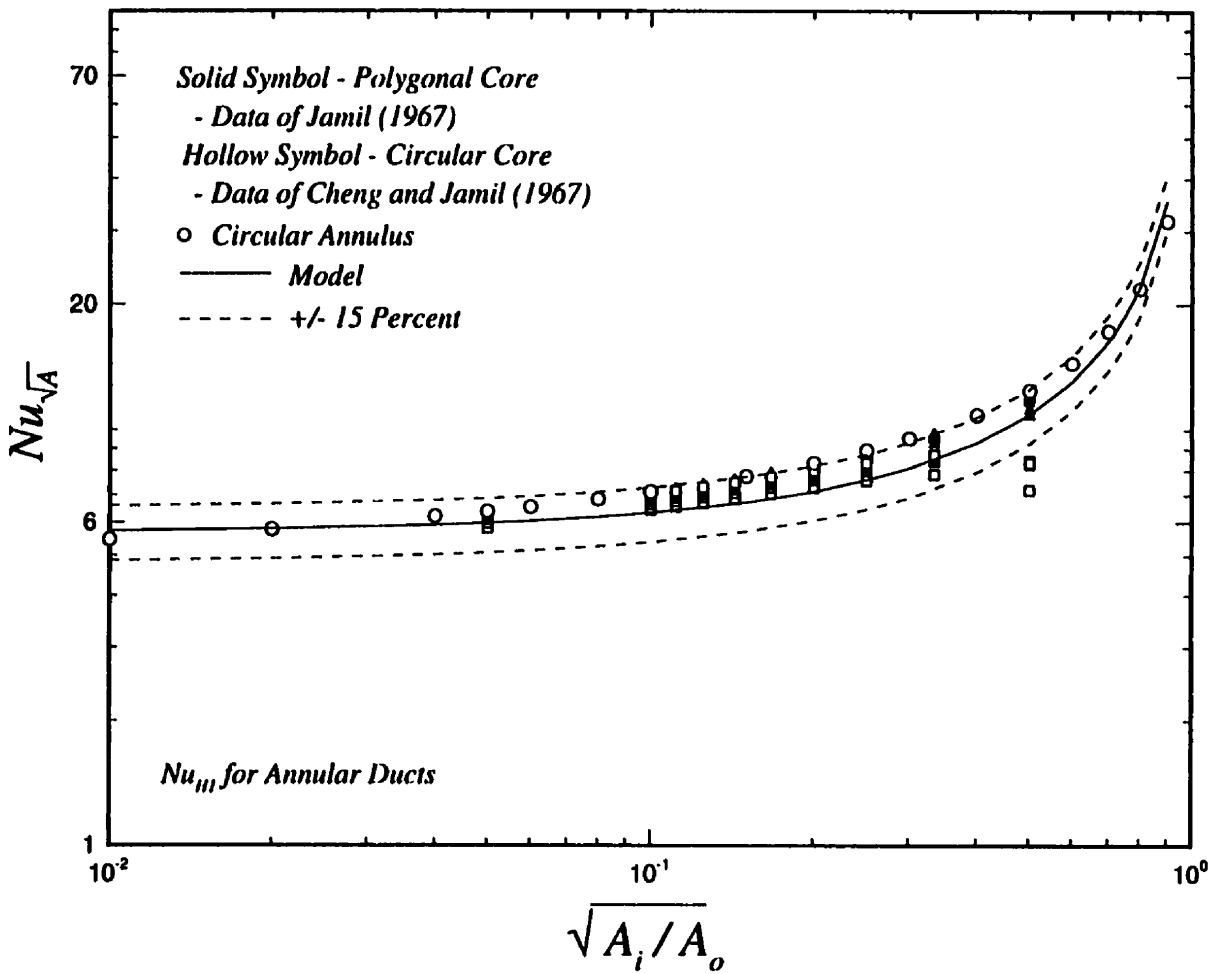

Fig. 4.18 - Fully Developed Flow Nu_{H1} in Doubly- Connected Ducts.

4.4 Developing Flow

In this section models for hydrodynamically developing flow and thermally developing flow will be developed by combining the asymptotic solutions for the entrance region and the fully developed flow models developed in the previous section. The asymptotic models will be combined using the Churchill and Usagi (1972) method discussed earlier in Section 4.2.2.

4.4.1 Apparent Friction Factor

In the entrance region where the boundary layer thickness is small, the results are similar for all ducts regardless of geometry. An analytical result for the apparent friction factor in the entrance region of the circular duct was derived by Shapiro et al. (1954) using several methods. The leading term in the solution for any characteristic length $\mathcal{L}$ is given by

$$f_{app}Re_{\mathcal{L}} = \frac{3.44}{\sqrt{z^+}} \tag{4.21}$$

which is valid for $z^+ = z/(\mathcal{L}\,Re_{\mathcal{L}}) \leq 0.001$.

This solution is independent of the duct shape and may be used to compute the apparent friction factor in the entrance region of most ducts.

For the particular case of predicting the apparent friction factor in a duct,a model may be developed by combining the developing flow, Eq. (4.21), and fully developed flow, fRe_{fd}, asymptotes in the following form:

$$f_{app}Re = \left\{ \left(\frac{3.44}{\sqrt{z^+}} \right)^n + (fRe_{fd})^n \right\}^{1/n} \tag{4.22}$$

A model which is valid over the entire duct length for many different geometries may

be obtained by substituting the model for the fully developed friction factor Reynolds number group developed earlier, Eq. (4.14), into the above equation. The resulting general model is

$$f_{app}Re_{\sqrt{A}} = \left[\left\{ \frac{3.44}{\sqrt{z^+}} \right\}^2 + \left\{ 8\sqrt{\pi} \left(\frac{\pi}{4} \frac{(1+\epsilon^2)}{\sqrt{\epsilon}\,\mathbf{E}(\sqrt{1-\epsilon^2})} \right) \right\}^2 \right]^{1/2} \tag{4.23}$$

where the characteristic length for $f_{app}Re$, fRe, and z^+ is now $\mathcal{L} = \sqrt{A}$ rather than the hydraulic diameter.

The correlation parameter n may be chosen such that the RMS differences between the predicted results and the numerical or analytical results is minimized. The parameter n was found to vary between 1.5 and 3.6 with an optimal value $n \approx 2$ for all duct shapes. The above model accurately predicts the data for all of the duct shapes examined in this study. The proposed model is considerably simpler than that of Shah (1978) and Yilmaz (1990) and also does not contain the incremental pressure drop factor K_∞. Since the solution of Shapiro et al. (1954) for the entrance region accounts for both the wall shear and the increase in momentum due to the accelerating core, there is no need to introduce the term K_∞. Thus the proposed model is now only a function of duct length z^+ and aspect ratio ϵ, whereas the models of Shah (1978) and Yilmaz (1990) are functions of many more parameters. Table 4.7 compares the percent difference and the RMS difference of the proposed model with the models of Shah (1978) and Yilmaz (1990) for a number of geometries. Also presented in Table 4.7 is the optimal value of the parameter n which minimizes the RMS difference for each geometry. It is apparent that choosing a single value of $n \approx 2$ does not introduce large errors and simplifies the model considerably.

Comparisons between numerical data and the new model for the geometries in Table 4.7 are presented in Figs. 4.19-4.24 for a range of z^+. With the exception of the eccentric annular duct at large values of r^* and e^*, the proposed model predicts almost all of the developing flow data available in the literature to within ± 12 percent.

Table 4.7

Comparison of RMS and Percent Differences*

in Developing Flow Models

Geometry	Shah (1978)	Yilmaz (1990)	Proposed Model			
	min/max	min/max	min/max	RMS	$n^\dagger$	($n = 2$) RMS
Circle	± 1.9	-0.3/2.7	-2.73/1.05	1.20	2.01	1.71
Circular Annulus $r_i/r_o = 0.05$	± 2.0	-17.0/1.2	-2.61/1.18	1.27	2.18	2.51
Circular Annulus $r_i/r_o = 0.10$	± 1.9	-17.4/1.9	-1.97/1.09	0.77	2.14	1.73
Circular Annulus $r_i/r_o = 0.50$	± 2.2	-10.2/0.9	-1.13/6.96	1.87	2.07	1.99
Circular Annulus $r_i/r_o = 0.75$	± 2.1	-5.4/1.3	-1.44/7.17	2.12	2.04	2.16
Square $b/a = 1$	± 2.3	-2.4/1.6	-1.48/2.27	1.41	1.95	1.61
Rectangle $b/a = 0.5$	± 1.9	-2.1/6.7	-1.48/2.27	1.14	1.98	1.16
Rectangle $b/a = 0.2$	± 1.7	-1.5/5.0	-1.11/1.89	1.10	2.15	2.04
Parallel Plates $b/a \to 0$	± 2.4	-1.6/1.8	-1.22/0.86	0.60	2.32	3.33
Isosceles Triangle $2\phi = 30°$	-	-1.1/0.9	-1.30/4.41	1.75	1.71	4.91
Isosceles Triangle $2\phi = 60°$	± 2.4	-0.6/1.1	-0.63/5.97	2.35	1.70	5.16
Isosceles Triangle $2\phi = 90°$	-	1.6/5.2	-7.28/0.85	2.04	2.03	2.08
Eccentric Annulus $e^* = 0.5$, $r^* = 0.5$	-	-5.5/3.0	-2.06/1.97	1.71	1.50	8.72
Eccentric Annulus $e^* = 0.5$, $r^* = 0.1$	-	-9.1/16	-2.22/2.29	1.66	1.66	5.08
Eccentric Annulus $e^* = 0.7$, $r^* = 0.3$	-	-10.3/3.1	-10.89/8.39	7.56	1.86	7.72
Eccentric Annulus $e^* = 0.9$, $r^* = 0.1$	-	-11.4/0.2	-13.96/5.87	5.94	2.38	7.30
Eccentric Annulus $e^* = 0.9$, $r^* = 0.5$	-	-9.9/-3.5	-35.13/9.44	13.34	3.61	18.14
Ellipse $b/a = 1$	-	-	-2.97/3.75	2.53	1.96	2.56
Ellipse $b/a = 0.5$	-	-	-2.98/5.77	3.77	1.97	3.85
Ellipse $b/a = 0.2$	-	-	-5.75/7.59	5.62	1.69	7.01
Circular Sector $2\phi = 11.25°$	-	-	-9.42/3.03	3.67	2.01	3.68
Circular Sector $2\phi = 22.5°$	-	-	-1.70/5.10	1.57	1.73	4.22
Circular Sector $2\phi = 45°$	-	-	-1.14/12.1	3.73	1.62	6.69
Circular Sector $2\phi = 90°$	-	-	-1.60/16.72	4.63	1.75	5.69
Pentagon	-	-	-3.46/12.75	5.79	1.76	6.41
Trapezoid $\phi = 72°$, $b/a = 1.123$	-	-	-4.96/11.35	6.05	1.55	8.68

* %diff= $(Analytical - Predicted)/(Analytical) \times 100$

† Optimal value

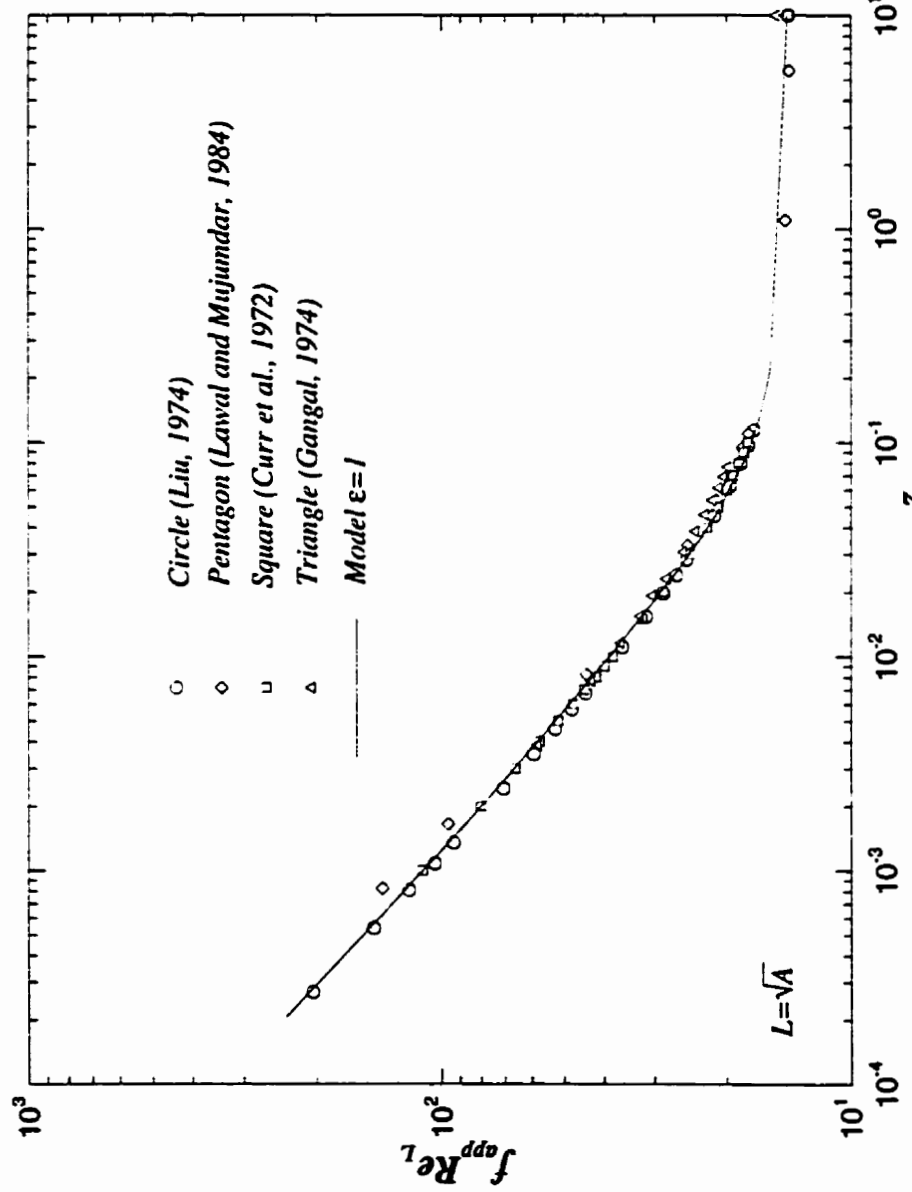

Fig. 4.19 - $f_{app}Re_{\sqrt{A}}$ for Polygonal Ducts.

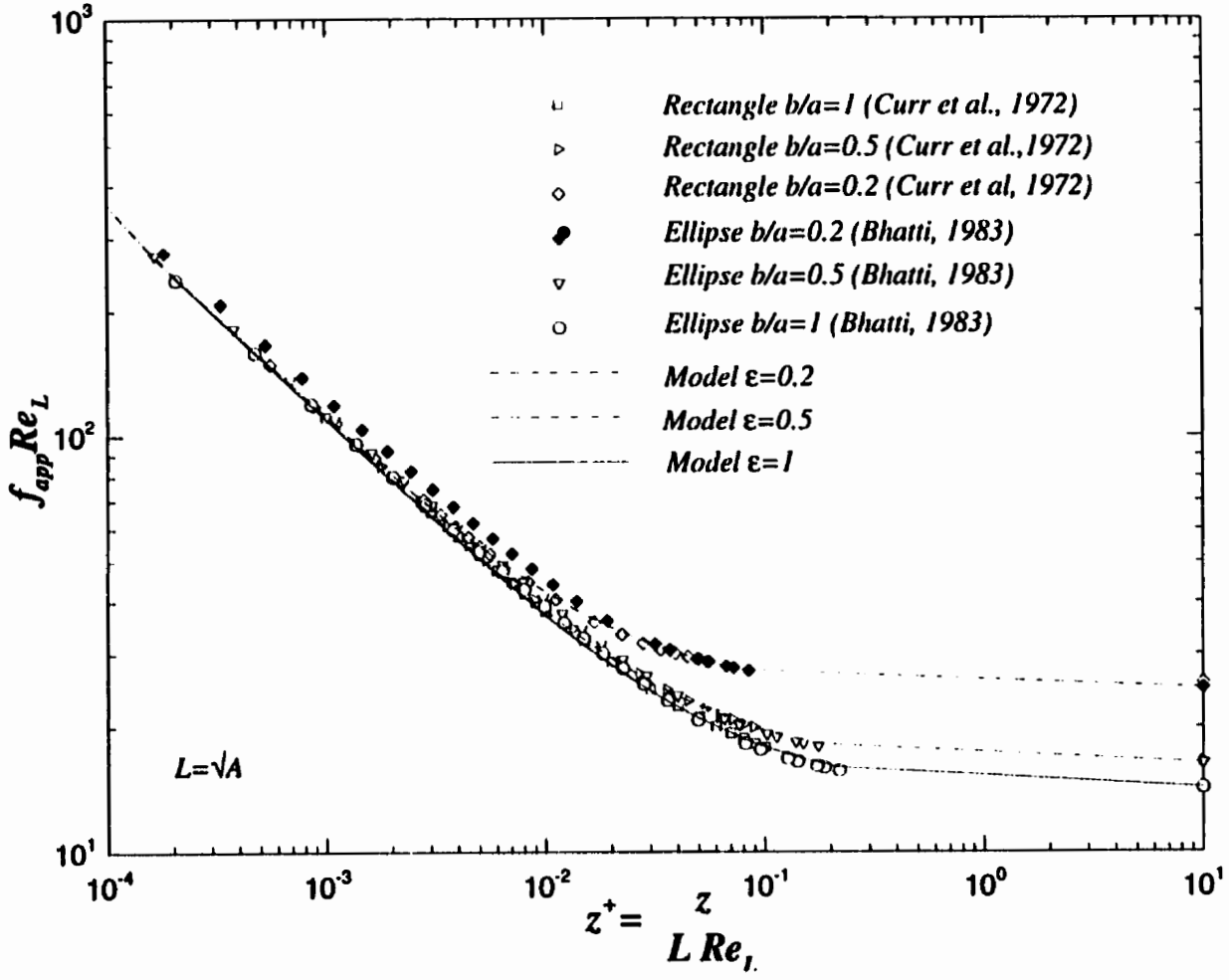

Fig. 4.20 - $f_{app}Re_{\sqrt{A}}$ for Flat Ducts.

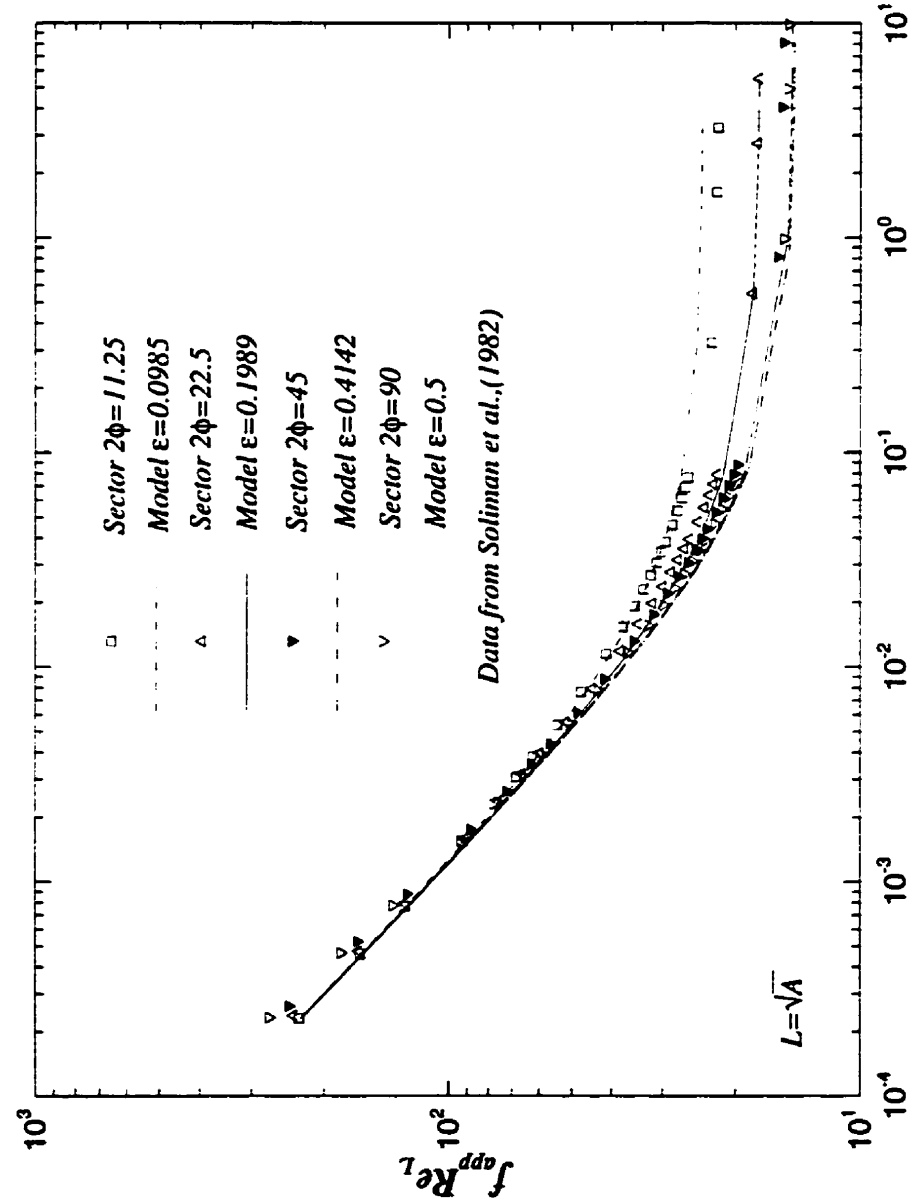

Fig. 4.21 - $f_{app}Re_{\sqrt{A}}$ for Circular Sector Ducts.

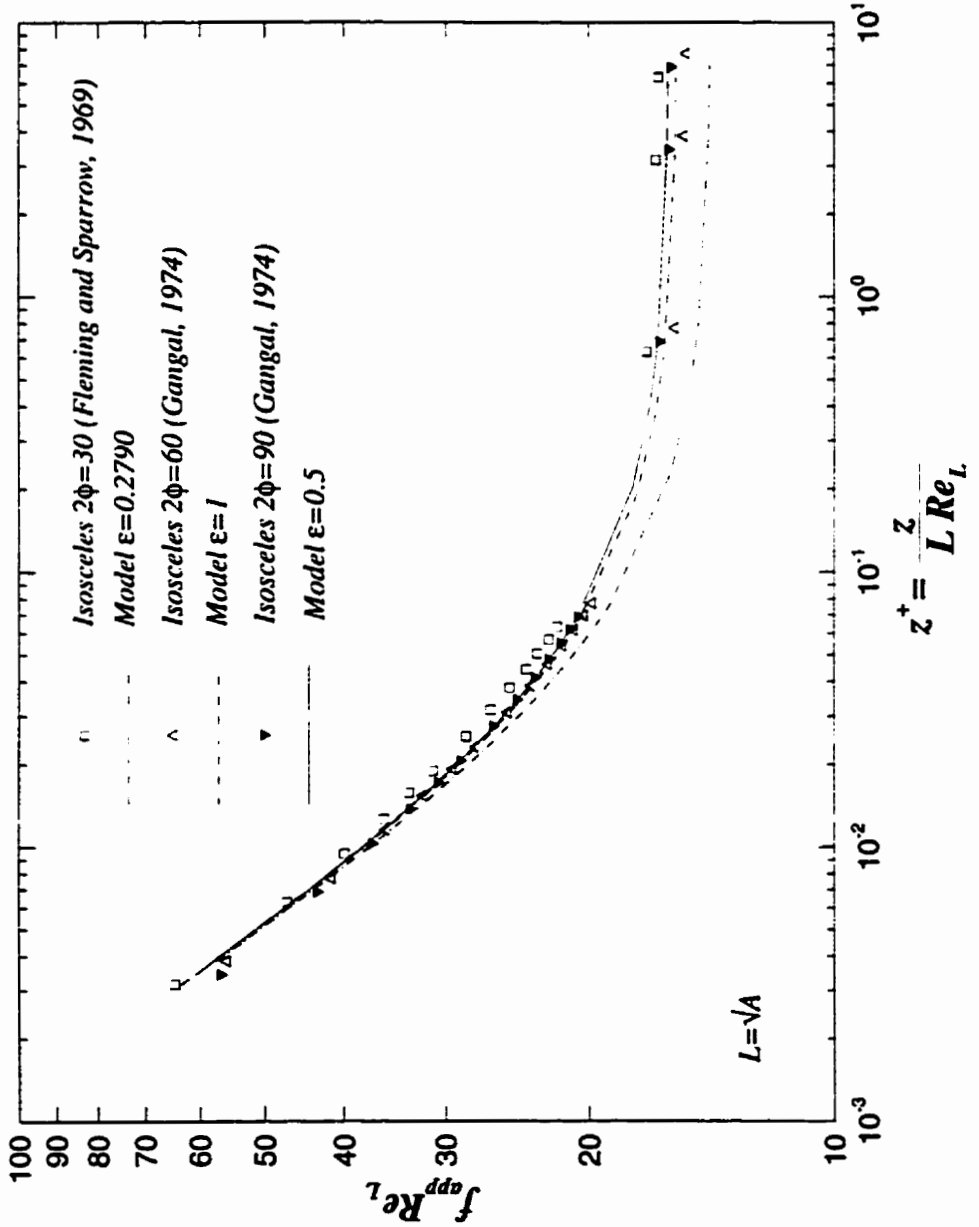

Fig. 4.22 - $f_{app}Re_{\sqrt{A}}$ for Isosceles Triangle Ducts.

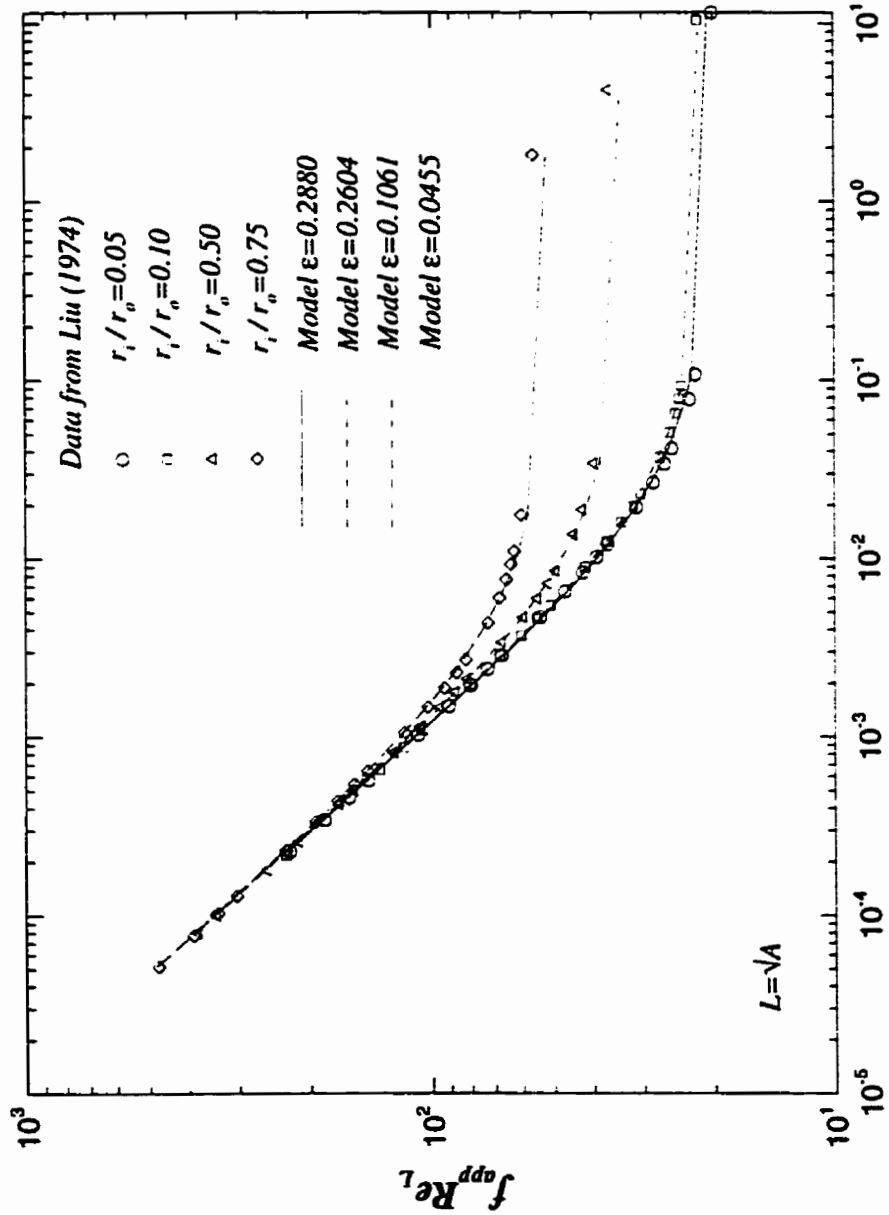

Fig. 4.23 - $f_{app}Re_{\sqrt{A}}$ for Circular Annular Ducts.

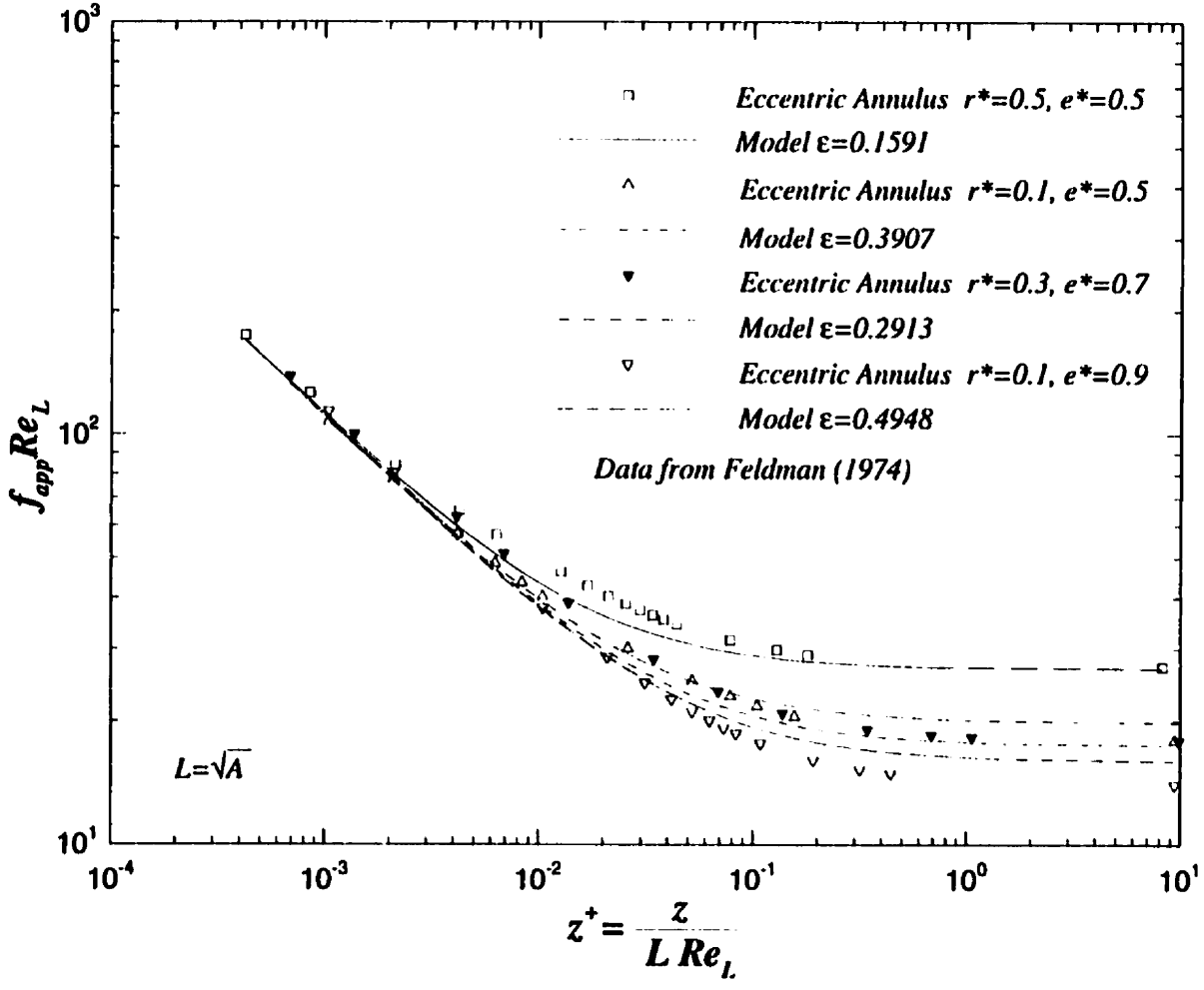

Fig. 4.24 - $f_{app}Re_{\sqrt{A}}$ for Eccentric Annular Ducts.

The proposed model provides equal or better accuracy than the model of Yilmaz (1990) and is also much simpler. A comparison of the model with the data for the parallel plate channel is also provided. For this geometry $\sqrt{A} \rightarrow \infty$, however, this geometry may be accurately modeled as a rectangular duct with $\epsilon \leq 0.01$ or a circular annular duct with $r^* \leq 0.05$. Good agreement is obtained with the current model when the parallel plate channel is modeled as rectangular or annular duct having an aspect ratio equal to $\epsilon = 0.01$ or $r^* = 0.05$, respectively.

4.4.2 Nusselt Number (Graetz Problem)

The development of a model for the thermal entrance problem will be similar to the development of the model for the hydrodynamic entrance problem. A general model for the thermal entrance problem may be developed by combining a generalized Leveque model for the entrance region with the fully developed flow result using the Churchill and Usagi (1972) asymptotic correlation method.

In the entrance region where the thermal boundary layer thickness is small, the results are weak functions of the geometry. A generalized Leveque model for the thermal entrance region may be presented in terms of the friction factor Reynolds number group fRe (Shah and London (1978). For any characteristic length $\mathcal{L}$ this result may be written in compact form:

$$Nu_{\mathcal{L}} = C_1 C_2 \left(\frac{fRe_{\mathcal{L}}}{z^*_{\mathcal{L}}} \right)^{\frac{1}{3}} \tag{4.24}$$

where the constant C_1 determines whether the Nusselt number is an average or local value and the constant C_2 determines whether the boundary condition is UWT or UWF. This asymptotic result is valid in the entrance region of most geometries. Since Eq. (4.24) is a function of the friction factor Reynolds number group, it is a weak function of the duct shape. Since the value of fRe_{D_h} for most geometries lies between 12 and 24, Eq. (4.24) will vary only by 25 percent due to the 1/3 power on fRe.

Now, substituting the model for the friction factor Reynolds number group $fRe_{\sqrt{A}}$ developed earlier, into Eq. (4.24), a simple Leveque model is obtained for the elliptical duct:

$$Nu_{\sqrt{A}}(z^*) = C_1 C_2 \left(\frac{8\sqrt{\pi}\left(\frac{\pi}{4}\frac{(1+\epsilon^2)}{\sqrt{\epsilon}\,\mathbf{E}(\sqrt{1-\epsilon^2})}\right)}{z^*_{\sqrt{A}}} \right)^{\frac{1}{3}} \tag{4.25}$$

This new result differs by only 1.2 percent compared with results derived by Someswara et al. (1967) and James (1970), and 1.5 percent compared with the model derived by Richardson (1980), for the elliptic duct. This new model is also much simpler than the models of Someswara et al. (1967), James (1970), and Richardson (1980) which all required complex numerical integrations. Richardson (1980) also provided a series approximation to avoid numerical integration. Equation (4.14) predicts the values of fRe for most ducts within $\pm$ 15 percent. An error of $\pm$15 percent in fRe will only result in an error of $\pm$ 5 percent in Nu. Thus, Eq. (4.25) will accurately predict the Nusselt number in the thermal entrance region for most of the ducts shown in Figs. 1.4 and 1.5, regardless of shape.

A model which is valid over the entire range of dimensionless duct lengths may be developed by combining Eq. (4.25) with Eq. (4.20) using the Churchill-Usagi (1972) asymptotic correlation method. The form of the proposed model is

$$Nu(z^*) = \left(\left\{ C_1 C_2 \left(\frac{fRe}{z^*} \right)^{\frac{1}{3}} \right\}^n + (Nu_{fd})^n \right)^{1/n} \tag{4.26}$$

Now using the result for the fully developed friction factor, Eq. (4.14), presented earlier, and the result for the fully developed flow Nusselt number, Eq. (4.20), developed earlier, a new model is proposed having the form:

$$Nu_{\sqrt{A}}(z^*) = \left[\left\{ C_1 C_2 \left(\frac{f Re_{\sqrt{A}}}{z^*_{\sqrt{A}}} \right)^{\frac{1}{3}} \right\}^5 + \left\{ C_3 \left(\frac{f Re_{\sqrt{A}}}{8\sqrt{\pi}\epsilon^{\gamma}} \right) \right\}^5 \right]^{\frac{1}{5}} \tag{4.27}$$

where the constants C_1, C_2, C_3 and γ are given in Table 4.8. These constants define the various cases for local or average Nusselt number and isothermal or isoflux boundary conditions. The above model is based upon the solutions for the elliptic duct geometry.

Table 4.8
Constants for Thermally Developing Flow Model

	Local	**Average**
C_1	1	1.5
	Isothermal (T)	**Isoflux (H)**
C_2	0.427	0.517
C_3	3.24	3.86
	Upper Bound	**Lower Bound**
γ	1/10	-3/10

Comparisons of this new model with data from Shah and London (1978) for the ducts summarized in Table 3.1 reveal that it predicts the numerical data for many geometries within ±20 percent. In order to provide a model which is more accurate for predicting the results of the geometries listed in Table 3.1, the constants C_2 and C_3 have been modified such that the predicted curve represents the mean value of similar geometries at each value of the aspect ratio $\epsilon = b/a$. The modified constants are summarized in Table 4.9. The accuracy of the model with the modified constants is improved to ± 12 percent with a few exceptions. Comparisons of this new model with predictions of the models of Yilmaz and Cihan (1993, 1995) are given in Table 4.10.

An optimal value of the correlation parameter n may be obtained for each geometry. In the interest of simplicity it has been chosen to be a constant without introducing significant error. Analysis of the available data has shown that the correlation parameter varies between 2.5 and 8 with an optimal value of $n \approx 5$ for all duct shapes. The proposed model is considerably simpler than that of Yilmaz and Cihan (1993, 1995) (see Table 3.2) and is valid for both boundary conditions (UWT or UWF) and for local and average conditions. In addition, to its simplicity, the new model is also more flexible, in that both thermal boundary conditions may be handled, whereas the models of Yilmaz and Cihan (1993, 1995) are different for each thermal boundary condition.

Table 4.9
Modified Constants for Thermally Developing Flow Model

	Local	**Average**
C_1	1	1.5
	Isothermal (T)	**Isoflux (H)**
C_2	0.409	0.501
C_3	3.01	3.66
	Upper Bound	**Lower Bound**
γ	1/10	-3/10

A comparison the proposed model with the available data (Shah and London, 1978) is presented in Figs. 4.25-4.27. Table 4.10 presents a summary of the maximum and minimum differences between the data and the proposed model. A comparison of the proposed model with the models of Yilmaz and Cihan (1993, 1995) is also presented in Table 4.10. Good agreement between the model and data is observed for all of the geometries except the isosceles triangular duct for the UWT boundary condition. In the case of the elliptic duct, no published data are available for comparison. However,

Table 4.10

Comparison of Percent Differences* Between Models and Data for Thermally Developing Flow

Geometry	$Nu^T_{\sqrt{A}}(z^*)$ (Average)		$Nu^H_{\sqrt{A}}(z^*)$ (Local)	
	Proposed Model	Yilmaz and Cihan (1993)	Proposed Model	Yilmaz and Cihan (1995)
Circle	-1.24/8.57	-0.47/-3.89	-1.60/5.27	-3.83/0.70
Rectangle $\epsilon = 1$	-7.53/-1.07	-3.52/0.58	-2.76/1.73	-3.95/4.80
Rectangle $\epsilon = 0.5$	-4.26/1.38	-0.86/4.16	-3.16/1.31	-4.1/0.24
Rectangle $\epsilon = 0.25$	3.01/10.85	0.54/7.43	1.80/7.01	0.44/8.20
Rectangle $\epsilon = 0.167$	3.84/11.86	3.32/1.59	-	-
Rectangle $\epsilon \rightarrow 0$	1.6/10.0	0.24/3.70	-9.93/7.03	-2.2/5.86
Isosceles Triangle $2\phi = 30°$	25.75/3.92	33.8/0.88	-	-
Isosceles Triangle $2\phi = 60°$	-12.11/-6.81	-4.36/-1.29	-7.24/-2.09	-4.79/-1.38
Isosceles Triangle $2\phi = 90°$	-24.45/1.56	-12.28/-1.97	-9.88/3.35	-3.72/0.76
Semi-Circle $\epsilon = 0.5$	-	-	-7.90/7.78	-0.91/8.83
†Ellipse $\epsilon = 0.9$	2.16/6.78	-	-1.25/4.74	-4.7/-1.2
†Ellipse $\epsilon = 0.8$	0.66/6.72	-2.66/-1.06	-1.71/2.91	-5.8/-0.8
†Ellipse $\epsilon = 0.6$	-1.17/-9.16	1.4/4.7	-1.43/-6.82	-

* %diff= $(Analytical - Predicted)/(Analytical) \times 100$

† Comparison of proposed model with results predicted by model of Yilmaz and Cihan (1993,1995)

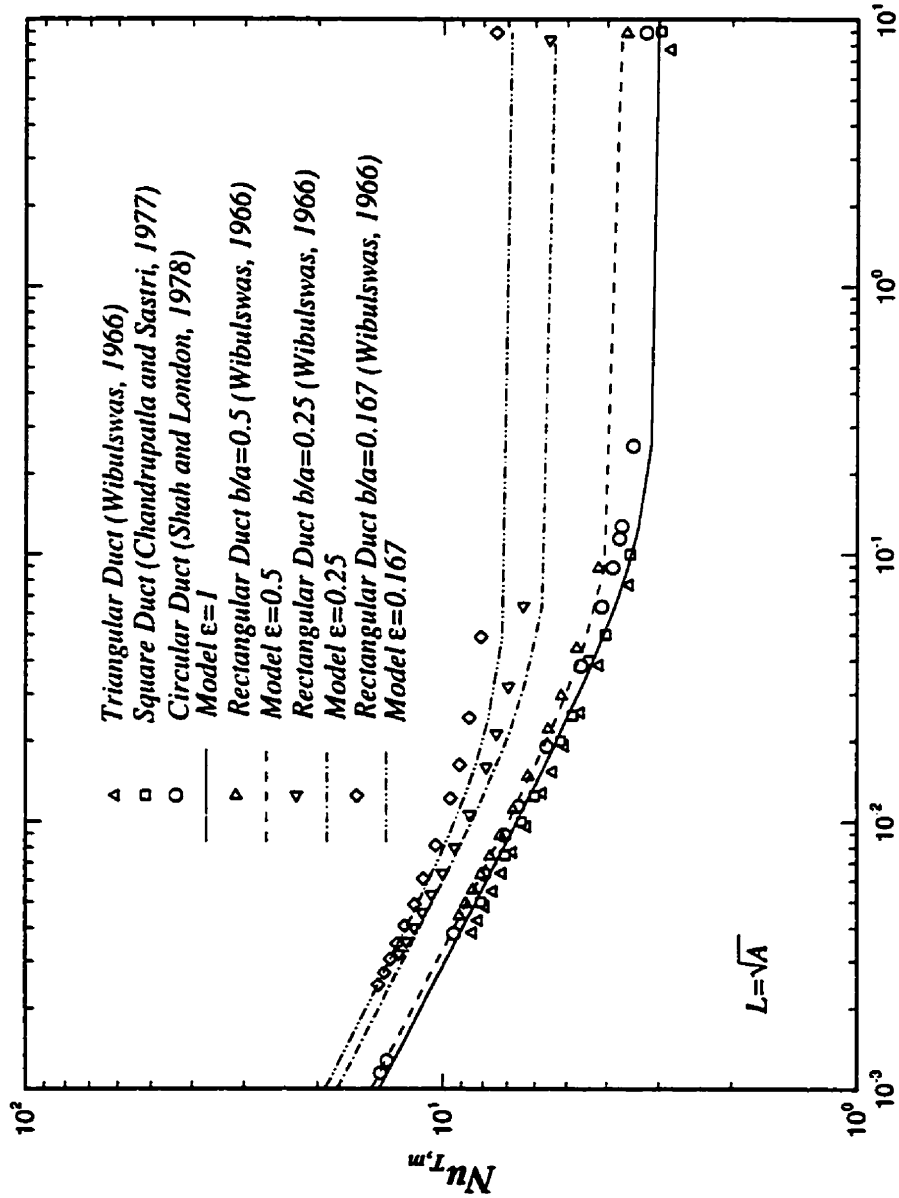

Fig. 4.25 - Thermally Developing Flow $Nu_{T,m}$.

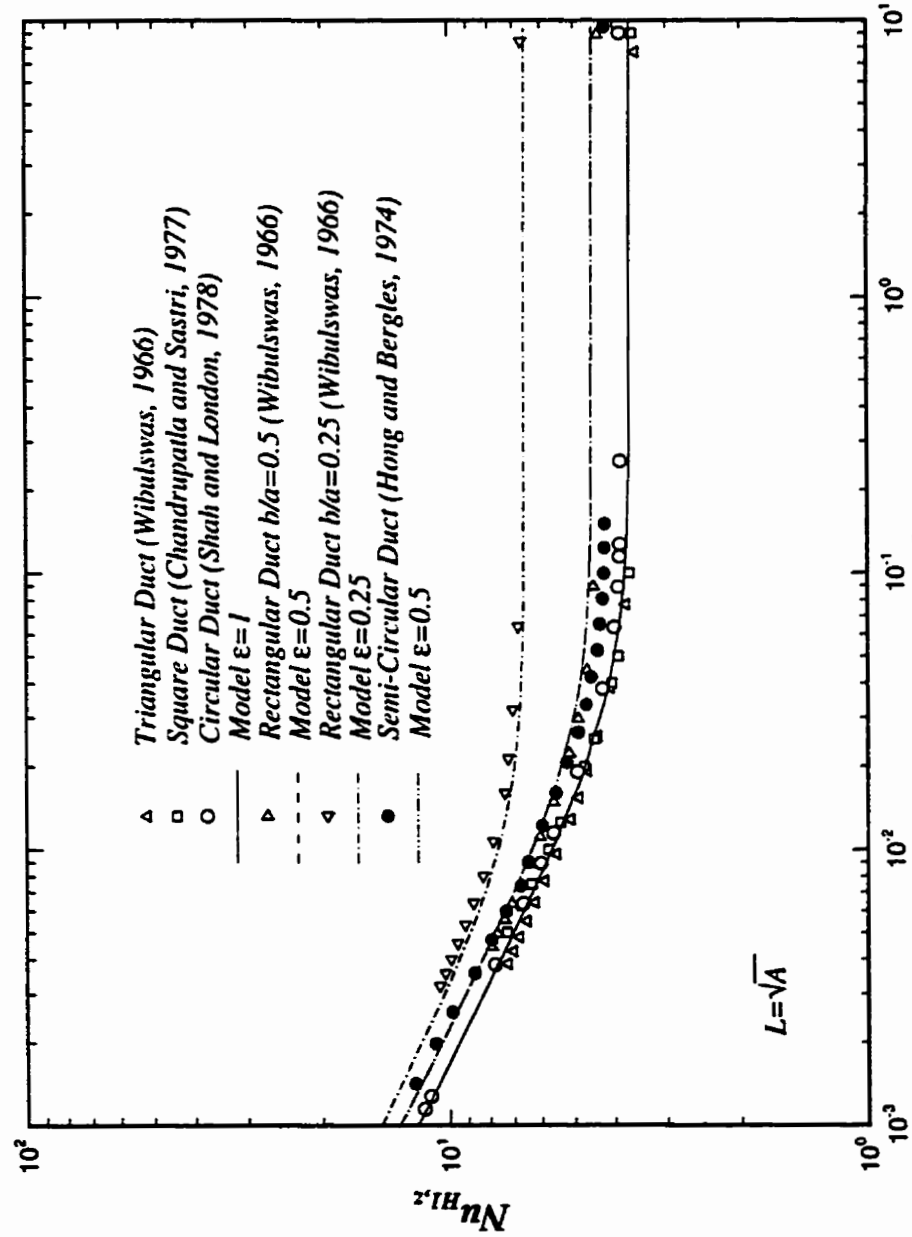

Fig. 4.26 - Thermally Developing Flow $Nu_{H1,z}$.

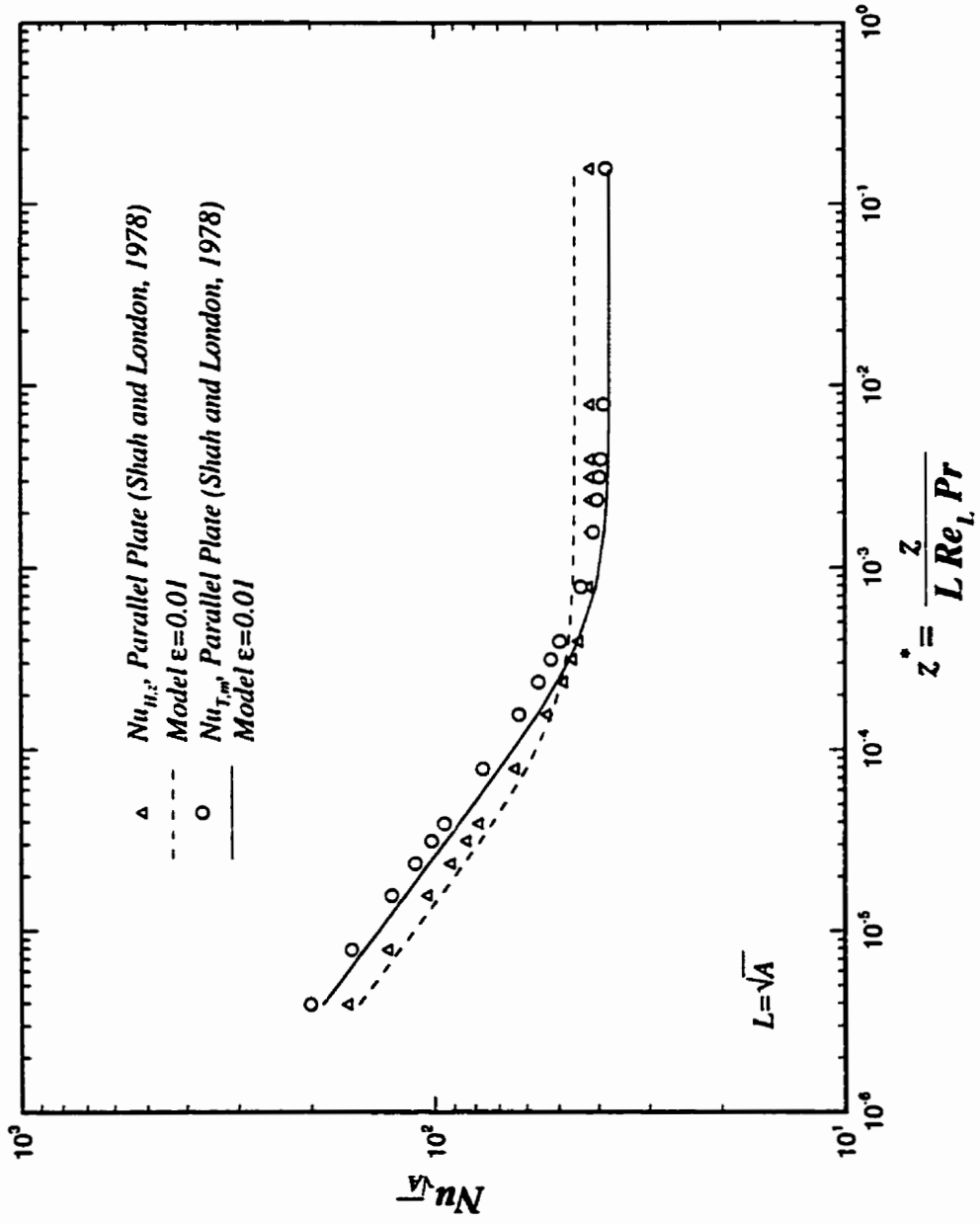

Fig. 4.27 - Thermally Developing Flow Between Parallel Plates

Yilmaz and Cihan (1993, 1995) provide comparisons of their model with their own unpublished numerical data. A comparison of the proposed model with that of Yilmaz and Cihan (1993, 1995) shows that good agreement should be obtained if direct comparison with their data were possible. Also, the proposed model is developed from asymptotic solutions for the elliptic duct. Thus the model is expected to provide very accurate results for the elliptic duct geometry. This particular geometry is extremely important in heat exchanger design where larger heat transfer coefficients are often desired without seriously compromising size and pressure drop constraints. A comparison with the data for the parallel plate channel is also provided. For this geometry $\sqrt{A} \rightarrow \infty$, however, this geometry is accurately approximated by the rectangular duct when $\epsilon = 0.01$. Good agreement is obtained with the current model when the parallel plate channel is modeled as a finite area duct with low aspect ratio. In all cases the proposed model provides equal or better accuracy than the models of Yilmaz and Cihan (1993, 1995) and is also much simpler. Finally, the proposed model is able to determine local or average Nusselt numbers, whereas the models of Yilmaz and Cihan (1993, 1995) were developed for the average Nusselt number (UWT) and local Nusselt number (UWF).

4.4.3 Nusselt Number (Combined Entrance)

The final problem analyzed in this Chapter is simultaneously developing flow or the combined entrance region. A model which is valid for most non-circular ducts may be developed using the same approach proposed by Churchill and Ozoe (1973a,b). Churchill and Ozoe (1973a,b) developed a model for the circular duct which is valid for all Prandtl numbers over the entire range of dimensionless duct lengths, by combining a composite model for the Graetz problem with a composite solution for the flat plate. In the combined entrance region, the boundary layer behaviour is very similar to flow over a flat plate as $z^* \rightarrow 0$.

A new model for the combined entrance region may be developed by combining the solution for a flat plate with the model for the Graetz flow problem developed earlier. The proposed model takes the form

$$y(z) = \left(\{y_{z\to 0}(Pr)\}^m + \{y_{z\to 0}^n + y_{z\to\infty}^n\}^{m/n} \right)^{1/m} \tag{4.28}$$

which is similar to that proposed by Churchill and Ozoe (1973a,b) for the circular duct. This model is a composite solution of three asymptotic solutions.

The solution for a flat plate (Schlichting 1979) may be compactly written as:

$$Nu_z = C_4 C_5 \sqrt{Re_z} Pr^{1/3} \tag{4.29}$$

where C_4 determines whether a local or average value is desired, and C_5 determines whether (UWT) or (UWF) is desired. The above result must now be converted to a form containing the dimensionless duct length z^* as the dependent variable. The resulting solution for any characteristic length $\mathcal{L}$ becomes:

$$Nu_{\mathcal{L}} = \frac{C_4 C_5}{\sqrt{z^*} Pr^{1/6}} \tag{4.30}$$

where C_4 takes a value of 1 (local) or 2 (average) and C_5 takes the value 0.332 (UWT) or 0.453 (UWF).

Based upon comparisons with available data, the solution given above may be combined with the earlier model for the Graetz problem, Eq. (4.27). This results in the following model for simultaneously developing flow in a duct of arbitrary cross-sectional shape

$$Nu_{\sqrt{A}}(z^*) = \left[\left(\left\{C_1C_2\left(\frac{fRe_{\sqrt{A}}}{z^*_{\sqrt{A}}}\right)^{\frac{1}{3}}\right\}^5 + \left\{C_3\left(\frac{fRe_{\sqrt{A}}}{8\sqrt{\pi}\epsilon^\gamma}\right)\right\}^5\right)^{m/5} + \left\{\frac{C_4C_5}{\sqrt{z^*_{\sqrt{A}}}Pr^{1/6}}\right\}^m\right]^{1/m} \tag{4.31}$$

The parameter m was determined to vary between 3 and 6 with an optimal value of $m \approx 5$ for all duct shapes. The above model is valid for $0.1 < Pr < \infty$ which is typical for most low Reynolds number flow heat exchanger applications.

Comparisons with the available data are provided in Tables 4.11 and 4.15 which summarize the RMS value and the (min/max) range of the error. Good agreement is obtained with the data for the circular duct and parallel plate channel. Note that comparison of the model for the parallel plate channel was obtained by considering a rectangular duct having an aspect ratio of $\epsilon = 0.01$. Good agreement is also obtained for the case of the square duct for all Prandtl numbers. Comparison of the model with data for the rectangular duct at various aspect ratios, Table 4.14, and two triangular ducts, Table 4.15, shows that larger errors arise. The data used for comparison in Tables 4.14 and 4.15 were obtained by Wibalswas (1966). In this work, the effects of transverse velocities in both the momentum and energy equations were ignored. Comparison of the data for the square duct at $Pr = 1.0$ obtained by Chandrupatla and Sastri (1978) which includes the effects of transverse velocities with the data of Wibulswas (1966) for $Pr = 0.72$ shows that the discrepancy is likely due to the data and not the model.

The accuracy for each case may be improved by obtaining the optimal value of the parameter m. However, this introduces an additional parameter into the model which is deemed unnecessary for purposes of heat exchanger design. The proposed model predicts most of the available data for the combined entry problem to within ± 15

percent and may be used to predict the heat transfer characteristics for other non-circular ducts for which there are presently no data.

Table 4.11

Comparison of Model with Data for Circular Duct

RMS and (min/max)

Pr	$Nu_{z,T}$	$Nu_{m,T}$	$Nu_{z,H}$
0.7	1.98 (-4.53/1.48)	5.29 (-14.14/5.15)	5.39 (-0.08/6.70)
2.0	4.60 (-7.37/-0.08)	7.22 (-17.65/-0.60)	4.34 (-0.61/6.27)
5.0	6.56 (-10.5/-0.07)	11.04 (-24.26/-0.60)	2.55 (-2.09/4.69)

Table 4.12

Comparison of Model with Data for Parallel Plate Channel

RMS and (min/max)

Pr	$Nu_{m,T}$	$Nu_{z,H}$
0.1	9.76 (-17.93/10.14)	N/A
0.7	5.27 (-4.37/7.76)	3.29 (-1.39/8.92)
2.0	3.88 (-0.03/6.44)	2.82 (-1.69/7.48)
5.0	4.28 (-2.81/12.3)	2.08 (-0.43/4.50)

Table 4.13

Comparison of Model with Data for Square Duct

RMS and (min/max)

Pr	$Nu_{z,H}$	$Nu_{m,H}$
0.1	12.71 (-0.20/15.08)	8.55 (-6.91/16.56)
1.0	2.47 (-2.30/4.67)	3.29 (-3.26/5.47)
10	2.50 (-4.22/-0.18)	2.82 (-3.63/3.07)

Table 4.14

Comparison of Model with Data for Rectangular Duct $Pr = 0.72$

RMS and (min/max)

$\epsilon = b/a$	$Nu_{m,T}$	$Nu_{z,H}$	$Nu_{m,H}$
1	12.88 (-17.68/1.13)	12.63 (-0.182/15.97)	6.19 (-1.39/16.20)
1/2	10.70 (-15.55/5.56)	12.40 (-0.11/15.90)	6.86 (-0.84/16.25)
1/3	9.09 (-13.74/7.40)	11.15 (-0.05/15.63)	7.46 (-0.37/14.96)
1/4	7.55 (-11.92/6.79)	11.00 (-0.04/15.67)	7.99 (-0.29/14.97)

Table 4.15

Comparison of Model with Data for Triangular Ducts $Pr = 0.72$

RMS and (min/max)

$Nu_{z,T}$	$Nu_{m,T}$	$Nu_{z,H}$	$Nu_{m,H}$
	Equilateral Triangle		
4.92 (-9.57/3.63)	10.89 (-17.96/0.75)	5.64 (-0.35/7.79)	2.77 (-3.63/9.05)
	Isosceles Right Triangle		
14.09 (-18.21/-0.53)	31.36 (-43.28/-3.985)	15.21 (-0.42/22.09)	7.88 (-16.23/20.07)

4.4.4 Hydrodynamic and Thermal Entrance Lengths

The hydrodynamic entrance length is traditionally defined as the point where the centerline velocity is equal to $0.99\,w_{max}$, whereas the thermal entrance length is defined as the point where the local Nusselt number is $1.05\,Nu_{fd}$, Shah and London (1978). New definitions for the thermal and hydrodynamic entrance lengths may be obtained from the proposed models. The new entrance lengths are defined as the value of z^+ and z^* where the value of $fRe_{\sqrt{A}}$ and $Nu_{\sqrt{A}}$ are five percent greater than the fully developed limit.

The resulting equations for the hydrodynamic and thermal entrance regions are:

$$z^+_{\sqrt{A}} = 0.9308\,\epsilon \left(\frac{\mathbf{E}(\sqrt{1-\epsilon^2})}{(1+\epsilon^2)} \right)^2 = \frac{L_{hy}}{\sqrt{A}\,Re_{\sqrt{A}}} \tag{4.32}$$

for the hydrodynamic entrance length, and

$$z^*_{\sqrt{A}} = 49.736\,\epsilon^{(2+3\gamma)} \left(\frac{C_1\,C_2}{C_3} \right)^3 \left(\frac{\mathbf{E}(\sqrt{1-\epsilon^2})}{(1+\epsilon^2)} \right)^2 = \frac{L_{th}}{\sqrt{A}\,Pr\,Re_{\sqrt{A}}} \tag{4.33}$$

for the thermal entrance length.

These equations predict the length of the duct for which entrance effects are negligible. The conventional definitions given by Eqs. (2.29) and (2.30) are also referred to as settling lengths (Shah and London, 1978). The alternative definitions proposed above, define the region of influence of the hydrodynamic and thermal entrance regions. If a duct is shorter than the lengths predicted by Eqs. (4.32) and (4.33), entrance effects will be significant.

The equations given above reduce to $z^+ \approx 0.57$ and $z^* \approx 0.077$ for the circular duct. The larger value of the hydrodynamic entrance length as compared to Eq. (2.29) is a result of the new definition. Note that Eq. (4.32) cannot be used to predict the point

where hydrodynamic boundary layers merge, since it is based upon the average value of the *apparent* friction factor. However, it may be used to determine an approximate value by considering the local value of the *apparent* friction factor by dividing by a factor of four. This is a result of a change in the coefficient 3.44 in Eq. (4.22) to 1.72. This gives $z^+ \approx 0.14$, which is approximately three times the accepted value of $z^+ \approx 0.056$.

4.5 Summary

The models developed in this Chapter for the plain duct geometries are summarized below. These models may be used to predict the heat transfer and fluid friction characteristics for the geometries summarized in Table 3.1 provided that the smallest corner angle is greater than 15 degrees. The models provide an accuracy of ± 12 percent for the FDF, TFDF, TDF, HDF problems and an accuracy of ± 15 percent for the SDF problem.

Fully Developed Flow (FDF) Model, $z^+ \to \infty$

$$fRe_{\sqrt{A}} = 8\sqrt{\pi}\left(\frac{\pi}{4}\frac{(1+\epsilon^2)}{\sqrt{\epsilon}\,\mathbf{E}(\sqrt{1-\epsilon^2})}\right) \tag{4.34}$$

Hydrodynamically Developing Flow (HDF) Model, $z^+ > 0$

$$f_{app}Re_{\sqrt{A}} = \left[\left\{\frac{3.44}{\sqrt{z^+_{\sqrt{A}}}}\right\}^2 + \left\{fRe_{\sqrt{A}}\right\}^2\right]^{1/2} \tag{4.35}$$

Thermally Fully Developed Flow (TFDF) Model, $z^+ \to \infty$, $z^* \to \infty$

$$Nu_{\sqrt{A}} = C_2\left(\frac{fRe_{\sqrt{A}}}{8\sqrt{\pi}\epsilon^\gamma}\right) \tag{4.36}$$

Thermally Developing Flow (TDF) Model, $z^+ \to \infty$, $z^* > 0$

$$Nu_{\sqrt{A}}(z^*) = \left[\left\{ C_1 C_2 \left(\frac{f Re_{\sqrt{A}}}{z^*_{\sqrt{A}}} \right)^{\frac{1}{3}} \right\}^5 + \left\{ C_3 \left(\frac{f Re_{\sqrt{A}}}{8\sqrt{\pi}\epsilon^\gamma} \right) \right\}^5 \right]^{\frac{1}{5}} \tag{4.37}$$

Simultaneously Developing Flow (SDF) Model, $z^+ > 0$, $z^* > 0$

$$Nu_{\sqrt{A}}(z^*) = \left[\left\{ C_1 C_2 \left(\frac{f Re_{\sqrt{A}}}{z^*_{\sqrt{A}}} \right)^{\frac{1}{3}} \right\}^5 + \left\{ C_3 \left(\frac{f Re_{\sqrt{A}}}{8\sqrt{\pi}\epsilon^\gamma} \right) \right\}^5 + \left\{ \frac{C_4 C_5}{\sqrt{z^*_{\sqrt{A}}} Pr^{1/6}} \right\}^5 \right]^{\frac{1}{5}} \tag{4.38}$$

where the constants C_1, C_2, C_3, C_4, C_5 and γ are defined in Table 4.16.

Table 4.16

Constants for Thermally Developing Flow Models in Non-Circular Ducts

	Local	Average
C_1	1	1.5
	Isothermal (T)	**Isoflux (H)**
C_2	0.409	0.501
C_3	3.01	3.66
	Local	**Average**
C_4	1	2
	Isothermal (T)	**Isoflux (H)**
C_5	0.332	0.453
	Upper Bound	**Lower Bound**
γ	1/10	-3/10

Chapter 5

Experimental Procedures and Results

5.1 Introduction

This chapter discusses all aspects related to the experimental measurement of the j and f characteristics for various compact heat exchanger surfaces. In the sections which follow details of the experimental program, test facility, experimental procedure, data reduction procedures, experimental uncertainty, and test results are presented.

5.2 Experimental Program

The experimental program consists of two phases. In the first phase, the test fixture is analyzed to develop pressure loss correlations for reducing friction factors and to compare experimentally measured heat transfer coefficients with theoretical predictions. In the second phase, the Fanning friction factor f and Colburn factor j are determined from experimental measurements for ten plate fin arrangements. Each device is classified by orientation in the flow field (HPD) and fin pitch/type (CPI or SQ). The important surface parameters which are required in the data reduction

procedures are defined in Table 5.1. Surface and geometrical parameters for each of these devices are summarized in Tables 5.2 and 5.3. These parameters were determined using the program *Turb v3.1* developed by Long Manufacturing, (Lemczyk, 1997).

5.3 Experimental Facility and Procedure

An experimental facility for measuring the heat transfer and pressure drop characteristics of thermal enhancement devices was originally designed and assembled by Long Manufacturing Inc. of Oakville, Ontario, (Morely, 1996). The experiment was later transferred to the University of Waterloo and subsequently redesigned to provide a larger test core and symmetric cooling (Morely, 1997). Figure 5.1 presents a schematic of the experimental facility. Figure 5.2 shows the heat exchanger experiment. In the sections which follow details of the test fixture, test fluids, and sensors are discussed.

Table 5.1

Defintion of Surface Parameters

Parameter	Definition
Area Enhancement Ratio	$AER = \frac{A_{total}}{2(WL)_{channel}}$
Fin Area Ratio	$FAR = \frac{A_{fin}}{A_{total}}$
Entrance Reduction Ratio	$ERR = \frac{A_{free}}{HW}$
Fin Length	S_o
Hydraulic Diameter	$d_h = \frac{4V_{free}}{A_{surface}}$

Table 5.2

Summary of Surface Characteristics

Type	Designation	Material	AER	FAR	ERR	S_o $[mm]$	d_h $[mm]$
HPD	CPI-1	Aluminum	1.916	0.4783	0.8769	2.225	2.231
HPD	CPI-2	Aluminum	1.921	0.4190	0.8769	2.225	2.484
HPD	CPI-3	Aluminum	2.383	0.5804	0.8953	1.815	1.822
HPD	CPI-4	Brass	2.080	0.5194	0.8869	1.731	2.068
HPD	CPI-5	Brass	2.417	0.5863	0.8869	1.850	1.780
HPD	SQ-1	Aluminum	2.049	0.6319	0.9167	3.223	2.729
HPD	SQ-2	Aluminum	1.984	0.6223	0.9089	3.111	2.556
HPD	SQ-3	Aluminum	1.899	0.6096	0.8963	2.968	2.312
HPD	SQ-4	Aluminum	2.457	0.5931	0.9091	2.361	2.067
HPD	SQ-5	Aluminum	2.441	0.5904	0.9091	2.361	2.081

Table 5.3

Summary of Surface Dimensions†

Designation	H [mm]	λ [mm]	W [mm]	θ [deg]	t [mm]
CPI-1					
CPI-2					
CPI-3					
CPI-4					
CPI-5					
SQ-1					
SQ-2					
SQ-3					
SQ-4					
SQ-5					

$$4\,mm < \lambda < 12\,mm$$

$$20° < \theta < 90°$$

$$2\,mm < H < 3.5\,mm$$

$$1\,mm < W < 2\,mm$$

† Proprietary data. Only available from Long Manufacturing Inc.

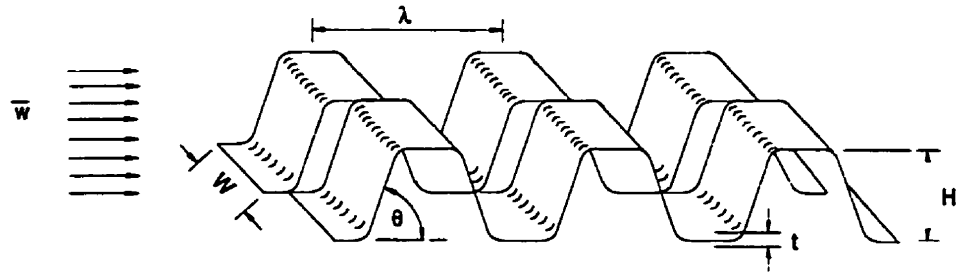

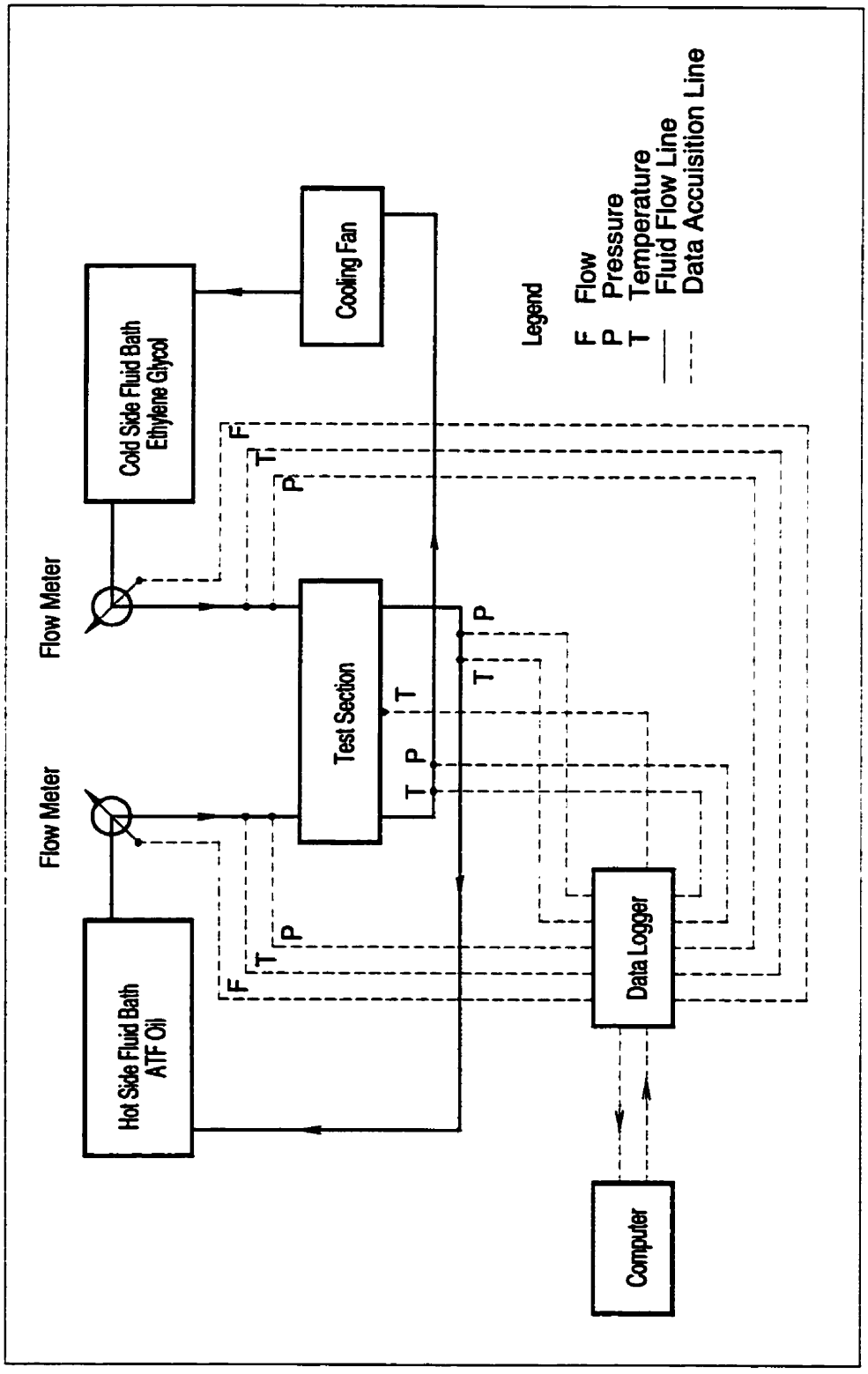

Fig. 5.1 - Schematic of Experimental Facility.

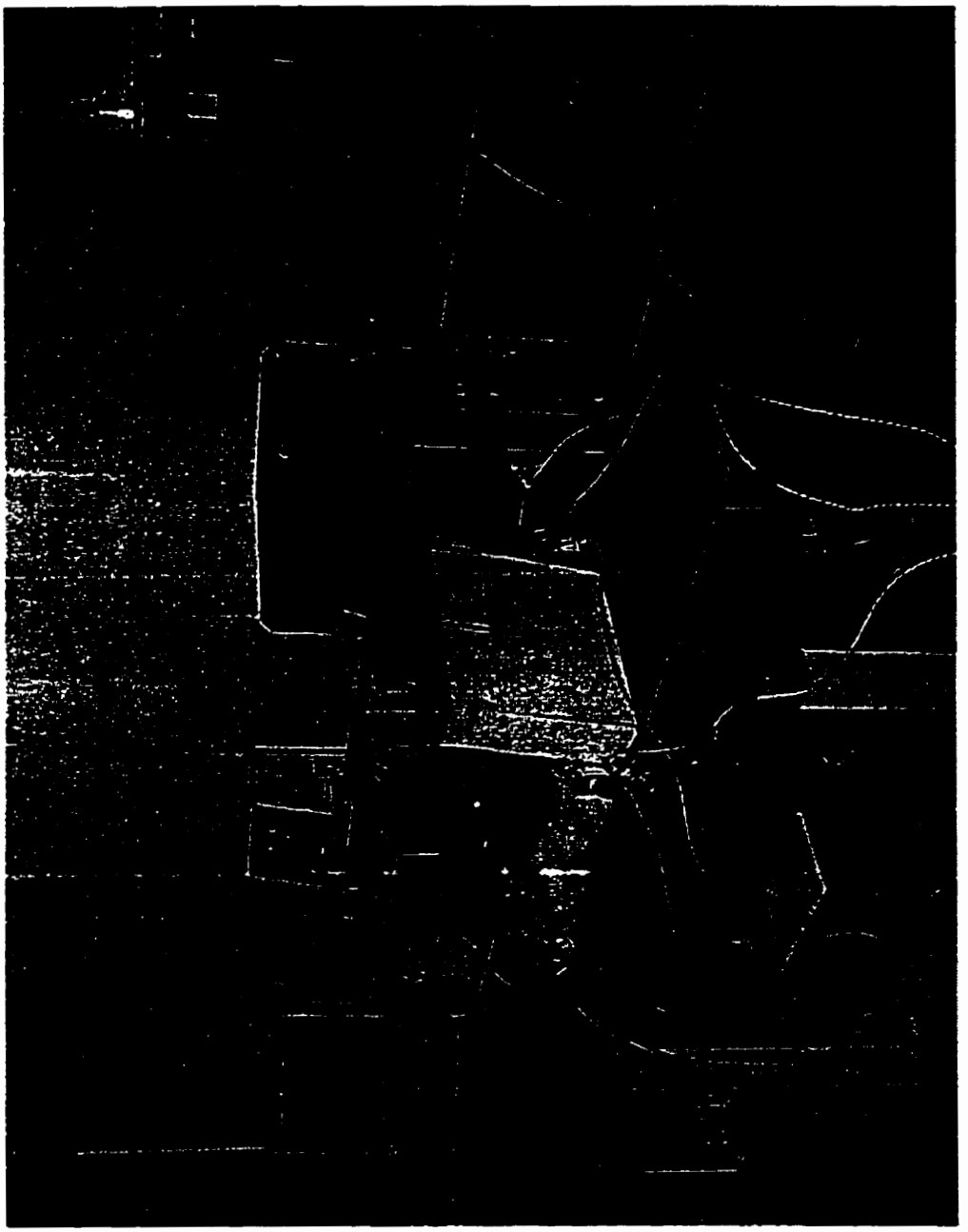

Fig. 5.2 - Waterloo Heat Exchanger Experiment.

5.3.1 Test Fixture

The test fixture is constructed from aluminum and is based upon a single pass shell and tube heat exchanger configuration. The test fixture may be operated in either a parallel flow or counterflow arrangement. The test core contains four channels, 11 inches in length and 1 inch in width, for placing plate fins. Various test cores have been machined which allow a variety of different plate fin heights to be tested. Automatic transmission oil was used as the working fluid and a 50 percent ethylene glycol and 50 percent water mixture was used as the coolant. Details of the test fixture are provided in Appendix B.

5.3.2 Fluid Baths

The experimental facility uses two *Lauda K20* variable flow rate constant temperature baths providing volumetric flow rates up to 5 gpm (330 cm^3/s). Flow in each bath is regulated by a pressure/suction pump. Each bath is equipped with a 1500 W heater allowing temperatures up to 250 $^\circ C$ to be obtained. The test fluid was Dexron III automatic transmission oil (Type H), while the coolant consisted of a 50 percent water and 50 percent ethylene glycol mixture. Each fluid bath may hold 18 L of fluid. An auxiliary cooler is connected in the coolant loop to prevent overheating of the coolant.

Oil and coolant properties have been obtained from the manufacturers by Long Manufacturing for a wide range of temperatures (Lemczyk and Molloy, 1996). These properties have been correlated to provide accurate interpolation of fluid properties. The required fluid property correlations are given below.

Type H Transmission Oil

$$\log_{10}(\mu) = 198.598 - 29.6011\,T^{1/2} + 1.46836\,T - 0.0245473\,T^{3/2} \tag{5.1}$$

$$\rho = 1159.7 - 11.0605\,T^{1/2} - 0.359005\,T \tag{5.2}$$

$$k = 0.178947 - 0.00267278\,T^{1/2} - 6.5788 \times 10^{-6}\,T \tag{5.3}$$

$$c_p = 237.467 + 66.7114\,T^{1/2} + 1.73041\,T \tag{5.4}$$

50-50 Ethylene Glycol - Water

$$\mu^{1/3} = 3.23858 - 0.310287\,T^{1/2} + 0.00761038\,T \tag{5.5}$$

$$\rho = 1416.3 - 22.2397\,T^{1/2} + 0.0703129\,T \tag{5.6}$$

$$k = -1.12878 + 0.151667\,T^{1/2} - 0.0035556\,T \tag{5.7}$$

$$c_p = 4302.06 - 186.873\,T^{1/2} + 7.45361\,T \tag{5.8}$$

The units for each property are μ $[kg/m \cdot s]$, ρ $[kg/m^3]$, k $[W/m \cdot K]$, and C_p $[J/kg \cdot K]$. Temperatures are specified in Kelvin $[K]$. Fluid properties are evaluated at the average value of the inlet and outlet temperatures for each fluid.

5.3.3 Temperature Measurement

Temperature measurements are obtained using four copper/constantan thermocouples. Temperatures are measured at the inlets and outlets of the test fixture. Each thermocouple was checked at various temperatures using a constant temperature bath and an ice/water mixture. Temperature measurement was determined to be accurate to $\pm$ 0.05 $°C$. Thermocouples were selected in pairs to ensure that the same temperature bias is measured to provide greater accuracy in the measurement of temperature differences. Temperature differences where determined to be measurable to within $\pm$0.1°C.

5.3.4 Pressure Measurement

Pressure measurements are obtained using two *XPro* pressure transducers. The pressure transducer on the upstream oil side is rated for 0-25 psig while the downstream pressure transducer is rated for 0-50 psia. It is necessary to measure absolute pressure on the downstream side since the *Lauda* baths are equipped with a pressure/suction

pump which produces a vacuum pressure on the downstream side at larger flow rates. Atmospheric pressure is measured using an aneroid barometer. Each transducer was calibrated using a dead weight tester. The results of the calibration were then fit using a linear regression analysis. Deviation of predicted results from measured results is less than ±1 percent.

5.3.5 Flow Measurement

Fluid flow rates are measured using two *Hoffer* flow meters with signal conditioners. Flow measurement is limited to the linear range of 0.75 gpm (47 cm^3/s) to 7.5 gpm (470 cm^3/s). The maximum flow rate obtainable with the test fixture is 2.25 gpm (140 cm^3/s). The flow meters were calibrated by Long Manufacturing using a mass flow meter for both test fluids. Calibration results were fit using a linear regression analysis. Deviation of predicted results from measured results is less than ±1 percent. Agreement between the two flow meters was found to be accurate within ±2 percent when both meters are connected in series.

5.3.6 Data Acquisition System

Data acquisition is fully automated using a *Campbell 21X* data logger attached to a personal computer. Real time monitoring of all measurements is displayed at all times. In addition, the instantaneous heat transfer rate in each fluid is displayed to determine when steady state conditions are reached. Data collection is operator initiated and a total of 60 data points are collected over a 3 minute interval. Average values of the 60 data points are then used in the data reduction procedures.

5.3.7 Specimen Preparation

Turbulator strip fin specimens are cut into 11 inch (27.94 cm) by 1 inch (2.54 cm) strips. A total of four specimens are required in the test core. In some instances it

is not possible to obtain a continuous specimen due to production dimensions. In these cases, two or three pieces are required to obtain the required test length. A set of four test plates have been machined to accommodate turbulator strip fins of various heights. Each set of plates is machined with a small interference to ensure good contact of the fin surfaces with the channel walls.

5.3.8 Test Procedure

After specimens were cut they were placed inside the test fixture and the fixture was checked for leaks. The fixture was then well insulated and each fluid was heated to an appropriate temperature. Tests were conducted with oil inlet temperatures of 115 $°C$ and 85 $°C$, while the coolant temperatures were initially set to 85 $°C$ and 65 $°C$, respectively. After each bath had reached its initial temperature level, the coolant flow rate was set to full flow and the oil flow rate was set to a starting flow rate of 30 cm^3/s. Conditions were then allowed to reach steady state before data acquisition began. The oil flow rate was then increased by 5 cm^3/s increments and the procedure repeated until the maximum oil flow rate was reached. Two tests were conducted at each oil inlet temperature to ensure repeatability.

5.4 Data Reduction

Experimental values for the Colburn j factor and the Fanning friction factor f are determined from the measurements of inlet and outlet temperatures, pressures, and volumetric flow rates. The friction factor f and Colburn factor j data are usually plotted versus the Reynolds number $Re_{d_h} = \frac{\overline{w} d_h}{\nu}$. The data reduction procedure has been programmed using the symbolic programming language of the Maple V4 mathematics package. The data reduction code is provided in Appendix C.

5.4.1 Friction Factor

Measurement of the friction factor may be conducted at the same time as the heat transfer measurements or separately using an isothermal fluid. If the friction factor is measured at the same time as the heat transfer coefficient it is referred to as a "hot" friction factor. Experimental values for "hot" friction factors should be the same as those measured using isothermal fluids if the effects of viscosity are not large or are taken into account when computing friction factors (Shah, 1985).

Pressure drop characteristics in the heat exchanger core are usually presented in terms of the Fanning friction factor f. They are related by the following expression (Shah, 1985)

$$f = \frac{d_h \rho_m}{4L}\left[\frac{\Delta p}{\frac{1}{2}\rho_m^2 \overline{w}^2} - \frac{1}{\rho_i}(1-\sigma^2+K_c) - 2\left(\frac{1}{\rho_o}-\frac{1}{\rho_i}\right) + \frac{1}{\rho_o}(1-\sigma^2-K_e)\right] \quad (5.9)$$

where Δp is the pressure drop in the core, L the core length, $\overline{w}$ is the average velocity based upon the minimum free flow frontal area, K_e and K_c are expansion and contraction loss coefficients at the entrance and exit of the core, and $\sigma = A_{free}/A_{front}$. Entrance and exit losses are significant for low values of σ and L and at high Reynolds numbers, for liquids at low Reynolds numbers the entrance and exit losses are negligible (Shah, 1985). If the temperature difference between the inlet and outlet is not large, then the fluid densities are approximately equal to the mean density ($\rho_i \approx \rho_o \approx \rho_m$), and the expression for the Fanning friction factor simplifies

$$f = \frac{d_h}{4L}\left[\frac{\Delta p}{\frac{1}{2}\rho_m \overline{w}^2} - K_c - K_e\right] \quad (5.10)$$

In obstructed flow applications such as flow normal to tube banks and flow through matrix or interrupted surfaces, entrance and exit loss effects are accounted for in the friction factor (Kays and London, 1984). Thus the definition of the friction factor simplifies with $K_e = 0$ and $K_c = 0$:

$$f = \frac{d_h}{4L}\left[\frac{\Delta p_{core}}{\frac{1}{2}\rho_m \overline{w}^2}\right] \tag{5.11}$$

where Δp_{core} is the total pressure drop across the heat exchanger core. It is related to the experimentally measured pressure drop across the test fixture by the following relation

$$\Delta p_{core} = \Delta p_{measured} - \Delta p_{losses} \tag{5.12}$$

Expressions for Δp_{losses} are developed in a later section. These expressions account for pressure losses due to the fluid hoses, pipe fittings, and manifolds. The experimentally measured friction factor then includes the effects of skin friction, profile drag, and local flow contraction and expansion losses within the finned surface.

5.4.2 Heat Transfer Coefficient

The average heat transfer rate may be determined from the experimental measurements by the following equation

$$\overline{Q} = \frac{(\dot{m}\, c_p\, \Delta T)_{hot} + (\dot{m}\, c_p\, \Delta T)_{cold}}{2} \tag{5.13}$$

where c_p is the heat capacity, $\dot{m}$ is the mass flow rate, and ΔT is the difference between inlet and outlet temperatures of the hot and cold fluids. The agreement between hot and cold side heat transfer rates was found to vary between $\pm$ 7.5 percent with an RMS value of 4-7 percent. This difference is likely due to the fact that the fluid properties defined by Eqs. (5.1-5.8) were obtained for similar fluids and not the actual fluids used in the experiments.

The overall heat transfer coefficient may be obtained from either a log mean temperature difference (LMTD) approach or an $\epsilon - NTU$ approach for a counterflow heat exchanger. Both approaches are discussed below.

The UA product is obtained from the average heat transfer rate $\overline{Q}$ and LMTD through

$$UA_{oil} = \frac{\overline{Q}}{\Delta T_{LMTD}} \tag{5.14}$$

where A_{oil} is the total inner surface area and ΔT_{LMTD} is the log mean temperature difference for the counterflow arrangement given by

$$\Delta T_{LMTD} = \frac{(T_{h,i} - T_{c,o}) - (T_{h,o} - T_{c,i})}{\ln\left(\frac{T_{h,i} - T_{c,o}}{T_{h,o} - T_{c,i}}\right)} \tag{5.15}$$

Alternatively, the overall heat transfer coefficient may be obtained using the $\epsilon - NTU$ approach. In this approach the effectiveness ϵ is defined by

$$\epsilon = \frac{\overline{Q}}{Q_{max}} = \frac{C_h(T_{h,i} - T_{h,o})}{C_{min}(T_{h,i} - T_{c,i})} \tag{5.16}$$

where $C_h = \dot{m}_h c_{p,h}$ and C_{min} is the lower of C_h or $C_c = \dot{m}_c c_{p,c}$. For a counterflow heat exchanger the $\epsilon - NTU$ relationship is

$$NTU = \frac{1}{1 - C_r} \ln\left(\frac{1 - \epsilon C_r}{1 - \epsilon}\right) \tag{5.17}$$

where $C_r = C_{min}/C_{max}$. Finally, the UA product is related to the number of transfer units (NTU) by

$$UA_{oil} = C_{min} NTU \tag{5.18}$$

The average heat transfer coefficient for the enhanced surface is related to the UA product through the following expression:

$$\frac{1}{UA_{oil}} = \frac{1}{\eta_o h_{oil} A_{oil}} + \frac{t_w}{A_w k_w} + \frac{1}{h_{cool} A_{cool}} \tag{5.19}$$

where A_{cool} is the coolant side or outer surface area, t_w is the thickness of the channel wall, k_w is the thermal conductivity of the channel wall, and η_o is the overall surface efficiency of the plate fin defined by

$$\eta_o = 1 - \frac{A_{fin}}{A_{total}}(1 - \eta_f) \tag{5.20}$$

The fin efficiency η_f may be computed using the definition for a straight fin (Kern and Kraus, 1972)

$$\eta_f = \frac{\tanh(mS_o)}{mS_o} \tag{5.21}$$

where $m = \sqrt{2h_{oil}/k_f t_f}$, S_o is the effective fin length, k_f is the thermal conductivity of the fin, and t_f is the thickness of the fin. This approach requires a numerical solution to compute the heat transfer coefficient h_{oil}, otherwise an iterative scheme may be used to determine the heat transfer coefficient.

The value of h_{cool} as a function of Reynolds number Re and Prandtl number Pr is determined in the next section. It was found that coolant side heat transfer coefficient varied very little (less than 10 percent) for each set of experiments, since the conditions on the coolant side remained approximately constant.

Experimental results for the average heat transfer coefficient are often written in terms of the Nusselt number

$$Nu_{d_h} = \frac{h_{oil} d_h}{k} \tag{5.22}$$

or the Colburn j factor defined as

$$j = \frac{Nu_{d_h}}{Re_{d_h} Pr^{1/3}} \tag{5.23}$$

where d_h is the hydraulic diameter of the enhanced channel.

5.4.3 Temperature Dependent Properties

The effect of temperature on fluid properties may be accounted for using equations provided by Webb (1994) for case where the test fluids are liquids. The constant property values of the Nusselt number and friction factor are related to the temperature dependent values through

$$\frac{Nu}{Nu_{cp}} = \left(\frac{\mu_w}{\mu_m}\right)^n \tag{5.24}$$

and

$$\frac{f}{f_{cp}} = \left(\frac{\mu_w}{\mu_m}\right)^m \tag{5.25}$$

where $n = -0.14$ for both heating and cooling and $m = 0.58$ for heating and $m = 0.54$ for cooling. The wall viscosity is calculated using an appropriate value of the wall temperature which may be determined from the following expression (Shah, 1985)

$$T_w = \frac{T_h/R_h + T_c/R_c}{1/R_h + 1/R_c} \tag{5.26}$$

where R_h and R_c are the hot and cold side film resistances, respectively.

Since temperature drops for each fluid are small, bulk values for the properties remain approximately constant. The viscosity correction factors for the present experimental results were determined to be on the order of 5 percent or less, due to the small temperature differences.

5.5 Thermal Characterization of Test Fixture

As part of the experimental program, the test fixture was tested without enhancement devices to provide a benchmark for the accuracy of the experiment, determine the pressure losses associated with the inlet and exit manifolds, and to determine a correlation for the coolant side heat transfer coefficient. Details of these experiments are presented in the sections which follow.

5.5.1 Coolant Side Heat Transfer Coefficient

In liquid-liquid heat exchangers the hot and cold side fluid resistances are of the same order of magnitude. If both resistances are to be determined from experimental measurements and one of the resistances remains constant while the other varies. the Wilson plot or modified Wilson plot techniques (Briggs and Young (1969), Shah (1985), Shah (1990), Khartabil and Christensen (1992)) may be employed to determine both fluid resistances. The procedure of Khartabil and Christensen (1992) is summarized below as it is the most general procedure for determining heat transfer coefficients using a non-linear least squares regression analysis. It reduces to a simple linear regression analysis if the exponent a in Eq. (5.27) is known a priori.

Beginning with the definition of the overall heat transfer coefficient Eq. (5.19), a model is proposed for the heat transfer coefficient on the unknown side in the form of

$$Nu_{D_h} = C_1 Re^a Pr^{1/3} = \frac{hD_h}{k} \tag{5.27}$$

The proposed model is then substituted into the definition of the overall heat transfer coefficient

$$\frac{1}{UA} = \frac{1}{C_1 Re^a Pr^{1/3}(Ak/D_h)} + C_2 \tag{5.28}$$

where C_2 represents the wall conduction resistance and film resistance which is constant and may be known or unknown.

Applying the method of least squares to Eq. (5.28) requires minimizing

$$S = \sum_{i=1}^{n} \left[\left(\frac{1}{UA}\right)_i - \frac{1}{C_1 Re_i^a [Pr^{1/3}(Ak/D_h)]_i} - C_2 \right]^2 \tag{5.29}$$

Minimizing Eq. (5.29) with respect to C_1, C_2, and a leads to the following equations for C_1 and C_2

$$\frac{1}{C_1} = \frac{n\sum_{i=1}^{n} \frac{(1/UA)_i}{Re_i^a W_i} - \sum_{i=1}^{n} \frac{1}{Re_i^a W_i} \sum_{i=1}^{n} \left(\frac{1}{UA}\right)_i}{n\sum_{i=1}^{n} \frac{1}{Re_i^{2a} W_i^2} - \left(\sum_{i=1}^{n} \frac{1}{Re_i^a W_i}\right)^2} \tag{5.30}$$

and

$$C_2 = \frac{\sum_{i=1}^{n} \frac{1}{Re_i^{2a} W_i^2} \sum_{i=1}^{n} \left(\frac{1}{UA}\right)_i - \sum_{i=1}^{n} \frac{(1/UA)_i}{Re_i^a W_i} \sum_{i=1}^{n} \frac{1}{Re_i^a W_i}}{n\sum_{i=1}^{n} \frac{1}{Re_i^{2a} W_i^2} - \left(\sum_{i=1}^{n} \frac{1}{Re_i^a W_i}\right)^2} \tag{5.31}$$

where

$$W_i = \frac{Pr_i^{1/3} Ak}{D_h} \tag{5.32}$$

The exponent a is then obtained by solving the following equation

$$\sum_{i=1}^{n} \frac{(1/UA)_i \ln(Re_i)}{Re_i^a W_i} - \frac{1}{C_1} \sum_{i=1}^{n} \frac{\ln(Re_i)}{Re_i^{2a} W_i^2} - C_2 \sum_{i=1}^{n} \frac{\ln(Re_i)}{Re_i^a W_i} = 0 \qquad (5.33)$$

If the exponent a is known a priori, then Eqs. (5.30,5.31) reduce to a linear regression problem. Data were analyzed using the general non-linear regression model.

Experiments were conducted to determine the coolant side heat transfer coefficient. The experiment was set up using one of the enhancement devices from Table 5.2 on the oil side with the oil flowing at the maximum attainable rate. The coolant side flowrate was then systematically varied following the procedure outlined earlier. Two data sets at each temperature level were obtained and analyzed using the procedure outlined above. In all experiments the conditions on the oil side remained essentially constant ensuring the validity of the Wilson plot method. In addition, the coolant side Prandtl number also remained constant, varying by less than 3 percent at each temperature level. All of the data for each temperature level were then analyzed using the mean value of the Prandtl number for the particular data set. This provided a smoother data set to analyze using the non-linear regression analysis.

A correlation at each temperature level was then determined. They are given below.

$$Nu(85°C) = 0.38467 Re^{0.56} Pr^{1/3} \qquad (5.34)$$

$$Nu(115°C) = 0.50882 Re^{0.52} Pr^{1/3} \qquad (5.35)$$

The results for each set of experiments are in good agreement with each other. Also the Reynolds number exponent a is approximately equal to the theoretical value of $a = 0.5$ predicted in boundary layer flows for the combined development of thermal and hydrodynamic boundary layers. The predictions from these two correlations vary by less than 5 percent from a correlation of all of the data.

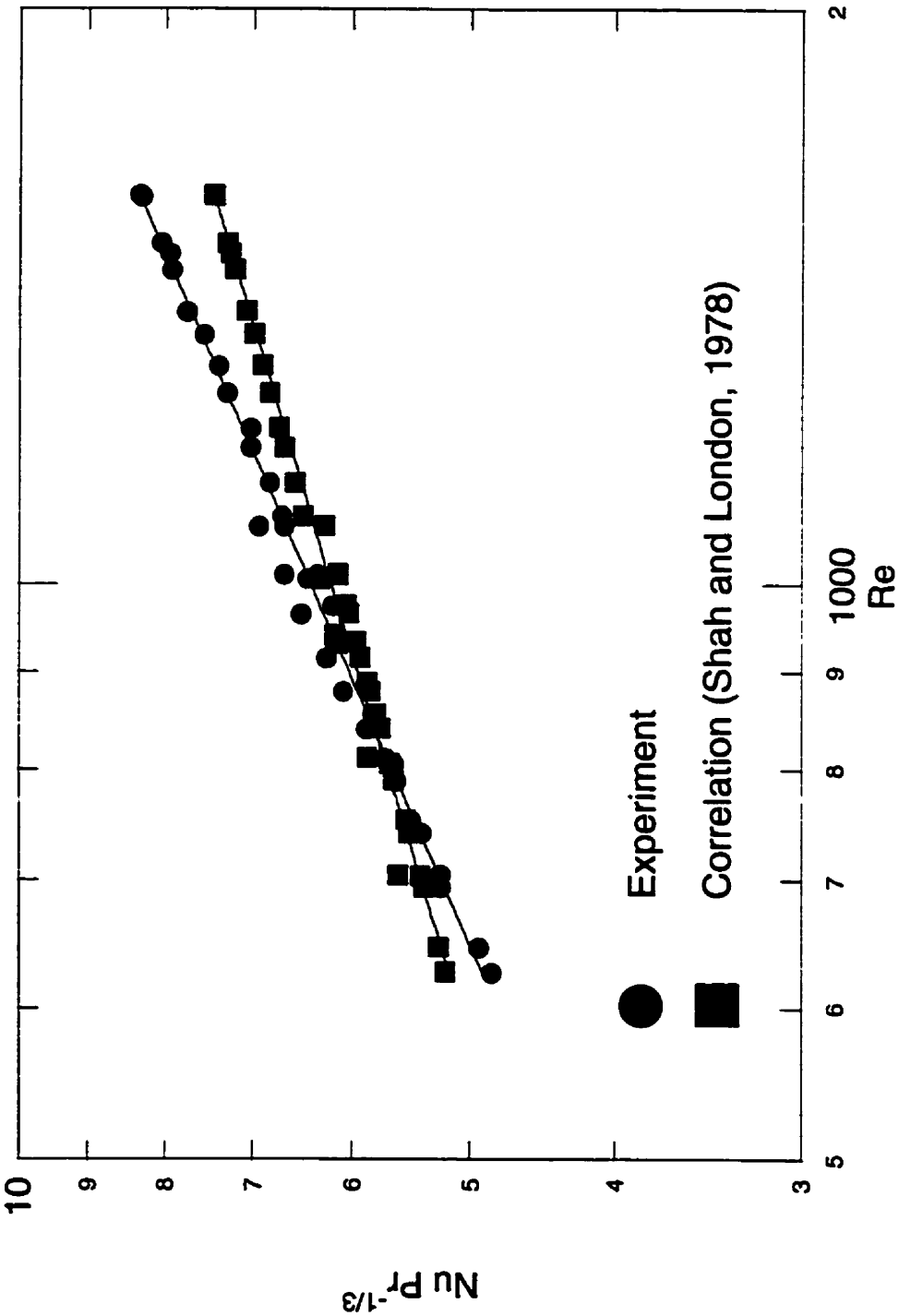

Fig. 5.3 - Coolant Side $Nu/Pr^{1/3}$.

The average correlation will be used for reducing the data for the turbulator experiments.

$$Nu_{cool} = 0.37049 Re^{0.565} Pr^{1/3} \tag{5.36}$$

The correlation given above is based upon the projected area $A_{projected} = 8LW$ of the coolant channels. If the total area ($2.8767 A_{projected}$) within the coolant channel is used to reduce the data, then very good agreement is obtained with the following correlation from Shah and London (1978)

$$Nu_{m,T} = 4.86 + \frac{0.06063 \left(\frac{L}{D_h RePr}\right)^{-1.2}}{1 + 0.09094 \left(\frac{L}{D_h RePr}\right)^{-0.7} Pr^{0.17}} \tag{5.37}$$

Equation 5.37 is for a parallel plate channel for the combined development of thermal and hydrodynamic boundary layers with one surface insulated. A comparison of the experimentally measured Nusselt number and the theoretical value is shown in Figure 5.3. Agreement between measured and theoretical is within 5.7 percent RMS. in the range of coolant side Reynolds numbers. The experimentally determined correlation. Eq. (5.36) will be used in all subsequent data reduction.

5.5.2 Bare Channel Heat Transfer Coefficient

The average heat transfer coefficient was also determined for the test fixture without enhancement devices. The hydrodynamic and thermal entrance lengths for a parallel plate channel may be determined from expressions provided in Shah and London (1978)

$$L_{hy} = D_h(0.3125 + 0.011 Re_{D_h}) \tag{5.38}$$

$$L_{th} = 0.0079735 D_h Re_{D_h} Pr \tag{5.39}$$

Using Eq. (5.38) the hydrodynamic entrance length for the test fixture was determined for the region leading up to the test channels. It was found for the range of volumetric flow rates and inlet conditions that the velocity profile is fully developed upon entering the test channels. Equation (5.39) also indicates that flow is thermally developing within each channel. Experimental results are compared with a solution obtained from Shah and London (1978) for flow in a rectangular channel for thermally developing flow.

The mean Nusselt number for the thermal entrance region in a rectangular channel may be computed from the following expression from Shah and London (1978) for thermally developing flow

$$Nu_{m,T} = 1.765 \left(\frac{L}{D_h Re_{D_h} Pr} \right)^{-1/3} \tag{5.40}$$

or a correlation from Shah and London (1978) for a parallel plate channel for simultaneously developing flow

$$Nu_{m,T} = 7.55 + \frac{0.024 \left(\frac{L}{D_h RePr} \right)^{-1.14}}{1 + 0.0358 \left(\frac{L}{D_h RePr} \right)^{-0.64} Pr^{0.17}} \tag{5.41}$$

The average heat transfer coefficient determined from experimental measurements using the test apparatus are compared with the theoretical results of Eq. (5.41) in Figure 5.4. Accurate results were obtained by including the surface area in the manifold portion of the test core where the flow field develops and using the effective flow length from entrance to exit. The RMS error for the data in Fig. 5.4 is 12.1 percent. In the bare channel experiments, the surface area in the manifold region accounts for approximately 34 percent of the total surface area when there is no enhancement. This value is reduced to approximately 15 percent when one of the surfaces summarized in Table 5.2 is placed in the test fixture. This additional heat transfer surface which is not accounted for in the data reduction of the turbulator

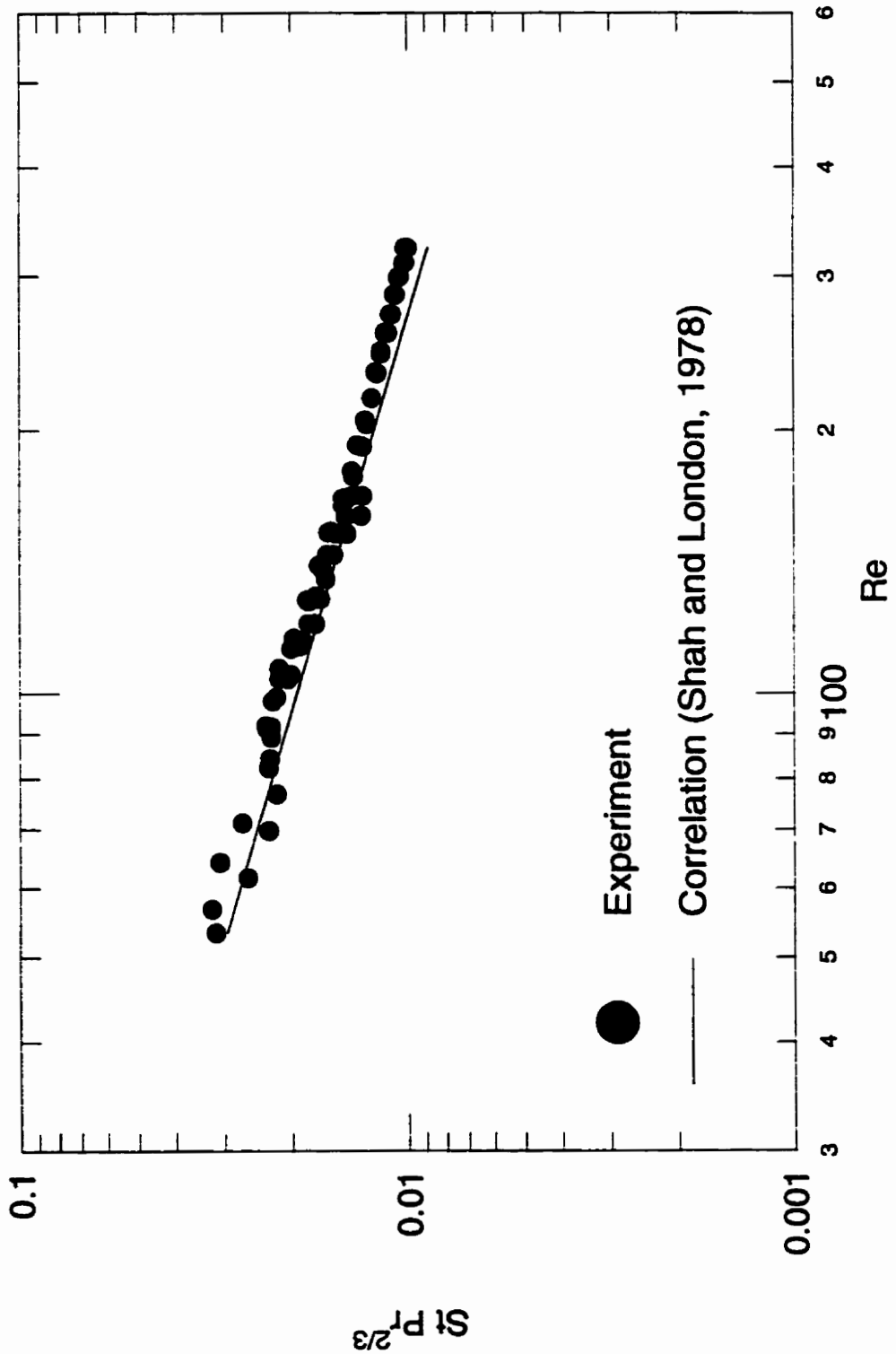

Fig. 5.4 - Comparison of Experimental Results with Prediction for a Bare Channel.

test data will result in a negligible effect since the effective heat transfer coefficient is much larger when turbulator strips are present.

5.5.3 Manifold Pressure Losses

The total pressure losses as a function of mass flow rate may be determined by testing the fixture without the turbulator strip fins in place. The theoretical total pressure drop across each test channel may be determined from the following expression for the friction factor

$$f Re_{D_h} = 20.904 \tag{5.42}$$

from Shah and London (1978) for a rectangular channel having an aspect ratio of $0.11 \approx 1/9$.

The total pressure drop in the channel is related to the friction factor by

$$\frac{\Delta p_{channel} D_h}{\frac{1}{2}\rho \overline{w}^2 4L} = \frac{20.904}{Re_{D_h}} \tag{5.43}$$

The pressure losses may now be determined from the following relation

$$\Delta p_{losses} = \Delta p_{measured} - \Delta p_{channel} \tag{5.44}$$

By conducting the experiment over a range of mass flow rates, a relation for the total pressure losses due to fluid hoses, pipe fittings and inlet and exit manifolds may be developed. An expression of the type

$$\Delta p_{losses} = C_3 \dot{m}^3 + C_2 \dot{m}^2 + C_1 \dot{m} + C_0 \tag{5.45}$$

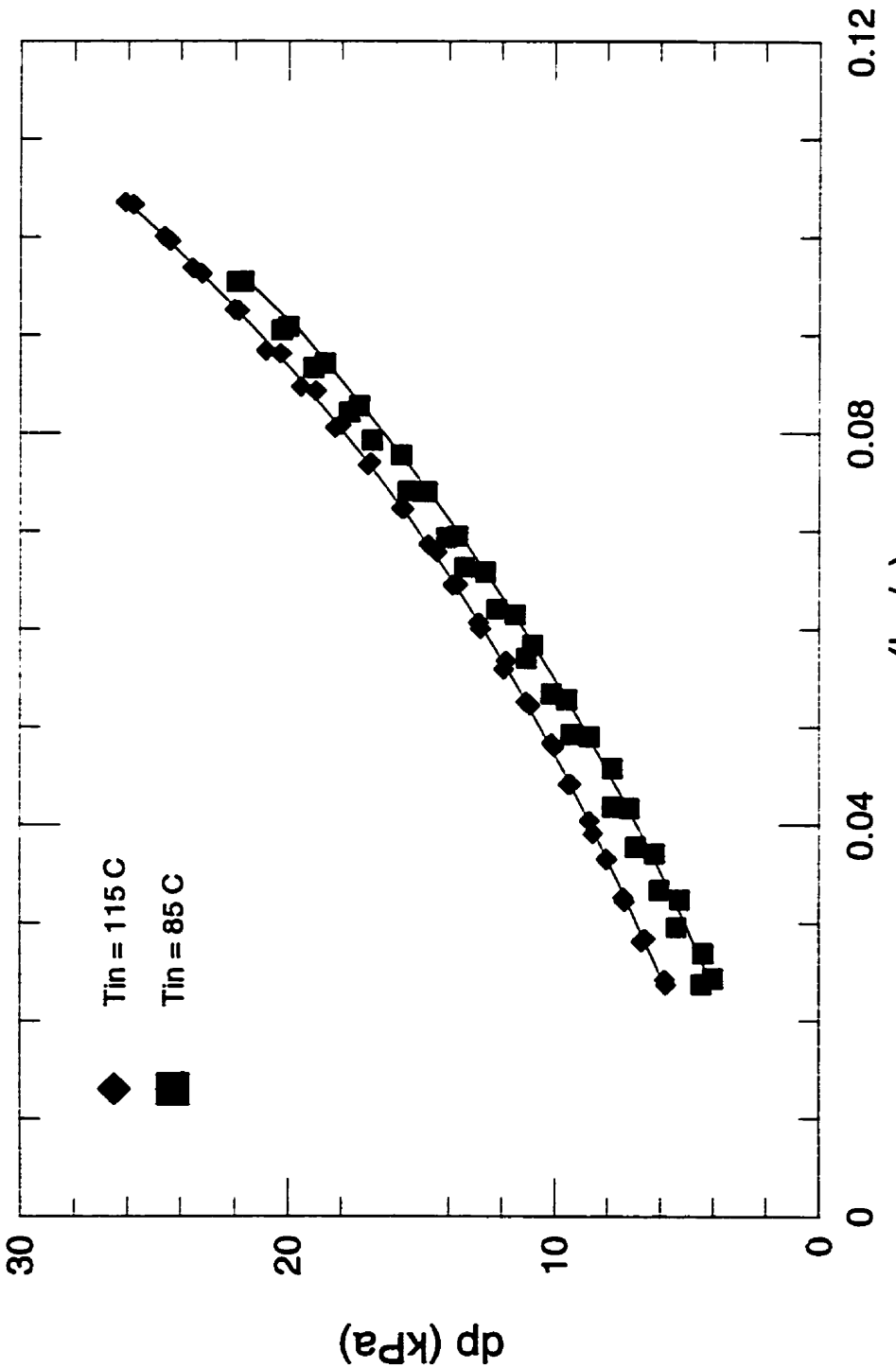

Fig. 5.5 - Pressure Losses of the Test Fixture.

where $\dot{m}$ is mass flow rate (kg/s). Expressions were developed for oil inlet temperatures of 115 $°C$ and 85 $°C$:

$$\Delta p_{115}(kPa) = 84641.19\,\dot{m}^3 - 110.13\,\dot{m}^2 + 150.16\,\dot{m} + 2.24 \tag{5.46}$$

$$\Delta p_{85}(kPa) = 2657.73\,\dot{m}^3 + 723.53\,\dot{m}^2 + 121.79\,\dot{m} + 0.675 \tag{5.47}$$

Due to the small range of plate channel heights (2.50 mm - 3.05 mm), only one set of plates (2.80 mm) were experimentally analyzed for pressure losses. Inlet and outlet pressure losses are mostly due to the inlet and exit manifolds. Differences in the pressure losses inside the test fixture entering and leaving the test core are negligible compared with the manifold losses. The experimentally determined pressure losses are shown in Fig. 5.5 along with the polynomial fits.

5.6 Experimental Uncertainty

The experimental uncertainty in measured values of f and j (or Nu) are usually within $\pm 5\%$ when the temperatures are accurately measured within $\pm 0.1°C$ and pressures accurately measured within $\pm 1\%$. The uncertainty in the Reynolds number is usually $\pm 2\%$ when the flow is measured accurately to within $\pm 0.7\%$ (Shah, 1985). The experimental uncertainty in the j and f results are a result of uncertainty in the experimental measurement of temperature, pressure, and flow rate and uncertainty in the thermal and fluid properties of the test fluids. A detailed uncertainty analysis has been undertaken and is summarized in Appendix C. The results of this analysis are summarized in Table 5.4.

The uncertainty in the Fanning friction factor and Reynolds number was determined to be 3.20 percent and 1.23 percent, respectively. The uncertainty in the Colburn j factor and Nusselt numbers have been determined to be 7.31-13.01 percent and 7.23-

12.96 percent, respectively. The upper limit in the j and Nu parameters is a result of smaller temperature differences being recorded for the lower oil inlet temperature tests. The uncertainties presented in Table 5.4, assume that the property correlations presented earlier in the Chapter are representative of the fluids used in the experiments. If the properties of the test fluids are not exactly the same as those predicted by the correlations, there will be an increase in the overall uncertainty. It is believed that the property correlations are extremely accurate for the glycol mixture and that the predictions for k, C_p, and ρ for the oil are also accurate as these properties do not vary significantly for other types of engine and transmission oil tabulated in Lemczyk and Molloy (1996). The viscosity of various types of transmission oils tabulated in Lemczyk and Molloy (1996) show more variation. The deviation from the mean value for all transmission oils at the elevated temperatures that the experiments were conducted, is between 5-15 percent, refer to Appendix D. Viscosity data for the Type-H transmission oil presented in Lemczyk and Molloy (1996) were obtained from one of the major automobile manufacturers, and are believed to be accurate.

Table 5.4

Uncertainty in f, j, and Re

Parameter	Uncertainty
f	3.20 %
j	13.01/7.31 %
Nu	12.96/7.23 %
Re	1.23 %
Pr	0.87 %

5.7 Experimental Results

Experimental results for the ten HPD type turbulator strips given in Table 5.2 are presented below. Simple correlations for each device have been obtained and are provided in Table 5.5. These correlations are used in a later section to assess the overall performance of each these devices for two criteria, constant mass flow rate, $\dot{m}$, and constant pumping power, $\dot{P}$. The degree of enhancement is generally much more important in the latter case as pumping power is usually a design constraint.

5.7.1 Turbulator Results

Experimental results for ten turbulator strips have been obtained. The data have been correlated using the following equations:

$$j = ARe_{d_h}^{a} \tag{5.48}$$

and

$$f = BRe_{d_h}^{b} \tag{5.49}$$

Values for the parameters A, a, B, and b for each device are summarized in Table 5.5. The correlations for the HPD devices should be used with caution and within the range of Reynolds numbers of the experiments. The data for these devices show that at higher Reynolds numbers, turbulence or inertial effects result in some flattening of the $f - Re$ and $j - Re$ curves. Graphical results presented in Figures 5.6-5.17 for each device along with a plot for each family of devices.

Table 5.5

Coefficients for Correlations

Fin	j		f	
Designation	A	a	B	b
CPI-1	0.2365	-0.2989	11.1777	-0.6083
CPI-2	0.2231	-0.3933	23.2454	-0.8265
CPI-3	0.3407	-0.4326	12.4490	-0.4572
CPI-4	0.2347	-0.3462	9.7672	-0.5072
CPI-5	0.2953	-0.4305	12.5845	-0.4590
SQ-1	0.2707	-0.2204	10.1229	-0.3874
SQ-2	0.3562	-0.2929	11.2634	-0.3974
SQ-3	0.2772	-0.2889	9.0467	-0.3819
SQ-4	0.2801	-0.4033	11.9566	-0.4457
SQ-5	0.2038	-0.2565	8.2743	-0.3328

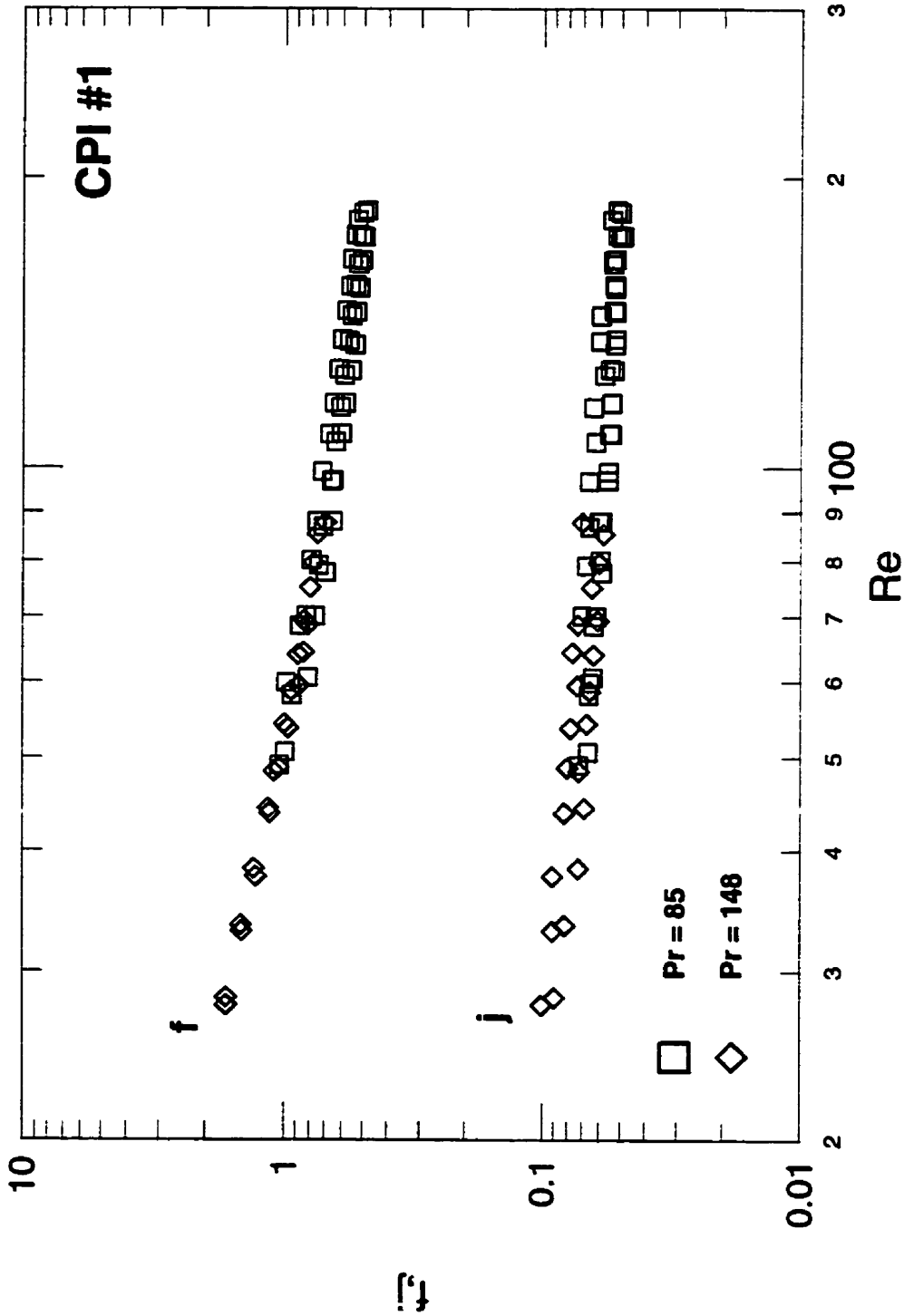

Fig. 5.6 - CPI-1 Experimental Data.

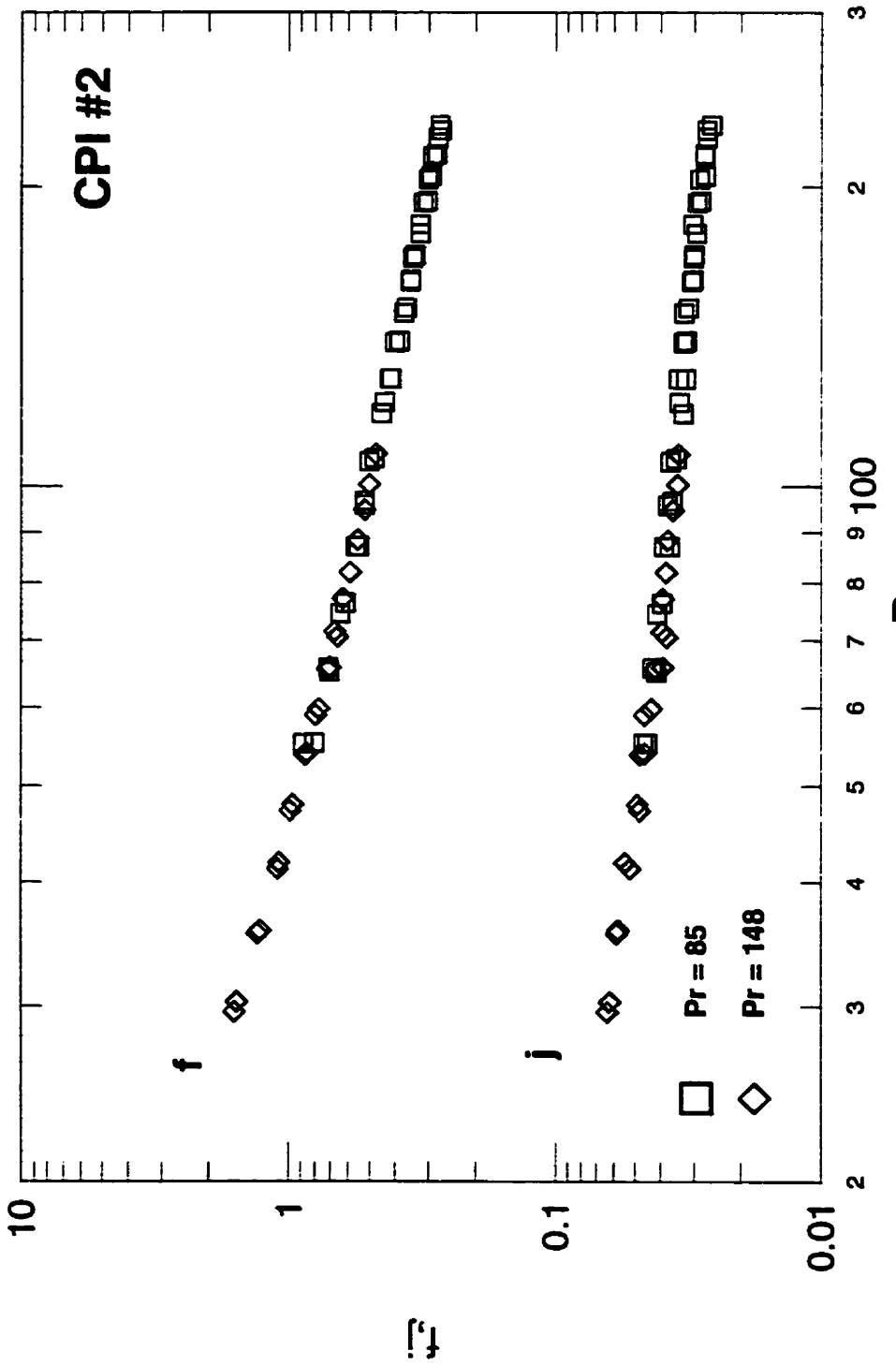

Fig. 5.7 - CPI-2 Experimental Data.

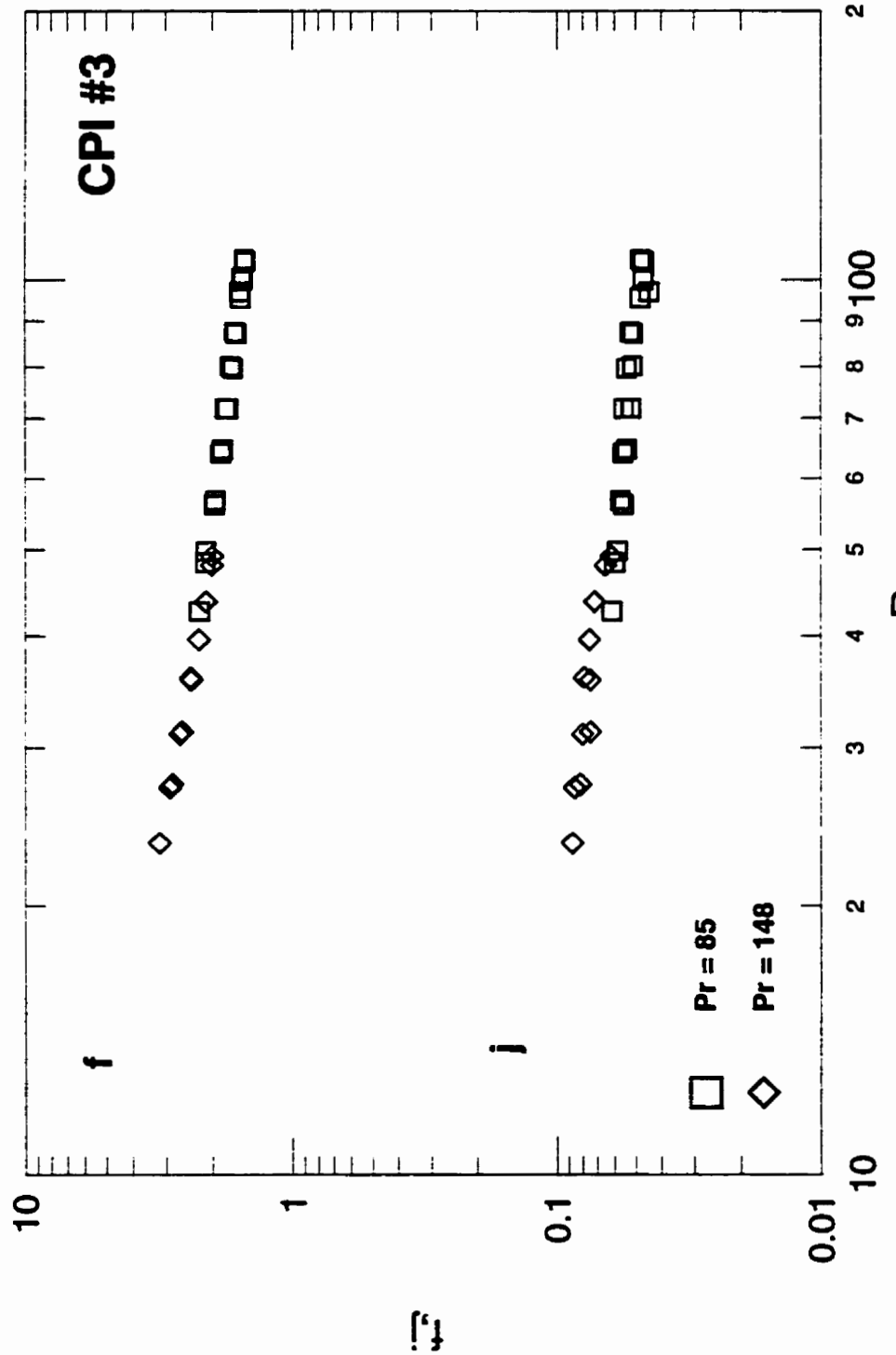

Fig. 5.8 - CPI-3 Experimental Data.

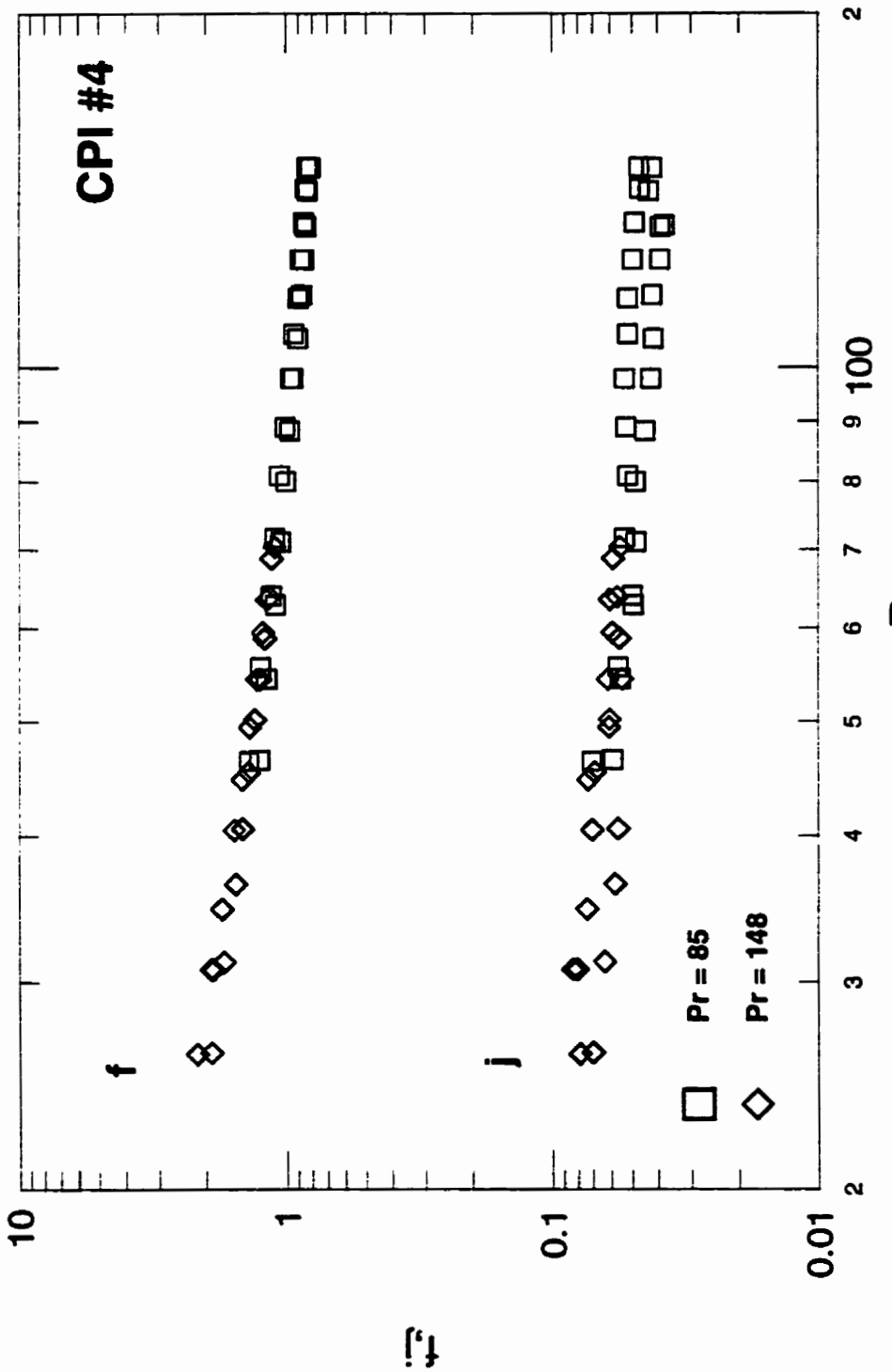

Fig. 5.9 - CPI-4 Experimental Data.

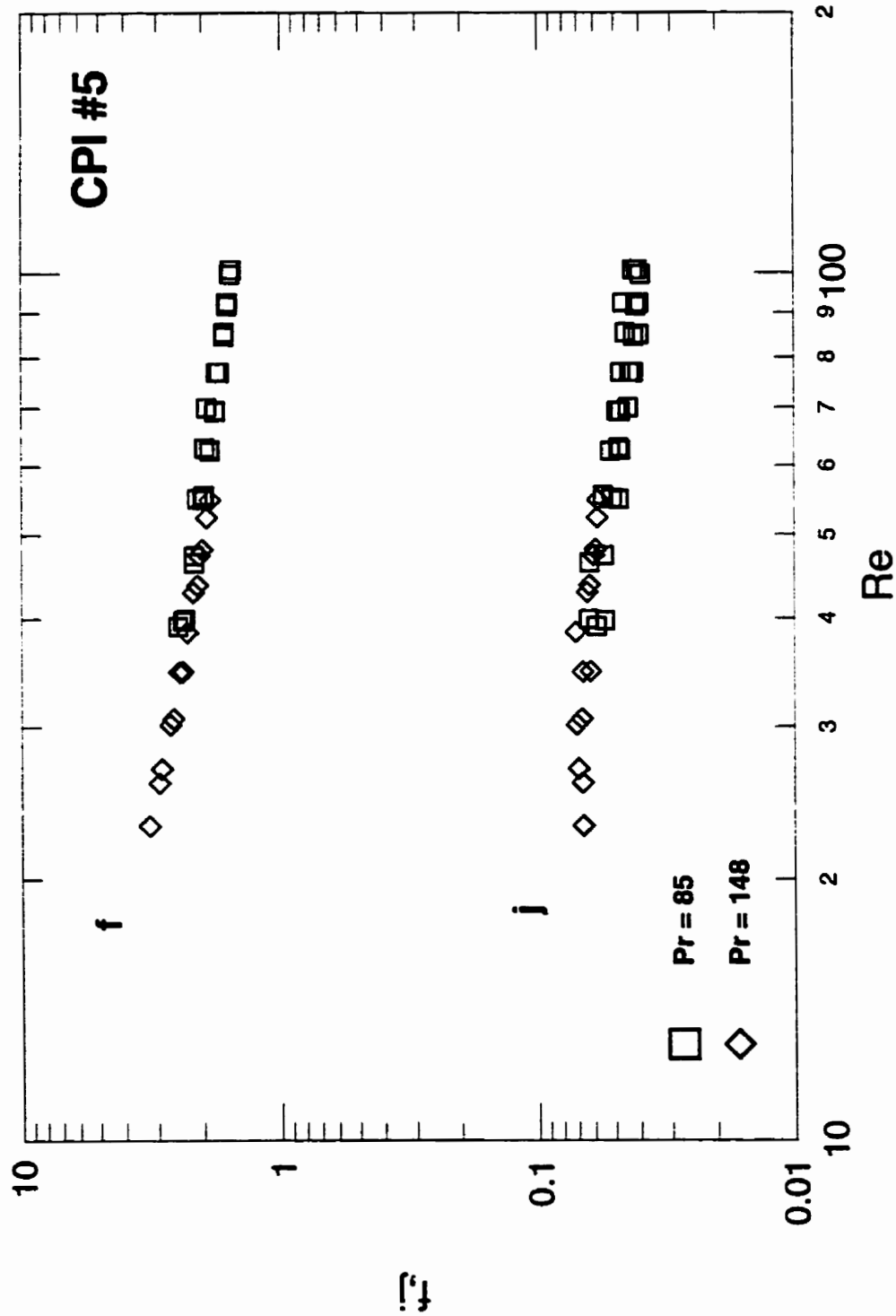

Fig. 5.10 - CPI-5 Experimental Data.

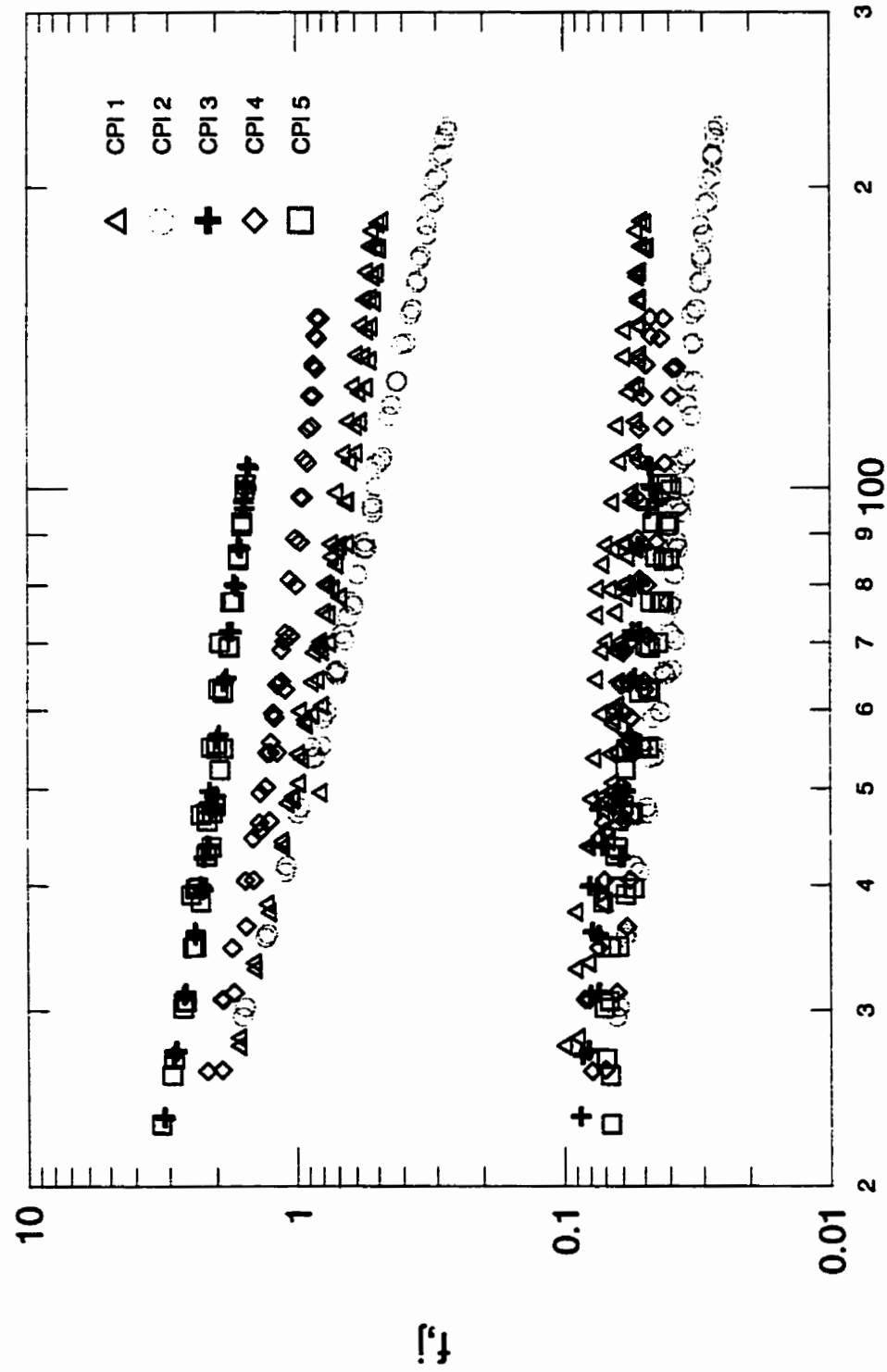

Fig. 5.11 - Comparison of all CPI Turbulator Strips.

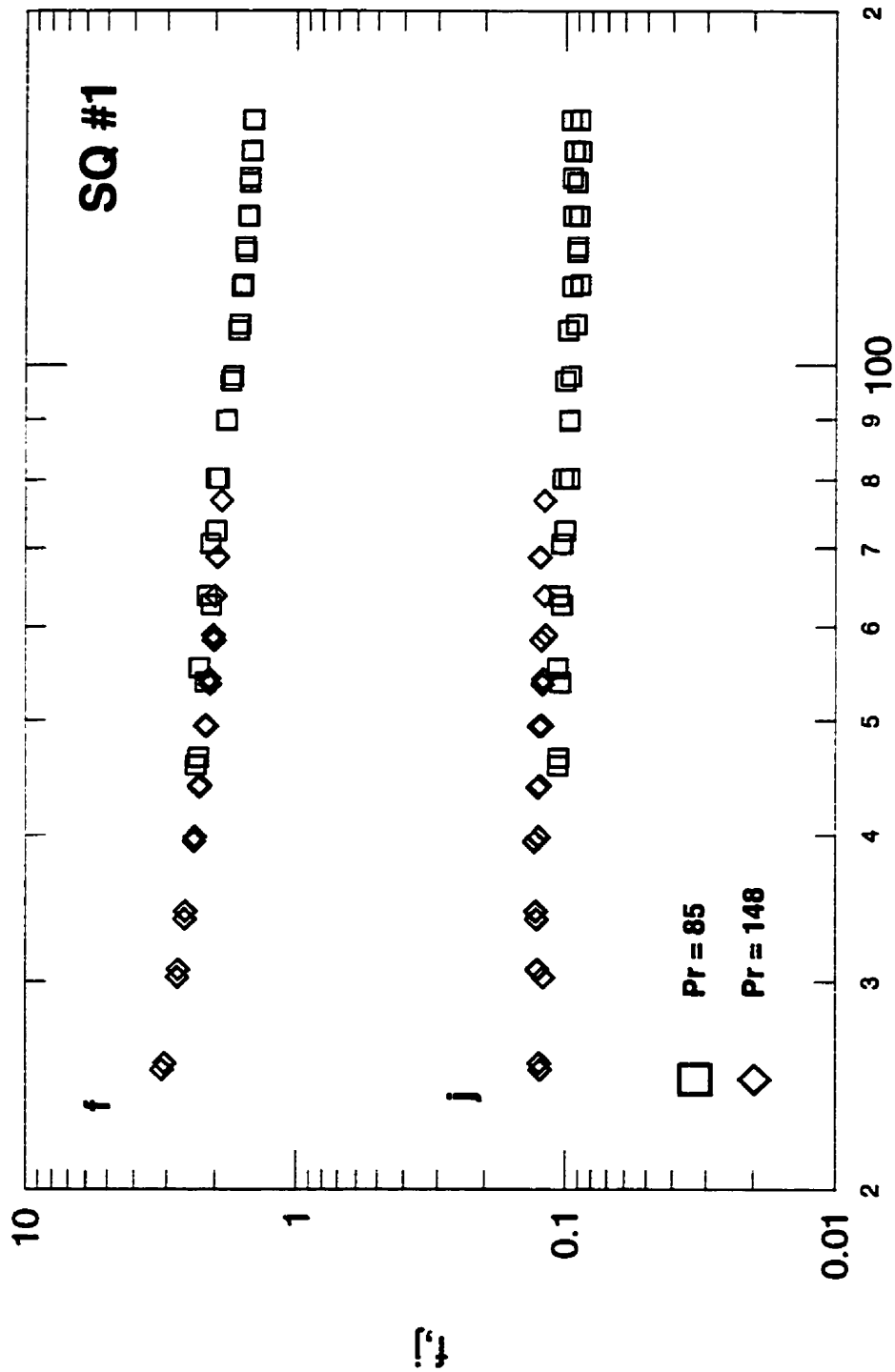

Fig. 5.12 - SQ-1

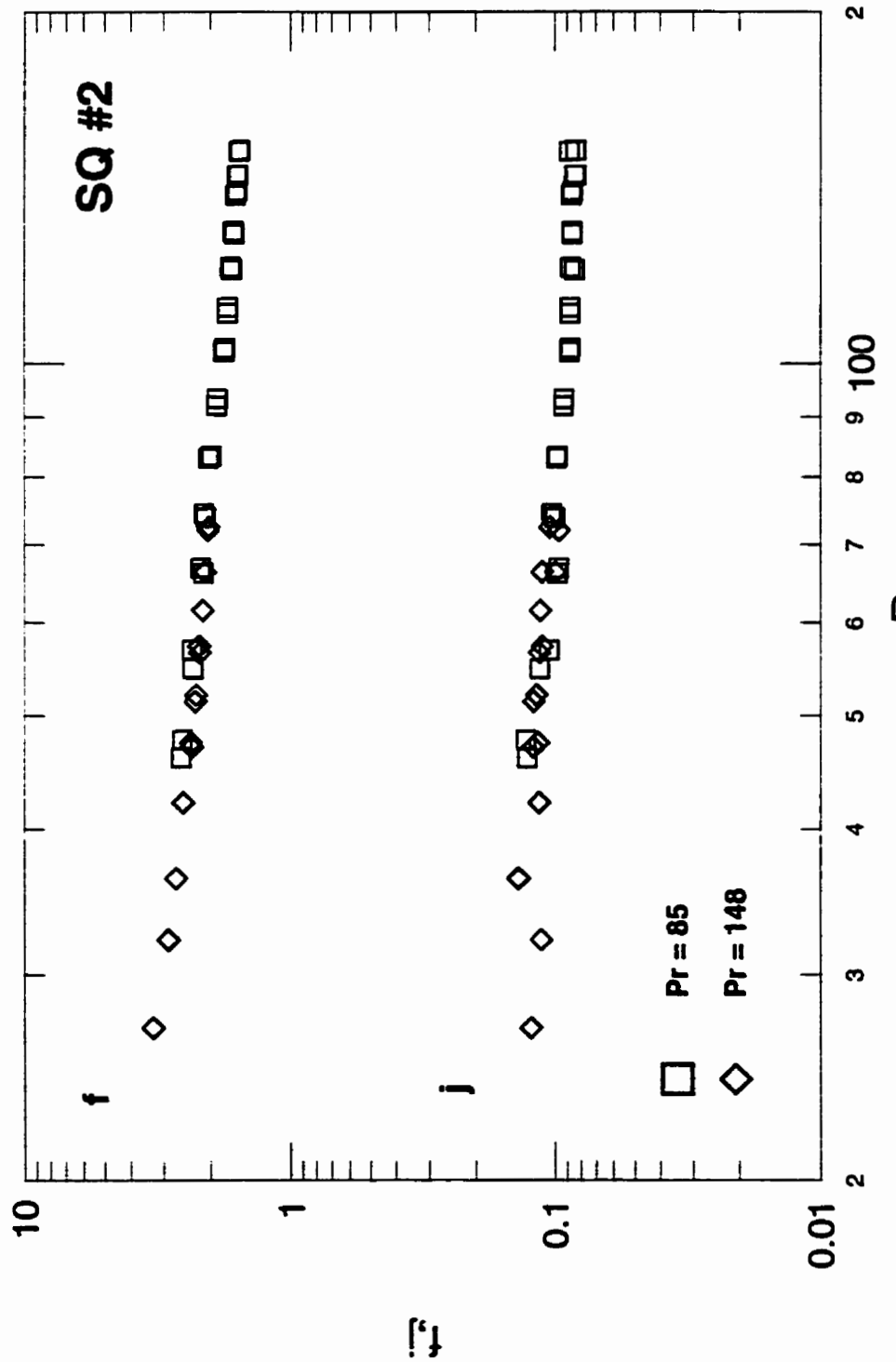

Fig. 5.13 - SQ-2

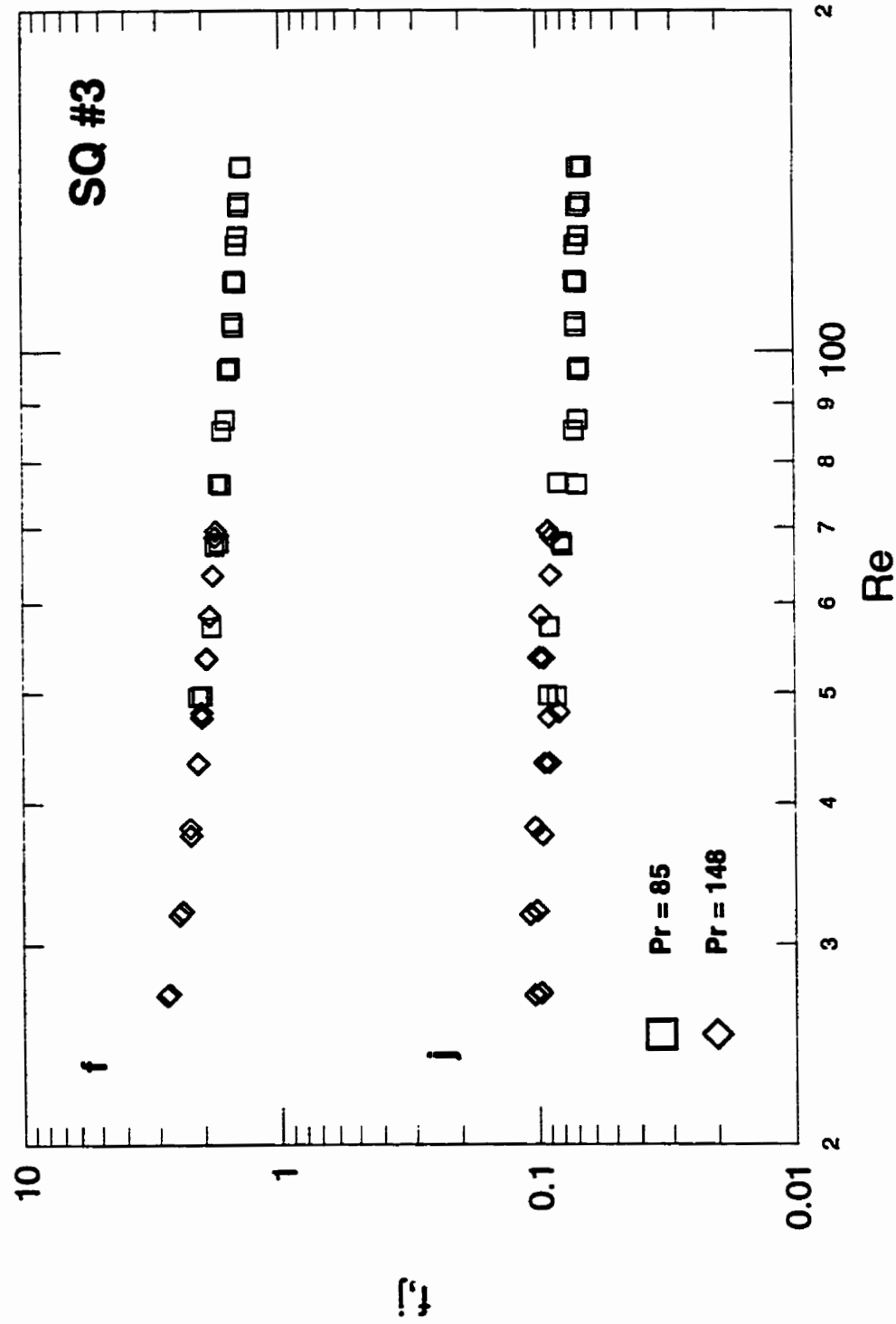

Fig. 5.14 - SQ-3 Experimental Data.

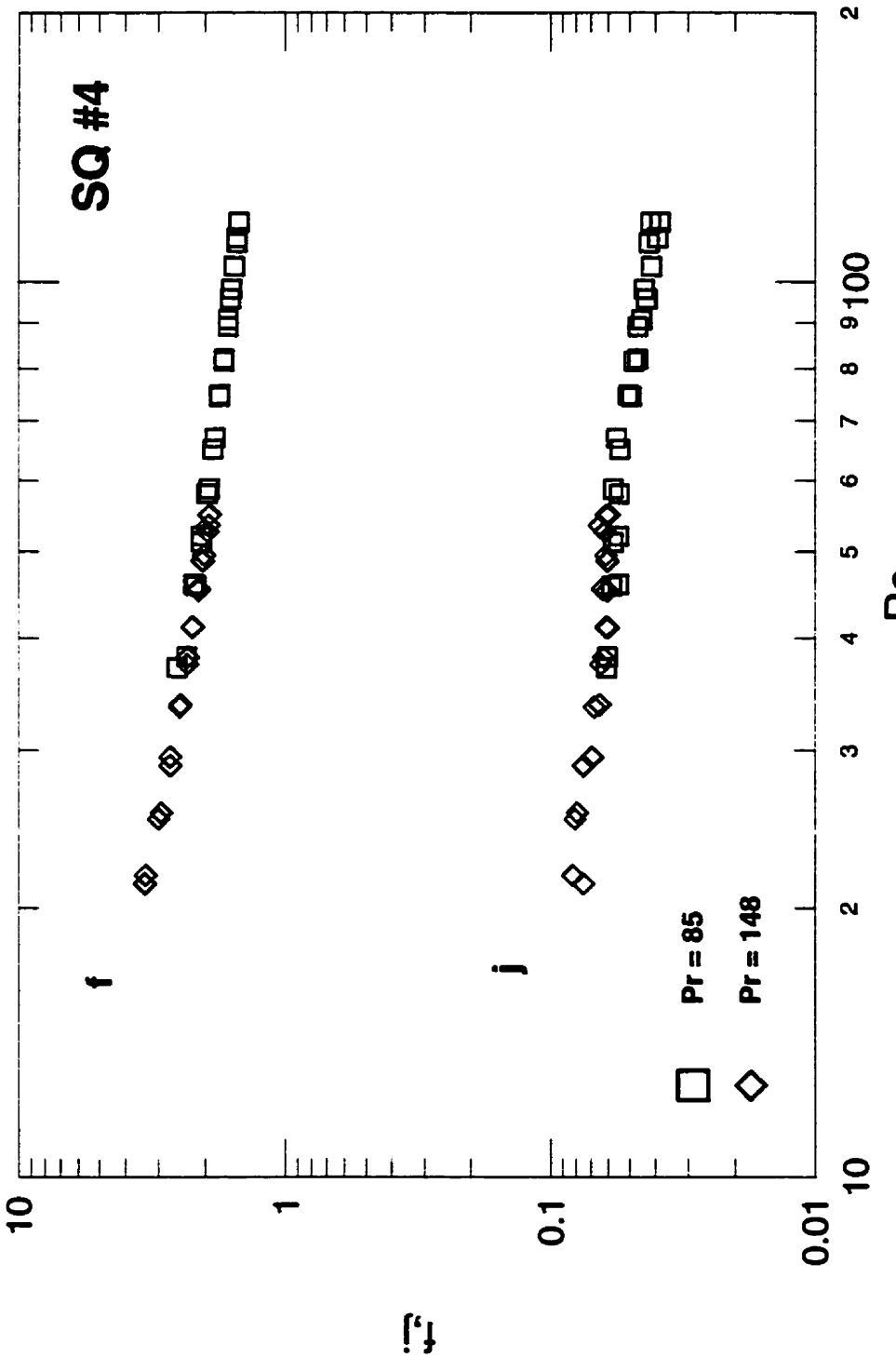

Fig. 5.15 - SQ-4 Experimental Data.

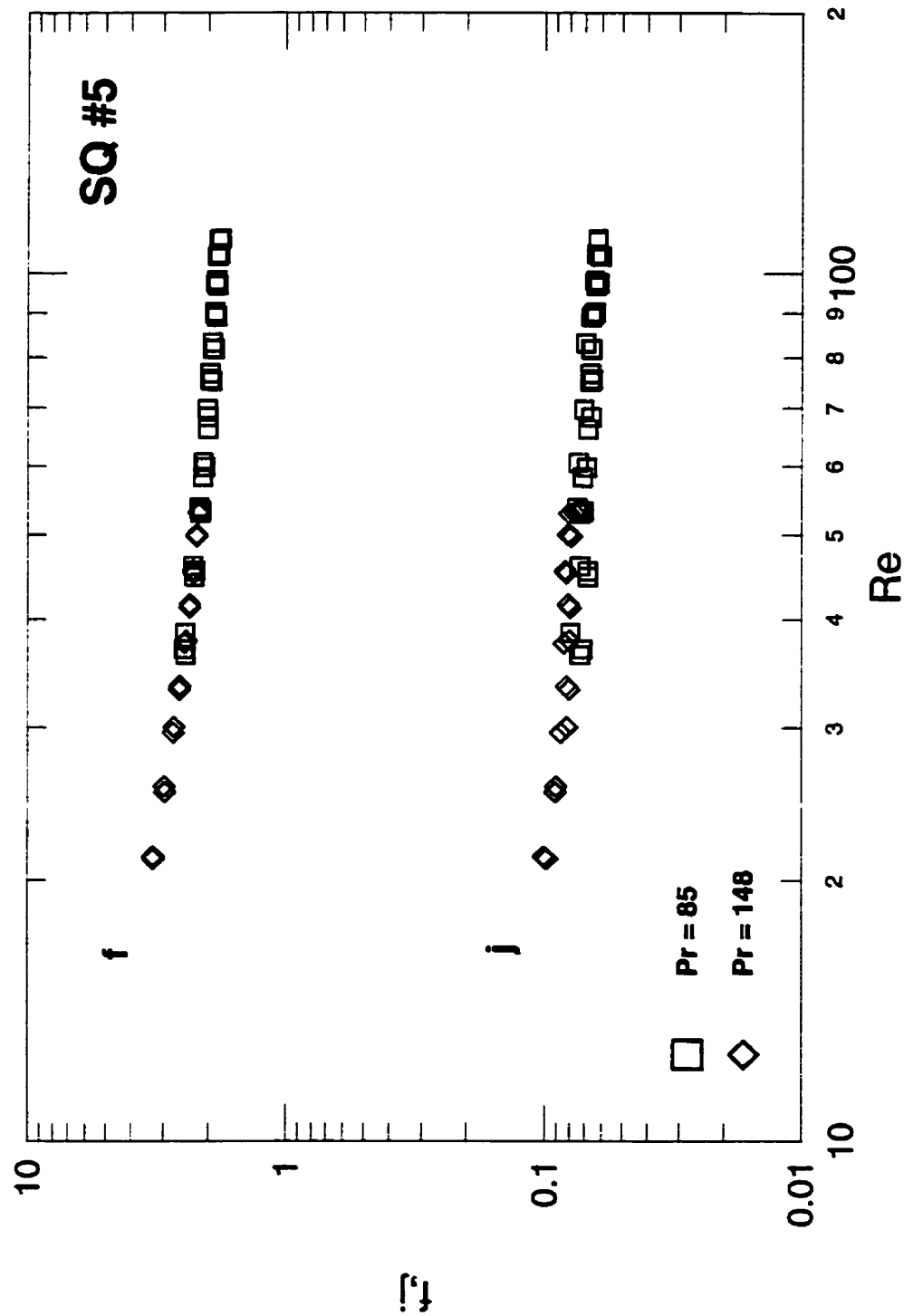

Fig. 5.16 - SQ-5 Experimental Data.

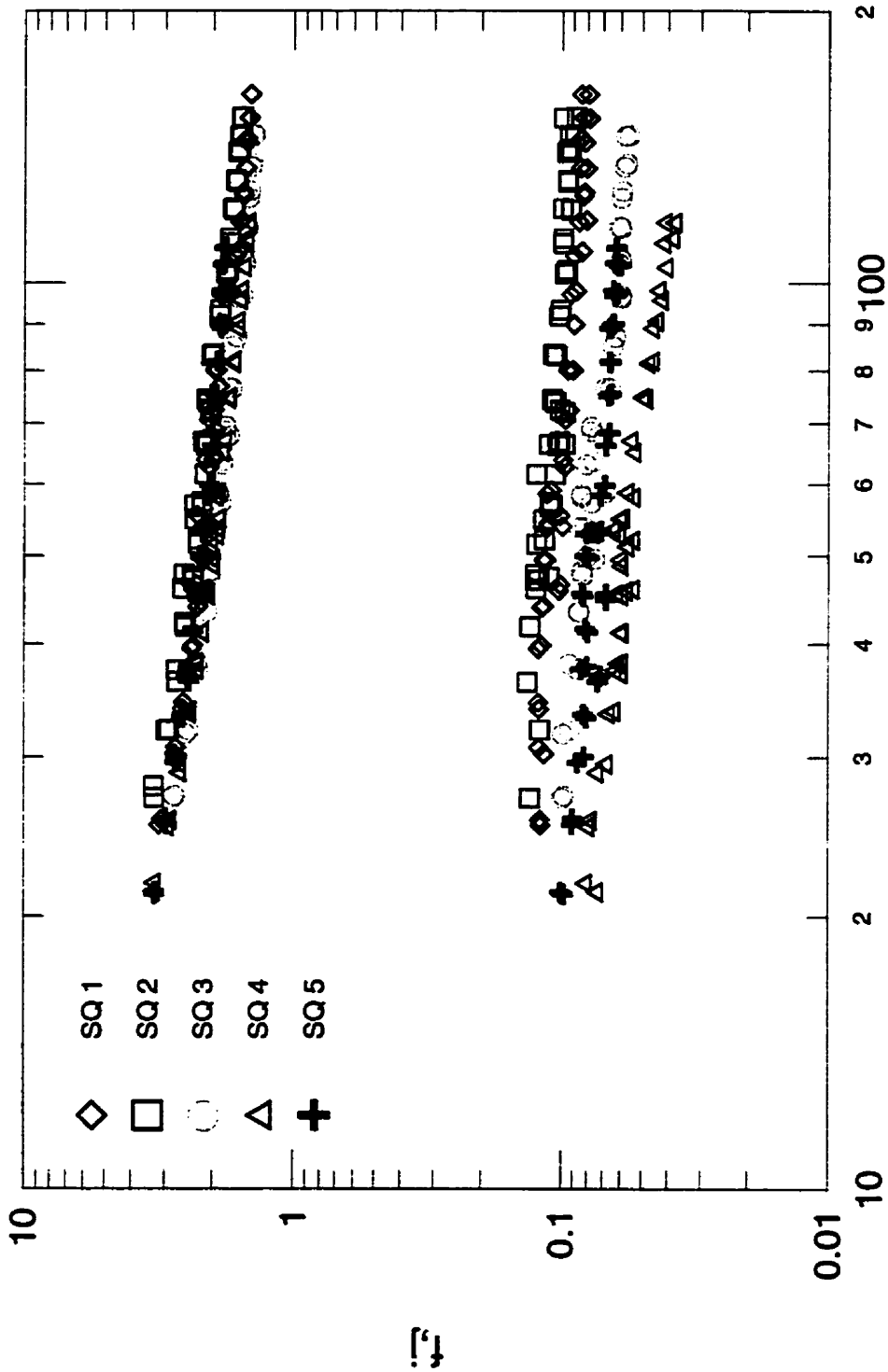

Fig. 5.17 - Comparison of all SQ Turbulator Strips.

5.7.2 Performance Evaluation

A comparison of all of the enhancement devices tested is presented below. The basis for comparison is provided by comparing the test results to the theoretical results which would arise at the same mass flow rate $\dot{m}$ if the channel did not contain a fin. The correlations developed earlier have been rescaled such that the Reynolds number is now based upon the hydraulic diameter of the bare channel $2H$. Later, the enhancement ratio is computed for constant mass flow rate and constant pumping power. More complex performance evaluation criteria are discussed in the text by Webb (1994). Many of these criteria involve design related issues.

The f and j factors in a smooth channel of aspect ratio $b/a \approx 0.1$ are given by relations from Shah and London (1978):

$$f_b = \frac{20.903}{Re_{D_h}} \tag{5.50}$$

and

$$j_b = 0.641 \frac{(fRe_{Dh})^{1/3}}{(L/D_h)^{1/3} Re_{D_h}^{2/3}} \tag{5.51}$$

where fRe_{D_h} is the friction factor Reynolds number group for a rectangular duct.

In order to assess the relative degree of enhancement of the devices examined in this Chapter, general relationships need to be developed which relate the enhanced channel to the bare or smooth channel. Webb (1994) discusses several methods to compare the performance of enhanced surfaces. Development of expressions for constant mass flow rate $\dot{m}$ and constant pumping power $\dot{P}$ is presented below.

The heat transfer coefficient is related to the Colburn j factor through the following expression

$$h = jc_p Pr^{-2/3} G \tag{5.52}$$

where $G = \rho\overline{w}$. Since it is the total enhancement which is of interest, that is the combined effects of the increase in surface area A and the increase in h, the following expression may be developed from Eq. (5.52).

$$\frac{(hA)_e}{(hA)_b} = \frac{j_e}{j_b}\frac{A_e}{A_b}\frac{G_e}{G_b} \tag{5.53}$$

The enhancement ratio may be written in terms of the Reynolds number Re as

$$\frac{(hA)_e}{(hA)_b} = \frac{j_e}{j_b}\frac{A_e}{A_b}\frac{Re_e}{Re_b} \tag{5.54}$$

The pumping power may be obtained from the following expression (Webb,1994)

$$\dot{P} = \left(\frac{fA_e}{A_c}\frac{G^2}{2\rho}\right)\left(\frac{GA_c}{\rho}\right) \tag{5.55}$$

where A_c is the cross-sectional area of the channel. The ratio of the pumping power in the enhanced channel to that for a smooth or bare channel is

$$\frac{\dot{P}_e}{\dot{P}_b} = \frac{f_e}{f_b}\frac{A_e}{A_b}\left(\frac{G_e}{G_b}\right)^3 \tag{5.56}$$

Once again, the above expression may be written in terms of the Reynolds number Re as

$$\frac{\dot{P}_e}{\dot{P}_b} = \frac{f_e}{f_b}\frac{A_e}{A_b}\left(\frac{Re_e}{Re_b}\right)^3 \tag{5.57}$$

Now if the expressions for the friction factor in the enhanced channel and smooth channel are known, the above expression for constant pumping power, that is $\dot{P}_e/\dot{P}_b = 1$, becomes

$$\frac{B(Re_e)^b}{(20.903/Re_b)}\frac{A_e}{A_b}\left(\frac{Re_e}{Re_b}\right)^3 = 1 \tag{5.58}$$

Equation 5.58 may be solved for the reduced Reynolds number which results in the enhanced channel

$$Re_e = \exp\left(\frac{\ln\left(\frac{20.903 Re_b^2}{B\,(A_e/A_b)}\right)}{3+b}\right) \tag{5.59}$$

In the sections which follow three measures of the degree of enhancement are presented.

Comparison of j and f with Bare Channel

In Figs. 5.18 and 5.19, the experimental correlations presented in Table 5.5 have been used to compare the friction factor and Colburn factor to that of the bare channel. Since the hydraulic diameters of the enhanced surfaces vary substantially from one another and from the value for the bare channel, all of the curves have been rescaled based upon the bare channel hydraulic diameter $2H$. This provides a proper basis for comparison at constant mass flow rate. The increase in pressure drop (or f) is significant with the HPD type devices as the Reynolds number increases. This large increase in pressure drop is primarily due to form drag.

Enhancement Ratio for Constant Mass Flow Rate $\dot{m}$

When the results are based upon the Reynolds number Re_{2H}, Eq. (5.54) becomes:

$$\frac{(hA)_e}{(hA)_b} = \frac{j_e}{j_b} AER \tag{5.60}$$

where AER is the area enhancement ratio defined earlier in the Chapter, see Table 5.1.

Plots of the enhancement ratio for $\dot{m} = Constant$ are presented in Figs. 5.20 and 5.21. The behavior of these devices is as expected. All of the devices demonstrate considerable heat transfer enhancement as a function of Reynolds number.

Enhancement Ratio for Constant Pumping Power $\dot{P}$

If the constraint for measuring the degree of enhancement is changed to constant pumping power significant reduction in the enhancement may result. The enhancement ratio is computed from Eq. (5.54) with Re_e determined from Eq. (5.59). The results have been computed using the correlations developed earlier for the friction factor and are plotted in Figs. 5.22 and 5.23. Once again, the results are based upon the bare channel Reynolds number Re_{2H}. In all cases there is still significant enhancement. This criterion represents a more realistic comparison. In most automotive applications pumping power is a limiting constraint followed by size.

5.8 Summary

This chapter presented the details of the experimental procedure and results for ten compact heat exchanger surfaces. Details of the data reduction procedure and thermal characterization of the test fixture were presented. The experiment was able to accurately measure the oil side and coolant side heat transfer coefficients. Agreement between experimental and theoretical values was within 12.1 percent RMS for the oil side and 5.7 percent RMS for the coolant side. Experimental uncertainty in Re was found to be 1.23 percent, 3.20 percent in f and 13.01/7.31 percent in j.

Correlations for ten turbulator strips were obtained for the range of Reynolds number $20 < Re < 200$. Finally, a simple performance study was undertaken such that the devices analyzed may be compared with each other and the degree of enhancement may be determined.

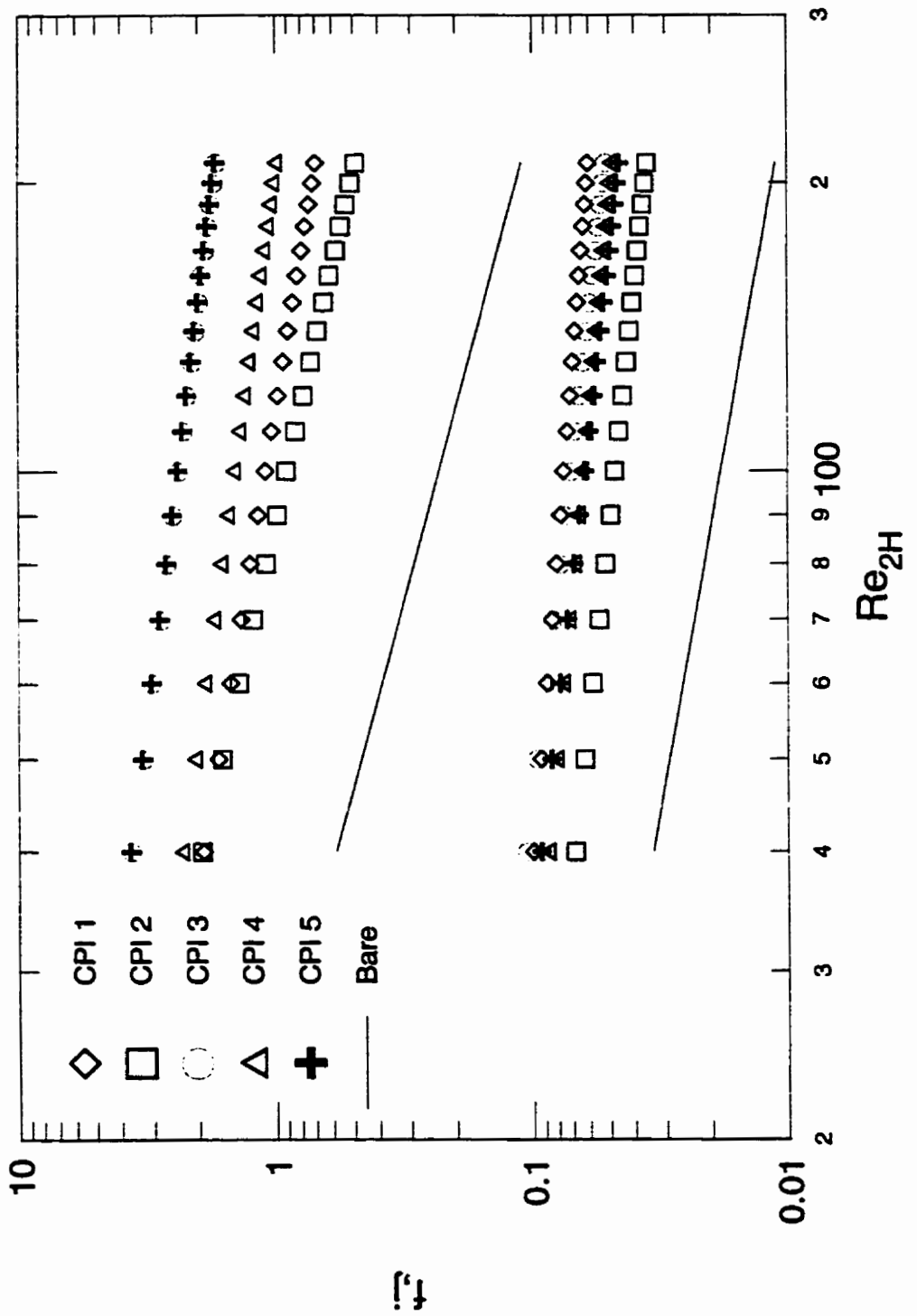

Fig. 5.18 - Comparison of all CPI Turbulator Strips with Bare Channel.

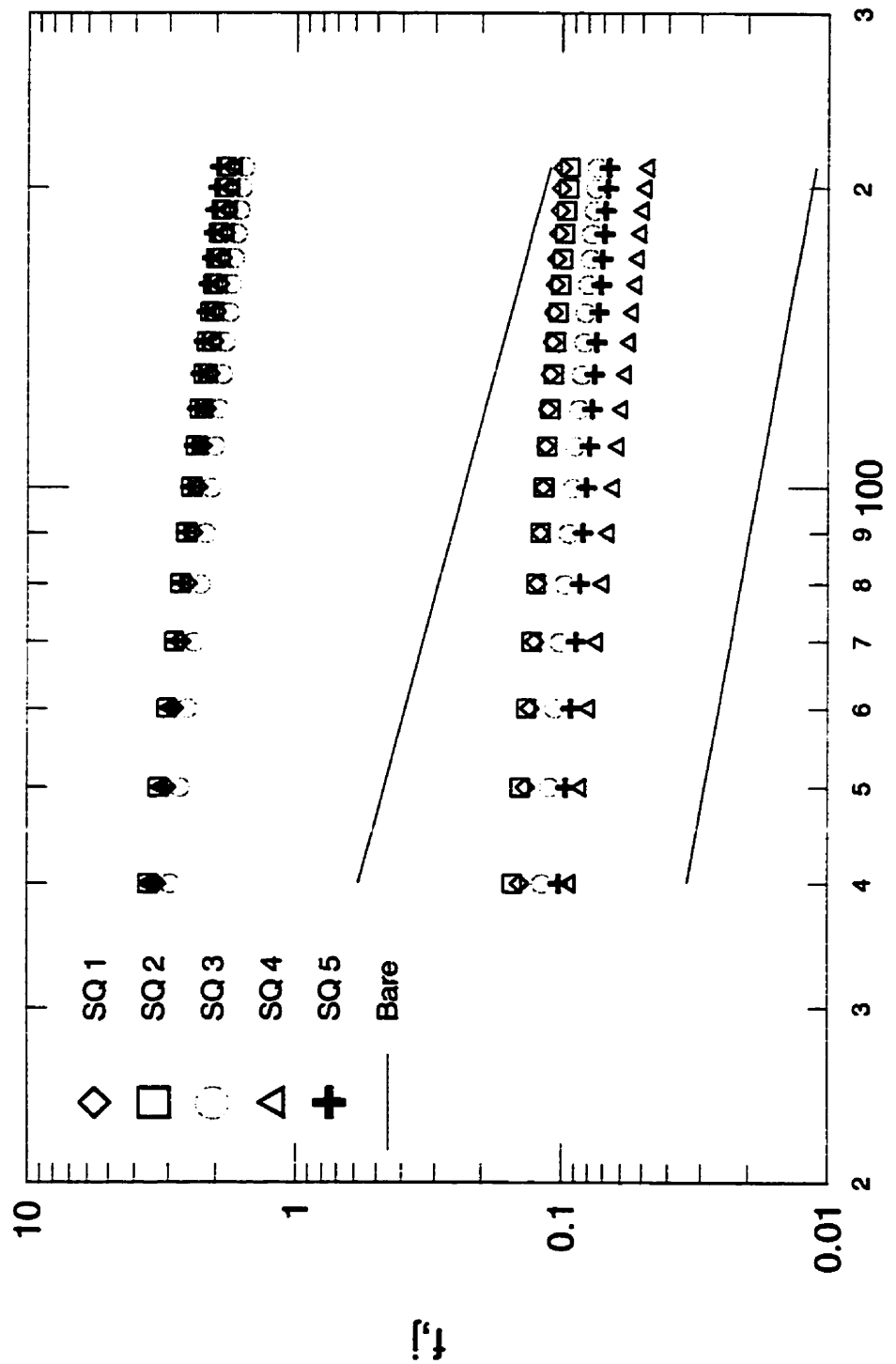

Fig. 5.19 - Comparison of all SQ Turbulator Strips with Bare Channel.

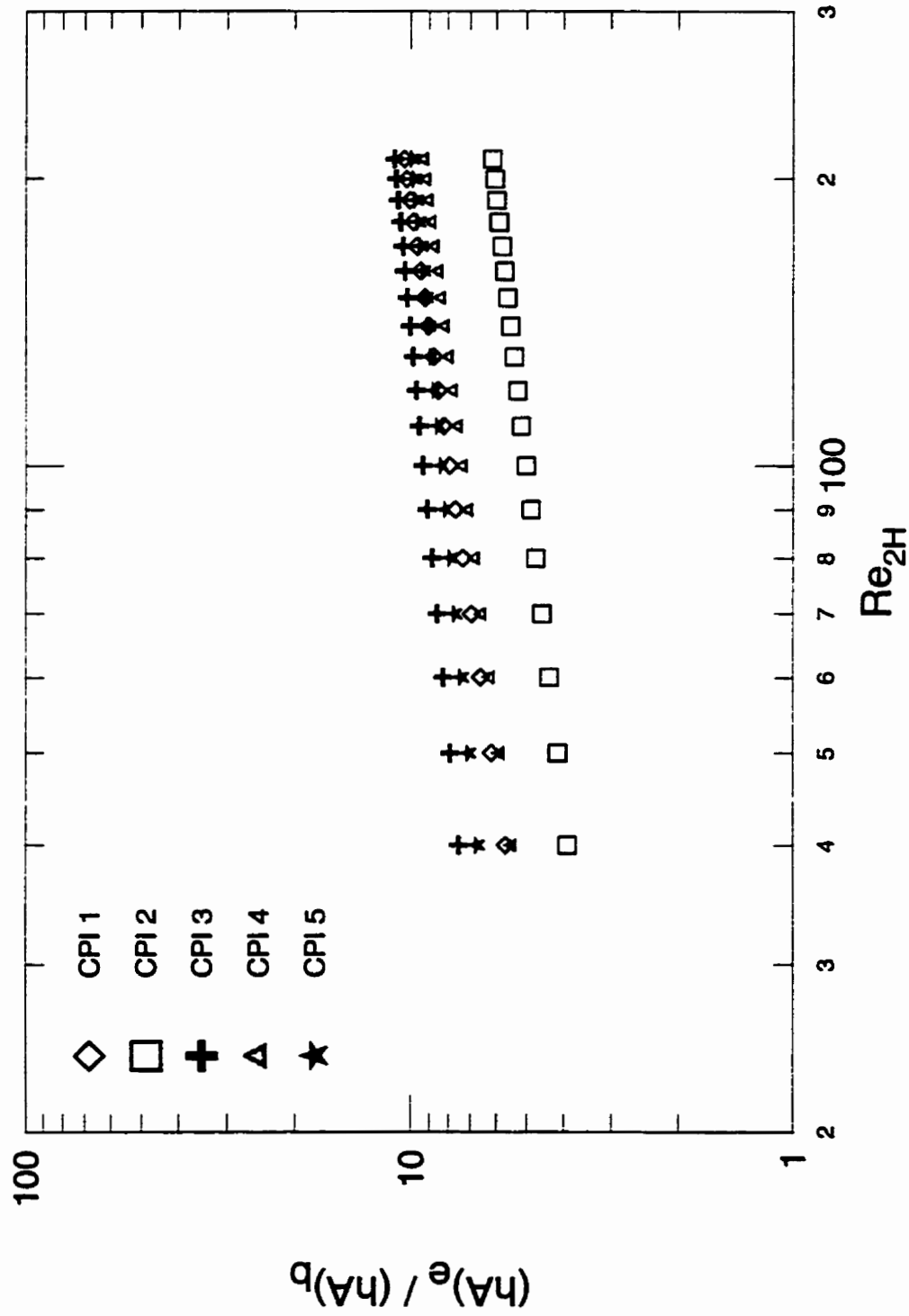

Fig. 5.20 - Enhancement Ratio for CPI Turbulator Strips with $\dot{m}$ = *Constant.*

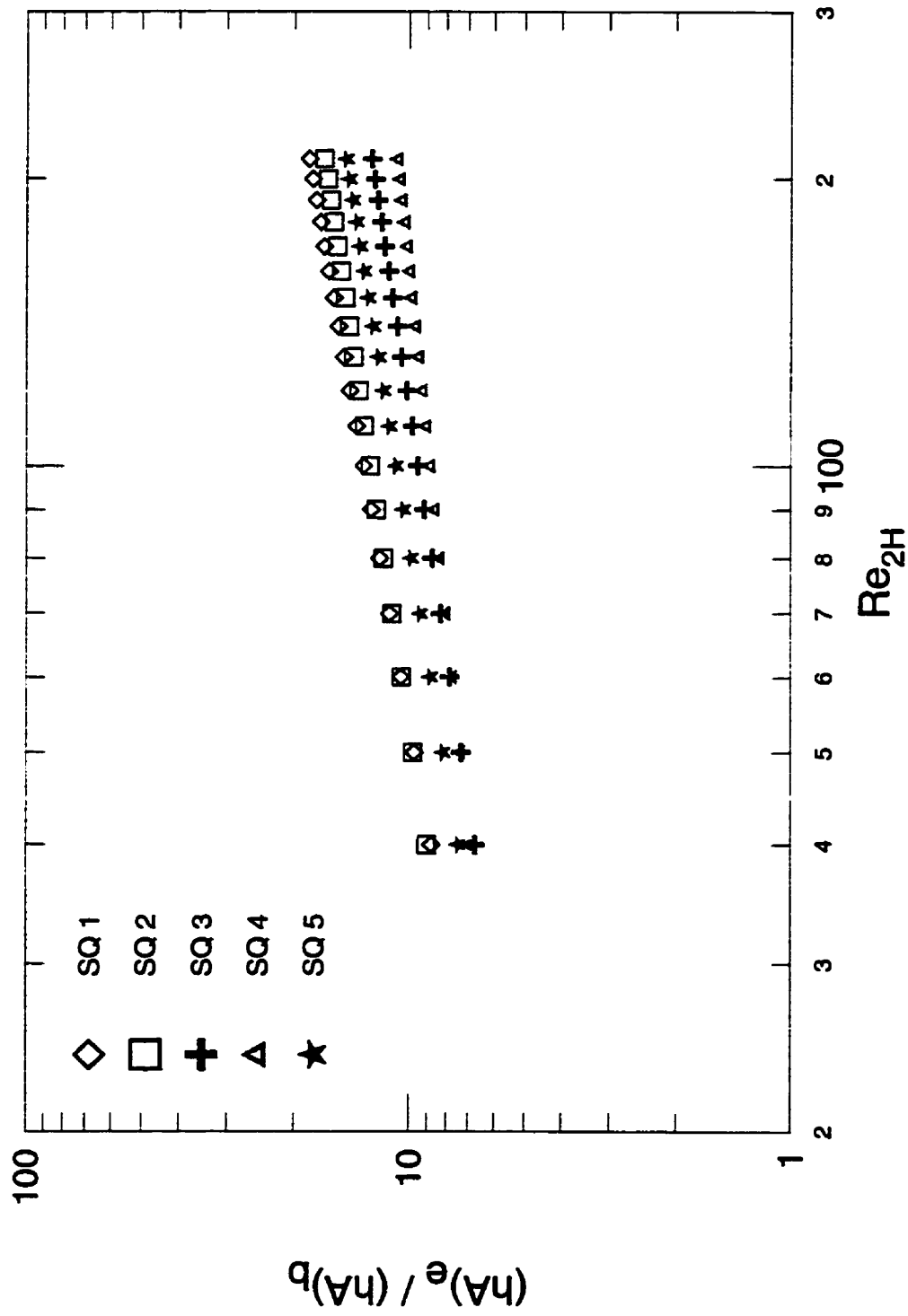

Fig. 5.21 - Enhancement Ratio for SQ Turbulator Strips with $\dot{m}$ = *Constant.*

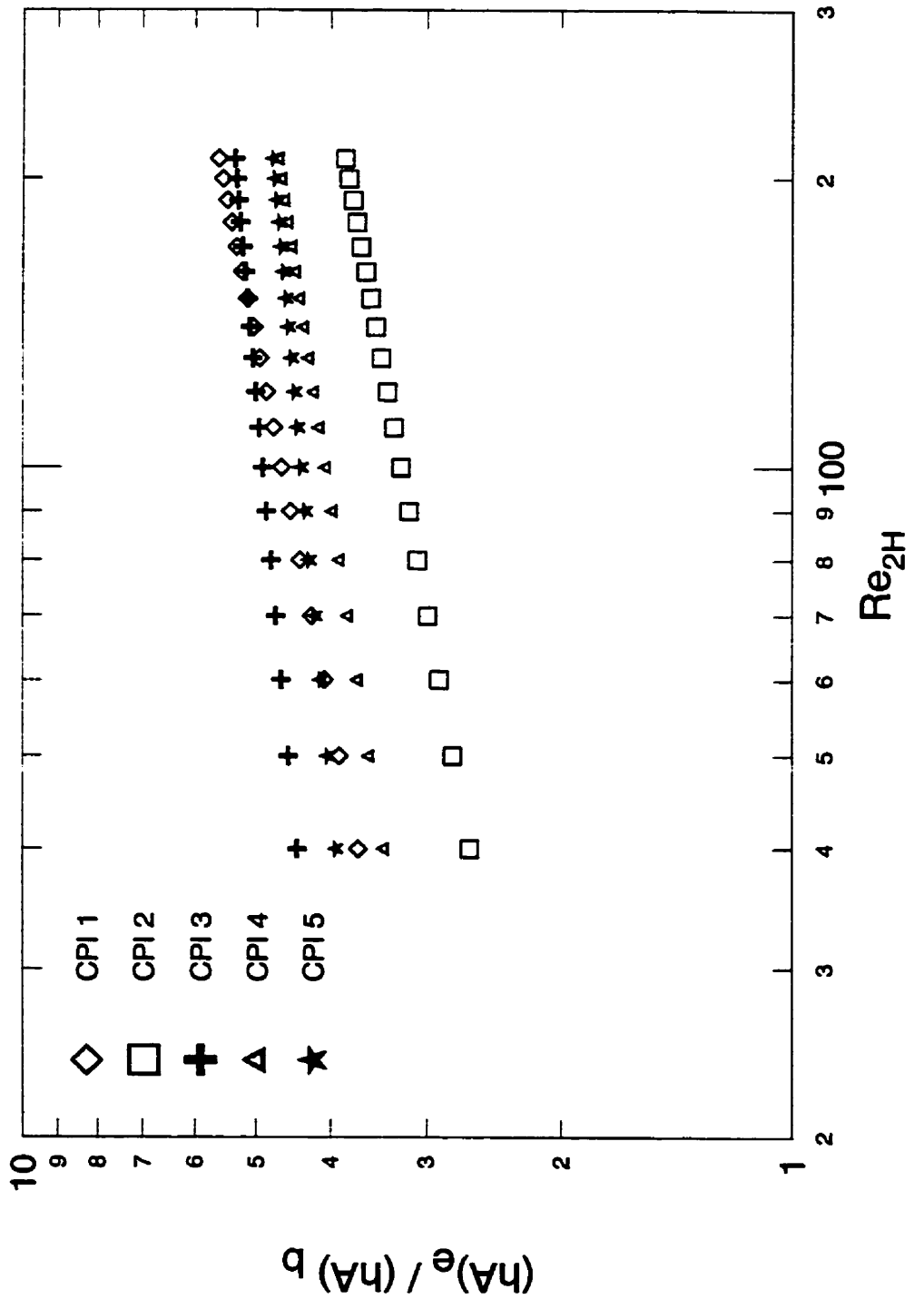

Fig. 5.22 - Enhancement Ratio for CPI Turbulator Strips with $\dot{P} = Constant$.

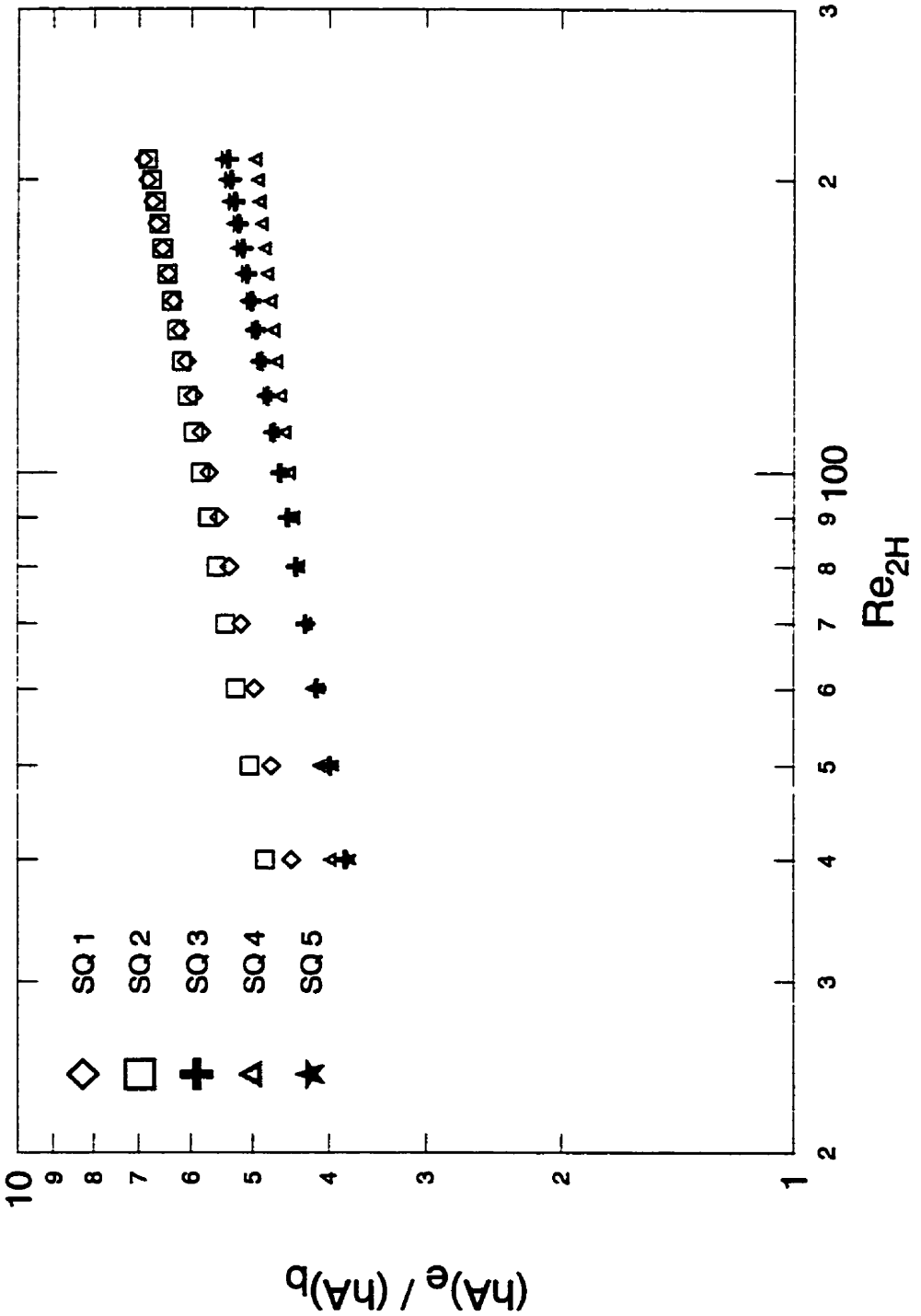

Fig. 5.23 - Enhancement Ratio for SQ Turbulator Strips with $\dot{P} = Constant$.

Chapter 6

Modelling and Analysis: Enhanced Channels

6.1 Introduction

Almost all compact heat exchangers utilize the plate fin as a means of increasing surface area and enhancing the heat transfer coefficient. Three configurations of the plate fin surfaces being considered are: continuous fin, interrupted fin, and the turbulator strip. The continuous plate fin consists of straight uninterrupted channels of non-circular shape. Thus, the models developed in Chapter 4 are directly applicable to this geometry. The interrupted strip fin or offset strip fin (OSF) and the turbulator strip are dealt with in this Chapter. Both devices are similar in construction, however, their orientation in the flow field, refer to Fig. 6.1, is the primary distinguishing feature in applications.

The present Chapter is divided into four sections. First, the approach to modelling is discussed for each device. Next, a review of the fundamental solutions of fluid dynamics and heat transfer which are used in the development of the proposed models is presented. In the final two sections, the development of models for the OSF and turbulator strip geometries are presented along with comparisons with experimental data for each device. In the case of the OSF, comparisons are made with existing

data from Kays and London (1984), while the turbulator model is compared with new data presented in the previous Chapter.

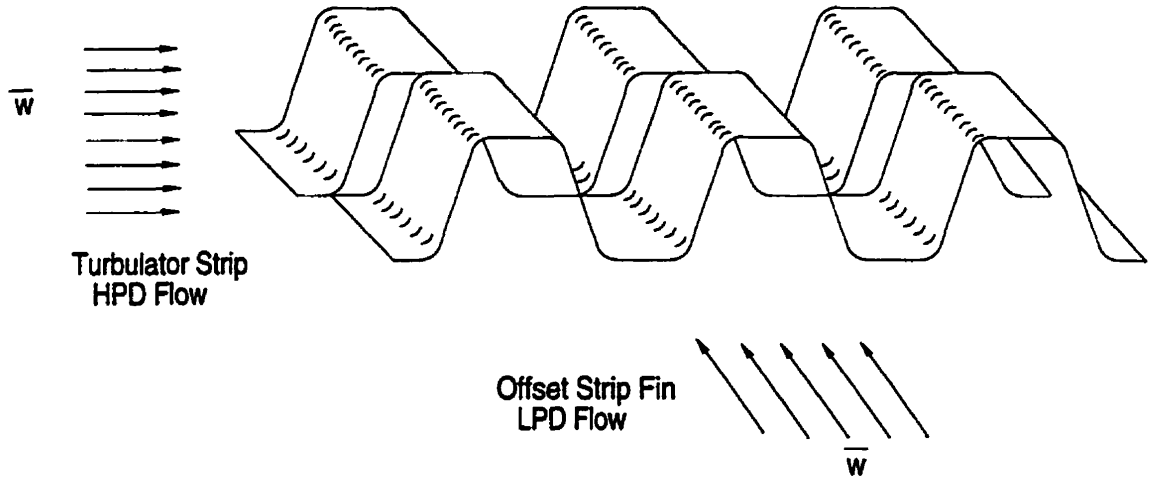

Fig. 6.1 - Interrupted Plate Fin Arrangements

6.2 Approach to Modelling

Models for both the OSF and turbulator geometries are developed by considering three distinct regions or flow regimes. These are: low Reynolds or creeping flow, laminar boundary layer flow, and turbulent boundary layer and/or inertial flow. Experimental data for both the OSF and turbulator geometries exhibit smooth transition from creeping flow to laminar boundary layer to turbulent like behavior. Models for these three regions or zones are developed and combined using the asymptotic correlation method proposed by Churchill and Usagi (1972).

The use of a three zone model to analyze heat transfer and fluid flow phenomena has been undertaken in the past by Hassani (1987) for natural convection from arbitrary three dimensional isothermal bodies, and by Achenbach (1995) for modelling heat transfer in packed beds. The work of Hassani (1987) involved combining the conduction or zero flow limit with the laminar and turbulent boundary layer solutions for natural convection problems. In the work of Achenbach (1995), the zero flow or

conduction limit for a packed bed was combined with the laminar and turbulent flow asymptotes for a single sphere.

Depending on the nature of the problem, a three zone model may be developed by combining the models or zones in the following manner:

$$y = \left[\{(y_o)^n + (y_{lam})^n\}^{m/n} + (y_{tur})^m\right]^{1/m} \tag{6.1}$$

or

$$y = \left[(y_o)^n + \{(y_{lam})^m + (y_{tur})^m\}^{n/m}\right]^{1/n} \tag{6.2}$$

where y_o denotes the creeping or low flow region, y_{lam} denotes the laminar boundary layer region, and y_{tur} denotes the turbulent or inertial flow region.

Models for these regions are developed from fundamental solutions reported in the heat transfer and fluid dynamics literature. These solutions accurately represent the observed trends in the experimental data. By considering a simple characteristic element of the OSF and turbulator geometries, the laminar and turbulent boundary layer models may be derived by performing simple force and energy balances. These models are then combined with the low flow asymptote using the form of Eqs. (6.1) or (6.2).

6.3 Review of Fundamental Solutions

The models which will be developed in this Chapter use several fundamental solutions from the heat transfer and fluid dynamics literature as building blocks. These solutions represent ideal geometries and flow conditions. Analytic, experimental and approximate analytical expressions will be reviewed for five types of flow conditions: laminar boundary layer, turbulent boundary layer, separated flow, creeping flow, and fully inertial flow.

6.3.1 Laminar Boundary Layer Flow

Solutions to the laminar boundary layer equations with pressure gradient, Eqs. (2.31-2.34), are reported in all convective heat transfer references (Kays and Crawford (1993), Burmeister (1993), Bejan (1995)). Solutions for three special cases of the wedge angle are summarized in Table 6.1 below. These solutions may be used as an indication of the effects of fin angle, width, and flow orientation. General expressions for the skin friction and heat transfer for any fin angle with $0 < \beta < 1$ are given below. This range covers the orientation from a flat plate to plane stagnation or a fin angle from 0° to 90°, refer to Fig. 6.2.

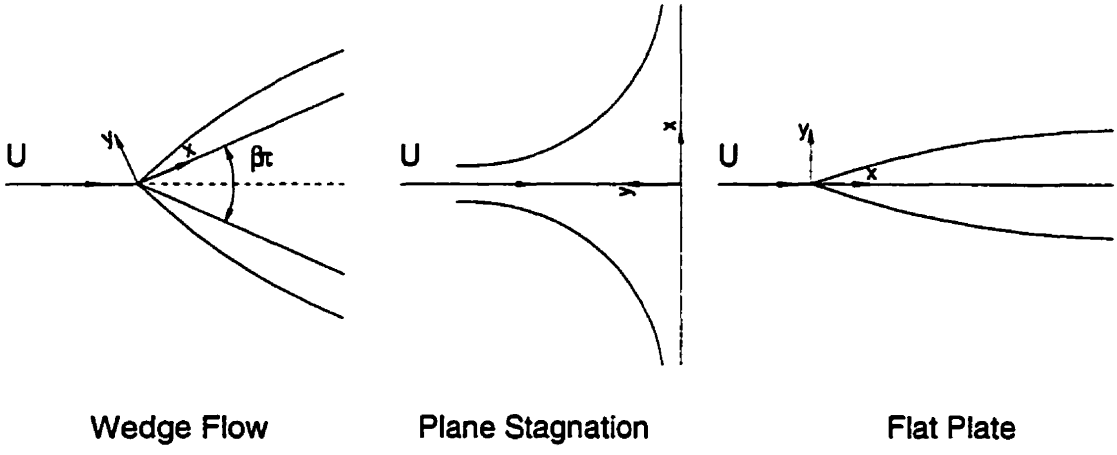

Fig. 6.2 - Flow Over a Wedge

Table 6.1

Summary of Heat Transfer and Friction in Wedge Flows

Flow Condition	β	$f''(0) = \frac{1}{2}C_{f,x}Re_x^{1/2}$	$Nu_x/Re_x^{1/2}$
Flat Plate	0	0.332	$0.332Pr^{0.33}$
Plane Stagnation	1	1.232	$0.570Pr^{0.40}$
Separated Flow	-0.1988	0	$0.224Pr^{0.25}$

The friction coefficient is defined as

$$C_{f,x} = 2f''(0)Re_x^{-1/2} \tag{6.3}$$

where $f''(0)$ is the solution to the boundary layer equations for the velocity gradient at the wall. It may be accurately determined from the following equation (Burmeister, 1993)

$$f''(0) = \frac{(1.225\beta + 0.244)^{0.534}}{\sqrt{2-\beta}} \tag{6.4}$$

for the range $0 < \beta < 1$.

The solution for the local Nusselt number in a wedge flow may be presented in terms of Eq. (6.4) by the following expression given in Cebeci and Bradshaw (1984) for the range $0 < \beta < 1$ and $Pr >> 1$

$$Nu_x = 1.12\left\{\frac{2}{2-\beta}\frac{f''(0)}{12}\right\}^{1/3} Pr^{1/3}Re_x^{1/2} \tag{6.5}$$

This expression reduces to

$$Nu_x = \begin{cases} 0.339Re_x^{1/2}Pr^{1/3} & \text{Flat Plate} \\ \\ 0.661Re_x^{1/2}Pr^{1/3} & \text{Plane Stagnation} \end{cases} \tag{6.6}$$

Average values of the friction and heat transfer coefficients for one wedge surface are related to the local values by means of the following expressions (Bejan (1995), Burmeister (1993))

$$\overline{C}_f = \frac{2}{3m+1}C_{f,x} \tag{6.7}$$

$$\overline{Nu}_L = \frac{2}{m+1}Nu_x \tag{6.8}$$

where $m = \beta/(2-\beta)$.

In the turbulator strip geometries, fluid flows over and around inclined surfaces. This flow field is neither similar nor dissimilar to the Falkner-Skan wedge flows, but possesses characteristics of both the flat plate and plane stagnation configurations, refer to Fig. 6.3.

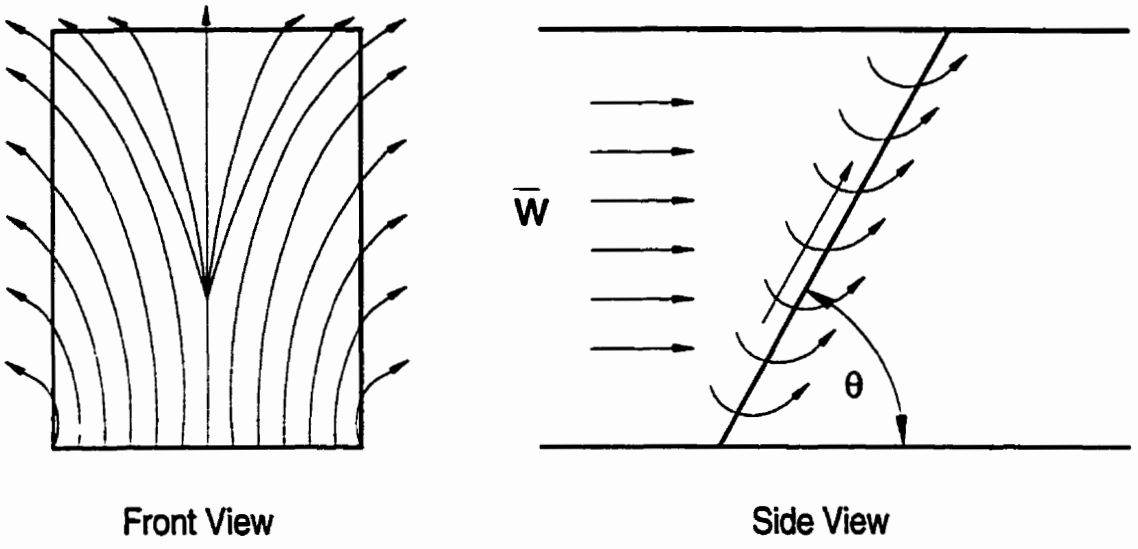

Fig. 6.3 - Three Dimensional Flow in a Turbulator Strip

A composite value for an inclined surface which is bounded by two parallel walls is proposed to take the form:

$$Nu_{eff} = Nu_{FP}\cos^2(\theta) + Nu_{PS}\sin^2(\theta) \tag{6.9}$$

and

$$C_{f,eff} = C_{f,FP}\cos^2(\theta) + C_{f,PS}\sin^2(\theta) \tag{6.10}$$

where FP denotes the flat plate component and PS denotes the plane stagnation component. These approximate expressions reduce to the flat plate and plane stagnation results as $0 < \theta < 90°$, and reduce to the arithmetic average at $\theta = 45°$.

6.3.2 Turbulent Boundary Layer Flow

At higher Reynolds numbers the flow becomes highly mixed and although laminar boundary layers may still be formed on the fin surfaces, the flow behaves in a turbulent like manner. Two important solutions which may be used to model the flow characteristics are the friction coefficient for a turbulent boundary layer on a smooth flat surface

$$\overline{C}_f = 0.074 Re_L^{-1/5} \tag{6.11}$$

and the Nusselt number

$$\overline{Nu}_L = 0.037 Re_L^{4/5} Pr^{1/3} \tag{6.12}$$

The above expressions are derived using the 1/7 power law rule for the turbulent velocity distribution. Details of the derivation of these semi-empirical solutions are available in most advanced fluid mechanics and heat transfer texts e.g. Schlichting (1979) and Knudsen and Katz (1958).

6.3.3 Separated Flow

Considerable heat transfer is also obtained in separated flows. This flow regime has been modelled analytically as a special case of the Falkner-Skan wedge flows (White, 1991) and has also been examined experimentally (Igarashi et al., 1975). An experimental relation which is valid in the rear of inclined flat plates for $\theta >$ 10°, rectangular cylinders and semi-circular cylinders was obtained by Igarashi et al. (1975) and is given by

$$Nu_X = 0.191 Re_H^{2/3} Pr^{1/3} \tag{6.13}$$

where H is the profile height and X is the chord length of the surface in cross-flow. In the present application, the flow in the wake region of the turbulator strip is such, that the chord length and profile height correspond to the width of the obstruction.

6.3.4 Creeping Flow

In the low Reynolds number region of the OSF geometries, characteristics of fully developed laminar flow in straight ducts become apparent. Regardless of the length of the interruption, Eqs. (2.29,2.30), dictate that fully developed flow conditions will prevail as $Re \rightarrow 0$. The models developed in Chapter 4 will be applicable in modelling flow through an interrupted channel. Of particular interest are the solutions for fully developed flow and for thermally developing flow in rectangular channels.

Creeping flow characteristics also appear in the low Reynolds number region of the turbulator geometries. These geometries are similar to consolidated media consisting of randomly shaped particles or packed columns typically found in the chemical process industries. The turbulator strip forms a continuous matrix surface which results in a complex flow field, refer to Fig. 6.4.

The friction factor in porous media for $Re \rightarrow 0$ has been derived by Carman (1956) using the Darcy flow model for a circular duct. The expression for the friction factor is usually presented in terms of an equivalent particle diameter. Since the turbulator strip is a continuous matrix, it is more appropriate to use a form which includes the hydraulic diameter of the channel rather than the equivalent spherical particle diameter. The analysis begins with

$$\frac{\Delta p}{L_e} = k_o \frac{16 \mu w_t}{d_h^2} \tag{6.14}$$

where k_o is called the Kozeny constant (Happel and Brenner (1965) and Churchill (1988)) for the packed or porous channel, L_e is the tortuous length of the channel

and w_t is the tortuous fluid velocity. The Kozeny constant has a value $k_o = 2$ for circular capillaries and $k_o = 3$ for a slit. For other shapes it typically takes a value somewhere between 1.5 and 3. A value of $k_o \approx 2.5$ is found experimentally for various non-circular capillaries , Carman (1956). Coincidentally, it is the average value of the slit and circular capillaries. Carman (1956) proceeded to introduce the tortuosity, L_e/L, and the tortuous velocity, $w_t = \overline{w}(L_e/L)$, to arrive at

$$\frac{\Delta p}{L_e} = k_o \frac{16\mu\overline{w}}{d_h^2}\left(\frac{L_e}{L}\right) \tag{6.15}$$

Now rewriting Eq. (6.15) in terms of the actual length of the channel or column gives:

$$\frac{\Delta p}{L} = k_o \frac{16\mu\overline{w}}{d_h^2}\left(\frac{L_e}{L}\right)^2 \tag{6.16}$$

The product of k_o and $(L_e/L)^2$ has been found experimentally to vary between 4 and 6 (Carman, 1956) and theoretical values for cylinders and spheres are reported by Happel and Brenner (1965) to lie between 4 and 7 for porosities between 0.1 and 0.9. Carman (1956) chose a value of $k_o\,(L_e/L)^2 \approx 5$ based upon the experimental data for flow of gases through a wide range of spherical, cubical, cylindrical and other non-spherical particles. This leads to

$$f = \frac{40}{Re_{dh}} \tag{6.17}$$

after introducing the definitions of the Fanning friction factor, the Reynolds number and the effective value of $k_o\,(L_e/L)^2$. The primary difference between the analysis reported above and that found in the literature (Carman (1956), Bird et al. (1962), Churchill (1987)) is the introduction of the specific surface and porosity concepts to define an effective particle diameter in place of the hydraulic diameter. This usually results in a slightly more complex expression. The result given by Eq. (6.17) is

generally valid below $Re_{d_h} < 10$. Above this critical value inertial effects become important.

An estimate for turbulator strips for the group $k_o\,(L_e/L)^2$ may be made by computing the value for the effective or tortuous flow length. In the turbulator strip geometries the fluid must flow around periodic obstacles of width W along a path having a wavelength λ. A typical flow path shown in Fig. 6.4 may be assumed to follow the wave form

$$f(x) = \frac{W}{2} \sin\left(\frac{4\pi x}{\lambda}\right) \tag{6.18}$$

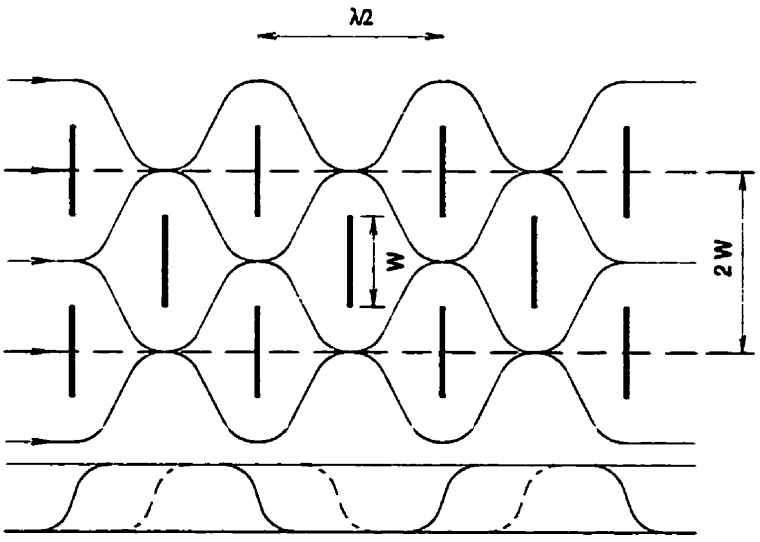

Fig. 6.4 - Sinusoidal Flow Through a Turbulator Strip

Now the effective flow length is the length of arc followed by Eq. (6.18). Using Eq. (6.18), the following expression may be derived for the turbulator strip:

$$k_o\left(\frac{L_e}{L}\right)^2 \approx 2.5\left(\frac{\int_0^\lambda \sqrt{1+f'(x)^2}\,dx}{\lambda}\right)^2 = C_o \tag{6.19}$$

Applying Eq. (6.19) along with the assumption that $k_o \approx 2.5$ results in values of $3.57 < k_o(L_e/L)^2 < 6.42$ for the turbulator geometries examined in Chapter 5. An average value for all ten turbulators gives $k_o(L_e/L)^2 \approx 4.61$, which is in the range of values typical for many packed beds. The creeping flow model for the turbulator geometry is taken to be:

$$f = \frac{8\,C_o}{Re_{d_h}} \tag{6.20}$$

where,

$$C_o = \frac{10}{\pi^2}\,(1+b^2)\,\mathbf{E}^2\left(\sqrt{\frac{b^2}{1+b^2}}\right) \tag{6.21}$$

and $\mathbf{E}(\cdot)$ is the complete elliptic integral of the second kind and $b = (2\pi W)/\lambda$.

Heat transfer at low Reynolds numbers in a porous parallel plate channel may be modelled as slug flow in a parallel channel containing no porous insert (Nield and Bejan, 1992). The solution for thermally fully developed flow with isothermal boundary condition is

$$Nu_H = 4.93 \tag{6.22}$$

where H is the channel height or wall to wall spacing. The slug flow model is applicable since the macroscopic velocity distribution in a porous channel is approximately uniform at every point in the cross-section and along the flow length.

6.3.5 Inertial Flow

At large flow rates or velocities, the flow within the enhanced geometries is affected by both profile drag and local expansion and contraction losses as the fluid meanders through the complex channel.

Drag Coefficients

In both the OSF and turbulator geometries form drag represents a significant component of the total pressure drop at large flowrates. Previous studies by Kays and Crawford (1993) and Joshi and Webb (1987) have suggested that the form drag component in an OSF array may be modelled using the potential flow solution for flow normal to a flat plate. The solution which is reported by both Lamb (1932) and Milne-Thompson (1968) is

$$C_D = \frac{2\pi}{\pi + 4} \approx 0.88 \tag{6.23}$$

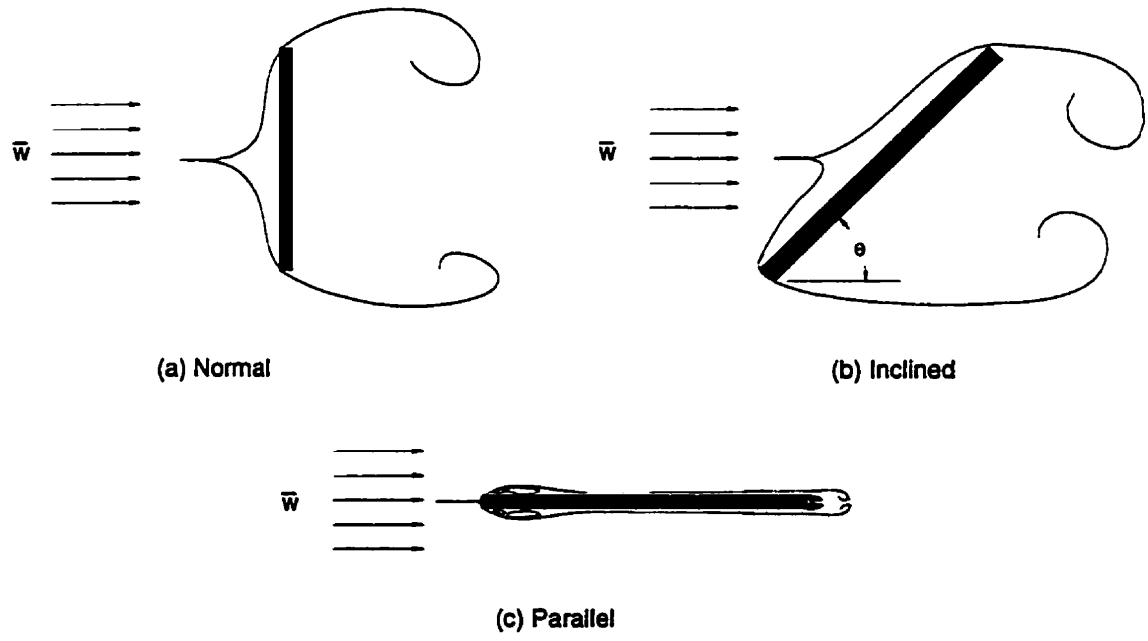

Fig. 6.5 - Flow Past a Flat Plate

If the fluid flows past an inclined plate, refer to Fig. 6.5, the drag coefficient based upon the chord length of the plate as reported by Lamb (1932) and Milne-Thompson (1968) is

Drag Coefficients

In both the OSF and turbulator geometries form drag represents a significant component of the total pressure drop at large flowrates. Previous studies by Kays and Crawford (1993) and Joshi and Webb (1987) have suggested that the form drag component in an OSF array may be modelled using the potential flow solution for flow normal to a flat plate. The solution which is reported by both Lamb (1932) and Milne-Thompson (1968) is

$$C_D = \frac{2\pi}{\pi + 4} \approx 0.88 \tag{6.23}$$

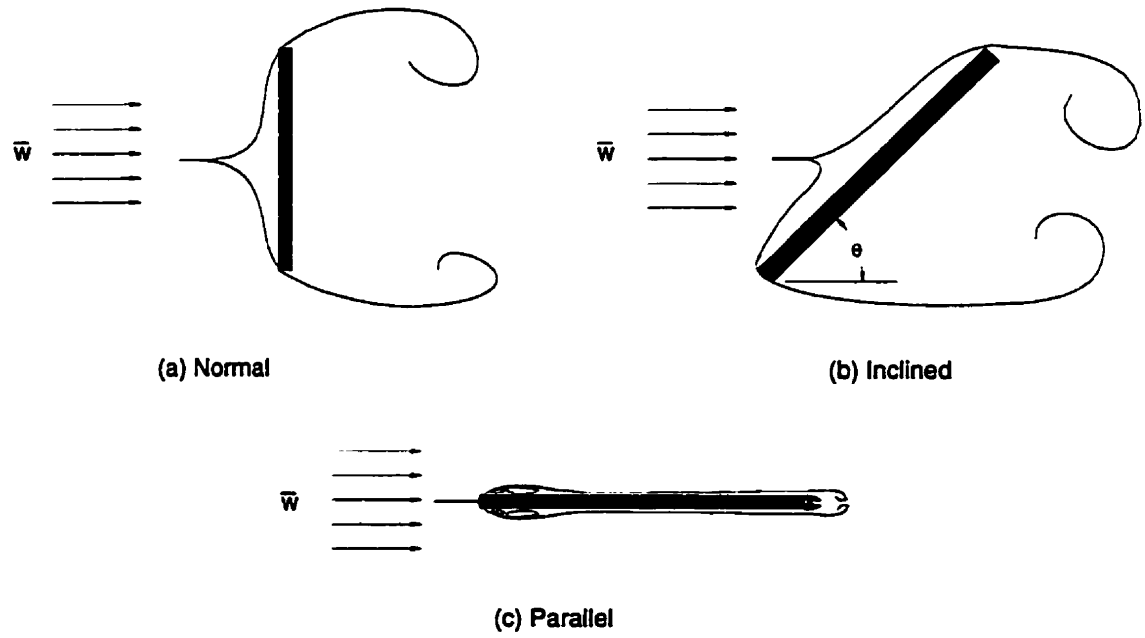

Fig. 6.5 - Flow Past a Flat Plate

If the fluid flows past an inclined plate, refer to Fig. 6.5, the drag coefficient based upon the chord length of the plate as reported by Lamb (1932) and Milne-Thompson (1968) is

$$C_D = \frac{2\pi \sin^2(\theta)}{\pi + 4\sin(\theta)} \tag{6.24}$$

Experimental values of the drag coefficient for two dimensional flow normal to flat plates and rectangular cylinders are typically in the range $0.89 < C_D < 2.4$, (Knudsen and Katz (1958), Blevins (1984)). Experimental results for flow past an inclined plate are also reported in Knudsen and Katz (1958) and Blevins (1984) and vary from $0.2 < C_D < 1.2$ for $20° < \theta < 90°$.

In the OSF geometries, a streamlined type of flow prevails, refer to Fig. 6.5c. The blunt leading edge of the interruption contributes a form drag component, however as a result of re-attachment of the boundary layer, the separation zone at the trailing edge of the interruption is small, and the drag coefficient may be taken to be Eq. (6.23). The experimental value for a rectangular plate of length L and thickness t having $L/t = 6$ is $C_D = 0.89$, Blevins (1984), which is in agreement with the potential flow solution. In the turbulator type geometries a large separation zone in the rear of the obstruction results in a much larger form drag contribution due to the lack of surface for boundary layer re-attachment. This behavior is typical of experimental data for many elongated bodies which are reported in Knudsen and Katz (1958). Data for rectangular and elliptic cylinders show a considerable decrease in the drag coefficient when the long axis of the body is oriented in the direction of flow. The drag coefficient for a rectangular plate having $L/t = 0.5$ is $C_D = 2.5$. For most of the turbulator geometries examined $L/t = 0.1$.

Flow past a fin surface within the turbulator geometries is primarily two dimensional since the flow is bound by the channel walls. The effect of fin angle has a considerable effect on the drag coefficient, since part of the flow is over the obstruction and part of the flow is around the obstruction. The following expression is proposed for modelling the drag coefficient

$$C_D \approx 2.4 f(\theta) \tag{6.25}$$

where

$$f(\theta) = \frac{(\pi + 4)\sin^2(\theta)}{\pi + 4\sin(\theta)} \tag{6.26}$$

Equation (6.25) was obtained by considering the effect of the inclination on the potential flow solution, i.e. Eq. (6.24) divided by Eq. (6.23) multiplied by the experimental value for the drag coefficient of a thin rectangular plate oriented normal to the flow $C_D(90°) \approx 2.4$.

Expansion and Contraction Losses

Finally, as the fluid flows through a turbulator strip it constantly encounters flow contractions and expansions as a result of the alternating rows which are out of phase with each other, refer to Fig. 6.6.

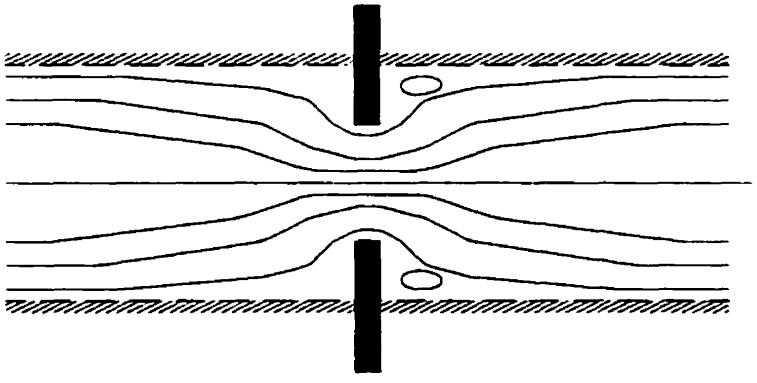

Fig. 6.6 - Flow Contraction and Expansion

The loss coefficients for a sudden contraction and a sudden expansion which the fluid experiences as it passes between the turbulator blades may be computed from the classic expressions reported in most fluid texts, e.g White (1987). The following expressions:

$$K_{SC} \approx 0.42\left(1-\beta^2\right) \tag{6.27}$$

and

$$K_{SE} = \left(1-\beta^2\right)^2 \tag{6.28}$$

are used to model the pressure drop which is a result of the sudden contraction and expansion within the turbulator geometry, where $K = \Delta p/(\frac{1}{2}\rho\overline{w}^2)$ and $\beta = A_i/A_o < 1$ is the area or blockage ratio. In most typical turbulator applications, the turbulator is composed of alternating rows which have the same width, i.e. $\beta = 0.5$. Thus, the total contribution of the expansion and contraction losses is found to be

$$K_{eff} \approx 0.878 \tag{6.29}$$

This value is also in agreement with values computed from graphical results reported in Kays and London (1984) for loss coefficients of tube bundles and parallel plate channels for various flow conditions. The effect of expansion and contraction losses within an OSF array are generally of the order of $K_{eff} < 0.1$ and will not be considered.

6.4 Modelling Offset Strip Fin Arrays

In this section the details of the model development for the OSF geometry are discussed. A typical OSF type geometry is shown in Fig. 6.7. The OSF is characterized by the interruption length L_f, the channel height H, the fin spacing s, and the fin thickness t. The model will be compared with data obtained from Kays and London (1984). The vast majority of these data were first published by Kays (1960), Briggs and London (1961), and London and Shah (1968). In all, nineteen sets of data are compared with the proposed model.

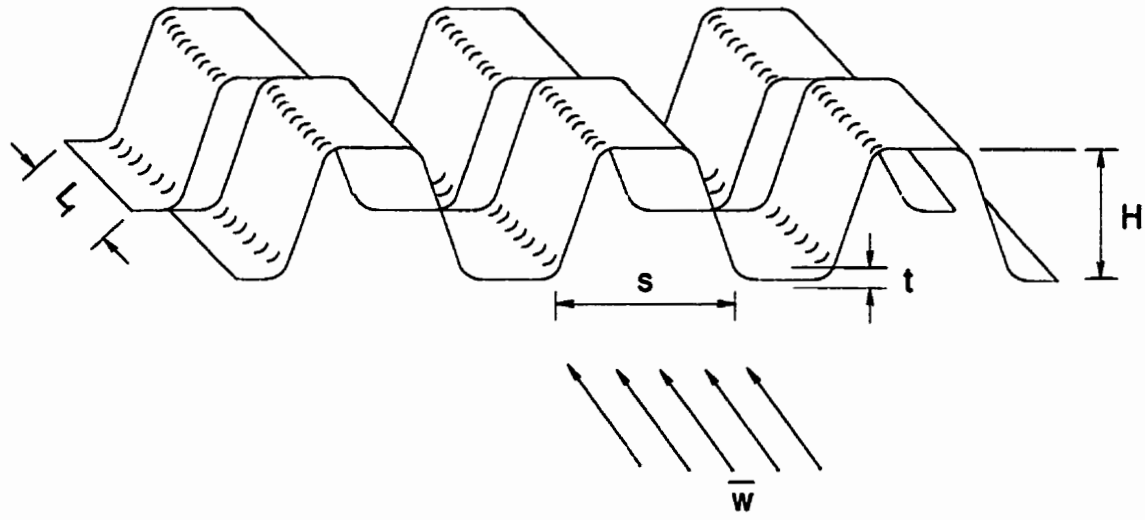

Fig. 6.7 - OSF Geometry

The following assumptions are made in the model development:

- Ideal surfaces, no burrs or scarfed edges
- Uniform surface dimensions throughout the array
- Complete destruction of boundary layers in the wake
- Negligible edge contributions
- Perfect contact at channel walls
- Isothermal surfaces

6.4.1 Friction Factor

Since the OSF is essentially an array of short rectangular (or other non-noncircular) ducts the friction factor should possess characteristic behavior of duct flow at low Reynolds numbers. In the limit $Re_{d_h} \rightarrow 0$ the value of f should approach the value for fully developed flow in a rectangular channel. In the limit of $Re_{d_h} \rightarrow \infty$ the value of f

should approach a constant value which is representative of the form drag component due to the finite fin thickness. Webb and Joshi (1982) developed a simple model by combining these asymptotic limits using the Churchill and Usagi (1972) correlation method. However, this model was only valid for OSF arrays having a channel aspect ratio $s/H < 0.25$. At larger values of the channel aspect ratio $s/H > 0.25$ the model provides poor correlation of the available data. The present model overcomes the deficiencies of the Webb and Joshi (1982) model by including additional terms in the laminar and turbulent asymptotes which capture the true physical behavior of the OSF array.

Laminar Region

In the laminar region, the flow field develops within each subchannel much the same as it does in a plain channel. A boundary layer is initiated on the subchannel walls and begins to grow. Depending upon the length of the subchannel, the flow may eventually become fully developed or remain partially developed when it leaves the subchannel. This suggests that the model developed in Chapter 4 for hydrodynamically developing flow may be used to predict the results in the laminar region. Figure 6.8 provides a comparison of a typical set of data obtained from Kays and London (1984) with several laminar and turbulent flow solutions. Comparison of the hydrodynamic entrance solution obtained by Shapiro et al. (1954), Eq. (3.1a), with OSF data from Kays and London (1984) shows that this solution overpredicts the friction factor. This overprediction is due to the fact that the entrance region solution not only accounts for the wall shear but also the increase in momentum of the inviscid core. The solution of Shapiro et al. (1954) also assumes a uniform entrance velocity distribution which is not present in the OSF application, (refer Fig. 6.9). Kays (Kays and Crawford, 1993) suggested better correlation is achieved by modelling the fin surface as a flat plate and accounting for the form drag component due to the finite edge thickness. This approach did not account for the low Reynolds number behavior which is apparent from Fig. 6.8.

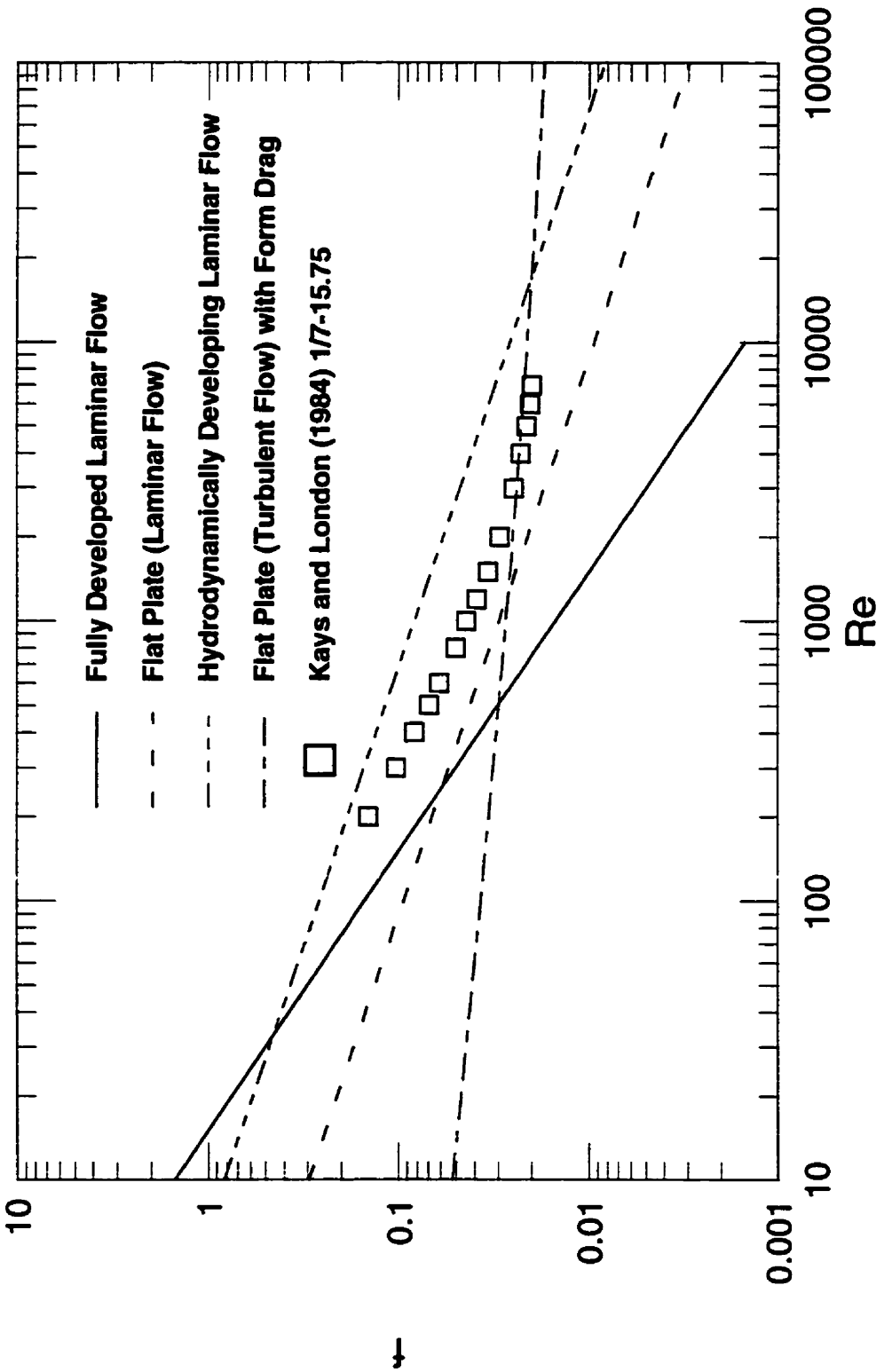

Fig. 6.8 - Comparison of Asymptotic Solutions with Data of Kays and London (1984) for 1/7-15.75.

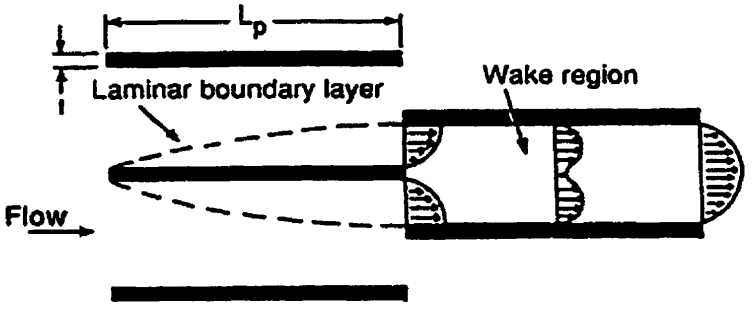

Fig. 6.9 - Velocity Distribution in an OSF Array.

The proposed laminar region model is taken to be a linear superposition of the Blasius solution for a flat plate and the fully developed friction factor for a rectangular duct

$$f_{lam} = \frac{\left(fRe_{D_h}\frac{d_h}{D_h}\right)}{Re_{d_h}} + 1.328\left(Re_{d_h}\frac{L_f}{d_h}\right)^{-1/2} \tag{6.30}$$

where fRe_{D_h} is the fully developed friction factor Reynolds number for the rectangular subchannel, D_h is the hydraulic diameter of the rectangular subchannel, d_h is the hydraulic diameter of the OSF array, and L_f is the length of the subchannel. A comparison of the laminar asymptotes is provided in Fig. 6.8 for a typical set of OSF data from Kays and London (1984). The above model represents the correct physical behavior for $Re_{d_h} \rightarrow 0$ or $L_f > 0.05 D_h Re_{D_h}$ and as Re_{d_h} increases or L_f decreases.

The proposed model may be interpreted in the following way. Upon leaving the subchannel the flow divides and enters two new subchannels. At this point, the velocity entering the new subchannel is zero at the centerline due to wall shear in the previous subchannel, (refer to Fig. 6.8. Since the centerline velocity is zero, the inlet velocity distribution is not uniform, which is a requirement for the hydrodynamically developing flow model presented in Chapter 4. As the flow begins to develop in the new subchannel, the velocity in the core region is less than that which would occur

if the inlet distribution were uniform. As a result of this lag, the boundary layer development is not affected by the inviscid core in the same way, and is similar to boundary layer development over a flat plate. In Shapiro et al. (1954) the authors point out that in the entrance region of a duct very near the inlet, boundary layer growth is very similar to that of a flat plate. However, as the core begins to accelerate, the boundary layer is unable to develop at the same rate as that for an isolated flat plate, since it is affected by the accelerating core.

Turbulent Region

The turbulent or non-laminar region may be modelled in a similar manner as done for the laminar region. The non-laminar region is generally characterized as having a turbulent wake (Joshi and Webb, 1987). In this region, the boundary layers which are formed are predominantly laminar but due to the wake effect, the behavior of the OSF is similar to that of a turbulent boundary layer. Performing a force balance on the subchannel results in the following expression:

$$\frac{\tau}{\frac{1}{2}\rho\overline{w}^2} = \frac{\tau_{wall}}{\frac{1}{2}\rho\overline{w}^2}\left(\frac{A_{wall}}{A_{wet}}\right) + C_D\left(\frac{A_{profile}}{A_{wet}}\right) \tag{6.31}$$

This expression may be written in terms of the turbulent boundary layer friction factor and drag coefficient given earlier. Equation (6.31) may be further simplified by assuming that $A_{wall}/A_{wet} \approx 1$ since the contribution of fin thickness to the total surface area is usually small, $< 5\%$, to give

$$f_{tur} = 0.074\left(Re_{d_h}\frac{L_f}{d_h}\right)^{-1/5} + \frac{(Ht + st/2)}{2L_f(H+s)}C_D \tag{6.32}$$

where H is the channel height, s is the width of the sub-channel, t is the thickness of the fin, and C_D is the form drag factor taken to be $C_D = 0.88$. Figure 6.3 shows the turbulent friction factor asymptote along with data for a typical OSF array from

Kays and London (1984). The data are in good agreement with the above expression in the region defined by $Re_{d_h} > 3000$.

Laminar - Transition - Turbulent Model

A general model which predicts the friction factor over the entire range of Reynolds numbers is developed by combining the the laminar and turbulent friction factors using the Churchill and Usagi (1972) correlation method.

The proposed model which is valid for the laminar - transition - turbulent region is given by

$$f = \left[\left\{ \frac{\left(f Re_{D_h} \frac{d_h}{D_h} \right)}{Re_{d_h}} + 1.328 \left(Re_{d_h} \frac{L_f}{d_h} \right)^{-1/2} \right\}^n + \left\{ 0.074 \left(Re_{d_h} \frac{L_f}{d_h} \right)^{-1/5} + \frac{(Ht + st/2)}{2L_f(H+s)} C_D \right\}^n \right]^{1/n} \tag{6.33}$$

where n is the correlation parameter. Values for n have been found to vary between $1.3 < n < 5$. A value of $n \approx 3$ provides excellent correlation for 19 data sets from Kays and London (1984). Comparison of the proposed model with data from Kays and London (1984) and the correlations developed by Manglik and Bergles (1995) will be provided after the development of a model for the analogous Colburn j factor.

6.4.2 Colburn j Factor

The Colburn j factor model is developed in essentially the same manner as the Fanning friction factor model. Since the OSF is essentially an array of short rectangular (or non-noncircular) ducts the Colburn j factor should possess characteristic behavior of duct flow at low Reynolds numbers. In the limit $Re_{d_h} \rightarrow 0$ the value of j should approach the value for fully developed flow in a rectangular channel. In the limit

$Re_{d_h} \rightarrow \infty$ the value of j should approach a value typical of turbulent boundary layer flow.

Laminar Region

In the laminar region, the Colburn j factor should possess characteristics of laminar duct flow. Kays (Kays and Crawford, 1993) suggested that the OSF can be modelled as a series of flat plates and that the j factor can be predicted by the analytical solution for a flat plate given by

$$j = 0.664 \left(Re_{L_f}\right)^{-1/2} \tag{6.34}$$

where L_f is the length of the interruption.

However, this relation tends to overpredict the data of Kays and London (1984), as shown in Fig. 6.4, and it has been suggested by Shah (1985), that better agreement with the data for OSF arrays is obtained using thermally developing flow solutions. such as the asymptotic solution proposed by Shah and London (1978):

$$j = 0.641 \left[\frac{f Re_{D_h}}{Re_{D_h}^2} \frac{D_h}{L_f}\right]^{1/3} \tag{6.35}$$

where $f Re_{D_h}$ is the fully developed friction factor Reynolds number group for the sub-channel. This result implies that a fully developed hydrodynamic boundary layer exists, whereas the flat plate model assumes that both hydrodynamic and thermal boundary layers develop simultaneously. In the laminar region the thermally developing flow solution underpredicts the data of Kays and London (1984). Both the flat plate model and the thermally developing flow asymptotic solutions are shown in Fig. 6.10 along with the turbulent boundary layer model and the fully developed laminar duct flow limit which is satisfied in the limit $Re_{d_h} \rightarrow 0$. It is clear from Fig. 6.10 that

both the fully developed laminar flow asymptote and the thermally developing flow asymptote characterize the laminar flow region.

If both the low Reynolds number limit $Re_{d_h} \rightarrow 0$ and the thermally developing flow asymptote are taken into consideration, then using the results presented in Chapter 4 for thermally developing flows gives:

$$j_{lam} = \left[\left(\frac{Nu_{D_h} \frac{d_h}{D_h}}{Re_{d_h} Pr^{1/3}} \right)^5 + \left(0.641 \frac{f Re_{D_h}^{1/3}}{Re_{d_h}^{2/3}} \left(\frac{d_h^2}{D_h L_f} \right)^{1/3} \right)^5 \right]^{1/5} \tag{6.36}$$

where fRe_{D_h} is the fully developed friction factor Reynolds number for the subchannel, Nu_{D_h} is the fully developed Nusselt number for the subchannel, D_h is the hydraulic diameter of the subchannel, d_h is the hydraulic diameter of the array, and Pr is the Prandtl number. This laminar flow model is plotted in Fig. 6.4 along with the flat plate model and the thermally developing and thermally fully developed models. Also presented in Fig. 6.4 is a typical OSF data set taken from Kays and London (1984). The above model represents the correct physical behavior for $Re_{d_h} \rightarrow 0$ or $L_f > 0.05 D_h Re_{D_h}$ and represents the correct physical behavior as Re_{d_h} increases or L_f decreases.

The proposed model may be interpreted in the following way. The data show that for $Re_{d_h} < 1000$ the flow is laminar. As the Reynolds number is decreased, the flow becomes more hydrodynamically developed. A typical OSF array has a subchannel length which is on the order of 1-10 mm, while the subchannel has a hydraulic diameter on the order of 2-3 mm. Using the approximate expression for predicting entry lengths, $L_{hy} \approx 0.05 D_h Re_{D_h}$, suggests that for most arrays the flow becomes hydrodynamically developed for $Re_{D_h} < 100$. This suggests that if $Re_{D_h} < 100$, the thermal boundary layer is more likely to be in a state of thermally developing flow. At $Re_{D_h} > 100$ the flow is more likely to be in a state of simultaneously developing flow and thus the flat plate model is more applicable. However, examination of Fig.

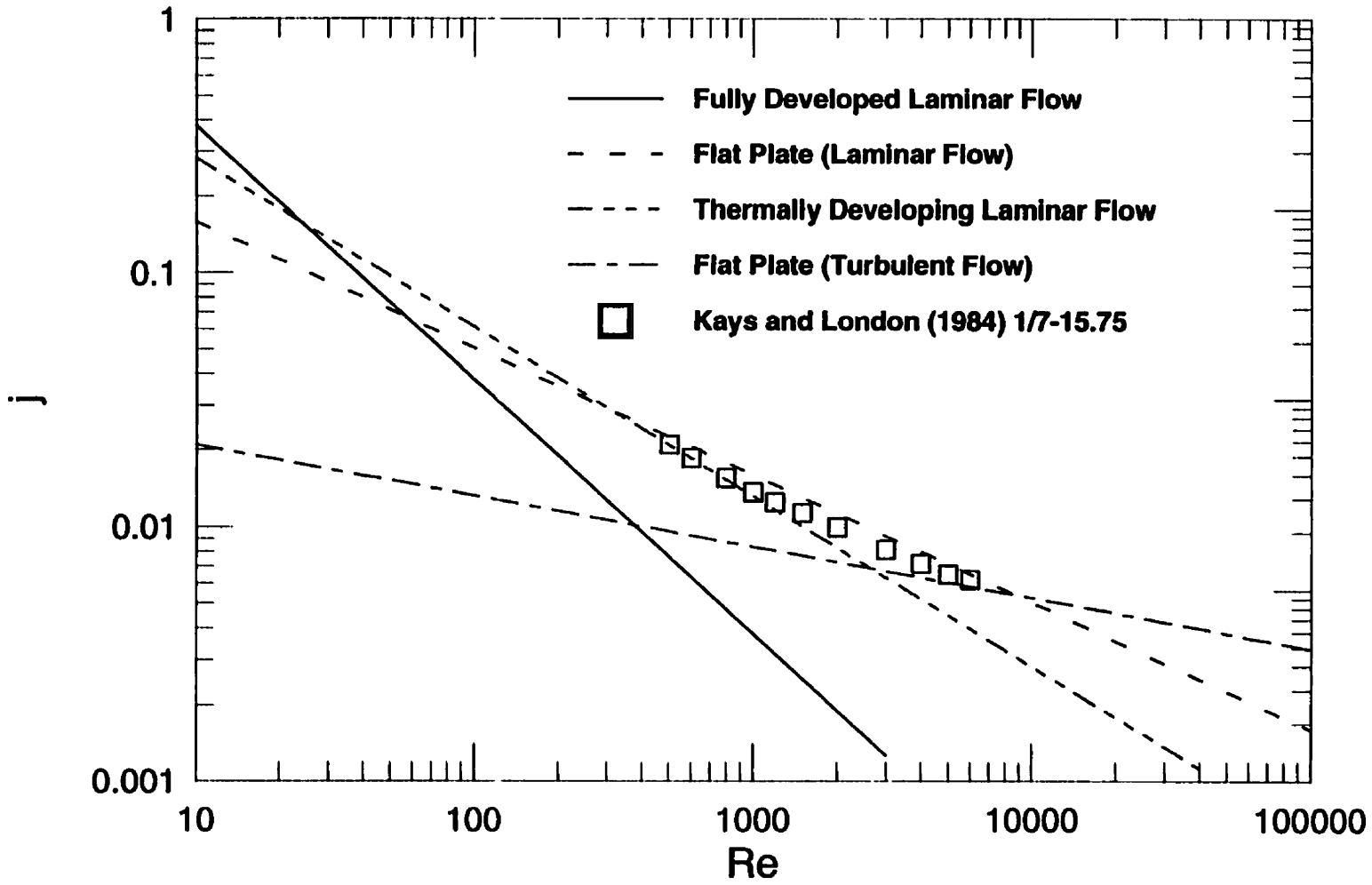

Fig. 6.10 - Comparison of Asymptotic Solutions with Data of Kays and London (1984) for 1/7-15.75.

6.10 shows that the results for Eqs. (6.34) and (6.35) are very close to each other in the region $100 < Re_{D_h} < 1000$ and both may predict results within 20 percent. Thus a model composed of the fully developed and thermally developed limits is more appropriate than one composed of the fully developed limit and the flat plate limit.

Turbulent Region

The turbulent or non-laminar region may be modelled in a similar manner as done for the laminar region. The non-laminar region is generally characterized as having a turbulent wake. In this region, the boundary layers which are formed are predominantly laminar but due to the wake effect, the behavior of the OSF is similar to that of a turbulent boundary layer. In the turbulent region the Colburn j factor is modelled using the Reynolds analogy $j = f/2$. Using the turbulent skin friction relation presented earlier gives:

$$j_{tur} = 0.037 \left(Re_{d_h} \frac{L_f}{d_h} \right)^{-1/5} \tag{6.37}$$

where L_f is the sub-channel length and d_h is the hydraulic diameter of the array. The turbulent model is shown in Fig. 6.10 along with data from Kays and London (1984). In the region defined by $Re_{d_h} > 5000$, the data agree well with Eq. (6.37).

Laminar - Transition - Turbulent Model

A general model which predicts the Colburn j factor over the entire range of Reynolds numbers is developed by combining the the laminar and turbulent models using the Churchill and Usagi (1972) correlation method.

The resulting model which is valid for the laminar - transition - turbulent region is given by

$$j = \left[\left\{ \left(\frac{Nu_{D_h} \frac{d_h}{D_h}}{Re_{d_h} Pr^{1/3}} \right)^5 + \left(\frac{0.641 f Re_{D_h}^{1/3}}{Re_{d_h}^{2/3}} \left(\frac{d_h^2}{D_h L_f} \right)^{1/3} \right)^5 \right\}^{m/5} + \left\{ 0.037 \left(Re_{d_h} \frac{L_f}{d_h} \right)^{-1/5} \right\}^m \right]^{1/m} \quad (6.38)$$

where m is the correlation parameter. Values for m are found to vary between $2 < m < 5$. A value of $m \approx 7/2$ provides excellent correlation for 19 data sets from Kays and London (1984). Comparisons of the proposed model with the data from Kays and London (1984) and the correlations developed by Manglik and Bergles (1995) are given in the next section.

6.4.3 Comparison of Models with Data

The proposed models are compared with nineteen sets of data for the OSF configuration which are available in tabular and graphical form in Kays and London (1984). Table 6.2 presents a summary of the optimal value of the correlation parameter for combining the laminar and turbulent models for each OSF data set. Excellent correlation is obtained for the friction factor data for most configurations. Examination of the Figs. 6.5-6.23 shows that the $1/8 - 15.61$, $1/9 - 24.12$, $1/9 - 25.01$, $1/10 - 19.74$, and $1/8 - 19.82D$ devices show possible effects of burred edges at high Reynolds numbers. If the fin edges are burred, an effective increase in the fin thickness will result in higher form drag contributions.

Good agreement between the proposed model and the OSF data is also achieved for all but four data sets for the Colburn j factor. Examination of Figs. 6.11-6.29 shows that for the $1/9 - 24.12$, $1/10 - 19.74$, $3/32 - 12.22$, and $1/6 - 12.18D$ devices, the model overpredicts at low values of the Reynolds number. At higher values of the Reynolds number, the data agree well with the model. This discrepancy may be due to experimental error. The experimental data provided in Kays and London (1984)

were obtained using air ($Pr \approx 0.71$) as a test fluid. At low velocities, tests conducted with air may experience a phenomena referred to as "rollover", (Shah, 1985). This phenomena results in measurements for the j factor which are lower than expected. Other factors, as outlined by Shah (1985), which may explain the trends in these data, are the effect of passage to passage non-uniformity and the presence of burrs.

Table 6.3 presents the RMS and (min/max) values of the percent differences for the case where a fixed value of the correlation parameter is used for all cases. The majority of the friction factor data are predicted within $\pm$ 20 percent while all but five data sets for the Colburn j factor data are predicted within $\pm$ 20 percent. Figures 6.11 - 6.29 compare the proposed models with the correlations developed by Manglik and Bergles (1995) and the data from Kays and London (1984). In almost all cases the correlations of Manglik and Bergles (1995) underpredict in regions of small and large Reynolds numbers when compared with the present model. Since the correlations are empirical fits, they are only valid within the range of the experimental data from which they were developed. Although Manglik and Bergles (1995) report that the model should be valid over the full range of Reynolds numbers, the present comparison indicates possible underprediction of the low Reynolds number flow characteristics. In the low Reynolds number region, the thermal and hydraulic characteristics should approach the characteristics of fully developed duct flow in the absence of mixed convection effects. In the high Reynolds number region, the present model also appears to predict the trends better. However, in most practical applications the the Reynolds number rarely exceeds 10000, Shah and Webb (1983). Thus, this does not pose any major problems in the applicability of the Manglik and Bergles (1995) correlation.

In a number of cases the the empirical correlations of Manglik and Bergles (1995) also provide poor correlation over the range of the available data. It is clear from Figs. 6.5-6.23 that the proposed model captures the correct physical behavior of the data. With the exception of five j data sets and two f data sets, in which the model either

overpredicts or underpredicts the data, good agreement between the proposed model and experimental data is achieved over a wide range of Reynolds numbers. Further validation of the model is in order for the low Reynolds region.

6.4.4 Effect of Subchannel Shape

Most OSF arrays are composed of rectangular sub-channels. However, in many applications, other shapes such as trapezoidal and sinusoidal may arise. The models developed for both the friction factor and the Colburn j factor may be applied to the these and other non-circular passage shapes, by simply providing the appropriate value for the fRe_{fd} and Nu_{fd} which appear in the models. These two dimensionless parameters can be accurately predicted using the models developed in Chapter 4. The geometric factor modifying the profile drag coefficient should also be adjusted based upon the actual profile area for the non-rectangular sub-channel.

Table 6.2

Comparison of Models with Data with Optimal Value of Blending Parameter

	f		j	
Designation	n	RMS	m	RMS
1/8-15.61	1.8	7.13	3.2	9.17
1/8-19.86	2.2	3.09	2.9	10.79
1/9-22.68	2.3	4.28	4.8	8.28
1/9-24.12	1.7	4.42	3.6	17.76
1/9-25.01	1.5	5.62	2.5	5.43
1/10-19.35	5.0	8.11	3.6	10.44
1/10-19.74	1.9	7.98	4.6	26.35
1/10-27.03	1.5	6.70	2.0	1.83
3/32-12.22	1.3	4.34	4.7	21.19
1/2-11.94 D	5.0	3.28	4.1	1.83
1/4-15.40 D	5.0	4.68	5.0	12.77
1/6-12.18 D	4.7	6.64	4.5	19.03
1/7-15.75 D	5.0	6.03	3.5	2.09
1/8-16.00 D	2.9	1.71	2.2	4.85
1/8-16.12 D	2.9	1.26	4.8	15.14
1/8-19.82 D	1.3	5.62	2.3	2.89
1/8-20.06 D	2.3	3.72	2.6	4.17
1/8-16.12 T	1.8	6.76	3.8	13.03
501 MOD	3.6	4.71	4.8	17.79

Table 6.3

Comparison of Models with Data with

Fixed Value of Blending Parameter

	f		j	
Designation	RMS	(min/max)	RMS	(min/max)
1/8-15.61	8.89	0.47/18.33	9.41	-13.90/11.95
1/8-19.86	4.61	2.96/7.35	10.63	-18.33/11.97
1/9-22.68	4.10	-1.11/7.48	9.49	-13.47/0.14
1/9-24.12	10.19	4.25/19.28	17.92	-29.06/10.87
1/9-25.01	13.33	9.17/22.52	8.17	-4.20/16.69
1/10-19.35	15.41	-19.54/-5.38	10.60	-19.73/7.12
1/10-19.74	9.92	-2.71/24.34	28.26	-45.35/2.50
1/10-27.03	13.58	8.76/18.30	10.58	6.29/16.07
3/32-12.22	16.65	12.13/20.11	22.60	-50.49/-2.03
1/2-11.94 D	10.85	-14.51/-2.45	2.40	-3.64/4.29
1/4-15.40 D	13.18	-16.41/-4.19	15.28	-24.10/0.10
1/6-12.18 D	13.87	-18.22/1.15	20.17	-39.46/-1.54
1/7-15.75 D	15.43	-20.81/-2.74	2.10	-2.53/4.25
1/8-16.00 D	4.06	-6.61/4.48	10.35	0.48/15.68
1/8-16.12 D	1.53	-2.13/-0.43	17.05	-24.87/-0.92
1/8-19.82 D	20.56	13.29/30.77	8.91	2.50/14.61
1/8-20.06 D	3.34	-0.38/7.30	7.16	-0.35/13.16
1/8-16.12 T	9.60	3.77/15.64	13.53	-21.55/5.11
501 MOD	4.76	-7.31/5.29	19.14	-29.57/8.14

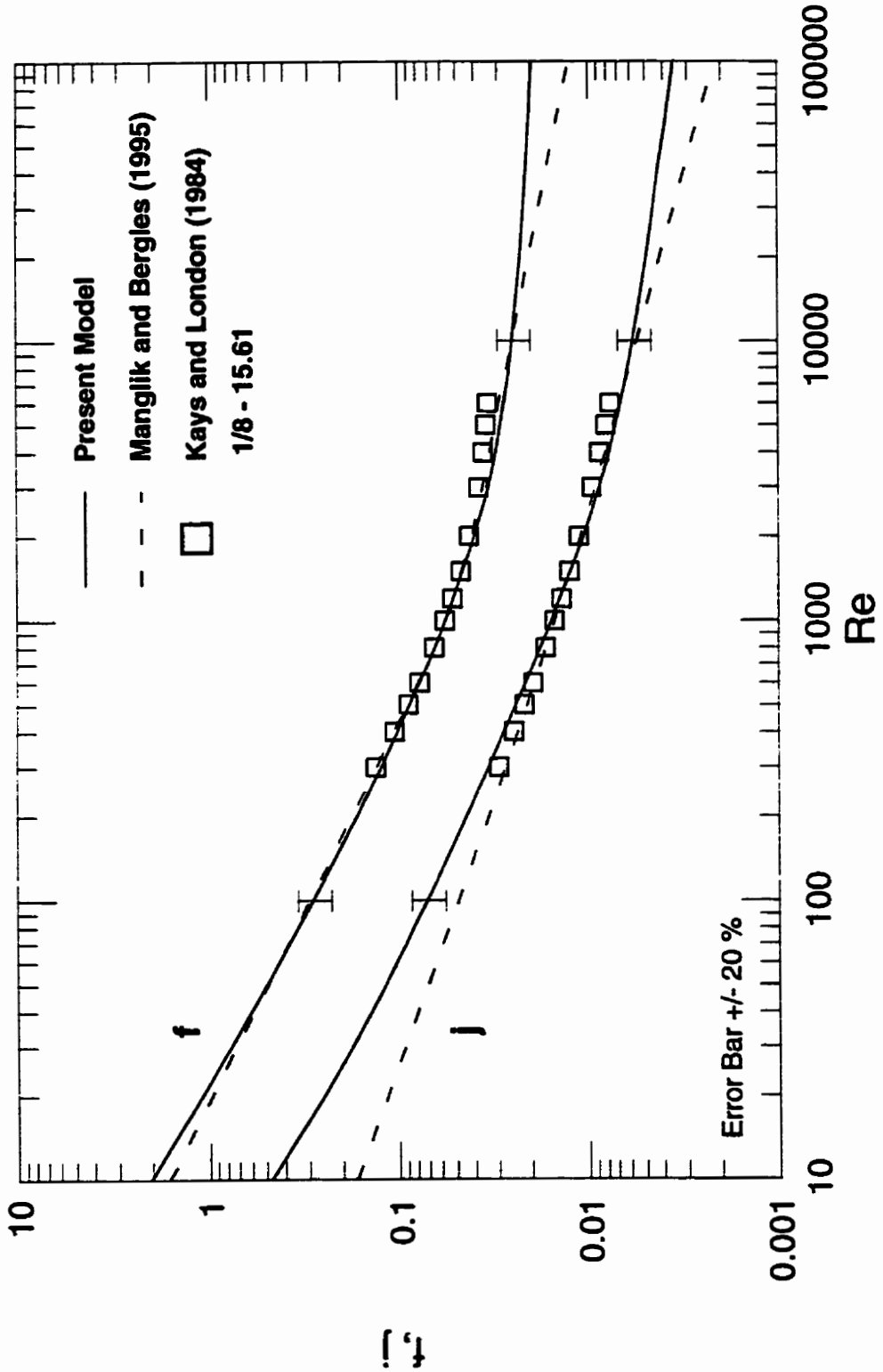

Fig. 6.11 - Comparison of Models with Data of Kays and London (1984) for 1/8-15.61.

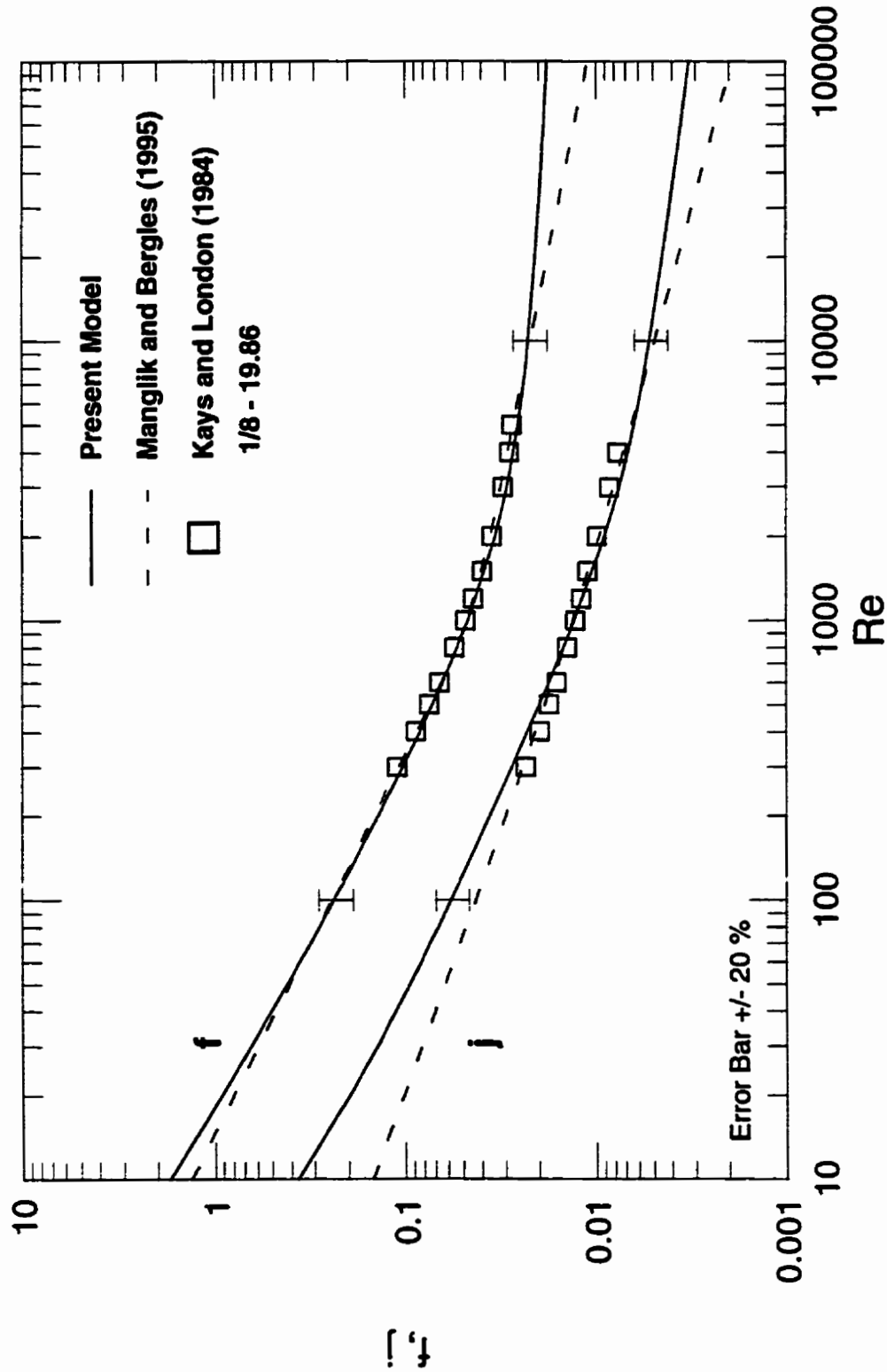

Fig. 6.12 - Comparison of Models with Data of Kays and London (1984) for 1/8-19.86.

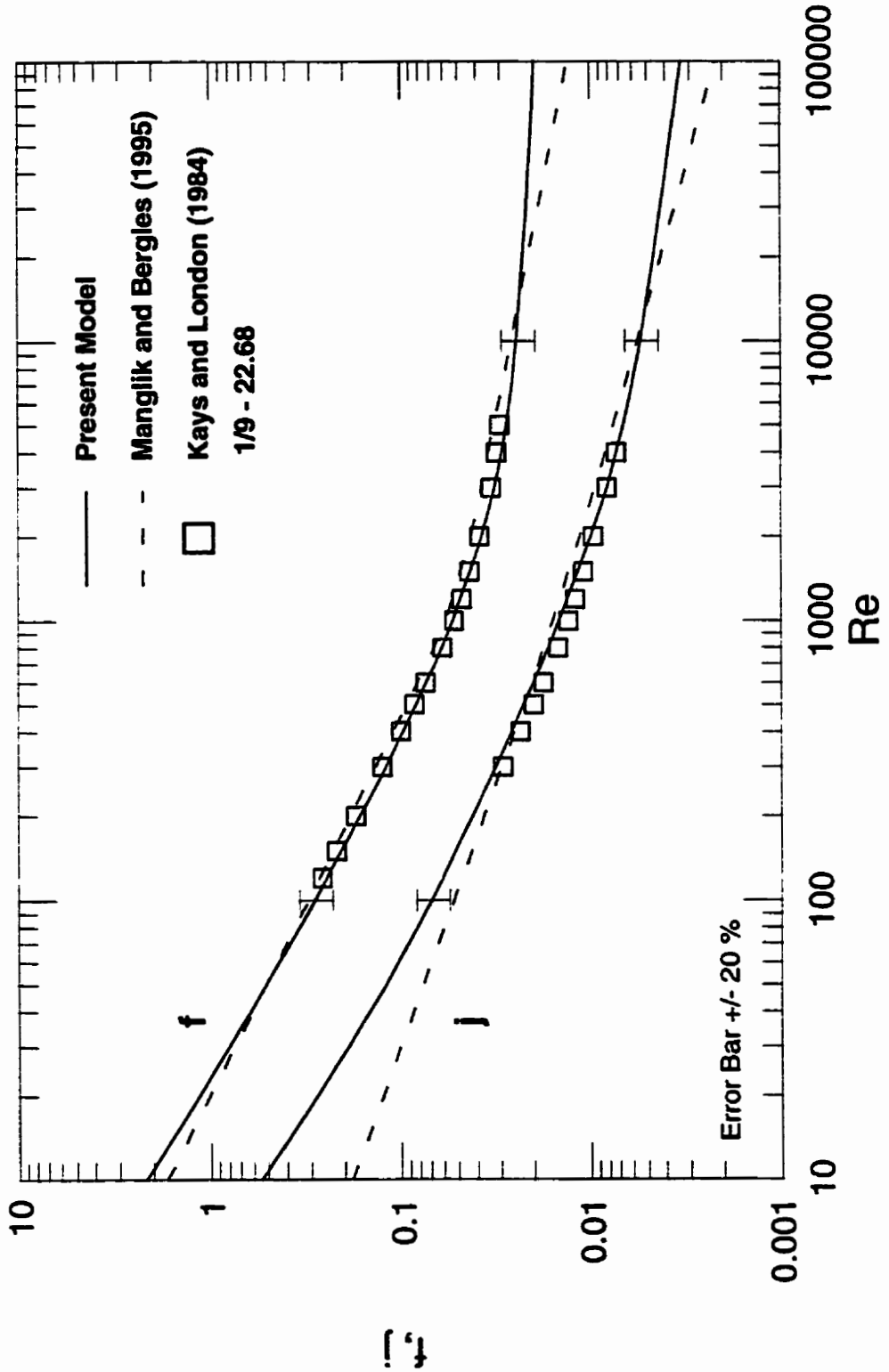

Fig. 6.13 - Comparison of Models with Data of Kays and London (1984) for 1/9-22.68.

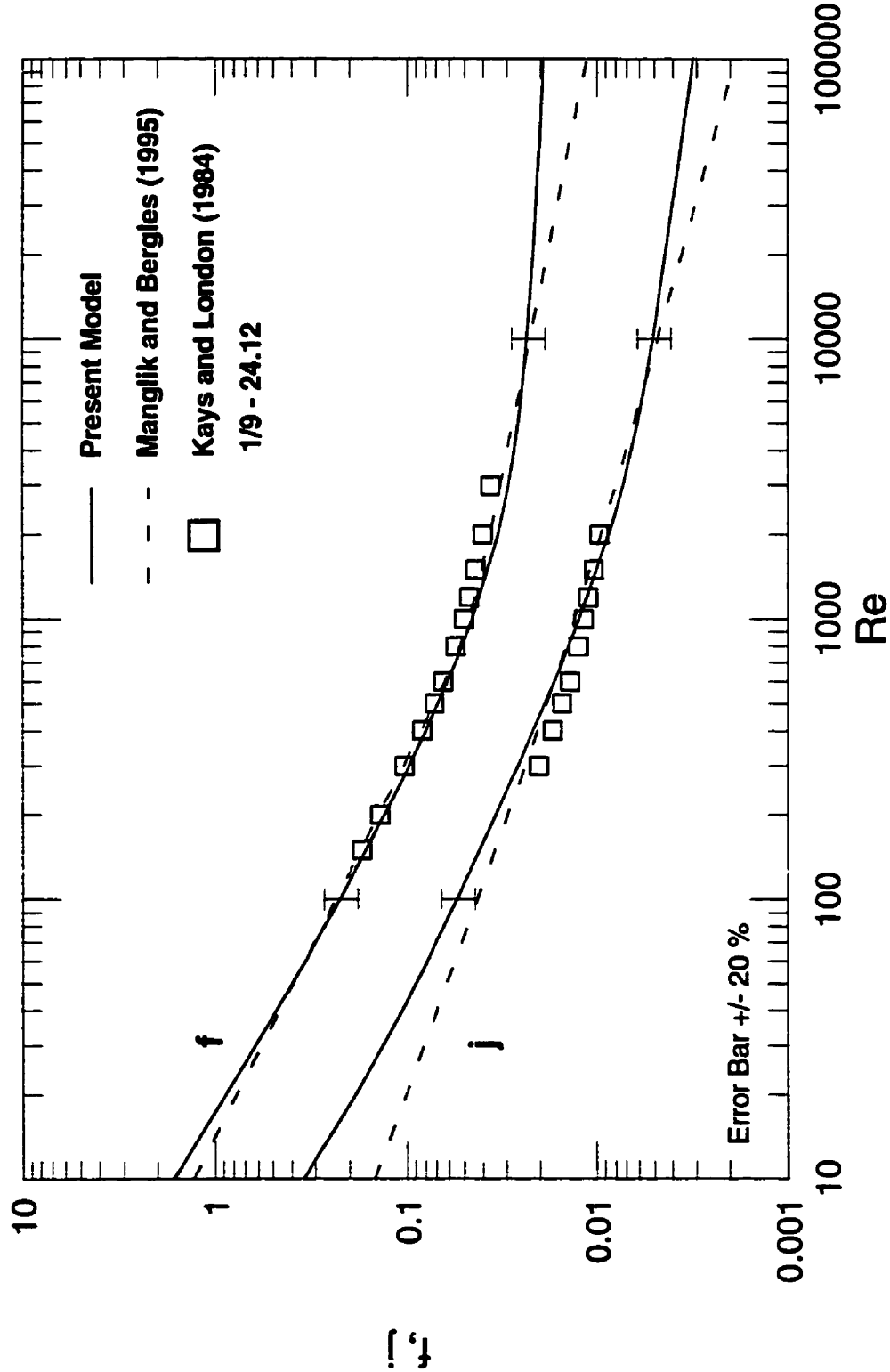

Fig. 6.14 - Comparison of Models with Data of Kays and London (1984) for 1/9-24.12.

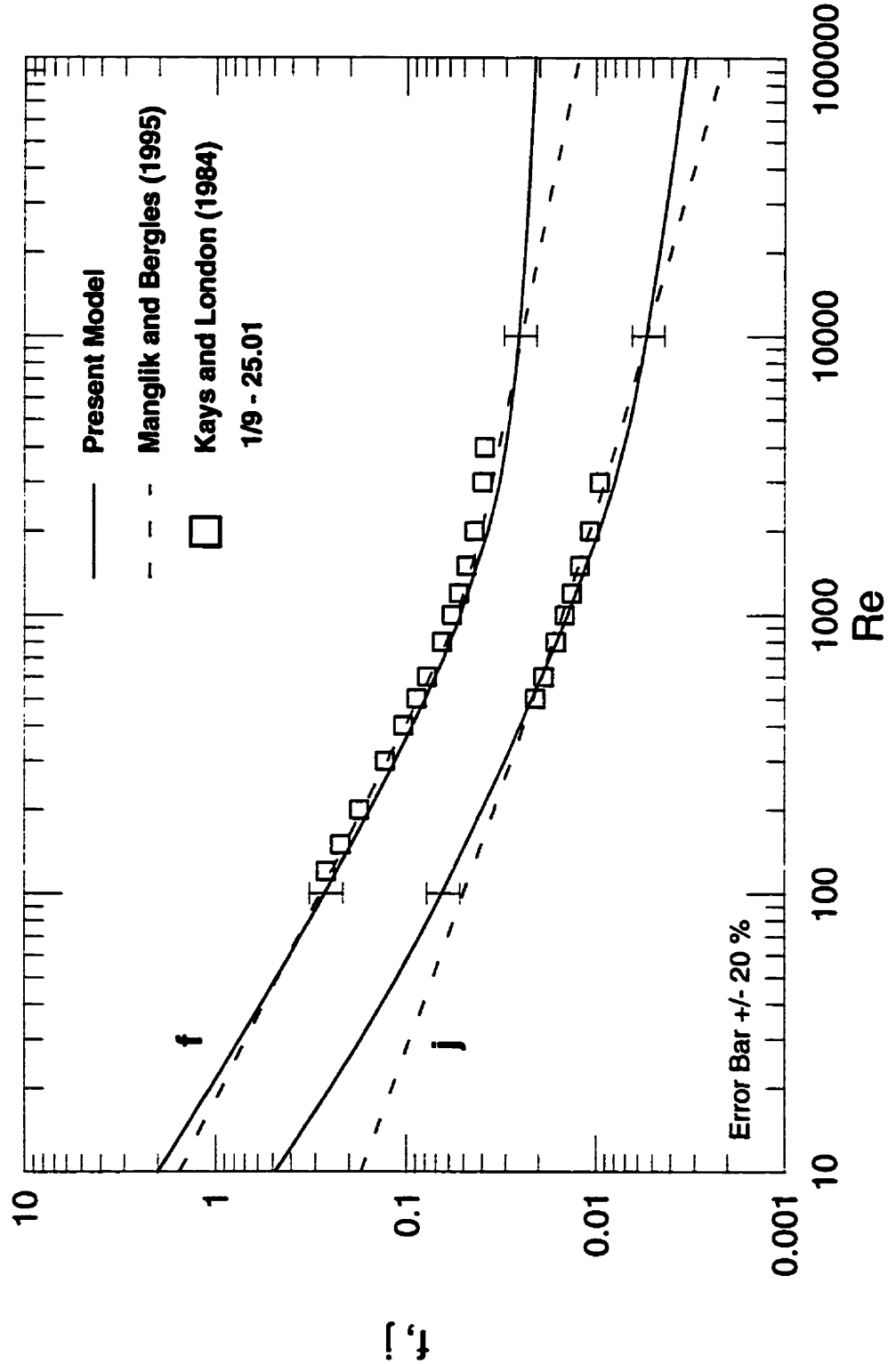

Fig. 6.15 - Comparison of Models with Data of Kays and London (1984) for 1/9-25.01.

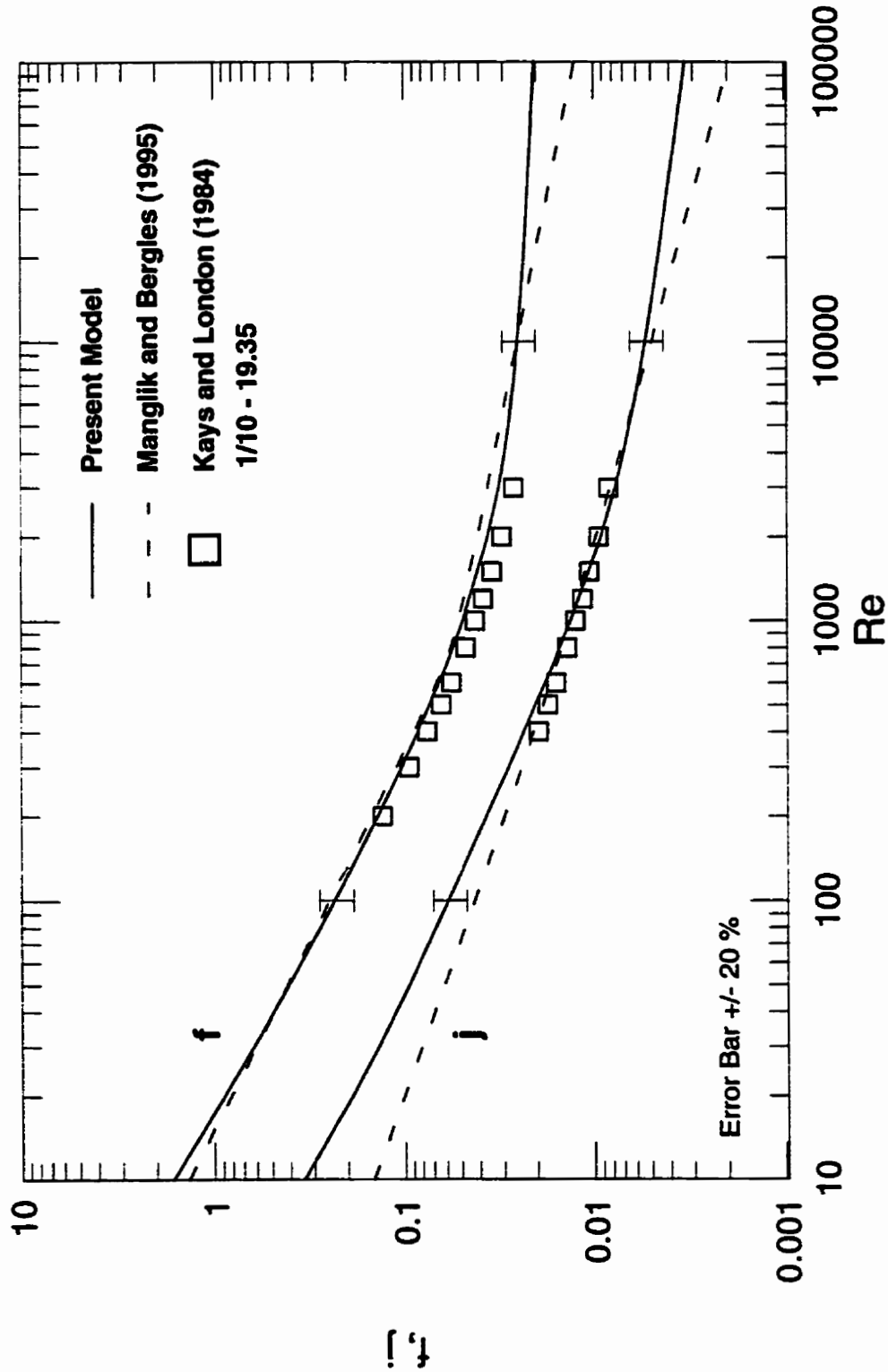

Fig. 6.16 - Comparison of Models with Data of Kays and London (1984) for 1/10-19.35

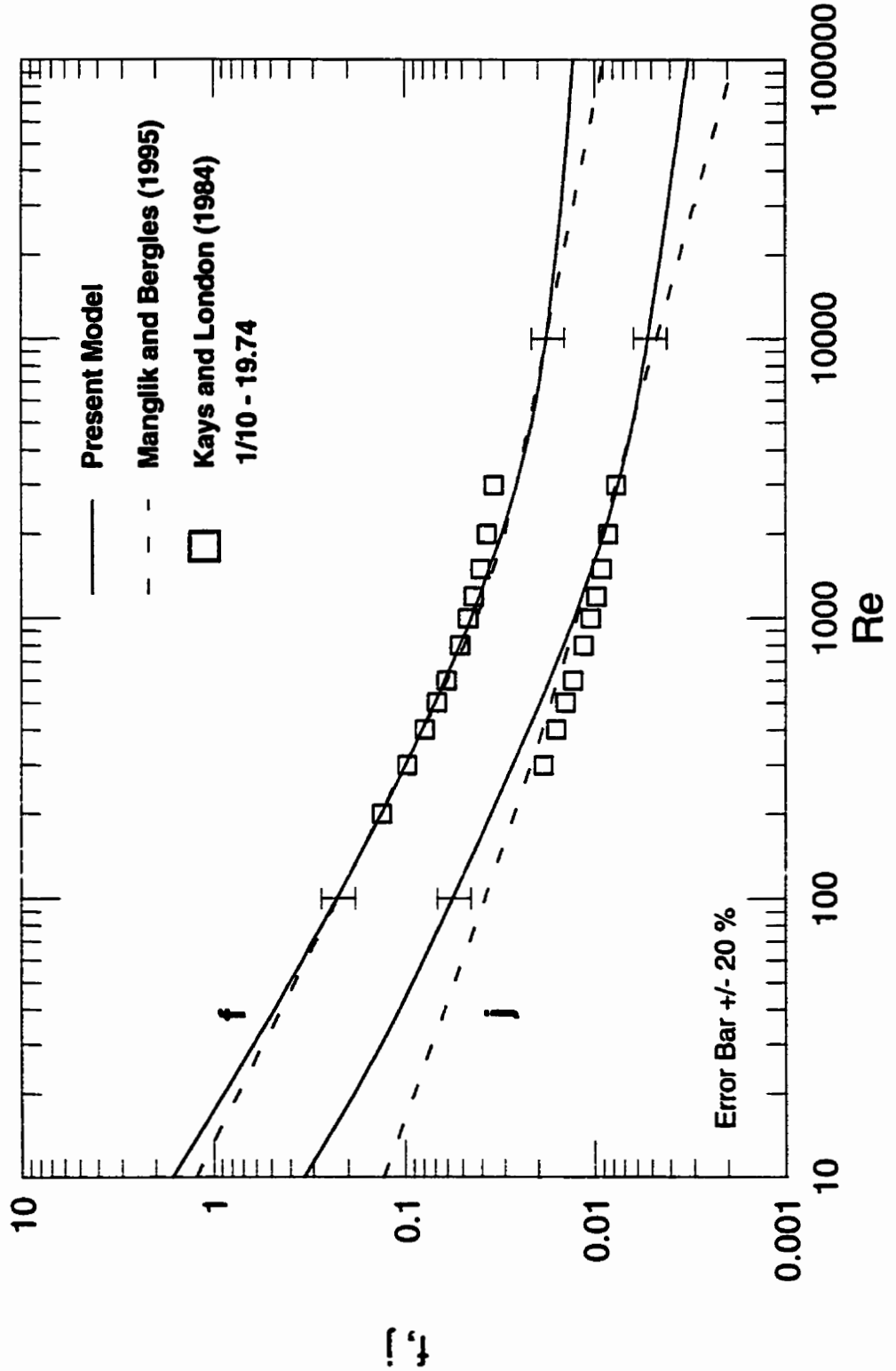

Fig. 6.17 - Comparison of Models with Data of Kays and London (1984) for 1/10-19.74.

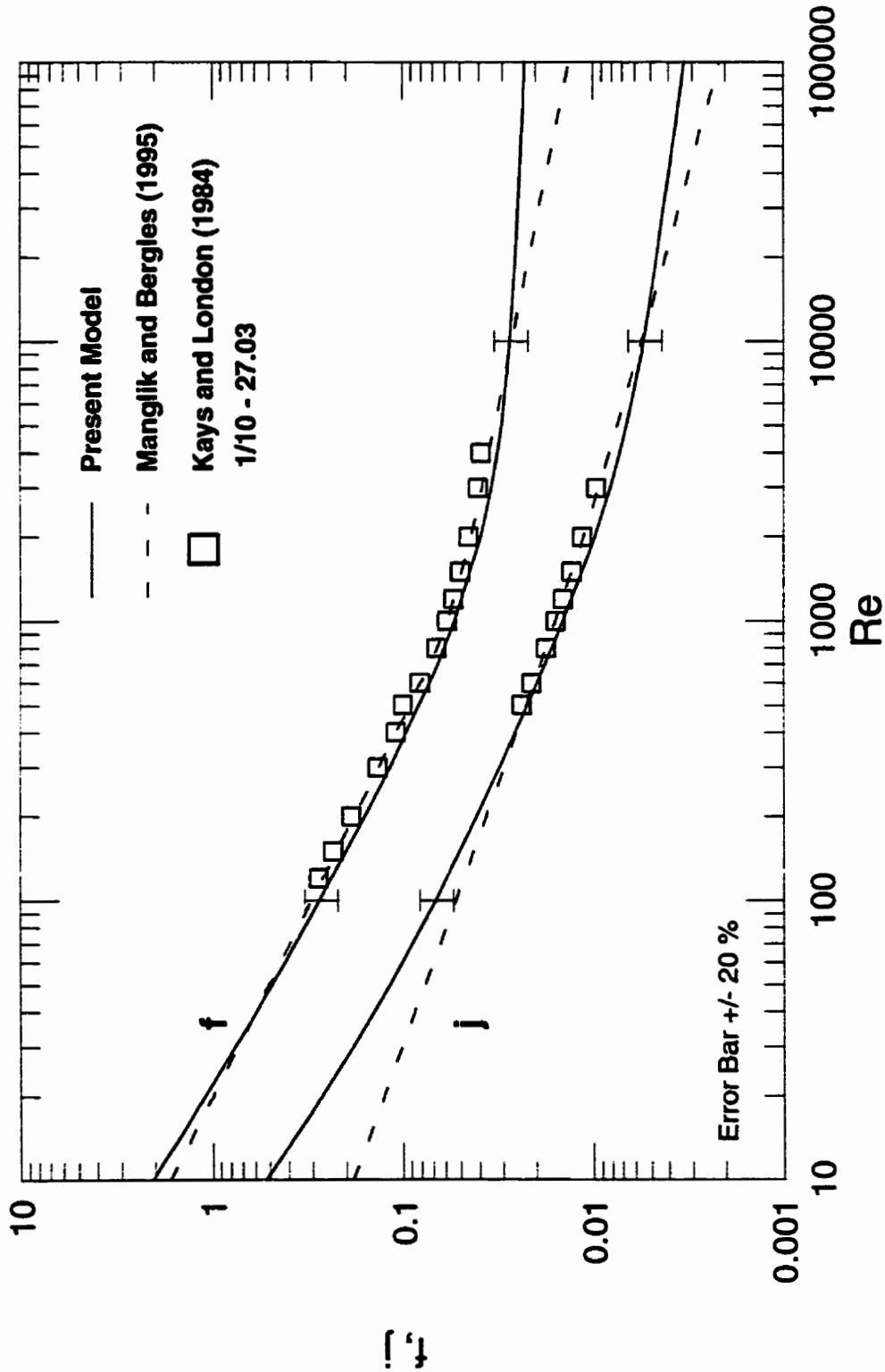

Fig. 6.18 - Comparison of Models with Data of Kays and London (1984) for 1/10-27.03.

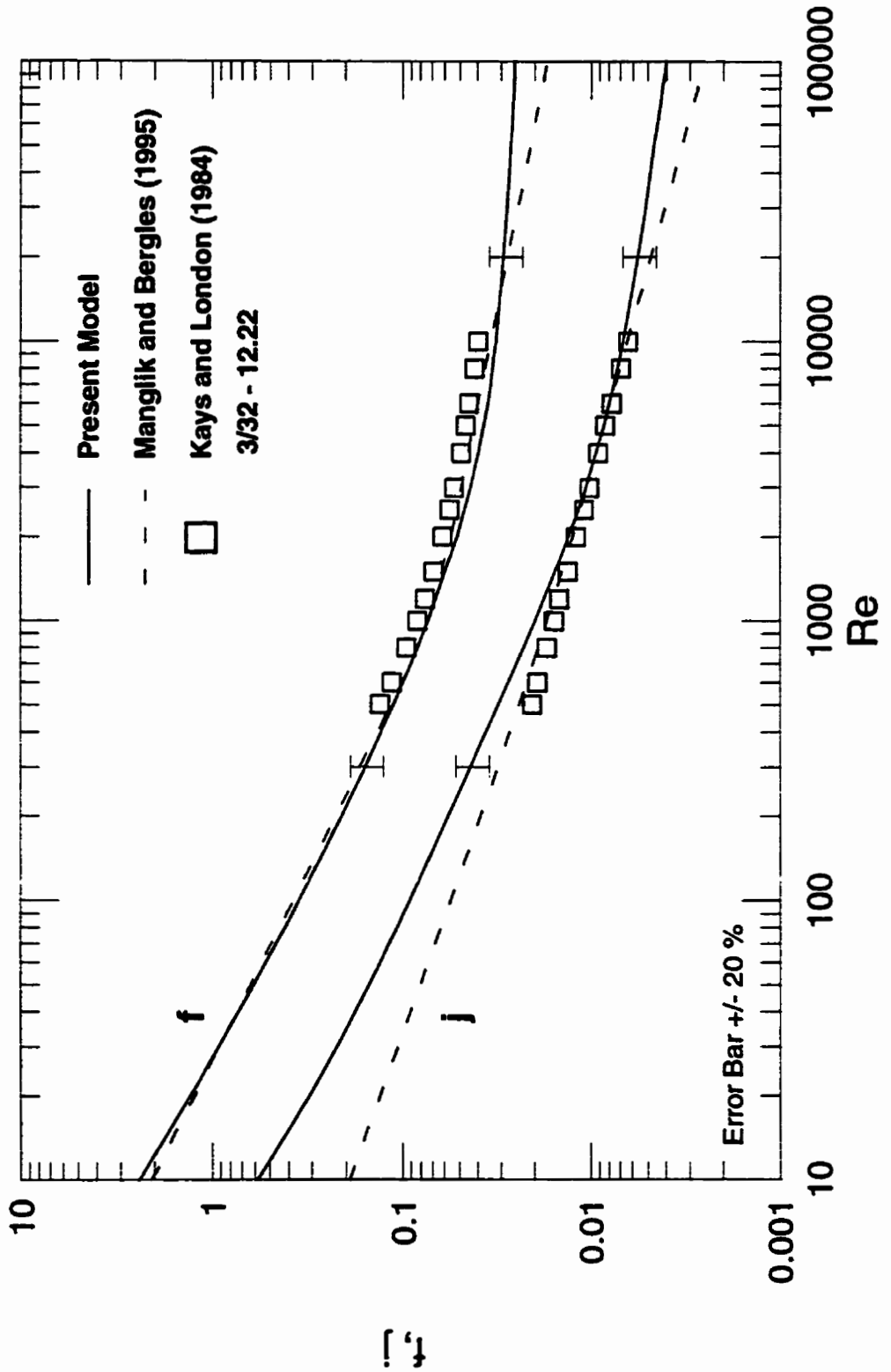

Fig. 6.19 - Comparison of Models with Data of Kays and London (1984) for 3/32-12.22.

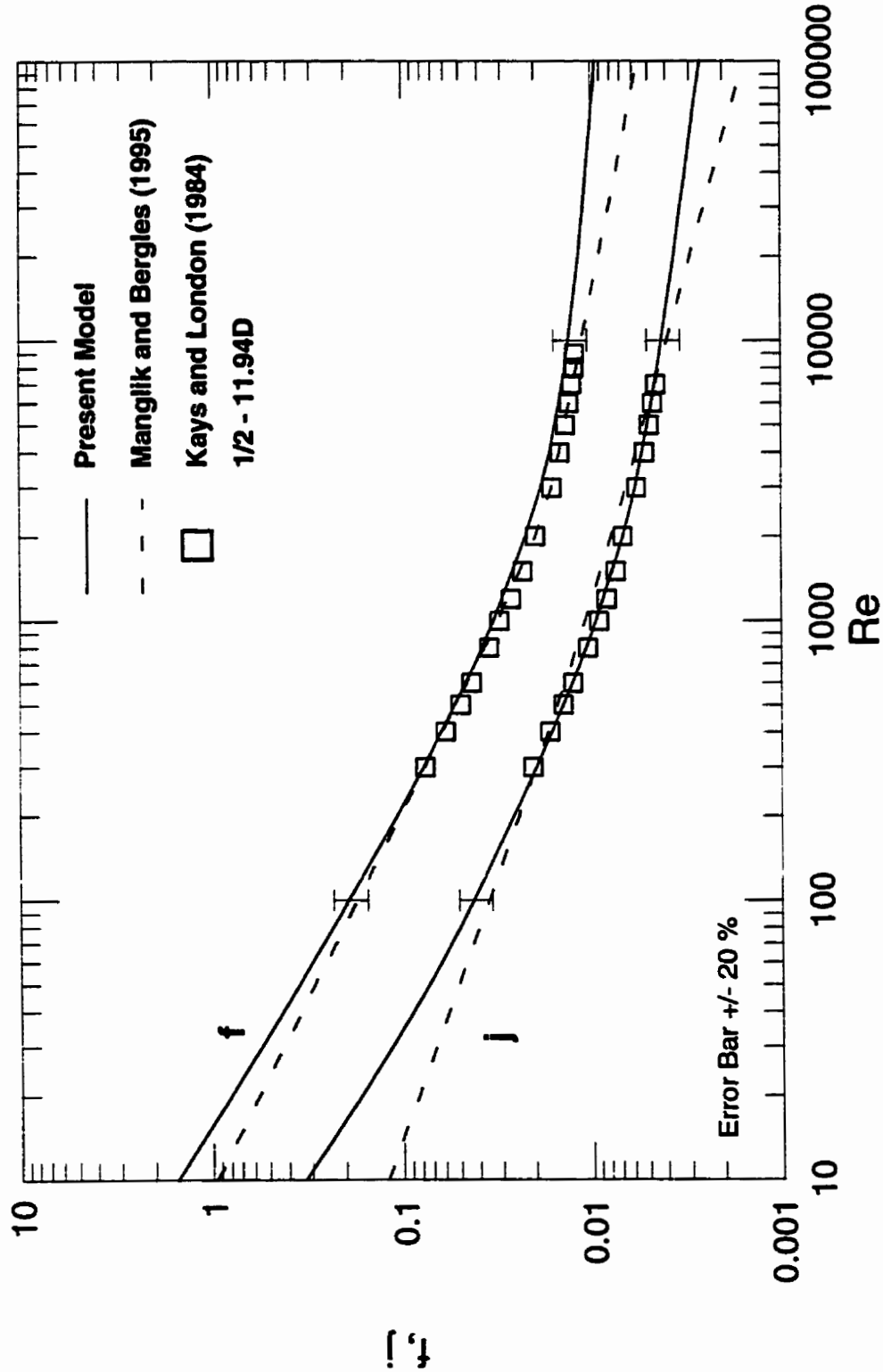

Fig. 6.20 - Comparison of Models with Data of Kays and London (1984) for 1/2-11.94D.

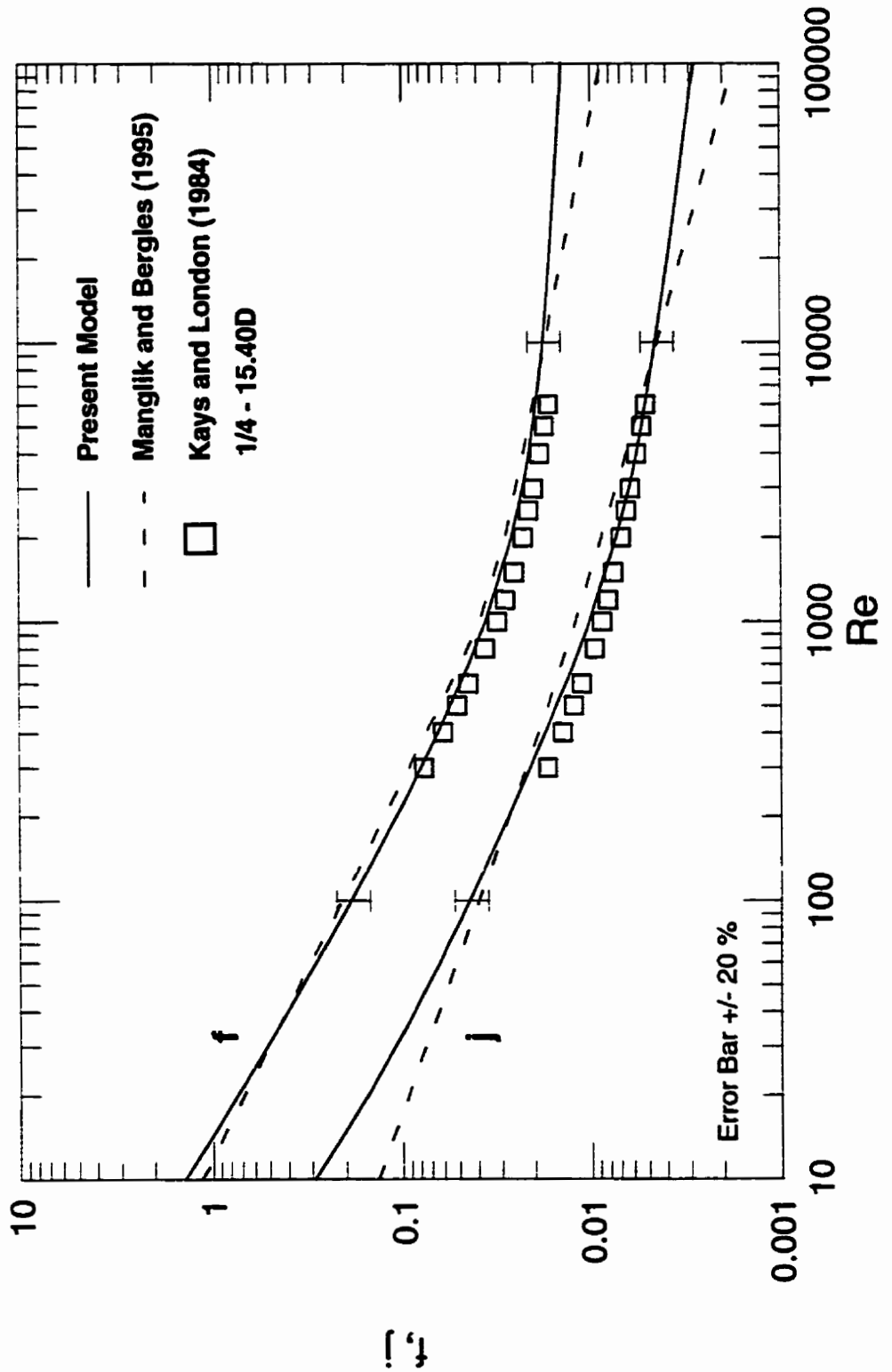

Fig. 6.21 - Comparison of Models with Data of Kays and London (1984) for 1/4-15.40D.

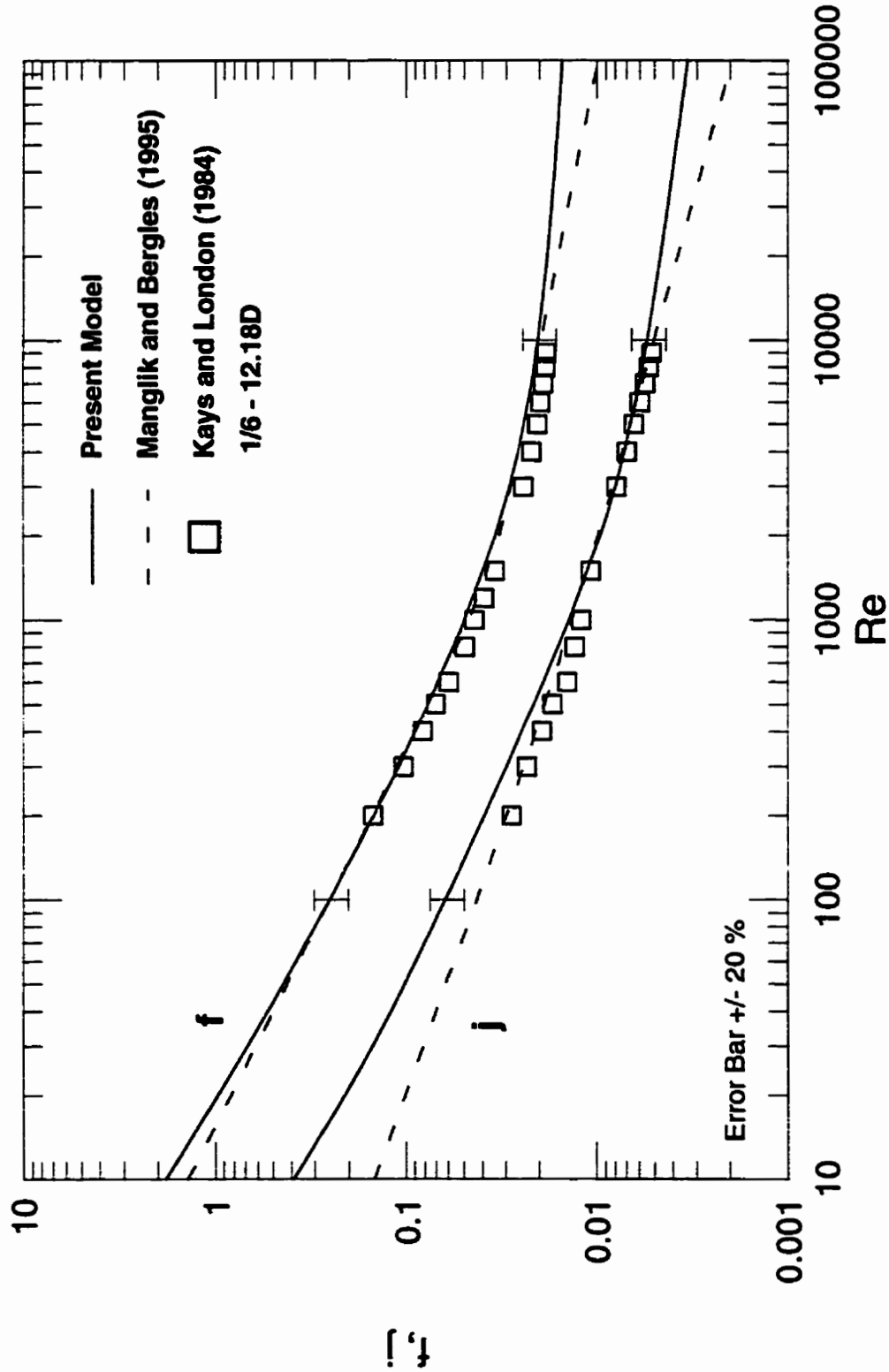

Fig. 6.22 - Comparison of Models with Data of Kays and London (1984) for 1/6-12.18D

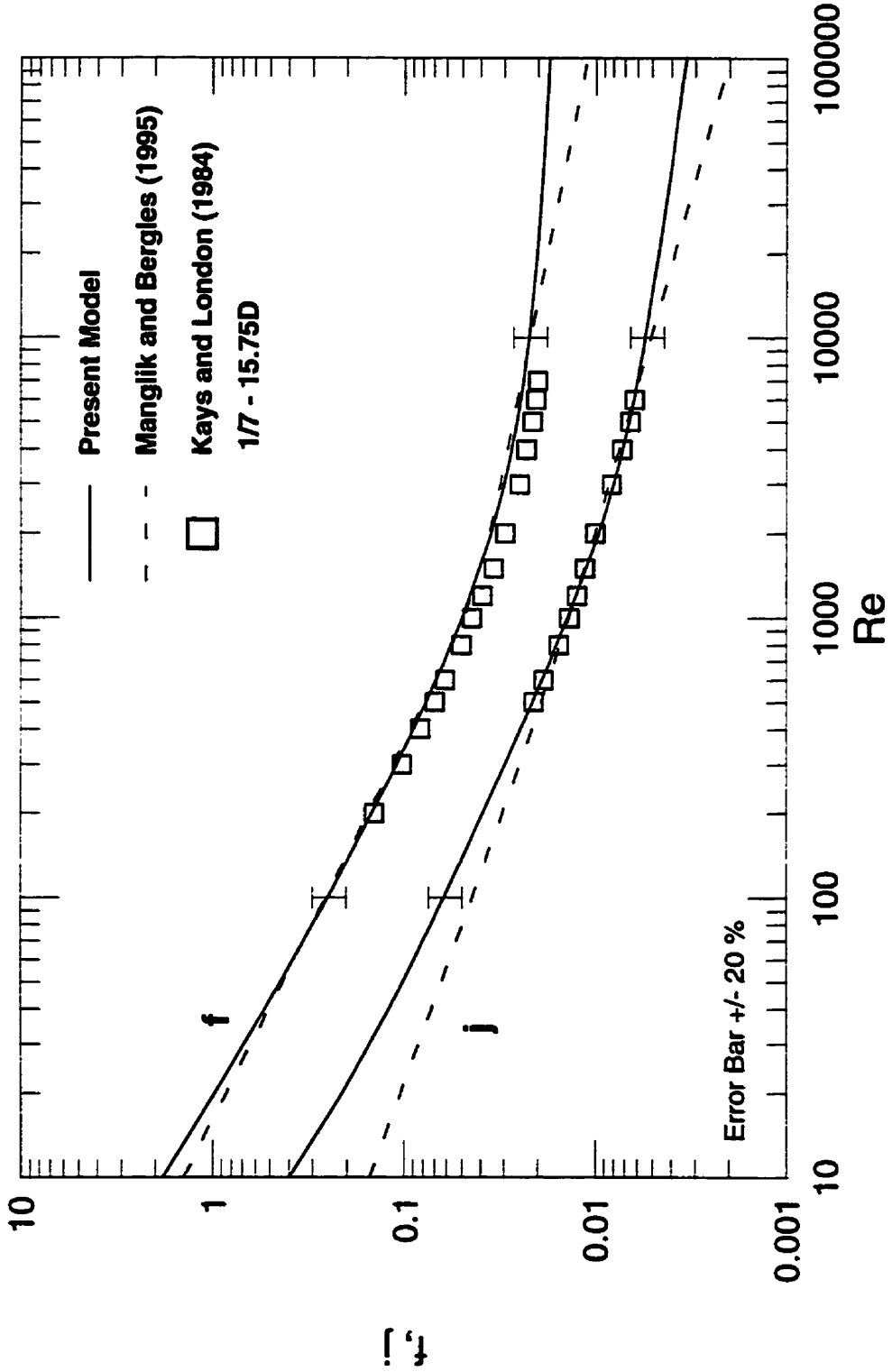

Fig. 6.23 - Comparison of Models with Data of Kays and London (1984) for 1/7-15.75D.

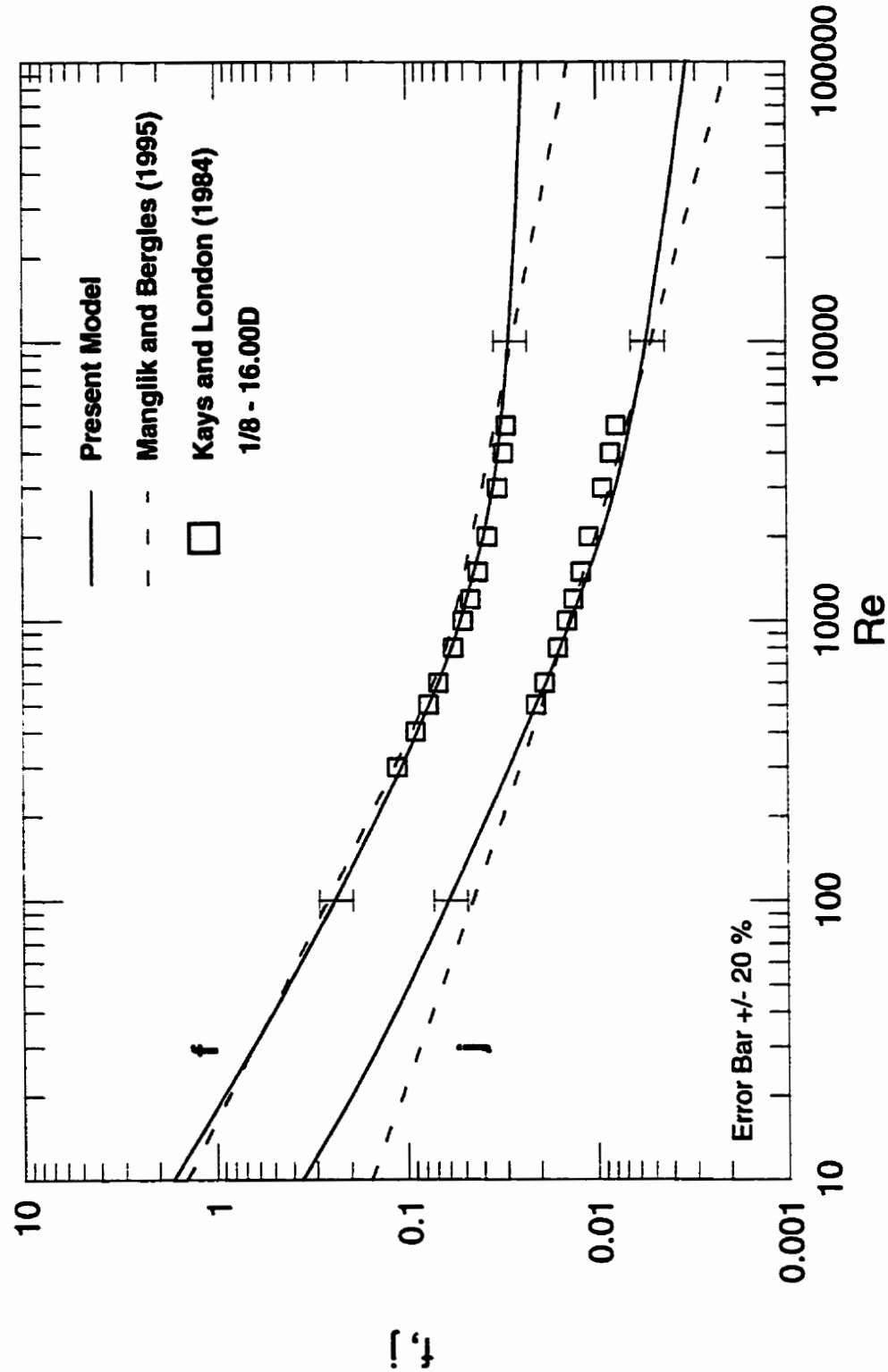

Fig. 6.24 - Comparison of Models with Data of Kays and London (1984) for 1/8-16.00D.

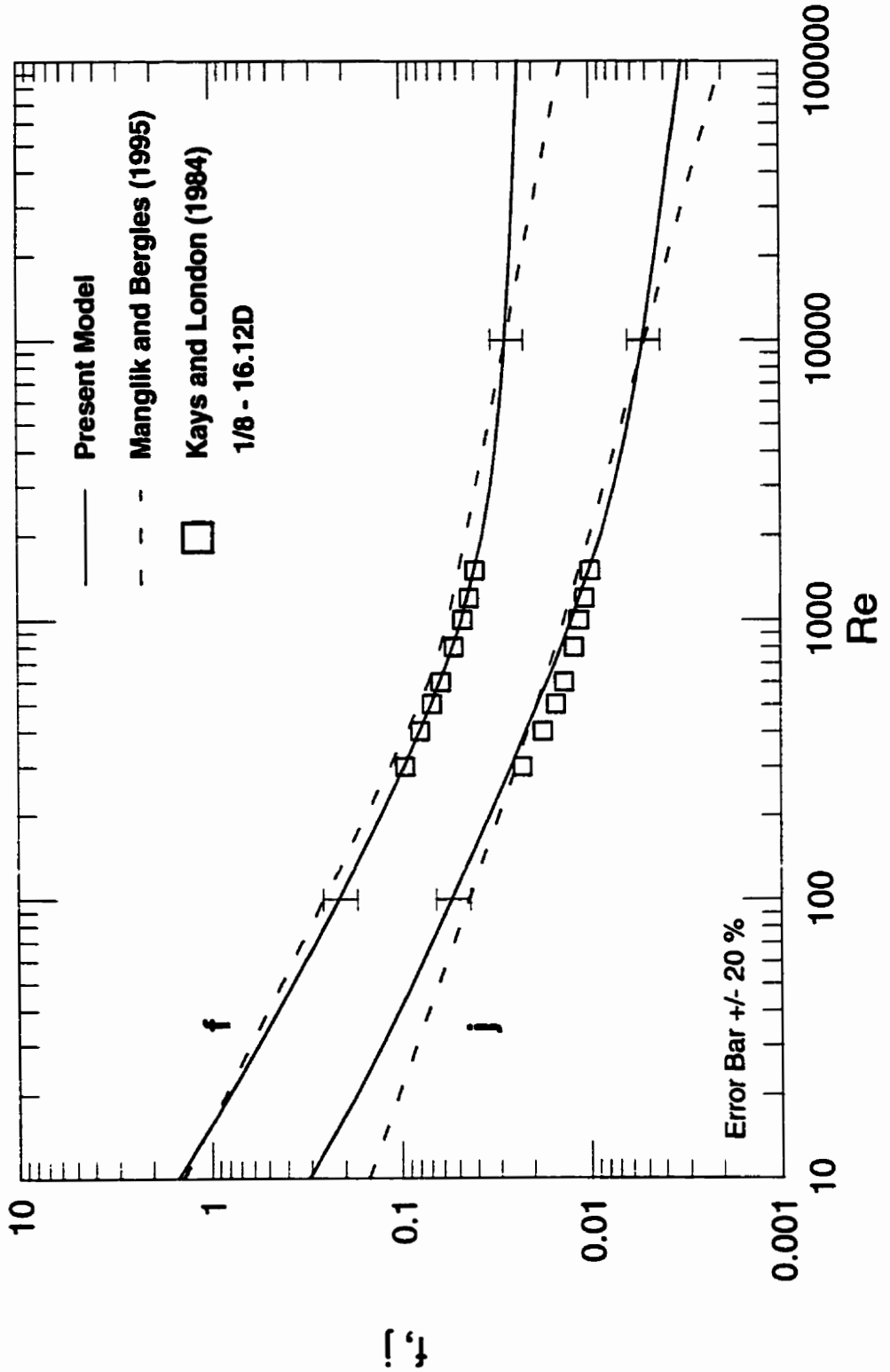

Fig. 6.25 - Comparison of Models with Data of Kays and London (1984) for 1/8-16.12D.

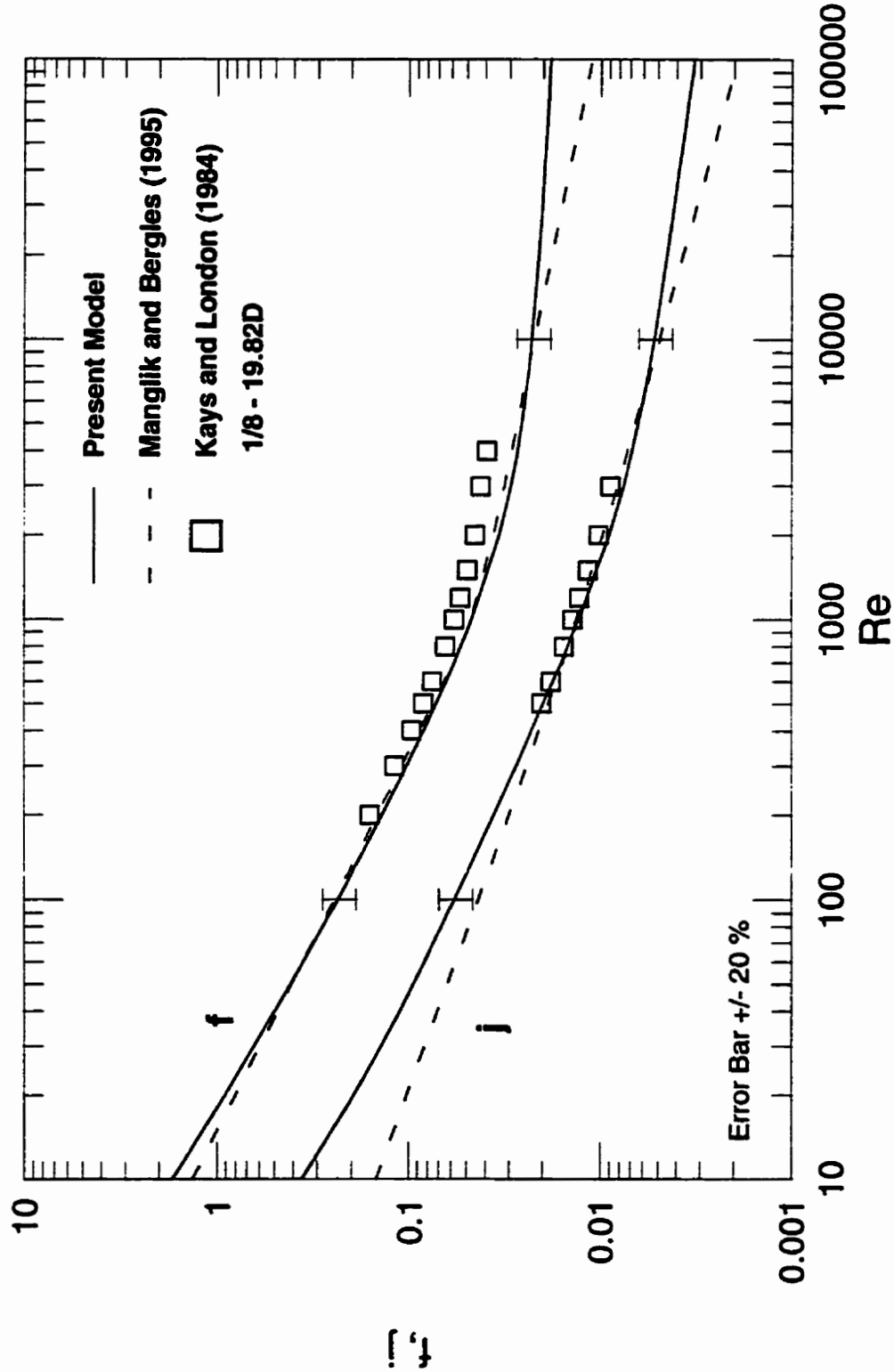

Fig. 6.26 - Comparison of Models with Data of Kays and London (1984) for 1/8-19.82D.

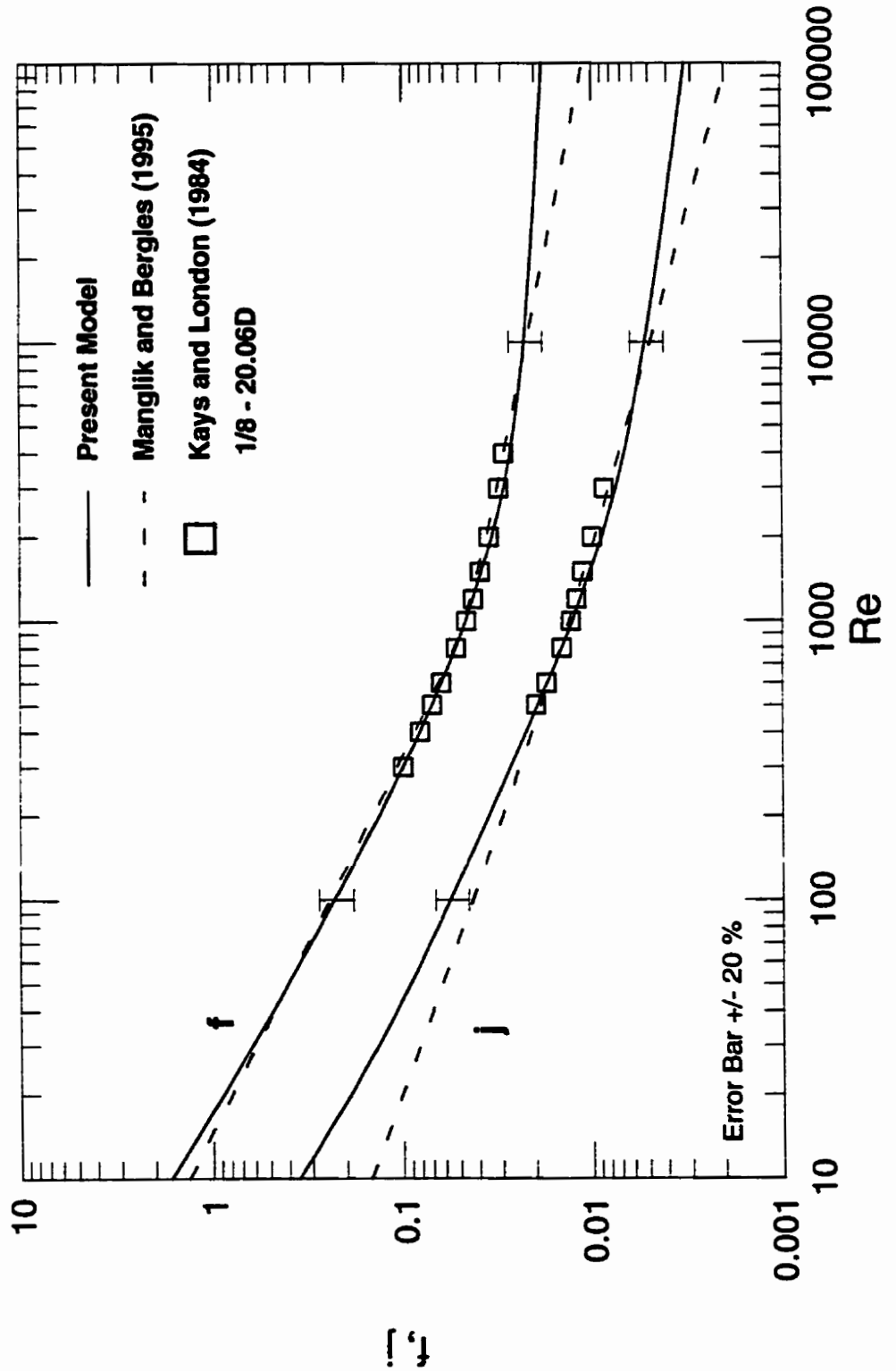

Fig. 6.27 - Comparison of Models with Data of Kays and London (1984) for 1/8-20.06D.

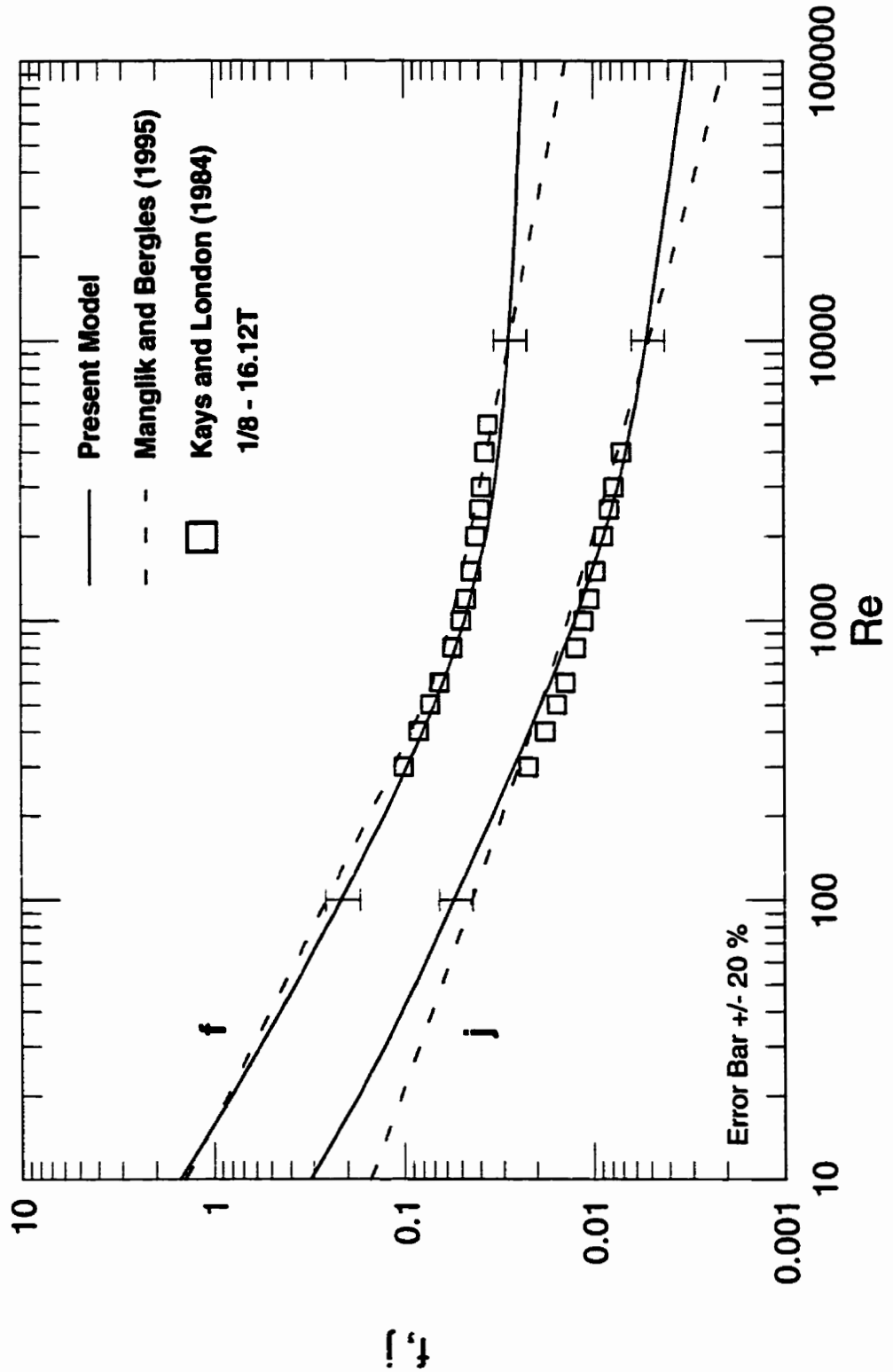

Fig. 6.28 - Comparison of Models with Data of Kays and London (1984) for 1/8-16.12T

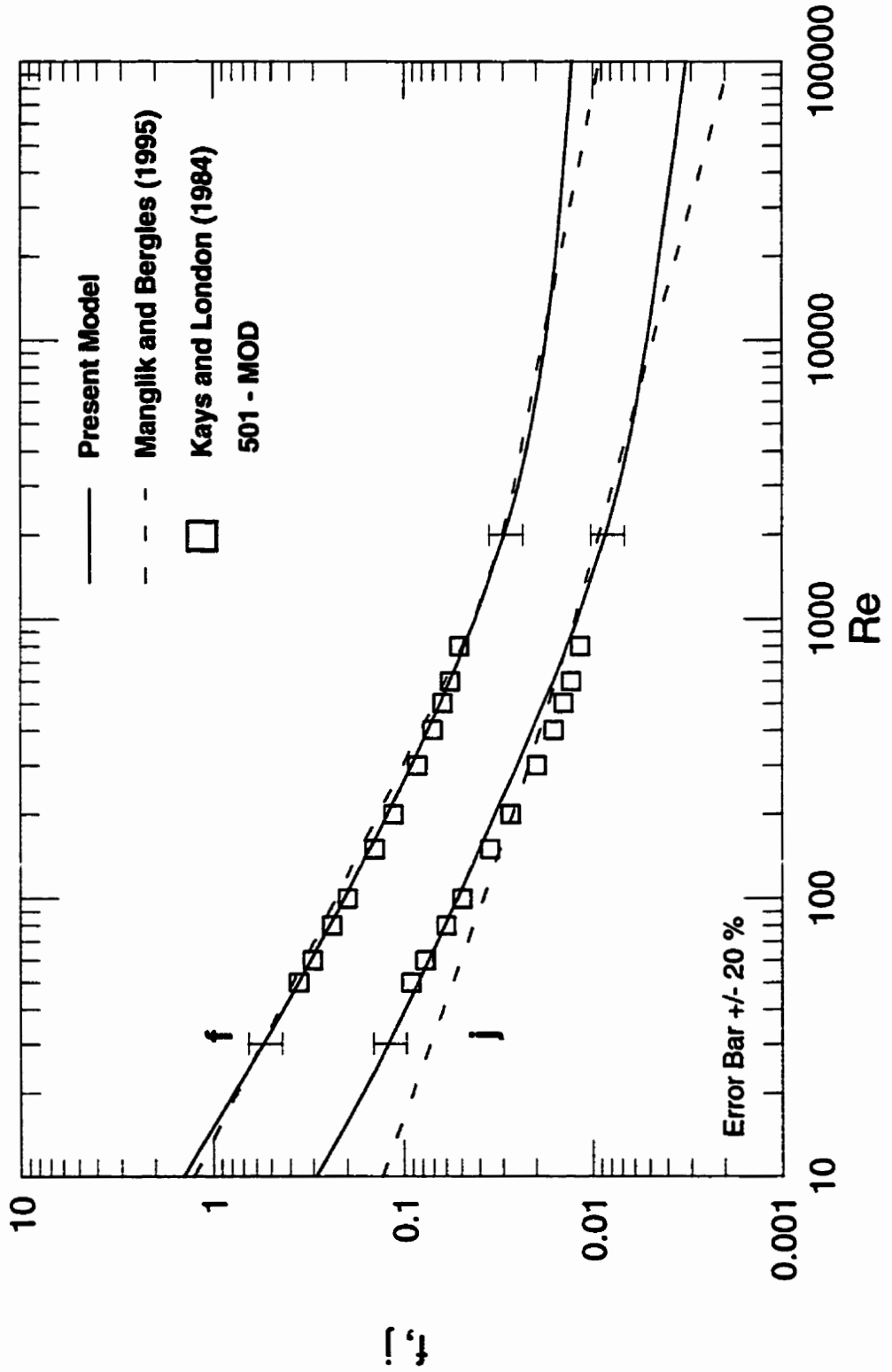

Fig. 6.29 - Comparison of Models with Data of Kays and London (1984) for 501-MOD.

6.5 Modelling Turbulator Strips

In this section the details of the model development for the turbulator type geometries are discussed. A typical turbulator geometry is shown in Fig. 6.30. The turbulator may be characterized by the blade width W, the channel height H, the wavelength λ, the fin thickness t, and fin angle θ. The fin angle for a curved profile may be nominally defined as:

$$\theta = \tan^{-1}(2H/\lambda) \tag{6.39}$$

The models developed in this section will be compared with experimental data for ten turbulator geometries provided in Chapter 5.

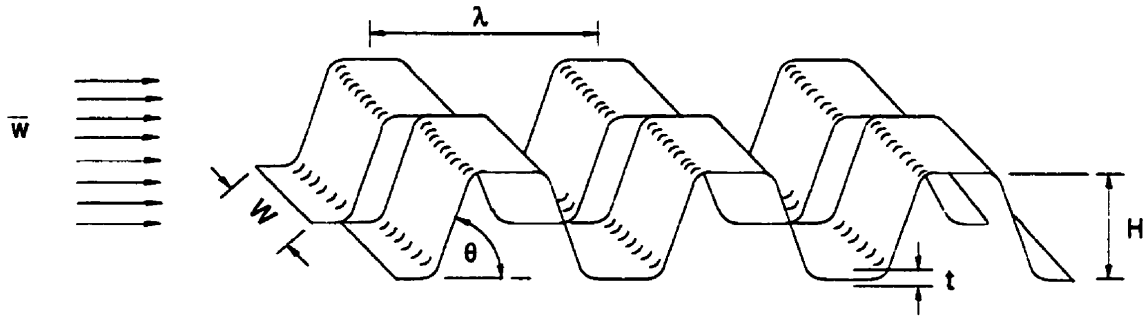

Fig. 6.30 - Turbulator Geometry

The following assumptions are made in the model development:

- Ideal surfaces, no burrs or scarfed edges
- Uniform surface dimensions throughout the array
- Large separation/recirculation zone in the rear of each fin
- Negligible edge contributions
- Perfect contact at channel walls
- Isothermal surfaces

6.5.1 Friction Factor

A friction factor model for the turbulator geometry shown in Fig. 6.30 may be developed by performing a simple force balance on a basic element or repeating cell which is shown below in Fig. 6.31.

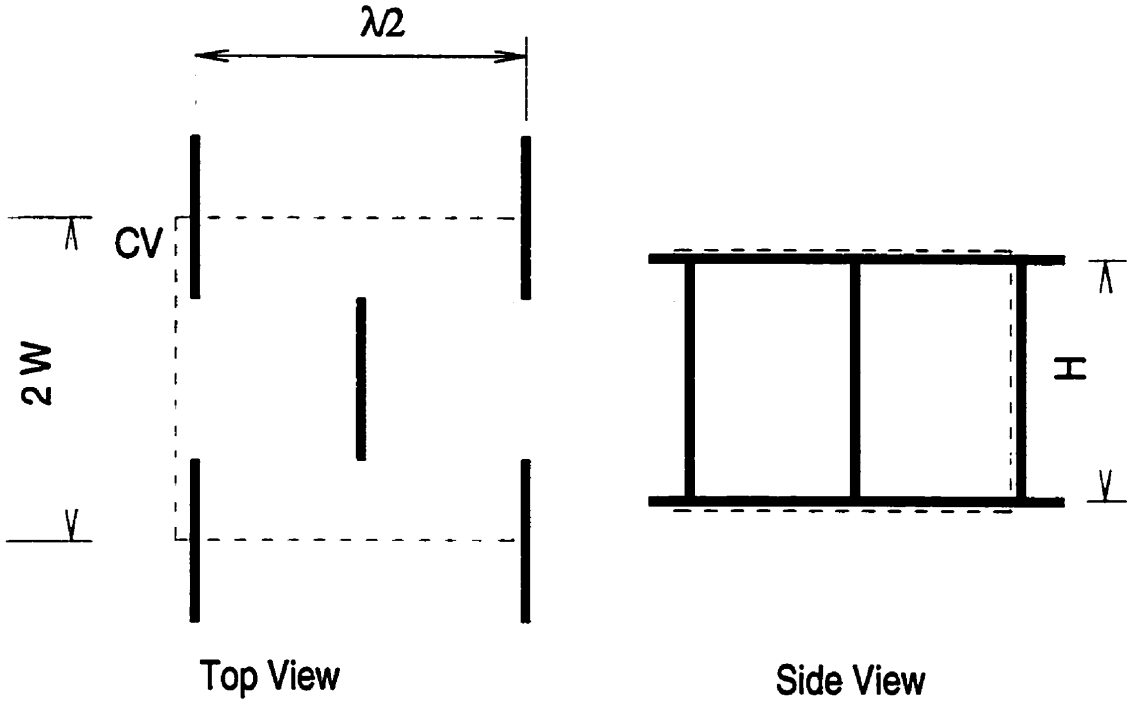

Fig. 6.31 - Basic Cell of Turbulator Strip

Using a basic cell of dimensions $2W \times \lambda/2 \times H$, a force balance gives:

$$\frac{\overline{\tau}}{\frac{1}{2}\rho\overline{w}^2} = \frac{\tau_{wall}}{\frac{1}{2}\rho\overline{w}^2}\left(\frac{A_{wall}}{A_{wet}}\right) + \frac{\tau_{fins}}{\frac{1}{2}\rho\overline{w}^2}\left(\frac{A_{fins}}{A_{wet}}\right) + C_D\left(\frac{A_{drag}}{A_{wet}}\right) + K_{eff}\left(2\frac{A_{front}}{A_{wet}}\right) \quad (6.40)$$

where $A_{wall} = 2W\lambda$, $A_{fin} = A_{wet} - A_{wall}$, $A_{front} = 2WH$, A_{drag} is the characteristic area that the drag coefficient is based upon, and $A_{wet} = (2\lambda W)AER$ is the total wetted surface area. The above expression may be written in terms of the friction coefficients for the fin surface and the channel walls:

$$f = f_{walls}\left(\frac{A_{walls}}{A_{wet}}\right) + f_{fins}\left(\frac{A_{fins}}{A_{wet}}\right) + C_D\left(\frac{A_{drag}}{A_{wet}}\right) + K_{eff}\left(2\frac{A_{front}}{A_{wet}}\right) \quad (6.41)$$

Since the drag and expansion/contraction coefficients are related to the fin surface they may be combined with the fin skin friction term in the following manner:

$$f = f_{walls}\left(\frac{A_{walls}}{A_{wet}}\right) + \left[f_{fins} + C_D\left(\frac{A_{drag}}{A_{fins}}\right) + K_{eff}\left(2\frac{A_{front}}{A_{fins}}\right)\right]\left(\frac{A_{fins}}{A_{wet}}\right) \quad (6.42)$$

The above expression represents an overall force balance on an element of the turbulator geometry. Now using the characteristic dimensions of the control volume Eq. (6.42) may be written as:

$$f = f_{walls}\left(\frac{1}{AER}\right) + \left[f_{fins} + C_D\left(\frac{A_{drag}}{A_{fins}}\right) + K_{eff}\left(2\frac{A_{front}}{A_{fins}}\right)\right]\left(1 - \frac{1}{AER}\right) \quad (6.43)$$

where AER is the area enhancement ratio defined in Chapter 5 as A_{wet}/A_{bare}.

Equation (6.43) is valid for both laminar and turbulent flow behavior. However, in the laminar region the C_D and K_{eff} terms are ignored as they only become significant at larger flow rates. Expressions will be developed using the fundamental solutions reviewed earlier, which model the friction factor on the channel walls and fin surfaces. The laminar and turbulent asymptotes will then be combined with the creeping flow asymptote using the Churchill and Usagi (1972) asymptotic correlation method in the form:

$$f = \left[\{(f_{cf})^m + (f_{lam})^m\}^{n/m} + (f_{tur})^n\right]^{1/n} \quad (6.44)$$

where m and n are correlation parameters to be chosen based upon comparisons with the experimental data.

Laminar Region

All of the experimental data for the various turbulators examined in Chapter 5 appear to have a low Reynolds number asymptote which is inversely proportional to the Reynolds number, $f \propto 1/Re$. This behavior is characteristic of the creeping flow regime which is observed in channels having complex flow paths such as flow through porous media.

Creeping flow through a complex channel or porous media was modelled by Carman (1956). This result is valid only for very small values of the Reynolds number $Re < 10$. The expression derived earlier for this region is

$$f_{cf} = \frac{8\,C_o}{Re_{d_h}} \tag{6.45}$$

where C_o is computed from Eq. (6.21).

At larger Reynolds numbers, boundary layers are thinner and the results indicate that the friction factor becomes inversely proportional to the square root of the Reynolds number, $f \propto 1/\sqrt{Re}$. Fluid friction on the channel walls is modelled as flow over a flat plate. The appropriate expression for predicting the contribution from the channel walls is

$$f_{wall} = 1.328 \left(Re_{d_h} \frac{\lambda}{d_h} \right)^{-1/2} \tag{6.46}$$

Fluid friction on the inclined fin surface is modelled as a combination of flow over a flat plate and plane stagnation flow. The solution for plane stagnation flow must be presented in terms of the average free stream velocity. Igarashi (1985) determined the appropriate velocity field from experimental measurements on the face of rectangular cylinders and plates oriented normal to a uniform flow field. The local velocity field in the vicinity of the stagnation point varied according to

$$w_\infty(x) = 1.65\frac{\overline{w}x}{W} \tag{6.47}$$

where W is the width of the plate or rectangular cylinder.

The appropriate expression for predicting the combined effects of plane stagnation and flat plate flow is modelled as

$$f_{fin} = 1.328\left(Re_{d_h}\frac{2S_o}{d_h}\right)^{-1/2}\cos^2(\theta) + 1.538\left(Re_{d_h}\frac{W}{d_h}\right)^{-1/2}\sin^2(\theta) \tag{6.48}$$

where S_o is the effective fin length.

As the angle of inclination increases to $\theta = 90°$ the expression above reduces to plane stagnation flow, and as the angle decreases the expression tends towards flow over a flat plate. Equation (6.48) models the leading side of the inclined surface. In the region to the rear, the flow is treated as a separated flow similar to flow over a bluff surface, and it is assumed that the wall shear is equal to zero.

Substituting the laminar boundary layer contributions into Eq. (6.38) with $K_{eff} = 0$ and $C_D = 0$ gives:

$$f_{lam} = \left\{1.328\left(Re_{d_h}\frac{\lambda}{d_h}\right)^{-1/2}\right\}\left(\frac{1}{AER}\right) \tag{6.49}$$
$$+\frac{1}{2}\left\{1.328\left(Re_{d_h}\frac{2S_o}{d_h}\right)^{-1/2}\cos^2(\theta) + 1.538\left(Re_{d_h}\frac{W}{d_h}\right)^{-1/2}\sin^2(\theta)\right\}\left(1 - \frac{1}{AER}\right)$$

Turbulent Region

At higher Reynolds numbers the flow behaves like a turbulent flow with inertial forces being dominant. The contribution of the channel walls to the friction factor may be computed from the following expression presented earlier:

$$f = 0.074 \left(Re_{d_h} \frac{\lambda}{d_h} \right)^{-1/5} \tag{6.50}$$

At very high Reynolds numbers only the form drag and loss coefficients are important. A form drag coefficient for the high Reynolds number asymptote was derived earlier using experimental and analytical results for flow past flat and inclined plates. Substituting the expressions for the form drag, Eq.(6.25), and effective loss coefficient, Eq. (6.29), derived earlier into Eq. (6.43), along with the turbulent skin friction component on the channel wall leads to

$$f_{tur} = 0.074 \left(Re_{d_h} \frac{\lambda}{d_h} \right)^{-1/5} \left(\frac{1}{AER} \right) + \left(1.2 \frac{(\pi + 4)\sin^2(\theta)}{\pi + 4\sin(\theta)} + 0.878 \sin(\theta) \right) \left(1 - \frac{1}{AER} \right) \tag{6.51}$$

The ratio of $A_{front}/A_{fins} = \sin(\theta)/2$ and $A_{drag}/A_{fins} = 1/2$, where the surface area of a single fin is taken to be $A_{fin} = 2HW/\sin(\theta)$ and $A_{drag} = HW/\sin(\theta)$, recalling that the potential flow solution for the drag coefficient for an inclined lamina, Eq. (6.24), is based upon the chord length rather than the profile height. This expression was found to be in good agreement with the trends observed in the experimental data for both small angles of inclination and nearly vertical obstructions.

The creeping flow, laminar boundary layer, and turbulent boundary layer asymptotes are plotted in Fig. 6.32 along with experimental data for one of the devices tested in Chapter 5.

Laminar - Transition - Turbulent Model

Having developed the appropriate asymptotic behavior for the friction factor, the results are now combined in the form of Eq. (6.44), where the correlation parameters

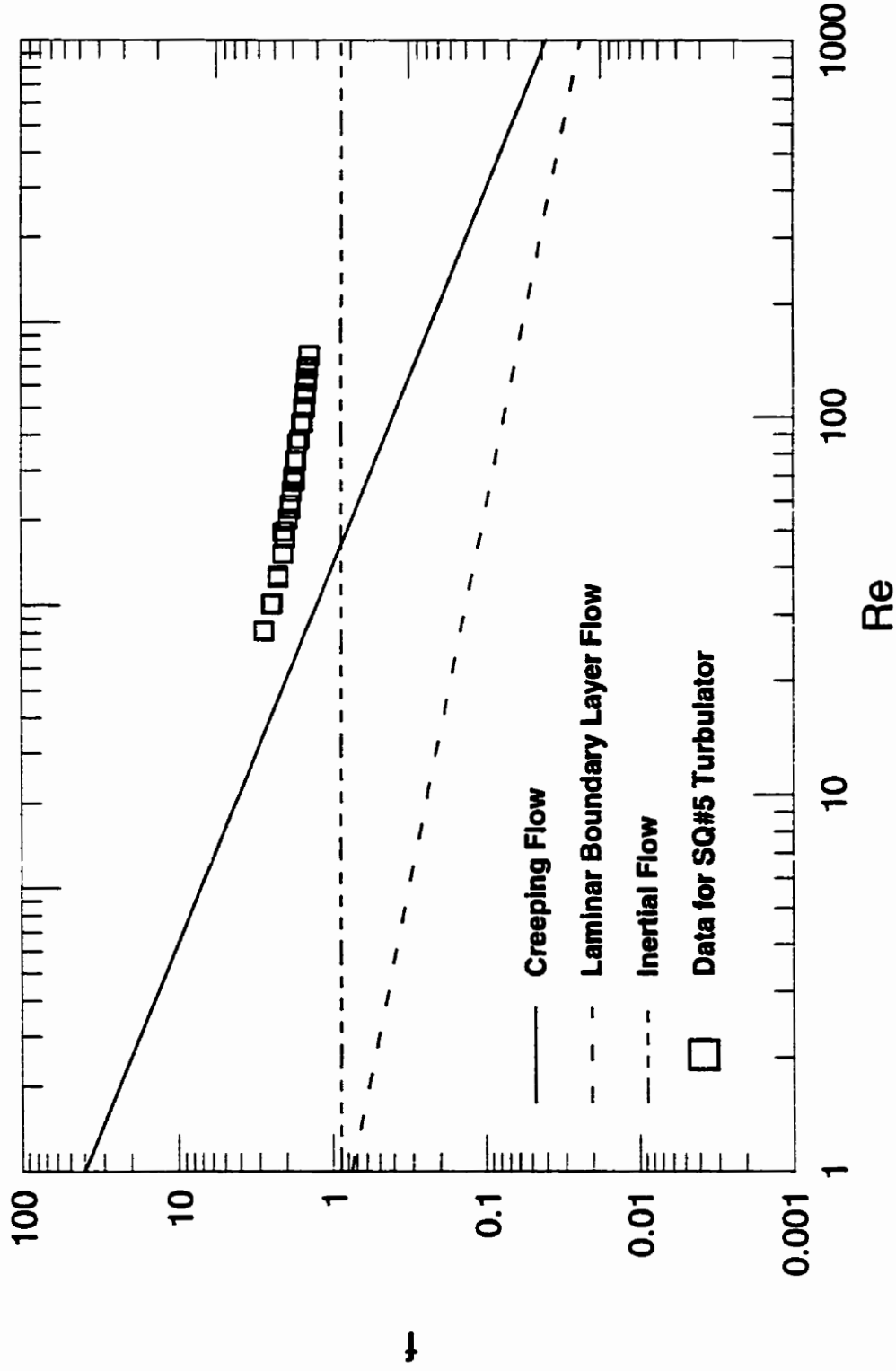

Fig. 6.32 - Comparison of Asymptotic Solutions with Data for a Typical Turbulator.

are $m \approx 1$ and $n \approx 6/7$. Examination of the model shows that the important parameters affecting the flow are the wave length of the convolutions λ, the surface area enhancement factor AER, fin width W, fin angle $\theta = \tan^{-1}(2H/\lambda)$ as a function of the channel spacing H, and the hydraulic diameter of the enhanced channel d_h. The fin thickness t is generally much smaller than the other characteristic dimensions and is not explicitly modelled. The effects of fin edge surface area are however, included through the enhancement factor AER. The nearly linear superposition of the three flow regimes is typical of fluid flow in complex channels and packed columns, Ergun (1952). Comparisons of the proposed model is provided after the development of a model for the Colburn j factor which is derived in the next section.

6.5.2 Colburn j Factor

A similar procedure is used to obtain a model for the Colburn j factor as used for the Fanning friction factor. Performing an energy balance on the same basic cell results in the following expression for the average heat transfer coefficient:

$$\overline{h}A_{wet} = \overline{h}_{wall}A_{wall} + \overline{h}_{fins}A_{fins} \tag{6.52}$$

Equation (6.52) may be written in terms of the Colburn j factor and the area enhancement ratio AER:

$$j = j_{wall}\left(\frac{1}{AER}\right) + j_{fins}\left(1 - \frac{1}{AER}\right) \tag{6.53}$$

Equation (6.53) is valid for both laminar and turbulent flow behavior. Expressions will be developed for the Colburn j factor on the channel walls and fin surfaces. The laminar and turbulent flow asymptotes may then be combined using the Churchill and Usagi (1972) asymptotic correlation method in the following form:

$$j = \left[(j_{cf})^p + \{ (j_{lam})^q + (j_{tur})^q \}^{p/q} \right]^{1/p} \tag{6.54}$$

where p and q are correlation parameters to be chosen based upon comparisons with the experimental data provided in Chapter 5.

Laminar Region

In the low Reynolds region the Colburn j factor will take the form:

$$j_{cf} = \frac{4.93}{Re_{d_h} Pr^{1/3}} \left(\frac{d_h}{H} \right) \tag{6.55}$$

This expression represents the creeping flow or fully developed limit for $Re_{d_h} \rightarrow 0$.

As the Reynolds number increases, boundary layers become thinner and the Colburn j factor should be proportional to $1/\sqrt{Re}$. Heat transfer on the channel walls may be modelled as flow over a flat plate. The appropriate expression for predicting the contribution from the channel walls is

$$j_{wall} = 0.664 \left(Re_{d_h} \frac{\lambda}{d_h} \right)^{-1/2} \tag{6.56}$$

Heat transfer on the inclined fin surface is modelled as a combination of flow over a flat plate and plane stagnation flow. Once again the plane stagnation flow solution must be converted to a form containing the average free stream velocity. Using Eq. (6.42), the appropriate expression for predicting the contribution of the fin surface is

$$j = \left\{ 0.664 \left(Re_{d_h} \frac{2S_o}{d_h} \right)^{-1/2} \cos^2(\theta) + 0.849 \left(Re_{d_h} \frac{W}{d_h} \right)^{-1/2} \sin^2(\theta) \right\} \tag{6.57}$$

where S_o is the effective fin length.

As the angle of inclination increases to $\theta = 90°$ the expression above reduces to plane stagnation flow, and as the angle decreases the expression tends towards flow over a flat plate. The above expression models only the leading surface of the fin. In the region to the rear, the flow is treated as a separated flow similar to that in the wake of a bluff body. In this region the heat transfer coefficient will be modelled by Eq. (6.13) for separated flow. The combined effect of the leading and rear faces is simply the arithmetic mean given by

$$j_{fins} = \frac{1}{2}\left\{0.664\left(Re_{d_h}\frac{2S_o}{d_h}\right)^{-1/2}\cos^2(\theta)+ \right.$$
$$\left. 0.849\left(Re_{d_h}\frac{W}{d_h}\right)^{-1/2}\sin^2(\theta) + 0.191\left(Re_{d_h}\frac{W}{d_h}\right)^{-1/3}\right\} \tag{6.58}$$

The complete laminar boundary layer model is now given by the following expression:

$$j_{lam} = \frac{1}{2}\left\{0.664\left(Re_{d_h}\frac{2S_o}{d_h}\right)^{-1/2}\cos^2(\theta) + 0.849\left(Re_{d_h}\frac{W}{d_h}\right)^{-1/2}\sin^2(\theta)\right.$$
$$\left. +0.191\left(Re_{d_h}\frac{W}{d_h}\right)^{-1/3}\right\}\left(1 - \frac{1}{AER}\right) + 0.664\left(Re_{d_h}\frac{\lambda}{d_h}\right)^{-1/2}\left(\frac{1}{AER}\right) \tag{6.59}$$

Turbulent Region

At higher Reynolds numbers it is assumed that the region between fins is fully occupied by a pair of symmetric recirculation bubbles. The average value of the heat transfer coefficient for both the fin surface and the channel walls is taken to be

$$j_{tur} = 0.191\left(Re_{d_h}\frac{W}{d_h}\right)^{-1/3} \tag{6.60}$$

Equation (6.60) has the same order of magnitude and Reynolds number exponent

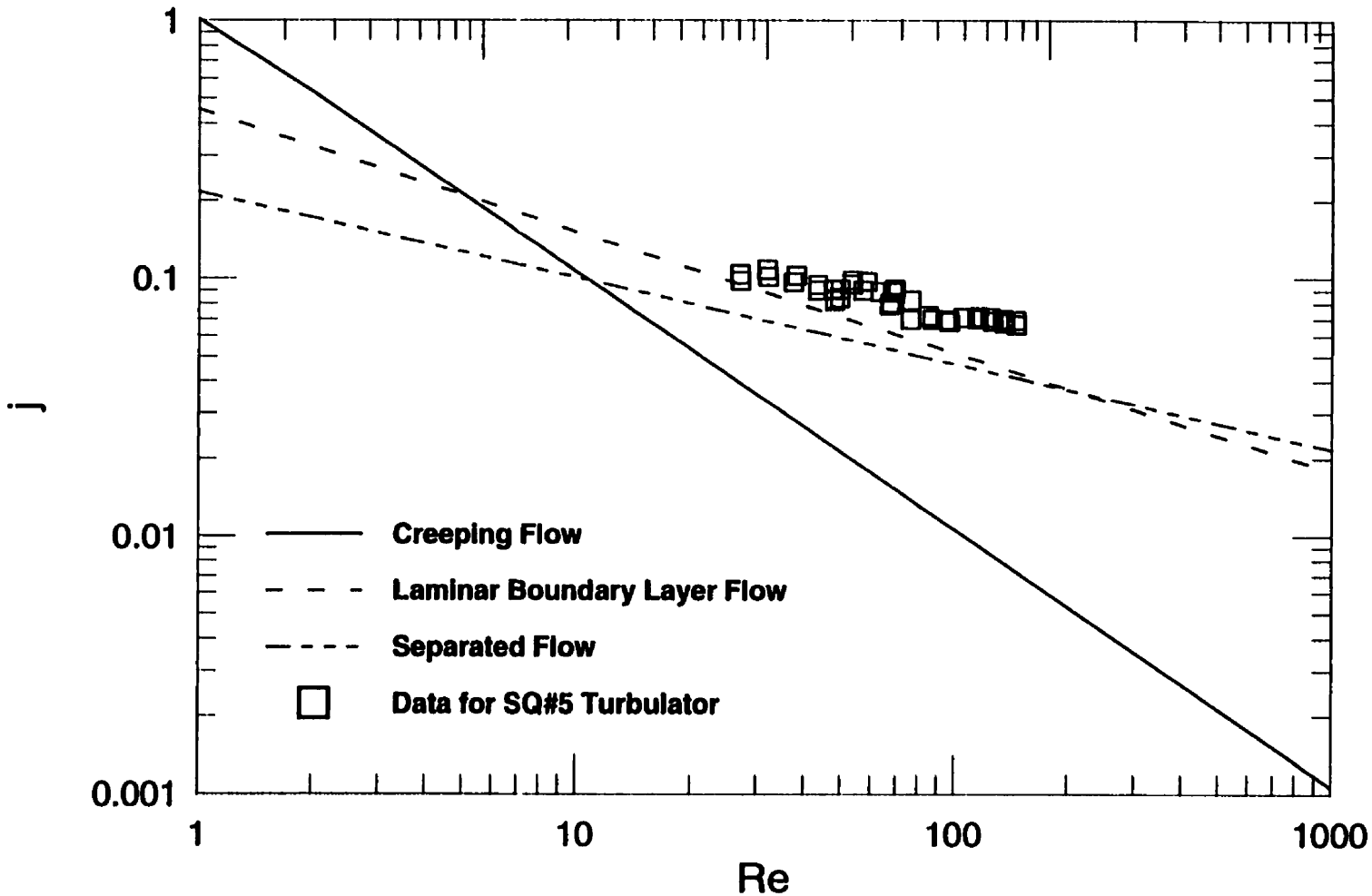

Fig. 6.33 - Comparison of Asymptotic Solutions with Data for a Typical Turbulator.

as the expression obtained from the numerical results of Patankar et al. (1977), Eq. (3.39). The creeping flow, laminar boundary layer, and turbulent region models are plotted in Fig. 6.26 along with experimental data for a typical turbulator geometry.

Laminar - Transition - Turbulent Model

Having developed the appropriate asymptotic behavior for the Colburn j factor, the results are now combined in the form of Eq. (6.54) proposed earlier, where the correlation parameters are $p \approx 9/2$ for all turbulators and $q \approx 7/5$ for turbulators with a straight profile and $q \approx 5$ for turbulators with a curved profile. Turbulators which have a curved profile allow the flow to become more three dimensional compared to those having a straight profile which tend to make the flow more two dimensional. As a result, the heat transfer coefficients are higher for the straight profiles. The blending parameter for the laminar and turbulent regions must be smaller for the straight profiles and larger for the curved profiles when interpolating in the transition region.

Examination of the model shows that the important parameters affecting the flow are the wave length of the convolutions λ, the surface area enhancement factor AER, fin width W, fin angle $\theta = \tan^{-1}(2H/\lambda)$ as a function of the channel spacing H, and the hydraulic diameter of the enhanced channel d_h. The fin thickness t is generally much smaller than the other characteristic dimensions and is not modelled explicitly. However, the effects of fin edge surface area are included through the enhancement factor AER.

6.5.3 Comparison of Models with Data

The proposed models are compared with ten sets of data for the turbulator configurations which are reported in Chapter 5. Table 6.4 presents a summary of the optimal value of the correlation parameters for combining the creeping flow, laminar

boundary layer and turbulent boundary layer models for each set of data. Excellent correlation is obtained for the friction factor data for all configurations tested. Good agreement between the proposed model and the turbulator data is also achieved for the Colburn j factor. The correlation parameters for the $CPI-2$ device were not tabulated, since this device is a special case of the $CPI-1$ device. The $CPI-2$ device has the same geometric configuration as the $CPI-1$ device except that every fourth row is replaced by a neutral surface containing no convolutions. This device is dealt with in a later section addressing the effects of bypass channels.

Table 6.5 presents the RMS and (min/max) values of the percent differences for the case where fixed values of the correlation parameters are used for all cases. The majority of the friction factor and Colburn j factor data are predicted within $\pm$ 20 percent. The large RMS difference reported for the $CPI-5$ and $SQ-4$ devices represents an average value of a biased error. All of the data for these two devices fall short of the model predictions, however, the model predicts the correct trends.

Figures 6.34 - 6.43 compare the proposed models with the turbulator data of Chapter 5. It is clear from Figs. 6.34-6.43 that the proposed model captures the correct physical behavior of the experimental data. With the exception of two j data sets, in which the data fall short of the model, excellent agreement between the proposed model and experimental data is achieved over a moderate range of Reynolds numbers. Further validation of the proposed model is in order for the low Reynolds and high Reynolds number regions.

6.5.4 Effect of Bypass Channels

If the turbulator strip contains neutral planes or bypass channels, the following expressions are proposed for modelling purposes:

$$f = \kappa \left(\frac{24}{Re_{d_h}} \frac{H}{d_h} \right) + (1 - \kappa) f_{turb} \tag{6.61}$$

and

$$j = \kappa \left(\frac{7.55}{Re_{d_h} Pr^{1/3}} \frac{H}{d_h} \right) + (1 - \kappa) j_{turb} \tag{6.62}$$

where $\kappa = N_{bypass}/N_{turb}$ is the bypass fraction and f_{turb}, j_{turb} are the friction factor and Colburn j factor for a given turbulator profile.

This approximate approach provides reasonable results for the $CPI-2$ device which contains 25 percent bypass using the $CPI-1$ turbulator profile. It is evident from Fig. 6.28, that the drag coefficient and expansion and contraction losses are not as significant in this configuration. Equations (6.61) and (6.62) assume that the bypass channels are concentrated as opposed to periodic which is the case for the $CPI-2$ device. The periodic nature of the bypass channels should have more effect on the friction data than the case where all of the bypass channels are concentrated in one region. This issue should be dealt with in more detail for future studies.

Table 6.4

Comparison of Models with Data with Optimal Value of Blending Parameter

	f			j		
Designation	m	n	RMS	p	q	RMS
CPI-1	1	0.99	5.80	3.0	4.0	10.21
CPI-2	-	-	-	-	-	-
CPI-3	1	0.85	4.23	4.0	5.0	13.42
CPI-4	1	1.00	3.95	5.0	5.0	17.69
CPI-5	1	0.87	4.85	5.0	5.0	29.50
SQ-1	1	0.79	3.59	5.0	1.25	12.31
SQ-2	1	0.71	2.98	5.0	1.25	7.82
SQ-3	1	0.80	1.49	5.0	1.75	9.97
SQ-4	1	0.85	2.11	4.5	5.0	35.92
SQ-5	1	0.81	5.27	5.0	4.0	9.37

Table 6.5

Comparison of Models with Data with

Fixed Values of Blending Parameter

	f		j	
Designation	RMS	(min/max)	RMS	(min/max)
CPI-1	8.25	-16.70/7.12	16.27	0.38/26.66
CPI-2	18.12	-37.50/20.08	17.44	-29.28/-7.70
CPI-3	6.57	-2.70/10.30	13.37	-22.31/-3.38
CPI-4	16.89	-29.98/-10.16	17.72	-34.98/4.28
CPI-5	5.94	-6.36/12.27	29.53	-41.18/-10.27
SQ-1	11.50	6.40/18.05	12.06	-25.47/23.20
SQ-2	18.88	14.58/23.97	8.95	-19.90/18.26
SQ-3	9.44	7.00/12.46	17.99	-28.95/-0.40
SQ-4	5.84	2.59/11.25	35.90	-52.41/-17.40
SQ-5	10.76	-0.30/17.91	9.38	-21.13/12.97

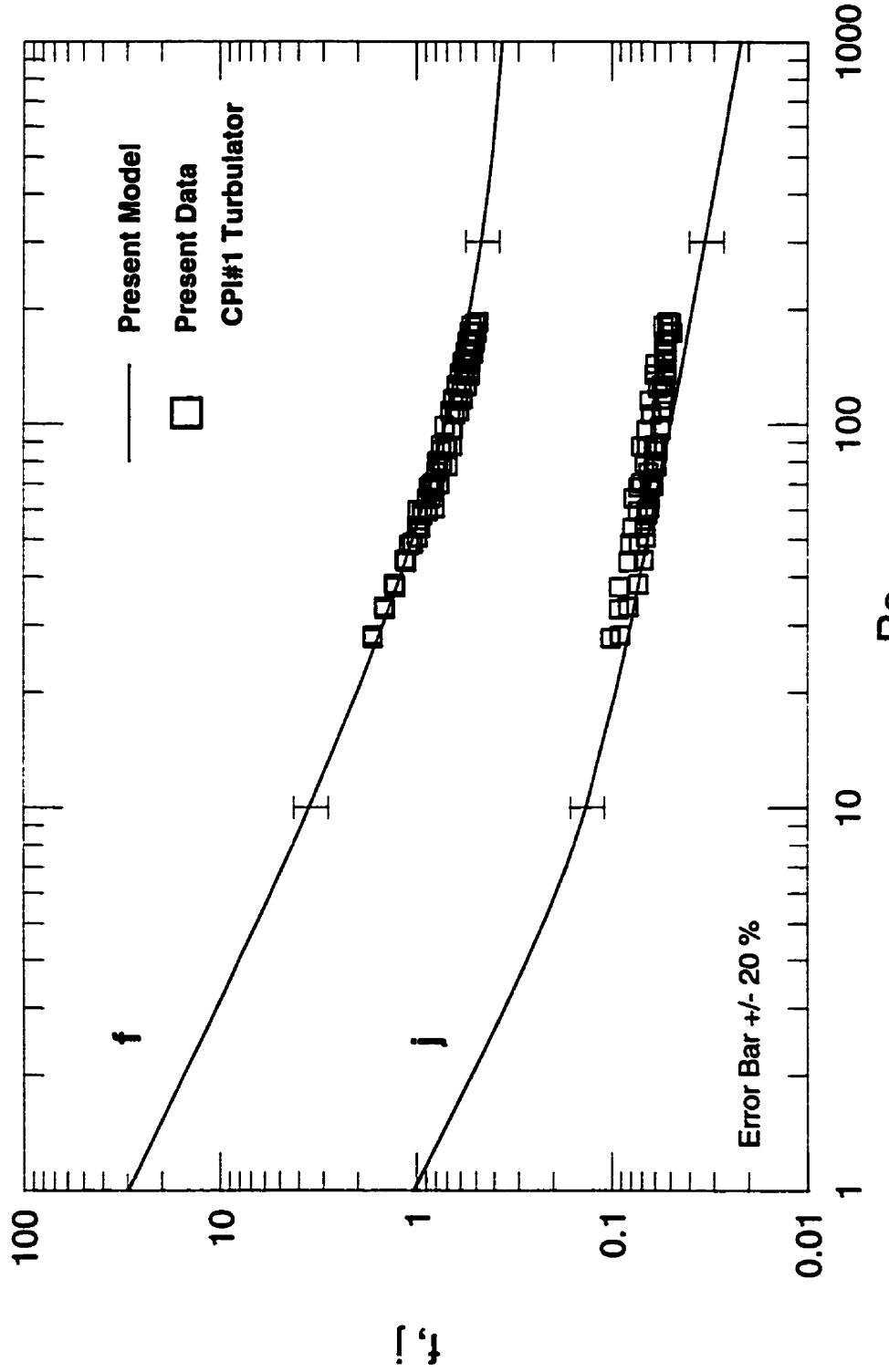

Fig. 6.34 - Comparison of Models with Data CPI-1 Turbulator.

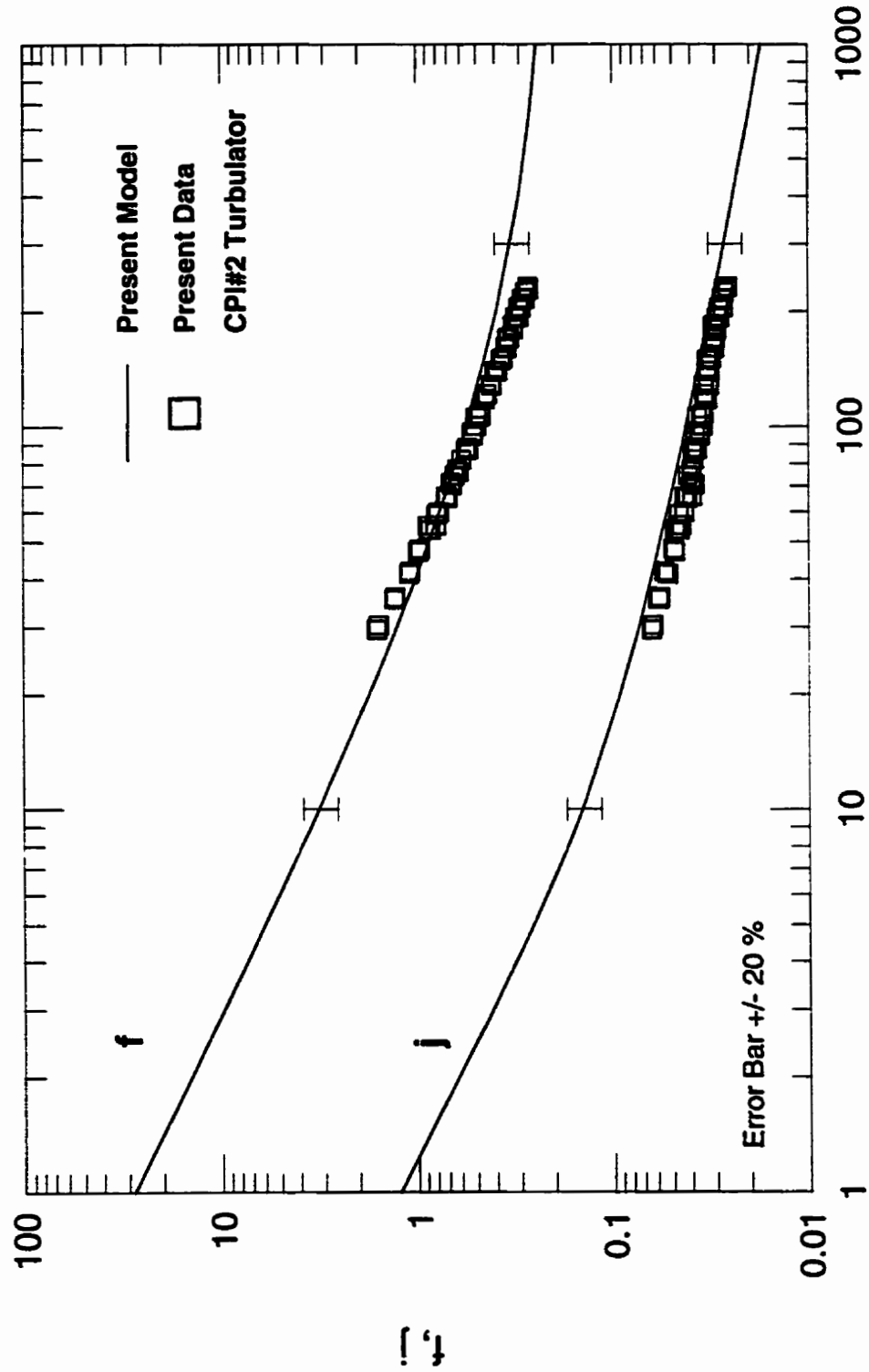

Fig. 6.35 - Comparison of Models with Data CPI-2 Turbulator.

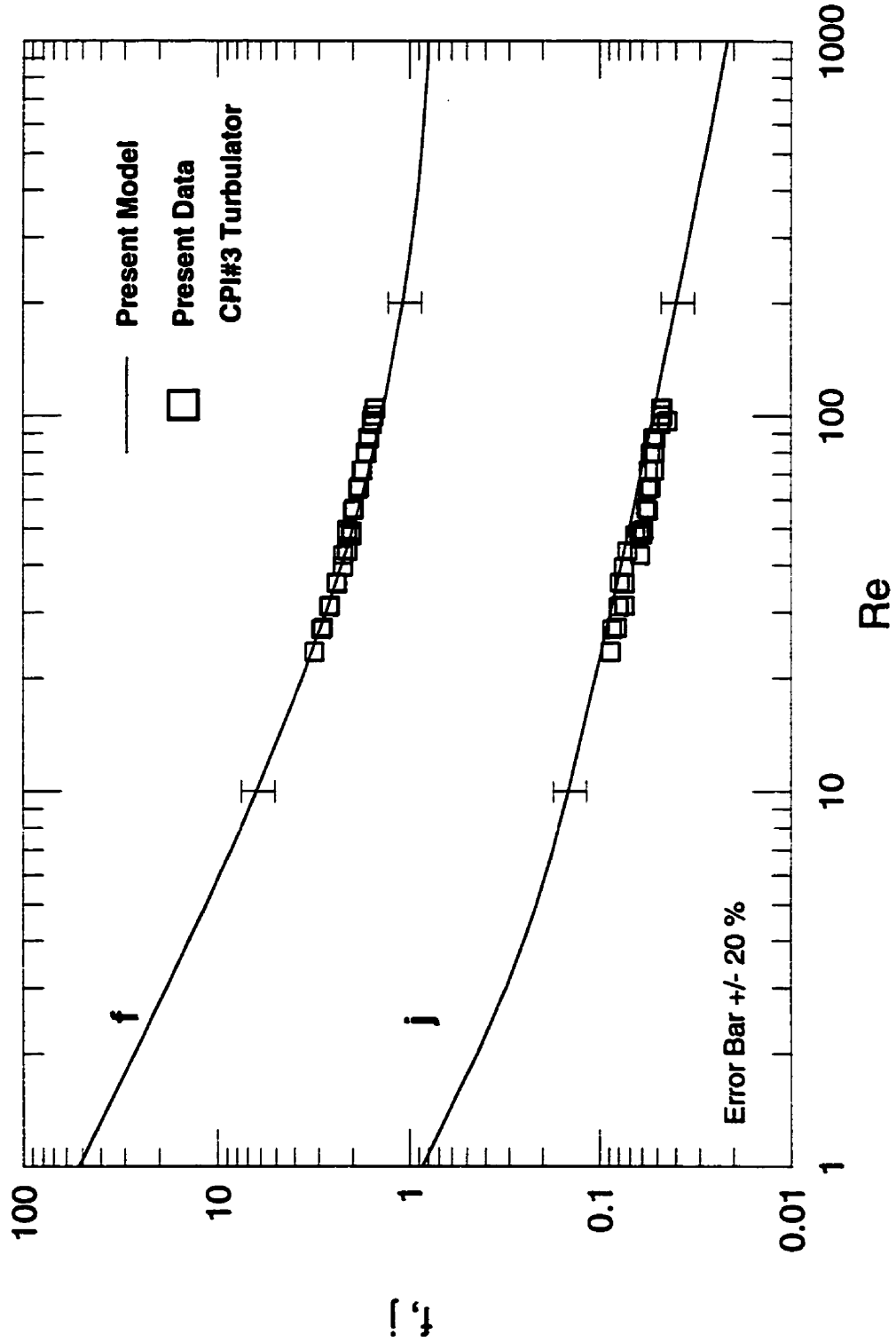

Fig. 6.36 - Comparison of Models with Data CPI-3 Turbulator.

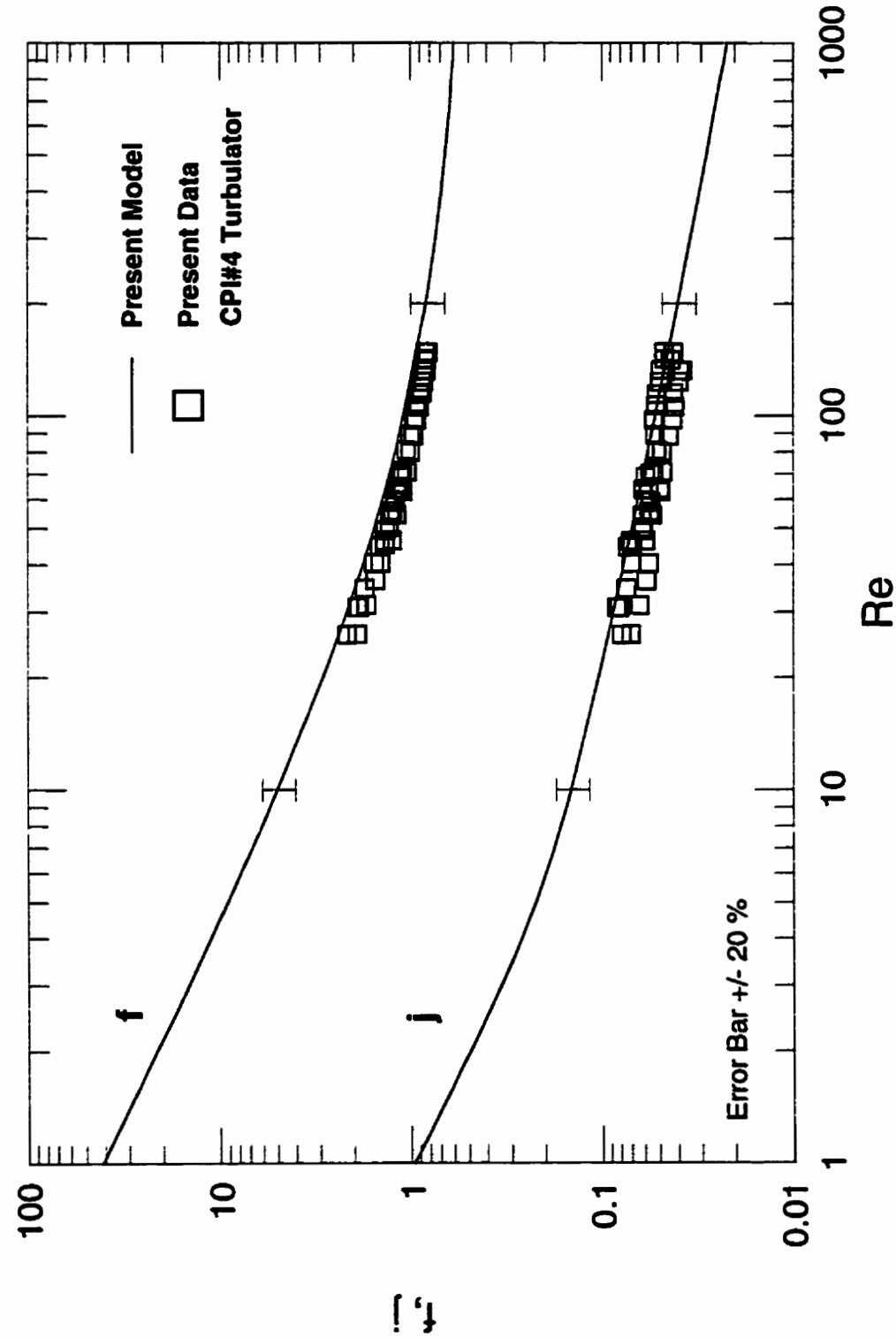

Fig. 6.37 - Comparison of Models with Data CPI-4 Turbulator.

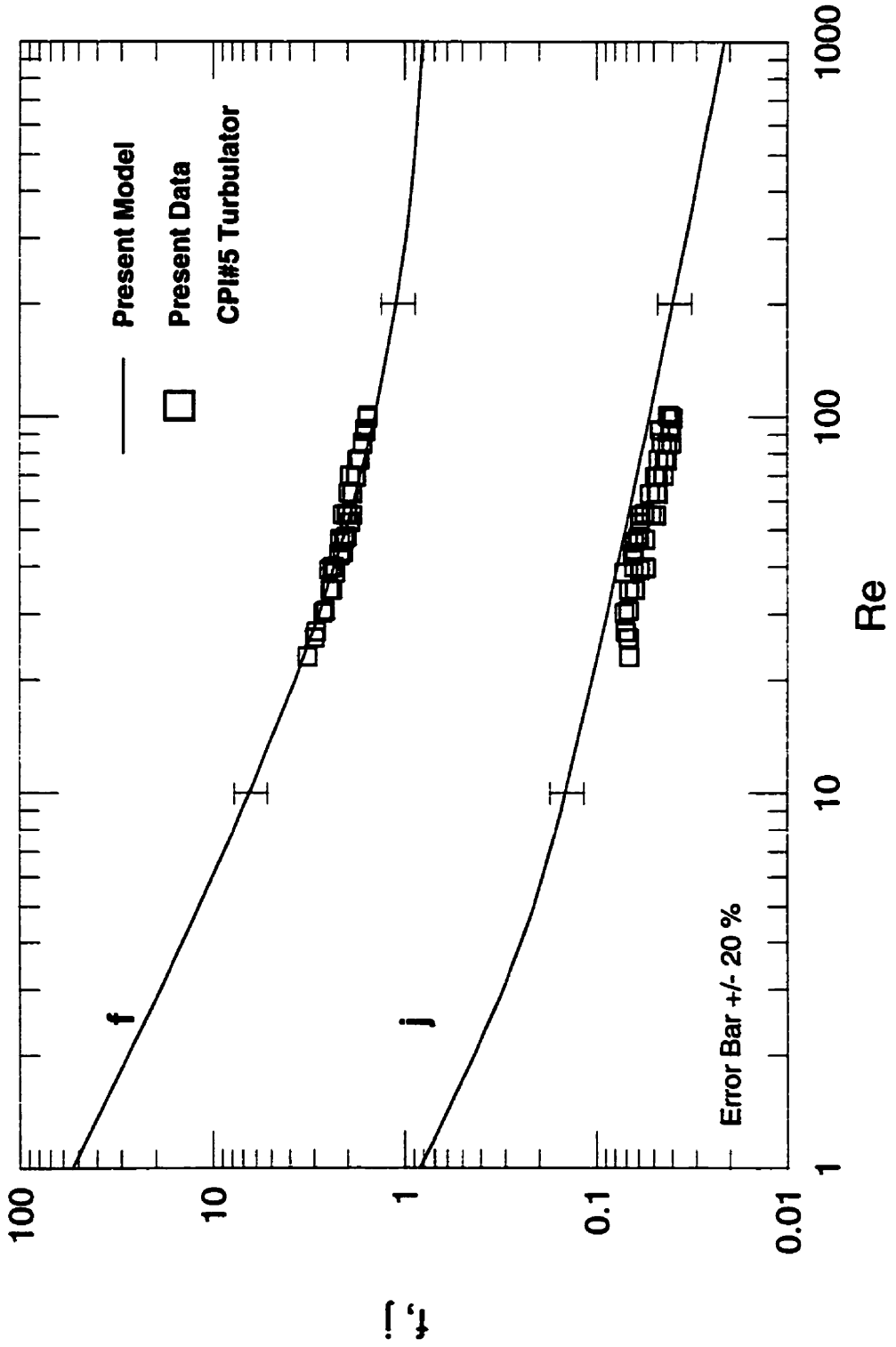

Fig. 6.38 - Comparison of Models with Data CPI-5 Turbulator.

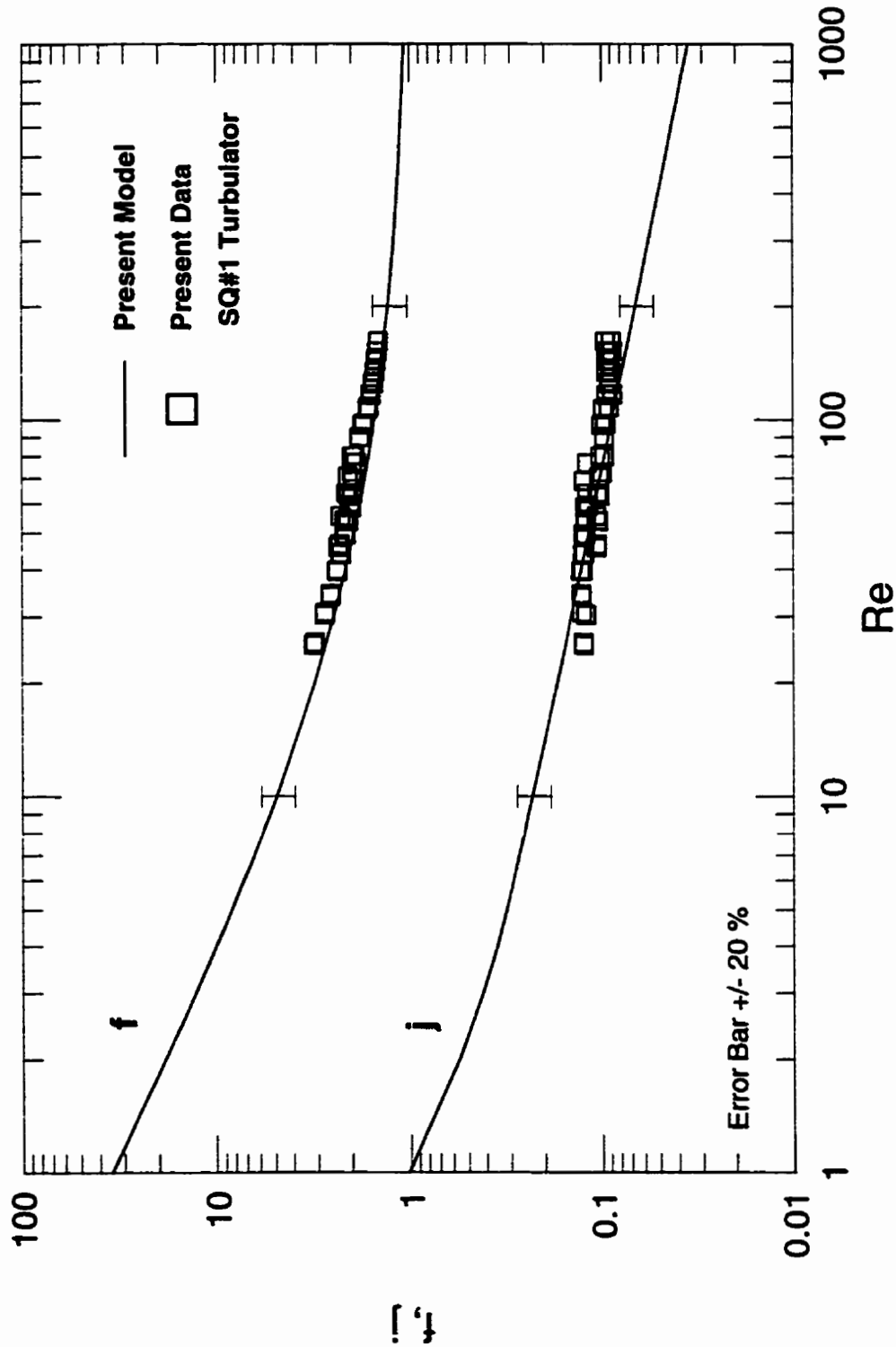

Fig. 6.39 - Comparison of Models with Data SQ-1 Turbulator.

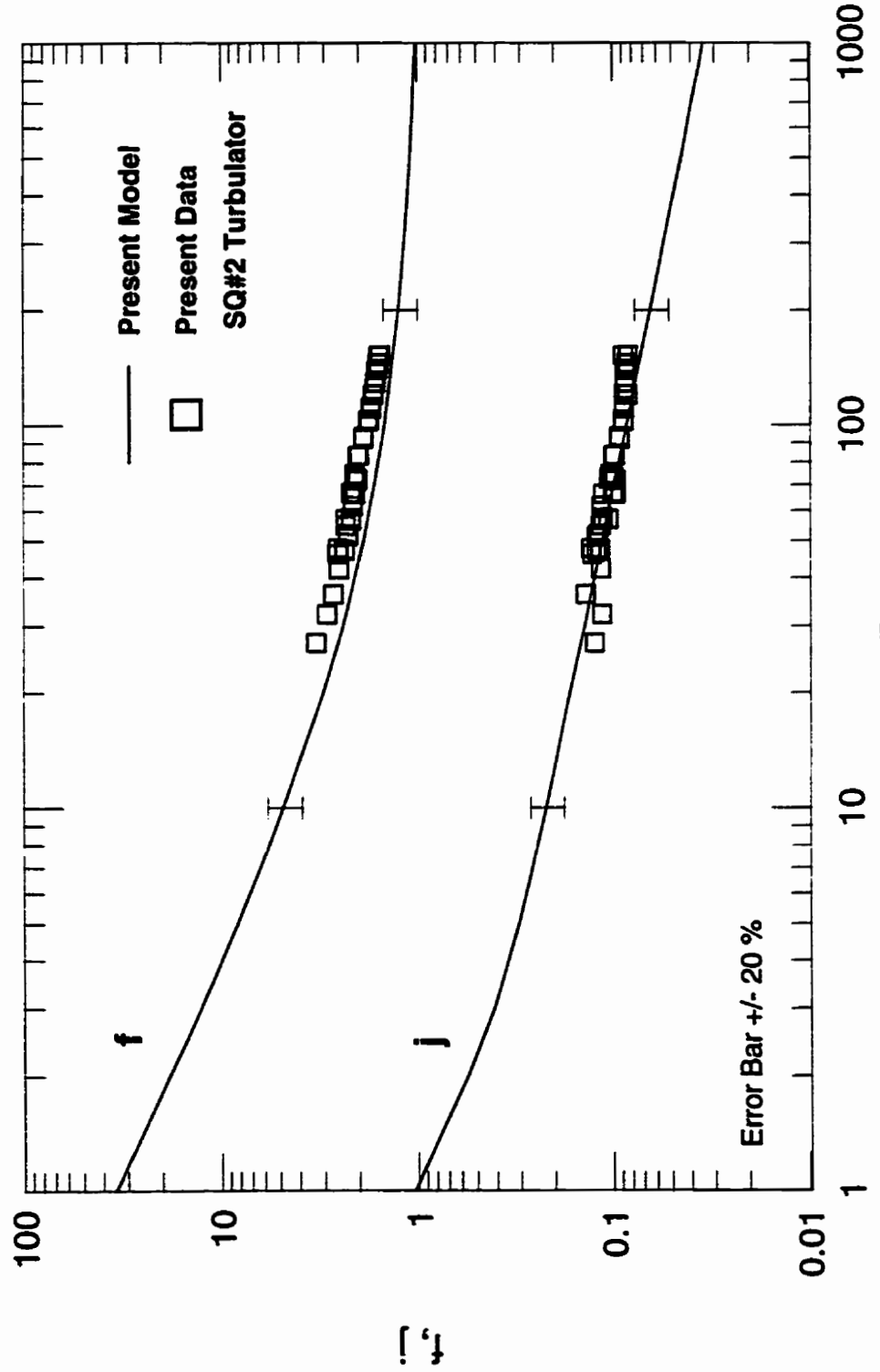

Fig. 6.40 - Comparison of Models with Data SQ-2 Turbulator.

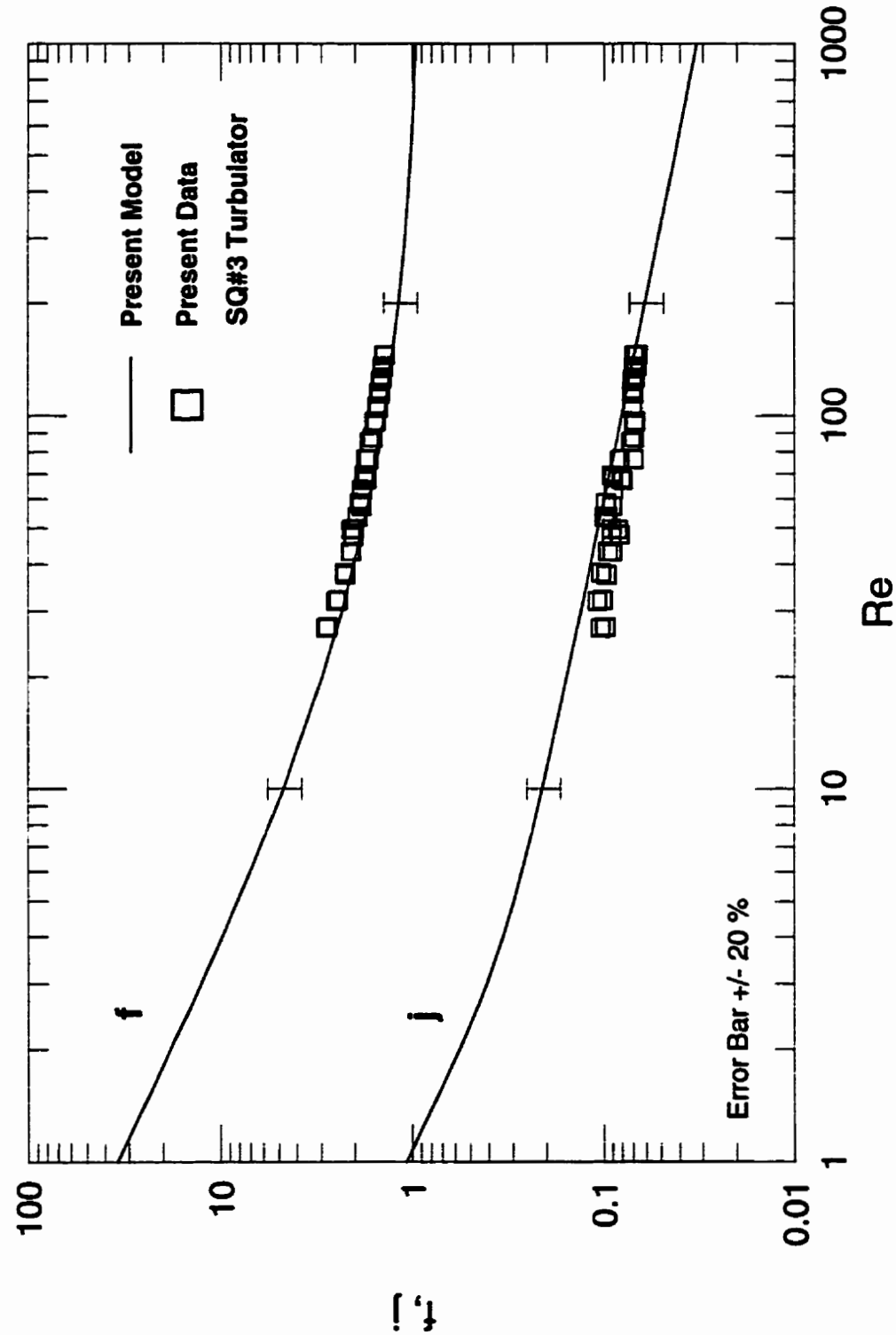

Fig. 6.41 - Comparison of Models with Data SQ-3 Turbulator.

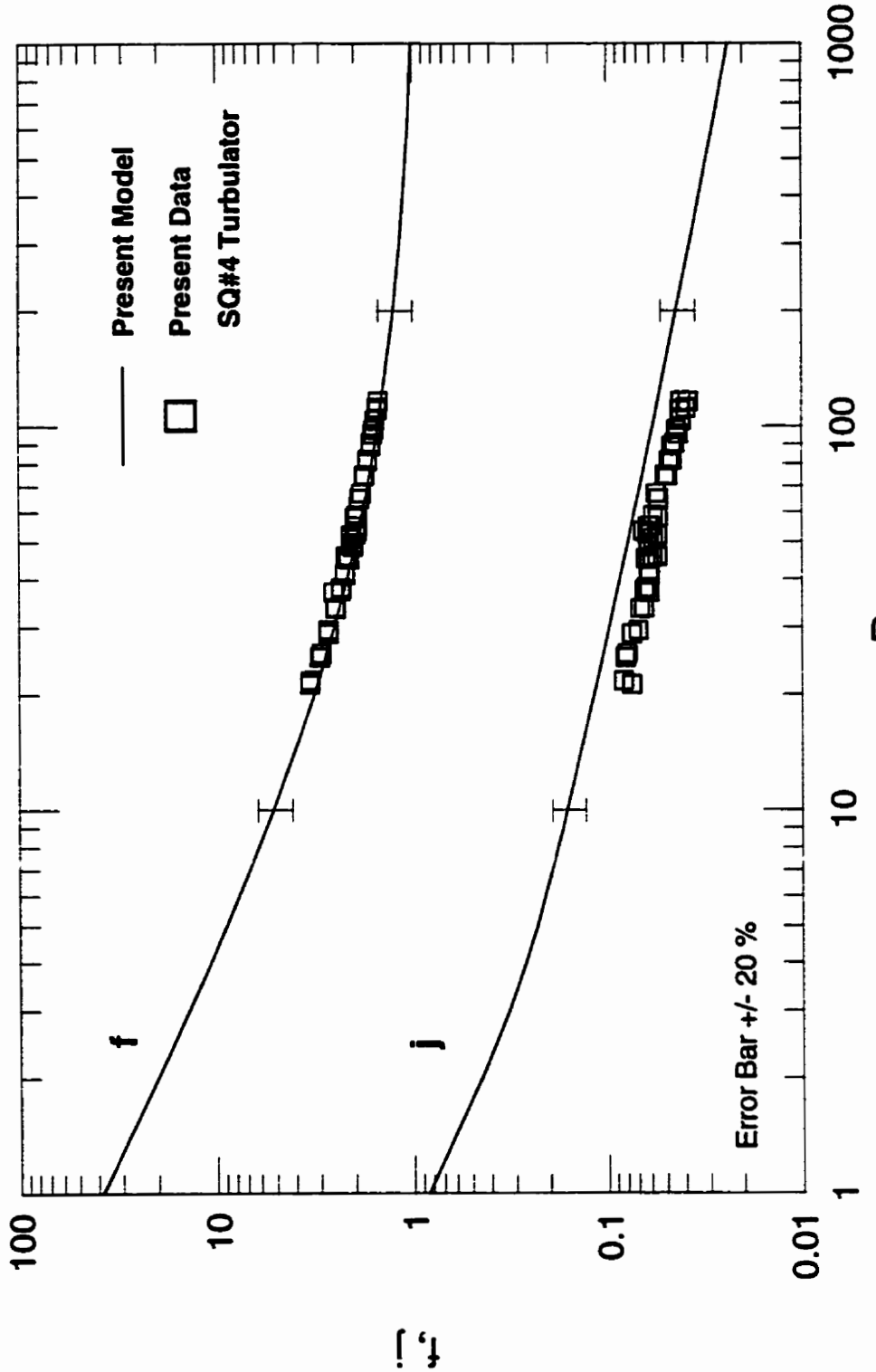

Fig. 6.42 - Comparison of Models with Data SQ-4 Turbulator.

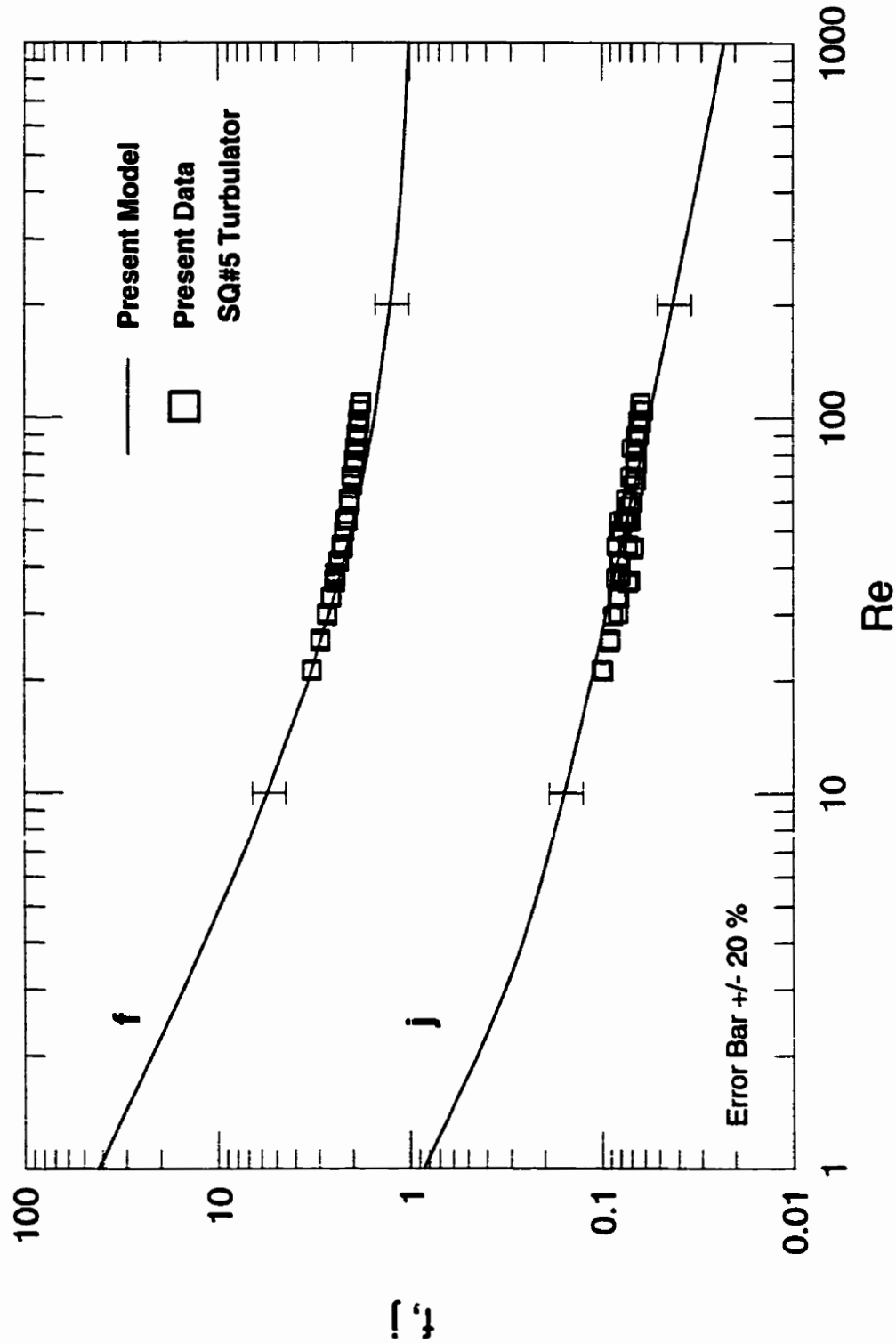

Fig. 6.43 - Comparison of Models with Data SQ-5 Turbulator.

6.6 Summary

Models were developed for two enhancement devices commonly found in compact heat exchangers. These models which were developed from analytic expressions can predict most OSF and turbulator strip friction factor and Colburn j factor data within $\pm$ 20 percent. The proposed models were developed for a wide range of Reynolds numbers which encompass the low flow or creeping flow regime and the high flow or turbulent region. Accurate prediction of the experimental data in the transition region was achieved by combining the laminar and turbulent regions using the asymptotic correlation method proposed by Churchill and Usagi (1972). The proposed models are summarized below, for both the OSF and turbulator geometries.

Offset Strip Fin Array

The basic equations for the OSF array are summarized below. The hydraulic diameter of the array is denoted by d_h, while the hydraulic diameter of the sub-channel is denoted by D_h.

Fanning f

$$f_{lam} = \frac{\left(f Re_{D_h} \frac{d_h}{D_h}\right)}{Re_{d_h}} + 1.328 \left(Re_{d_h} \frac{L_f}{d_h}\right)^{-1/2} \tag{6.63}$$

$$f_{tur} = 0.074 \left(Re_{d_h} \frac{L_f}{d_h}\right)^{-1/5} + 0.88 \left(\frac{(Ht + st/2)}{2L_f(H+s)}\right) \tag{6.64}$$

$$f = \left\{(f_{lam})^3 + (f_{tur})^3\right\}^{1/3} \tag{6.65}$$

Colburn j

$$j_{lam} = \left[\left(\frac{Nu_{D_h} \frac{d_h}{D_h}}{Re_{d_h} Pr^{1/3}} \right)^5 + \left(\frac{0.641 f Re_{D_h}^{1/3}}{Re_{d_h}^{2/3}} \left(\frac{d_h^2}{D_h L_f} \right)^{1/3} \right)^5 \right]^{1/5} \tag{6.66}$$

$$j_{tur} = 0.037 \left(Re_{d_h} \frac{L_f}{d_h} \right)^{-1/5} \tag{6.67}$$

$$j = \left\{ (j_{lam})^{7/2} + (j_{tur})^{7/2} \right\}^{2/7} \tag{6.68}$$

where

$$f Re_{D_h} = 23.94 - 30.05\epsilon + 32.37\epsilon^2 - 12.08\epsilon^3 \tag{6.69}$$

and

$$Nu_{D_h} = 7.45 - 16.9\epsilon + 22.1\epsilon^2 - 9.75\epsilon^3 \tag{6.70}$$

$0 < \epsilon = s/H < 1$ for a rectangular sub-channel. If subchannel is a geometry other than rectangular, fRe and Nu should be replaced by appropriate values for the particular geometry.

Turbulator Strips

The basic equations for the turbulator strip are summarized below. The hydraulic diameter of the array is denoted by d_h.

Fanning f

$$f_{cf} = \frac{8 C_o}{Re_{d_h}} \tag{6.71}$$

where

$$C_o = \frac{10}{\pi^2}\left(1+b^2\right)\mathbf{E}^2\left(\sqrt{\frac{b^2}{1+b^2}}\right) \tag{6.72}$$

and $\mathbf{E}(\cdot)$ is the complete elliptic integral of the second kind and $b = (2\pi W)/\lambda$.

$$f_{lam} = \left\{1.328\left(Re_{d_h}\frac{\lambda}{d_h}\right)^{-1/2}\right\}\left(\frac{1}{AER}\right) \tag{6.73}$$
$$+\frac{1}{2}\left\{1.328\left(Re_{d_h}\frac{2S_o}{d_h}\right)^{-1/2}\cos^2(\theta) + 1.538\left(Re_{d_h}\frac{W}{d_h}\right)^{-1/2}\sin^2(\theta)\right\}\left(1-\frac{1}{AER}\right)$$

$$f_{tur} = 0.074\left(Re_{d_h}\frac{\lambda}{d_h}\right)^{-1/5}\left(\frac{1}{AER}\right) + \left(1.2\frac{(\pi+4)\sin^2(\theta)}{\pi+4\sin(\theta)} + 0.878\sin(\theta)\right)\left(1-\frac{1}{AER}\right) \tag{6.74}$$

$$f = \left[\left(f_{cf}+f_{lam}\right)^{6/7} + \left(f_{tur}\right)^{6/7}\right]^{7/6} \tag{6.75}$$

Colburn j

$$j_{cf} = \frac{4.93}{Re_{d_h}Pr^{1/3}}\left(\frac{d_h}{H}\right) \tag{6.76}$$

$$j_{lam} = \frac{1}{2}\left\{0.664\left(Re_{d_h}\frac{2S_o}{d_h}\right)^{-1/2}\cos^2(\theta) + 0.849\left(Re_{d_h}\frac{W}{d_h}\right)^{-1/2}\sin^2(\theta)\right.$$
$$\left.+0.191\left(Re_{d_h}\frac{W}{d_h}\right)^{-1/3}\right\}\left(1-\frac{1}{AER}\right) + 0.664\left(Re_{d_h}\frac{\lambda}{d_h}\right)^{-1/2}\left(\frac{1}{AER}\right) \tag{6.77}$$

$$j_{tur} = 0.191 \left(Re_{d_h} \frac{W}{d_h} \right)^{-1/3} \tag{6.78}$$

$$j = \left[(j_{cf})^p + \{ (j_{lam})^q + (j_{tur})^q \}^{p/q} \right]^{1/p} \tag{6.79}$$

where $p = 9/2$ for all profiles and $q = 5$ for curved profiles and $q = 3/2$ for straight profiles.

In both the offset strip fin and turbulator strip geometries, the hydraulic diameter is defined as

$$d_h = \frac{4V_{free}}{A_{wet}} \tag{6.80}$$

Chapter 7

Summary and Conclusions

7.1 Summary of Present Research

This thesis examined the fluid friction and heat transfer characteristics for three typical geometries employed in heat exchanger design: the plain non-circular duct of constant cross-section, the rectangular offset strip fin, and the turbulator strip. Models for each of these geometries were developed for low Reynolds number flow conditions.

Analysis of the heat transfer and fluid friction data for straight non-circular ducts and channels revealed that scatter in the fully developed laminar flow data could be reduced using a characteristic length based upon the square root of the cross-sectional flow area, rather than the hydraulic diameter. The square root of the cross-sectional flow area was shown to be proportional to the equivalent circular duct diameter and also representative of the geometric mean of a vector normal to the duct wall. It was shown that this alternative definition for the characteristic length provided better correlation of the data over a wide range of duct aspect ratios, than could be achieved by the hydraulic diameter. This resulted in simple models being developed for fully developed flow conditions for the Nusselt number and friction factor - Reynolds number product. These simple models predict most of the available

data for most non-circular ducts to within ± 10%.

The fully developed flow models were later combined with simple asymptotic solutions for the hydrodynamic and thermal entrance regions to provide models which are valid over the entire range of dimensionless duct lengths for a large number of duct shapes. Models for the the hydrodynamic, thermal, and combined entrance problems were developed by combining the asymptotic solutions using a simple correlation method proposed by Churchill and Usagi (1972). These new models for the hydrodynamic and thermal entrance problems predict most of the available data to within ± 12% for the HDF and TDF problems, and ± 15% for the SDF problem. Models for the Nusselt number are valid for local and average conditions for both the uniform wall temperature (T) and uniform wall flux (H or H1) boundary conditions.

All of the models developed for straight non-circular ducts and channels may be used to predict the heat transfer and fluid friction characteristics in continuous plate fin compact heat exchangers. New models have been developed for predicting the heat transfer and fluid friction characteristics in heat exchangers utilizing the interrupted plate fin and turbulator strip geometries. These models which are based upon fundamental fluid dynamics and heat transfer theory, agree with experimental measurements to within ± 20% for both the Fanning friction factor, f, and Colburn j factor. Model comparisons for the interrupted strip fin were made with nineteen sets of data tabulated in Kays and London (1984), while model comparisons for the turbulator strip were made with ten sets of data obtained as part of this work.

All of the models developed for the plain duct and enhanced channel applications fulfill the need for simple and accurate predictive techniques. These models may also be incorporated into simulation and optimization codes which are routinely developed by manufacturers and designers of heat exchanger equipment.

7.2 Areas for Future Research

Several areas for future research which would benefit from a similar modelling approach are outlined below.

In the case of a straight non-circular duct, these are the effect of fully developed velocity distribution on fully developed and thermally developing flows, the effect of finite wall resistance and/or external heat transfer coefficient, and mixed convection effects at low Reynolds numbers.

- Solutions for fluids of non-newtonian character, i.e. power law fluids, exhibit similar characteristics to newtonian fluid flow. Since the parabolic velocity distribution is merely a special case of the general power law fluid, extension of the friction factor and Nusselt number models should not be difficult.

- Analysis of data for the parallel plate channel and circular duct for a wall having finite wall resistance shows that a universal resistance function may be found. This function may then be used to approximate results for non-circular ducts.

- The effect of external film coefficient also appears to be amenable to modelling. In most applications the exact boundary condition at the wall may lie somewhere in between the (T) or (H, H1) conditions depending upon the external heat transfer coefficient. Smooth transition from one wall condition to the other as a function of the external heat transfer coefficient allows for the development of a simple expression which relates these two wall conditions.

- Finally, at low Reynolds numbers, mixed convection effects may be important, especially in vertical ducts. Simple modelling to account for bouyancy assisted and opposed flows are available for a number of duct shapes. Development of more general models using the results of the present work would benefit the field.

In enhanced channel applications a number of issues still need to be resolved. These are: the effect of sub-channel shape for an offset-strip fin, the effect of fluid bypass channels, and the acquisition of data over a wider range of Reynolds numbers for the turbulator devices examined in Chapter 5.

- The models developed for the offset strip fin allow for the effect of sub-channel shape to be modelled. It was shown that sub-channel cross-sectional shape only affects results at low Reynolds number, i.e. the fully developed flow region. However, since all of the data in Kays and London (1984) for the interrupted strip fins are for the rectangular array, numerical or experimental data are required for verification.

- The effect of fluid bypass channels was studied for one turbulator configuration. The particular case examined was that of periodic placement of neutral planes or surfaces. The size and distribution of bypass channels needs to be addressed in more detail. A simple modelling approach similar to that proposed earlier may then be developed which accounts for the effects of fluid bypassing on the friction factor and heat transfer characteristics.

- Finally, the turbulator strip models have been developed over a wide range of Reynolds numbers. However, data has only been obtained in the intermediate region of the model, $10 < Re < 200$. Acquisition of data which span a wider Reynolds number range, $1 < Re < 1000$, would be beneficial for further validation and refinement of the turbulator models.

References

Achenbach, E., "Heat and Flow Characteristics of Packed Beds", *Experimental Thermal and Fluid Science*, Vol. 10, 1995, pp. 17-27.

Aggarwala, B.D. and Gangal, M.K., "Laminar Flow Development in Triangular Ducts", *Transactions of the CSME*, Vol. 3, 1975, pp. 231-233.

Asako, Y., Nakamura, H., and Faghri, M., "Developing Laminar Flow and Heat Transfer in the Entrance Region of Regular Polygonal Ducts", *International Journal of Heat and Mass Transfer*, Vol. 31, 1988, pp 2590-2593.

Bejan, A., *Heat Transfer*, Wiley, New York, 1993.

Bejan, A., *Convection Heat Transfer*, Wiley, New York, 1995.

Bejan, A., *Entropy Generation Minimization*, 1996, CRC Press.

Bender, E., "Druckverlust bei Laminarer Stromung im Rohreinlauf", *Chemie-Ingenieur Technik*, Vol. 41, 1969, pp. 682-686.

Bergles, A.E., *Chapter 11: Techniques to Augment Heat Transfer*, in *Handbook of Heat Transfer*, eds. W.M. Rohsenow, J.P. Hartnett, and Y.I. Cho, McGraw-Hill, New York, 1998.

Bhatti, M. S., "Laminar Flow in the Entrance Region of Elliptical Ducts", *Journal of Fluids Engineering*, Vol. 105, 1983, pp. 290-296.

Bird, R.B., Stewart,W.E., and Lightfoot, E.N., *Transport Phenomena*, Wiley, New York, 1960.

Blevins, R.D., *Applied Fluid Dynamics Handbook*, 1984, Van Nostrand Reinhold, New York.

Bodoia, J.R. and Osterle, J.F., "Finite Difference Analysis of Plane Poiseuille and Couette Flow Developments", *Applied Scientific Research A*, Vol. 10, 1961, pp. 265-276.

Botterill, J.S.M., *Chapter 6: Heat Transfer in Fluidized and Packed Beds*, in *Handbook of Heat Transfer Applications*, eds. W.M. Rohsenow, J.P. Hartnett, and E.N. Ganic, McGraw-Hill, New York, 1985.

Briggs, D.E, and London, A.L., "Heat Transfer and Flow Friction Characteristics of Five Offset Rectangular and Six Plain Triangular Plate Fin Heat Transfer Surfaces", *International Developments in Heat Transfer*, ASME, 1961, pp. 122-134.

Briggs, D.E. and Young, E.H., "Modified Wilson Plot Techniques for Obtaining Heat Transfer Correlations for Shell and Tube Heat Exchangers", *Chemical Engineering Progress Symposium Series*, Vol. 65, 1969, pp. 35-45.

Burmeister, L.C., *Convective Heat Transfer*, Wiley, New York, 1993.

Carman, P.C., *Flow of Gases Through Porous Media*, Butterworths Scientific Publications, London, 1956.

Cebeci, T. and Bradshaw, P., *Physical and Computational Aspects of Convective Heat Transfer*, Springer-Verlag, New York, 1984.

Chandrupatla, A.R. and Sastri, V.M.K., "Laminar Forced Convection Heat Transfer of a Non-Newtonian Fluid in a Square Duct", *International Journal of Heat and Mass Transfer*, Vol. 20, 1977, pp. 1315-1324.

Cheng, K.C., "Laminar Flow and Heat Transfer Characteristics in Regular Polygonal Ducts", *Proceedings of the International Heat Transfer Conference, 3rd AIChE*, Vol. 1, 1966, pp. 64-76.

Cheng, K. C., "Laminar Forced Convection in Regular Polygonal Ducts with Uniform Peripheral Heat Flux", *Journal of Heat Transfer*, Vol. 91, 1969, pp. 156-157.

Cheng, K.C. and Jamil, M., "Laminar Flow and Heat Transfer in Circular Ducts with Diametrically Opposite Flat Sides and Ducts of Multiply Connected Cross Sections", *Canadian Journal of Chemical Engineering*, Vol. 48, 1970, pp. 333-334.

Churchill, S.W., *Viscous Flows: The Practical Use of Theory*, Butterworths, Boston, MA, 1988.

Churchill, S. W. and Ozoe, H., "Correlations for Laminar Forced Convection with Uniform Heating in Flow over a Plate and in Developing and Fully Developed Flow in a Tube", *Journal of Heat Transfer*, Vol. 95, 1973, pp. 78-84.

Churchill, S. W. and Ozoe, H., "Correlations for Laminar Forced Convection in Flow Over an Isothermal Flat Plate and in Developing and Fully Developed Flow in an Isothermal Tube", *Journal of Heat Transfer*, Vol. 95, 1973, pp. 416-419.

Churchill, S. W. and Usagi, R., "A General Expression for the Correlation of Rates of Transfer and Other Phenomena", *American Institute of Chemical Engineers*, Vol. 18, 1972, pp. 1121-1128.

Curr, R.M., Sharma, D., and Tatchell, D.G., "Numerical Predictions of Some Three Dimensional Boundary Layers in Ducts", *Computer Methods in Applied Mechanics and Engineering*, Vol. 1, 1972, pp. 143-158.

Daigle, J., "Turbulizer Performance Experiments", ME 482 Project, University of Waterloo, 1997.

Drew, T. B., "Mathematical Attacks on Forced Convection Problems: A Review", *Transactions of the American Institute of Chemical Engineers*, Vol. 26, 1931, pp. 26-80.

Dubrovsky, E.V., "Experimental Investigation of Highly Effective Plate Fin Heat Exchanger Surfaces", *Experimental Thermal and Fluid Science*, Vol. 10, 1995, pp. 200-220.

Ebadian, M.A. and Dong, Z.F., "Chapter 5 Forced Convection, Internal Flow in Ducts", in *Handbook of Heat Transfer*, eds. W.M. Rohsenow, J.P. Hartnett, Y.I. Cho, McGraw-Hill, New York, 1998.

Ebadian, M. A., Topakoglu, H. C., and Arnas, O. A., "On the Convective Heat Transfer in a Tube of Elliptic Cross-Section Maintained Under Constant Wall Temperature", *Journal of Heat Transfer*, Vol. 108, 1986, pp. 33-39.

Eckert, E.R.G. and Drake, R.M., *Analysis of Heat and Mass Transfer*, McGraw-Hill, New York, 1972.

Eckert, E.R.G. and Irvine, T.F., "Flow in Corners of Passages with Non-Circular Cross-sections", *Transactions of the ASME*, Vol. 78, 1956, pp. 709-718.

Ergun, S, "Fluid Flow Through Packed Columns", *Chemical Engineering Progress*, Vol. 48, 1952, pp. 89-94.

Feldman, E.E., "The Numerical Solution of the Combined Thermal and Hydrodynamic Entrance Region of an Eccentric Annular Duct, Ph.D. Thesis, Carnegie-Mellon University, 1974.

Fleming, D.P. and Sparrow, E.M., "Flow in the Hydrodynamic Entrance Region of Ducts of Arbitrary Cross-section", *Journal of Heat Transfer*, Vol. 91, 1969, pp. 345-354.

Gangal, M.K., "Some Problems in Channel Flow", Ph.D Thesis, University of Calgary, 1974.

Gunn, D.J. and Darling, C.W.W., "Fluid Flow and Energy Losses in Non-Circular Conduits", *Transactions of the Institution of Chemical Engineers*, Vol. 41, 1963, pp. 163-173.

Hagan, S.L. and Ratkowsky, D.A., "Laminar Flow in Cylindrical Ducts Having Regular Polygonal Shaped Cores", *Canadian Journal of Chemical Engineering*, Vol. 46, 1968, pp. 387-388.

Haji-Sheikh, A., Mashena, M., and Haji-Sheikh, M.J., "Heat Transfer Coefficient in Ducts with Constant Wall Temperature", *Journal of Heat Transfer*, Vol. 105, 1983, pp. 878-883.

Happel, J. and Brenner, H., *Low Reynolds Number Hydrodynamics*, Noordhoff International Publishing, 1965.

Hassani, A, *An Investigation of Free Convection Heat Transfer from Bodies of Arbitrary Shape*, Ph.D. Thesis, University of Waterloo, 1987.

Holman, J.P., *Experimental Methods for Engineers*, McGraw-Hill, New York. 1984.

Hong, S.W. and Bergles, A.E., "Augmentation of Laminar Flow Heat Transfer in Tubes by Means of Twisted Tape Inserts", *Technical Report HTL-5, ISU-ERI-Ames-75011*, Iowa State University, 1974.

Hornbeck, R.W., "Laminar Flow in the Entrance Region of a Pipe" *Applied Scientific Research A*, Vol. 13, 1964, pp. 224-232.

Huntly, E.S., *Dimensional Analysis*, Rinehart, New York, 1951.

Igarashi, T., "Heat Transfer from a Square Prism to an Air Stream", *International Journal of Heat and Mass Transfer*, Vol. 28, 1985, pp. 175-181.

Igarashi, T., Hirata, M., and Nishiwaki, N., "Heat Transfer in Separated Flows: Part 1, Experiments on Local Heat Transfer from the Rear of a Flat Plate Inclined to an Air Stream", *Heat Transfer, Japanese Research*, Vol. 4, 1975, pp. 11-32.

Incropera, F.P. and DeWitt, D. P., *Fundamentals of Heat and Mass Transfer*, Wiley, New York, 1990.

Jakob, M., *Heat Transfer Vol. 1*, John Wiley and Sons Inc., New York, 1949.

James, P. A., "Forced Convection Heat Transfer in Narrow Passages", *Canadian Journal of Chemical Engineering*, Vol. 48, 1970, pp. 330-332.

Jamil, M., "Laminar Forced Convection in Noncircular Ducts", M.S. Thesis, University of Alberta, 1967.

Joshi, H.M. and Webb, R.L., "Heat Transfer and Friction in the Offset Strip Fin Heat Exchanger", *International Journal of Heat and Mass Transfer*, Vol. 30, 1987, pp. 69-84.

Kakac, S. and Liu, H., *Heat Exchangers: Selection, Rating, and Thermal Design*, CRC Press, Boca Raton, 1998.

Kakac, S., Shah, R.K., and Aung, W., *Handbook of Single Phase Convective Heat Transfer*, Wiley, New York, 1987.

Kakac, S. and Yener, Y., "Laminar Forced Convection in the Combined Entrance Region of Ducts", in *Low Reynolds Number Heat Exchangers*, ed. S. Kakac, R. K. Shah and A. E. Bergles, pp. 165-204, Hemisphere Publishing, Washington, 1983.

Kalinin, E.K. and Dreitser, G.A., "Heat transfer Enhancement in Heat Exchangers", in *Advances in Heat Transfer*, ed. J.P. Hartnett, T.F. Irvine, Y.I. Cho, and G.A. Greene, pp. 159-332, Academic Press, New York, 1998.

Kays, W.M., "Basic Heat Transfer and Flow Friction Characteristics of Six Compact High Performance Heat Transfer Surfaces", *Journal of Engineering Power*, Vol. 82, 1960, pp. 27-34.

Kays, W.M., and Crawford, M.E., *Convective Heat and Mass Transfer*, McGraw-Hill, New York, 1993.

Kays, W.M. and London, A.L., *Compact Heat Exchangers*, McGraw-Hill, New York, 1984.

Kays, W.M. and Perkins, H.C., *Chapter 7: Forced Convection, Internal Flow in Ducts*, in *Handbook of Heat Transfer Fundamentals*, eds. W.M. Rohsenow, J.P. Hartnett, and E.N. Ganic, McGraw-Hill, New York, 1985.

Kelkar, K.M. and Patankar, S.V., "Numerical Prediction of Heat Transfer and Fluid Flow in in Rectangular Offset Fin Arrays", *Numerical Heat Transfer*, 1985, ASME HTD-52, pp. 21-28.

Kern, D.Q. and Kraus, A.D., *Extended Surface Heat Transfer*, McGraw-Hill, New York, 1972.

Khartabil, H.F. and Christensen, R.N., "An Improved Scheme for Determining heat Transfer Correlations from Heat Exchanger Regression Models with Three Unknowns", *Experimental Thermal and Fluid Science*, Vol. 5, 1992, pp. 808-819.

Knudsen, J.G. and Katz, D.L., *Fluid Dynamics and Heat Transfer*, McGraw-Hill, New York, 1958.

Lakshminarayanan, R. and Haji-Sheikh, A., "Entrance Heat Transfer in Isosceles and Right Triangular Ducts", *Journal of Thermophysics and Heat Transfer*, Vol. 6, 1992, pp. 167-171.

Lamb, H., *Hydrodynamics*, Cambridge University Press, 1932.

Langhaar, H.L., "Steady Flow in the Transition Length of a Straight Tube", *Journal of Applied Mechanics*, Vol. 9, 1942, pp. A55-A58.

Langhaar, H.L., *Dimensional Analysis and Theory of Models*, Wiley, New York, 1951.

Lauwerier, H.A., "The Use of Confluent Hypergeometric Functions in Mathematical Physics and the Solution of an Eigenvalue Problem", *Applied Scientific Research*, Vol. A2, 1951, pp. 184-204.

Lawal, A. and Mujumdar, A.S., "Forced Convection Heat Transfer to a Power Law Fluid in Arbitrary Cross-section Ducts", *Canadian Journal of Chemical Engineering*, Vol. 62, 1984, pp. 326-333.

Lemczyk, T.F., "Turbulizer CFD Analysis Research Report", Advanced Engineering Report No. NP-326, Long Manufacturing, 1992.

Lemczyk, T.F., "Research Topics in Low Reynolds Flow Heat Exchangers", Long Manufacturing, 1994.

Lemczyk, T.F., *Turb v3.1 User's Manual*, Long Manufacturing, 1997.

Lemczyk, T.F. and Molloy, D., "Fluid Properties Research Report: Advanced Engineering NP-329", Long Manufacturing, 1996.

Liu, J., "Flow of a Bingham Fluid in the Entrance Region of an Annular Tube", M.S. Thesis, University of Wisconsin, 1974.

London, A.L. and Shah, R.K., "Offset Rectangular Plate Fin Surfaces - Heat Transfer and Flow Friction Characteristics", *Journal of Engineering Power*, Vol. 90, 1968, pp. 218-228.

MaClaine-Cross, I.L., "An Approximate Method for Calculating Heat Transfer and Pressure Drop in Ducts with Laminar Flow", *Journal of Heat Transfer*, Vol. 91, 1969, pp. 171-173.

Manglik, R.M. and Bergles, A.E., "The Thermal-Hydraulic Design of the Rectangular Offset Strip Fin Compact Heat Exchanger", in *Compact Heat Exchangers: A Festschrift for A.L. London*, pp. 123-149, eds. R.K. Shah, A.D. Kraus, and D. Metzger, Hemisphere Publishing, Washington, 1990.

Manglik, R.M. and Bergles, A.E., "Heat Transfer and Pressure Drop Correlations for the Rectangular Offset-Strip-Fin Compact Heat Exchanger", *Experimental Thermal and Fluid Science*, Vol. 10, 1995, pp. 171-180.

McComas, S.T., "Hydrodynamic Entrance Lengths for Ducts of Arbitrary Cross-Section", *Journal of Basic Engineering*, Vol. 89, 1967, pp. 847-850.

McAdams, W.H., *Heat Transmission*, McGraw-Hill, New York, 1942.

Miller, R.W. and Han, L.S., "Pressure Losses for Laminar Flow in the Entrance Region of Ducts of Rectangular and Equilateral Triangular Cross-Section", *Journal of Applied Mechanics*, Vol. 38, 1971, pp. 1083-1087.

Milne-Thomson, L.M., *Theoretical Hydrodynamics*, Dover, 1968.

Moffat, R.J., "Describing Uncertainties in Experimental Results", *Experimental Thermal and Fluid Science*, Vol. 1, 1988, pp. 3-17.

Morley, P., "Heat Transfer and Pressure Drop Analysis of Heat Exchangers", Student Work Report, Long Manufacturing, 1996.

Morley, P., "Compact Heat Exchanger Performance", ME 482 Project, University of Waterloo, 1997.

Muzychka, Y.S. and Yovanovich, M.M., "Modeling Fricton Factors in Non-Circular Ducts for Developing Laminar Flow", AIAA Paper 98-2492, 2nd Theoretical Fluid Mechanics Meeting, Albuquerque, NM, 1998.

Muzychka, Y.S. and Yovanovich, M.M., "Modeling Nusselt Numbers for Thermally Developing Laminar Flow in Non-Circular Ducts", AIAA Paper 98-2586, 7th AIAA/ASME Joint Thermophysics and Heat Transfer Conference, Albuquerque, NM, 1998.

Newman, J., "Extension of the Leveque Solution", *Journal of Heat Transfer*, Vol. 91, 1969, pp. 177-178.

Newman, J., "The Graetz Problem", in *The Fundamental Principles of Current Distribution and Mass Transport in Electrochemical Cells*, ed. A. J. Bard, Vol. 6, pp. 187-352, Dekker, 1973.

Nield, D.A. and Bejan, A., *Convection in Porous Media*, Springer-Verlag, New York, 1992.

Obot, N. T., "Determination of Incompressible Flow Friction in Smooth Circular and Non-Circular Passages: A Generalized Approach Including Validation of the Nearly Century Old Hydraulic Diameter Concept", *Journal of Fluids Engineering*, Vol. 110, 1988, pp. 431-440.

Panton, R.L., *Incompressible Flow*, Wiley, New York, 1985.

Patankar, S.V., Liu, C.H., Sparrow, E.M., "Fully Developed Flow and Heat Transfer in Ducts Having Streamwise Periodic Variations of Cross-sectional Area", *Journal of Heat Transfer*, Vol. 99, 1977, pp. 180-186.

Patankar, S.V., "Numerical Prediction of Flow and Heat Transfer in Compact Heat Exchanger Passages", in *Compact Heat Exchangers: A Festschrift for A.L. London*, pp. 191-204, eds. R.K. Shah, A.D. Kraus, and D. Metzger, Hemisphere Publishing, Washington, 1990.

Raithby, G.D. and Hollands, K.G.T., "Chapter 4 Natural Convection", in *Handbook of Heat Transfer*, eds. W.M. Rohsenow, J.P. Hartnett, Y.I. Cho, McGraw-Hill, New York, 1998.

Rapely, C.W., Stainsby, R., and Webb, A.I.C., " Developing Laminar Flow in Elliptical Ducts Via the F.E.M.", *Numerical Methods in Laminar and Turbulent Flow, Proceedings of the 4th International Conference*, 1985, pp. 51-62.

Ratkowsky, D.A. and Epstein, N., "Laminar Flow in Regular Polygonal Shaped Ducts with Circular Centered Cores", *Canadian Journal of Chemical Engineering*, Vol. 46, 1968, pp. 22-26.

Refai, G.A. and Yovanovich, M.M., "Analytical Method for Forced Convection from Flat Plates, Circular Cylinders, and Spheres", *Journal of Thermophysics and Heat Transfer*, Vol. 9, 1995, pp. 516-523.

Richardson, S. M., "Extended Leveque Solutions for Flows of Power Law Fluids in Pipes and Channels", *International Journal of Heat and Mass Transfer*, Vol. 22, 1978, pp. 1417-1423.

Richardson, S. M. "Leveque Solution for Flow in an Elliptical Duct", *Letters in Heat and Mass Transfer*, Vol. 7, 1980, pp. 353-362.

Rohsenow, W.M. and Choi, H.Y., *Heat, Mass, and Momentum Transfer*, Prentice-Hall, Englewood Cliffs, NJ, 1961.

Rohsenow, W.M., Hartnett, J.P., and Ganic, E.N., eds. *Handbook of Heat Transfer Fundamentals*, McGraw-Hill, New York, 1985a.

Rohsenow, W.M., Hartnett, J.P., and Ganic, E.N., eds. *Handbook of Heat Transfer Applications*, McGraw-Hill, New York, 1985b.

Rohsenow, W.M., Hartnett, J.P., and Cho, Y.I., eds. *Handbook of Heat Transfer*, McGraw-Hill, New York, 1998.

Rouse, H., ed. *Advanced Fluid Mechanics*, Wiley, New York, 1959.

Sahnoun, A. and Webb, R.L., "Prediction of Heat Transfer and Friction for the Louver Fin Geometry", *Journal of Heat Transfer*, Vol. 114, 1992, pp. 893-900.

Schlichting, H.V., *Boundary Layer Theory*, McGraw-Hill, New York, 1979.

Schmidt, F.W. and Newell, M.E., "Heat Transfer in Fully Developed Laminar Flow Through Rectangular and Isosceles Triangular Ducts", *International Journal of Heat and Mass Transfer*, Vol. 10, 1967, pp. 1121-1123.

Sellars, J. R., Tribus, M., and Klein, J. S., "Heat Transfer to Laminar Flow in a Round Tube or Flat Conduit - The Graetz Problem Extended", *Transactions of the ASME*, Vol. 78, 1956, pp. 441-448.

Shah, R.K., "Laminar Flow Friction and Forced Convection Heat Transfer in Ducts of Arbitrary Geometry", *International Journal of Heat and Mass Transfer*, Vol. 18, 1975, pp. 849-862.

Shah, R. K., "A Correlation for Laminar Hydrodynamic Entry Length Solutions for Circular and Non-Circular Ducts", *Journal of Fluids Engineering*, Vol. 100, 1978. pp. 177-179.

Shah, R.K., "Compact Heat Exchangers", in *Heat Exchangers*, eds. S. Kakac, A.E. Bergles, and F. Mayinger, pp. 111-151, McGraw-Hill, New York, 1981.

Shah, R.K., "Fully Developed Laminar Flow Forced Convection in Channels", in *Low Reynolds Number Heat Exchangers*, eds. S. Kakac, R.K. Shah and A.E. Bergles, pp. 75-164, Hemisphere Publishing, Washington, 1983.

Shah, R.K., "Research Needs in Low Reynolds Number Flow Heat Exchangers", in *Low Reynolds Number Heat Exchangers*, eds. S. Kakac, R.K. Shah and A.E. Bergles. pp. 983-1000, Hemisphere Publishing, Washington, 1983.

Shah, R.K., "Chapter 4, Part 3: Compact Heat Exchangers", in *Handbook of Heat Transfer Applications*, eds. W.M. Rohsenow, J.P. Hartnett, and E.N. Ganic, McGraw-Hill, New York, 1985.

Shah, R.K., "Assessment of Modified Wilson Plot Techniques for Obtaining Heat Exchanger Design Data", *Heat Transfer 1990*, Vol. 5, 1990, pp. 51-56.

Shah, R.K. and Bhatti, M.S., Chapter 3: Laminar Convective Heat Transfer in Ducts, in *Handbook of Single Phase Convective Heat Transfer*, eds. S. Kakac, R.K. Shah and W. Aung, Wiley, New York, 1987.

Shah, R. K. and London, A.L., "Thermal Boundary Conditions and Some solutions for Laminar Duct Flow Forced Convection", *Journal of Heat Transfer*, Vol. 96, 1974, pp. 159-165.

Shah, R.K. and London, A.L., *Advances in Heat Transfer, Supplement 1, Laminar Forced Flow Convection in Ducts*, Academic Press, New York, 1978.

Shah, R.K. and Sekulic, D.P., "Chapter 17 Heat Exchangers", in *Handbook of Heat Transfer*, eds. W.M. Rohsenow, J.P. Hartnett, Y.I. Cho, McGraw-Hill, New York, 1998.

Shah, R.K. and Webb, R.L., "Compact and Enhanced Heat Exchangers", in *Heat Exchangers: Theory and Practice*, eds. J. Taborek, G.F. Hewitt, N. Afghan, pp. 425-468, McGraw-Hill, New York, 1983.

Shah, V.L. and Farnia, K., "Flow in the Entrance of Annular Tubes", *Computers and Fluids*, Vol. 2, 1974, pp. 285-294.

Shapiro, A.H., Siegel, R., and Kline, S.J., " Friction Factor in the Laminar Entry Region of a Smooth Tube", *Proceedings of the 2nd U.S. National Congress of Applied Mechanics*, 1954, pp. 733-741.

Shih, F.S., "Laminar Flow in Axisymmetric Conduits by a Rational Approach", *Canadian Journal of Chemical Engineering*, Vol. 45, 1967, pp. 285-294.

Siegel, R., "The Effect of Heating on Boundary Layer Transition for Liquid Flow in a Tube", Sc.D. Thesis, Massachusetts Institute of Technology, 1953.

Soliman, H.M., "Laminar Heat Transfer in Annular Sector Ducts", *Journal of Heat Transfer*, Vol. 109, 1987, pp. 247-249.

Soliman, H.S., Munis, A.A., and Trupp, A.C., "Laminar Flow in the Entrance Region of Circular Sector Ducts", *Journal of Applied Mechanics*, Vol. 49, 1982, pp. 640-642.

Someswara Rao, S., Pattabhi Ramacharyulu, N., Krishnamurty, V., "Laminar Forced Convection in Elliptic Ducts", *Applied Scientific Research*, Vol. 18, 1967, pp. 185-193.

Sparrow, E.M., "Analysis of Laminar Forced Convection Heat Transfer in Entrance Region of Flat Rectangular Ducts", *NACA Technical Note 3331*, 1955.

Sparrow, E.M. and Haji-Sheikh, A., "Laminar Heat Transfer and Pressure Drop in Isosceles Triangular, Right Triangular, and Circular Sector Ducts", *Journal of Heat Transfer*, Vol. 87, 1965, pp. 426-427.

Sparrow, E.M. and Haji-Sheikh, A., "Flow and Heat Transfer in Ducts of Arbitrary Shape with Thermal Boundary Conditions", *Journal of Heat Transfer*, Vol. 91, 1966, pp. 351-358.

Sparrow, E.M. and Lin, S.H., "The Developing Laminar Flow and Pressure Drop in the Entrance Region of Annular Ducts", *Journal of Basic Engineering*, Vol. 86, 1964, pp. 827-834.

Sparrow, E.M., Lin, S.H., and Lundgren, T.S., " Flow Development in the Hydrodynamic Entrance Region of Tubes and Ducts", *The Physics of Fluids*, Vol. 7, 1964, pp. 338-347.

Sparrow, E.M., Baliga, B.R., and Patankar, S.V., "Heat Transfer and Fluid Flow Analysis of Interrupted Wall Channels, With Application to Heat Exchangers", *Journal of Heat Transfer*, Vol. 99, 1977, pp. 4-11.

Stephan, K., "Warmeubergand und Druckabfallbei Nicht Ausgebildeter Laminarstromung in Rohren und in Ebenen Spalten", *Chem-Ing-Tech*, Vol. 31, 1959, pp. 773-778.

Taylor, E.S., *Dimensional Analysis for Engineers*, Oxford University Press, Oxford, 1974.

Teertstra, P.M., Yovanovich, M.M., and Culham, J.R., "Pressure Loss Modeling for Surface Mounted Cuboid-Shaped Packages in Channel Flow", *IEEE Transactions Components, Packaging, and Manufacturing Technology*, Part A, Vol. 20, 1998, pp. 463-471.

Vennard, J.L. and Street, R.L., *Elementary Fluid Mechanics*, Wiley, New York, 1982.

Webb, R.L., *Chapter 17: Enhancement of Single Phase Heat Transfer*, in *Handbook of Single Phase Convective Heat Transfer*, eds. S. Kakac, R.K. Shah and W. Aung, Wiley, New York, 1987.

Webb, R.L., *Principles of Enhanced Heat Transfer*, John Wiley, New York, 1994.

Webb. R.L., "Advances in Modeling Enhanced Heat Transfer Surfaces", *Proceedings of the 10th International Heat Transfer Conference*, 1995, pp. 445-459.

Webb, R.L. and Joshi, H.M., "Prediction of the Friction Factor for the Offset Strip Fin Matrix", *ASME/JSME Thermal Engineering Joint Conference*, Vol. 1, ASME, pp. 461-470.

Wieting, A.R., "Empirical Correlations for Heat Transfer and Flow Friction Characteristics of Rectangular Offset-Fin Plate-Fin Heat Exchangers", *Journal of Heat Transfer*, Vol. 97, 1975, pp. 488-490.

White, F.M., *Viscous Fluid Flow*, McGraw-Hill, New York, 1974.

White, F.M., *Fluid Mechanics*, McGraw-Hill, New York, 1987.

White, F.M., *Viscous Fluid Flow*, McGraw-Hill, New York, 1991.

Wibulswas, P., "Laminar Flow Heat Transfer in Noncircular Ducts", Ph.D. Thesis, London University, 1966.

Worsoe-Schmidt, P. M., "Heat Transfer in the Thermal Entrance Region of Circular Tubes and Annular Passages with Fully Developed Laminar Flow", *International Journal of Heat and Mass Transfer*, Vol. 10, 1966, pp. 541-551.

Yilmaz, T., "General Equations for Pressure Drop for Laminar Flow in Ducts of Arbitrary Cross Sections", *Journal of Energy Resources Technology*, Vol. 112, 1990, pp. 220-223.

Yilmaz, T. and Cihan, E., "General Equation for Heat Transfer for Laminar Flow in Ducts of Arbitrary Cross-Sections", *International Journal of Heat and Mass Transfer*, Vol. 36, 1993, pp. 3265-3270.

Yilmaz, T. and Cihan, E., "An Equation for Laminar Flow Heat Transfer for Constant Heat Flux Boundary Condition in Ducts of Arbitrary Cross-Sectional Area", *Journal of Heat Transfer*, Vol. 117, 1995, pp. 765-766.

Yovanovich, M. M., "New Nusselt and Sherwood Numbers for Arbitrary Isopotential Bodies at Near Zero Peclet and Rayleigh Numbers", AIAA Paper 87-1643, 1987a.

Yovanovich, M. M., "Natural Convection from Isothermal Spheroids in the Conductive to Laminar Flow Regimes", AIAA Paper 87-1587, 1987b.

Yovanovich, M.M., Lee, S., and Gayowsky, T.J., " Approximate Analytic Solution of Laminar Forced Convection from an Isothermal Plate", AIAA Paper 92-0248, Presented at the 30th Aerospace Sciences Meeting and Exhibit, Reno, NV, 1992.

Yovanovich, M.M. and Muzychka, Y.S., "Solutions of Poisson Equation within Singly and Doubly Connected Domains", AIAA Paper 97-3880, National Heat Transfer Conference, Baltimore MD, 1997.

Yovanovich, M. M., Teertstra, P. M., and Culham, J. R. "Modeling Transient Conduction from Isothermal Convex Bodies of Arbitrary Shape", *Journal of Thermophysics and Heat Transfer*, Vol. 9, 1995, pp. 385-390.

Yuan, S.W., *Foundations of Fluid Mechanics*, Prentice Hall, Englewood Cliffs, NJ, 1967.

Zarling, J.P., "Application of Schwarz-Neumann Technique to Fully Developed Laminar Heat Transfer in Non-Circular Ducts", *Journal of Heat Transfer*, Vol. 99, 1976, pp. 332-335.

Zarling, J.P., "Application of the Schwarz-Neumann Technique to Fully Developed Laminar Heat Transfer in Non-Circular Ducts", *ASME Paper 76-WA/HT-49*, 1976.

Appendix A

Dimensional Analysis

Dimensional analysis using the Buckingham Π theorem has been applied to many physical phenomena such as fluid flow, heat transfer, stress and strain, and electromagnetic field theory (Huntly (1951), Langhaar (1951), Taylor (1974)). The basic theory of dimensional analysis is still presented in most elementary fluid mechanics texts e.g. Vennard and Street (1982) and White (1987), however, its inclusion in heat transfer texts is non-existent, except for the early texts by McAdams (1942) and Rohsenow and Choi (1961). Dimensional analysis using the Buckingham Π theorem is one of several methods for determining the important non-dimensional groups in problems which contain many dimensional parameters.

In many of the classic texts on dimensional analysis (Huntly (1951), Langhaar (1951), Taylor (1974)), examples are given only for simple geometries such as the circular duct or circular cylinder. Application to non-circular geometries assumes a knowledge of concepts such as the hydraulic diameter or other equivalent length scales. In this section, application of the Buckingham Π theorem to two of the problems being examined, namely HFDF and TFDF will be conducted from a general perspective. The results of this analysis will be applied to several different geometries and a simple model will be developed which is valid for all of the geometries of interest.

In order to apply the Π theorem, the number of Π groups must be determined. The Π

theorem states that if there are m variables and r fundamental units, then there will be $(m-r)$ Π groups. However, this classical approach does not always yield a solution. In such cases, the value of r is then decreased by one and the method repeated. This approach is usually presented in more elementary texts such as Vennard and Street (1982) and White (1987). A more formal approach is adopted in texts on dimensional analysis (Huntly (1951), Langhaar (1951), Taylor (1974)) and is summarized in the advanced level texts by Rouse (1959), Yuan (1967) and Panton (1985). The number of Π groups for a given problem is determined by examining the dimensional matrix and determining its rank. The rank of the dimensional matrix is the order of the largest square sub-matrix which has a non-zero determinant. If more than one sub-matrix with a non-zero determinant is found, then there exists several combinations of repeating variables which may yield a solution. It should also be pointed out that more than one solution may exist. In these cases, the analyst must use experience to decide which solution is appropriate.

The general approach outlined above will now be applied to the two fully developed flow problems being examined.

A.1 Hydrodynamic Problem

In the case of the fully developed fluid flow the friction factor f depends on several important variables in the form:

$$f(\overline{w}, -\frac{dp}{dz}, \mu, A, P) = 0 \tag{A.1}$$

In many of the references (Huntly (1951), Langhaar (1951), Taylor (1974), Vennard and Street (1982), White (1987)), the density of the fluid is also included in the Π analysis. Use of the fluid density is not required since the fully developed duct flow problem represents a balance of pressure and viscous forces. If density is included,

then an additional Π group results which is merely the Reynolds number. The analysis below excludes density, however, the second example considers this problem with density as an additional variable.

The dimensional matrix with density excluded is given below:

	$-\frac{dp}{dz}$	$\overline{w}$	A	P	μ
M	1	0	0	0	1
L	-2	1	2	1	-1
T	-2	-1	0	0	-1

In this case the rank of the matrix is determined to be three. One set of repeating variables may be chosen to be $\overline{w}$, μ and A. Now Eq. (A.1) may be rewritten as

$$\phi(\pi_1, \pi_2) = 0 \tag{A.2}$$

The Π groups are determined by examining the units of each set of variables and solving a set of algebraic equations which make each Π group dimensionless. After proceeding with the necessary steps in the analysis, the following Π groups are obtained:

$$\pi_1 = \frac{-\frac{dp}{dz}A}{\overline{w}\mu}, \quad \pi_2 = \frac{P}{\sqrt{A}} \tag{A.3}$$

Now in this case, since there are only two Π groups, Eq. (A.2) may be written in the form:

$$\frac{-\frac{dp}{dz}A}{\overline{w}\mu} = C\frac{P}{\sqrt{A}} \tag{A.4}$$

where C is a constant or it may be expressed as

$$\frac{-\frac{dp}{dz}A}{\overline{w}\mu}\frac{\sqrt{A}}{P} = C \tag{A.5}$$

Finally, by performing a control volume force balance at the wall of the duct one obtains the relation:

$$-\frac{dp}{dz}A = \overline{\tau}_w P \tag{A.6}$$

This leads to the final form of the dimensionless wall shear stress:

$$\frac{\overline{\tau}_w\sqrt{A}}{\overline{w}\mu} = C \tag{A.7}$$

This dimensionless group is sometimes referred to as the *Poiseuille* number *Po* (White (1991), Churchill (1988)). In this case the characteristic length is the square root of the cross-sectional flow area $\mathcal{L} = \sqrt{A}$.

Next, the hydrodynamic problem will be re-analyzed using the Π theorem while considering the fluid density as an additional variable. Therefore,

$$f(\overline{w}, -\frac{dp}{dz}, \mu, \rho, A, P) = 0 \tag{A.8}$$

The dimensional matrix for the modified problem is

	$-\frac{dp}{dz}$	$\overline{w}$	A	P	μ	ρ
M	1	0	0	0	1	1
L	-2	1	2	1	-1	-3
T	-2	-1	0	0	-1	0

Analysis of the matrix reveals that the rank is again three. The repeating variables may be chosen to be $\overline{w}$, ρ and A. This allows Eq. (A.8) to be written as

$$\phi(\pi_1, \pi_2, \pi_3) = 0 \tag{A.9}$$

Proceeding with the Π theorem analysis, the following Π groups will be formed:

$$\pi_1 = \frac{-\frac{dp}{dz}\sqrt{A}}{\rho \overline{w}^2}, \quad \pi_2 = \frac{\mu}{\rho \overline{w}\sqrt{A}}, \quad \pi_3 = \frac{P}{\sqrt{A}} \tag{A.10}$$

The reader should recognize the first Π group as the definition of the Darcy friction factor with the characteristic length $\sqrt{A}$ in place of the hydraulic diameter D_h, and the second Π group as the reciprocal of the Reynolds number based upon $\mathcal{L} = \sqrt{A}$ in place of the hydraulic diameter D_h.

Equation (A.9) may be written in the more familiar form:

$$\frac{-\frac{dp}{dz}\sqrt{A}}{\rho \overline{w}^2} = F\left(\frac{\mu}{\rho \overline{w}\sqrt{A}}, \frac{P}{\sqrt{A}}\right) \tag{A.11}$$

In both applications of the Π theorem, the Π group $P/\sqrt{A}$ appeared. It will be shown that this dimensionless parameter is an important geometric parameter which leads to the collapsing of the numerical data for many geometries onto a single curve. Finally, dimensional analysis also suggests that the characteristic length $\mathcal{L} = \sqrt{A}$ should be used to non-dimensionalize the hydrodynamic problem, rather than the hydraulic or equivalent diameter $D_h = 4A/P$. If the above examples are re-analyzed using the duct perimeter, P, as a repeating variable in place of the duct area, then the characteristic length suggested will change to the duct perimeter, $\mathcal{L} = P$.

A.2 Thermal Problem

The analysis for the thermal problem will be repeated based upon the analysis presented in Rohsenow and Choi (1961), except the cross-sectional area and perimeter will used in place of the diameter. The variables of interest for the thermal problem are listed below:

$$f(h, k, \mu, C_p, \rho, \overline{w}, A, P) = 0 \tag{A.12}$$

The dimensional matrix for the thermal problem is:

	h	k	μ	C_p	ρ	$\overline{w}$	A	P
M	1	1	1	0	1	0	0	0
L	0	1	-1	2	-3	1	2	1
T	-3	-3	-1	-2	0	-1	0	0
Θ	-1	-1	0	-1	0	0	0	0

Examination of the dimensional matrix reveals that a 4×4 matrix has a non-zero determinant. The repeating variables will be chosen to be $\overline{w}$, k, μ, and A. Having determined the rank of the matrix to be four, there will be four Π groups. Therefore the problem may be more compactly stated in the following dimensionless form of Eq. (A.12):

$$\phi(\pi_1, \pi_2, \pi_3, \pi_4) = 0 \tag{A.13}$$

Proceeding with the analysis, the resulting Π groups are found to be:

$$\pi_1 = \frac{h\sqrt{A}}{k}, \quad \pi_2 = \frac{P}{\sqrt{A}}, \quad \pi_3 = \frac{\mu C_p}{k}, \quad \pi_4 = \frac{\rho\overline{w}\sqrt{A}}{\mu} \tag{A.14}$$

Now in this case, since there are only four Π groups, Eq. (A.13) may be written in the following form:

$$\frac{h\sqrt{A}}{k} = F\left(\frac{\mu C_p}{k}, \frac{P}{\sqrt{A}}, \frac{\rho\overline{w}\sqrt{A}}{\mu}\right) \tag{A.15}$$

The results for the thermal problem provided Π groups similar to those in the previous section. As mentioned earlier, an equally valid analysis would also show that the perimeter P, would result as a characteristic length. However, it is important to point out that dimensional analysis did not produce dimensionless groups with the combination A/P as a characteristic length. This could only occur if both the perimeter and the area were included as repeating variables which would be redundant.

Appendix B

Test Fixture Specifications

The components of the test fixture discussed in Chapter 5 are shown in Figs. B.1-B.5. The fixture is composed of two test plates, two coolant jackets, two test fluid inlet/exit manifolds, and four coolant inlet/exit manifolds. In all, four sets of test plates have been machined which can accomodate plate fins having a height of 2.45 mm - 3.15 mm.

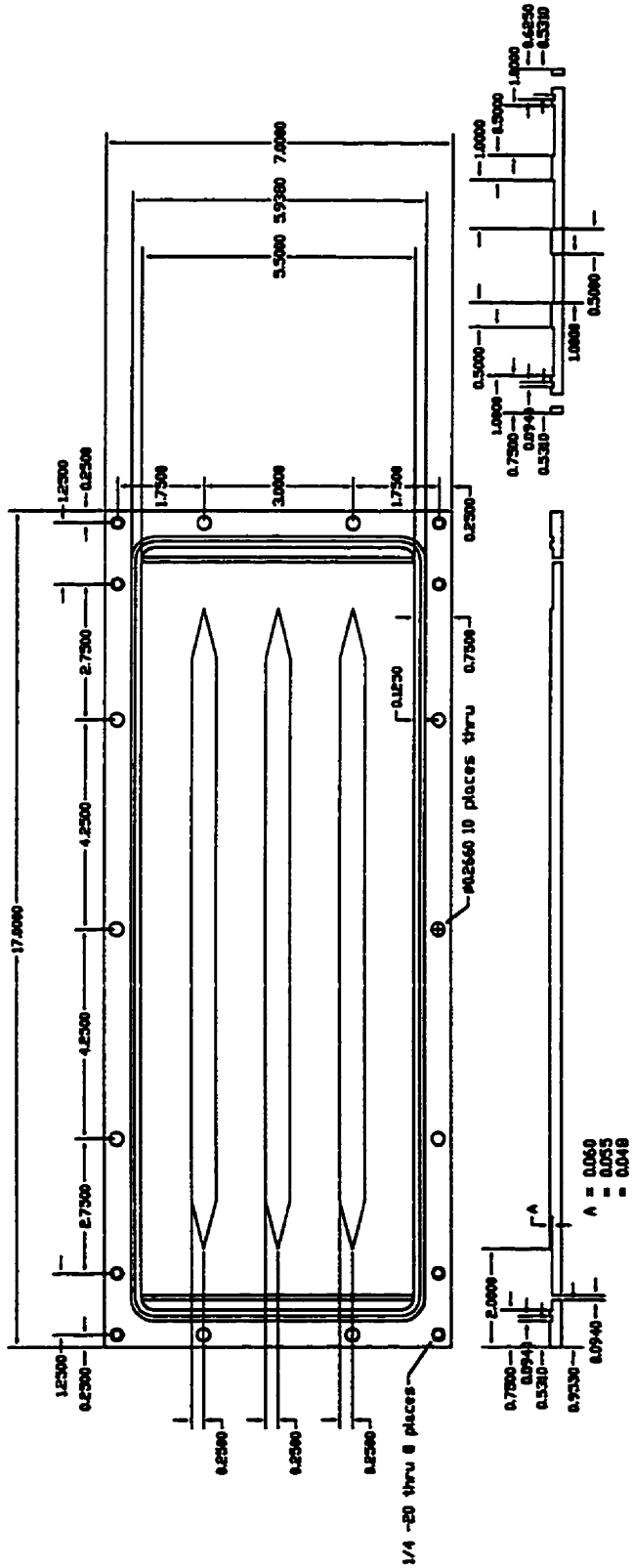

Fig. B.1 - Test Plate A.

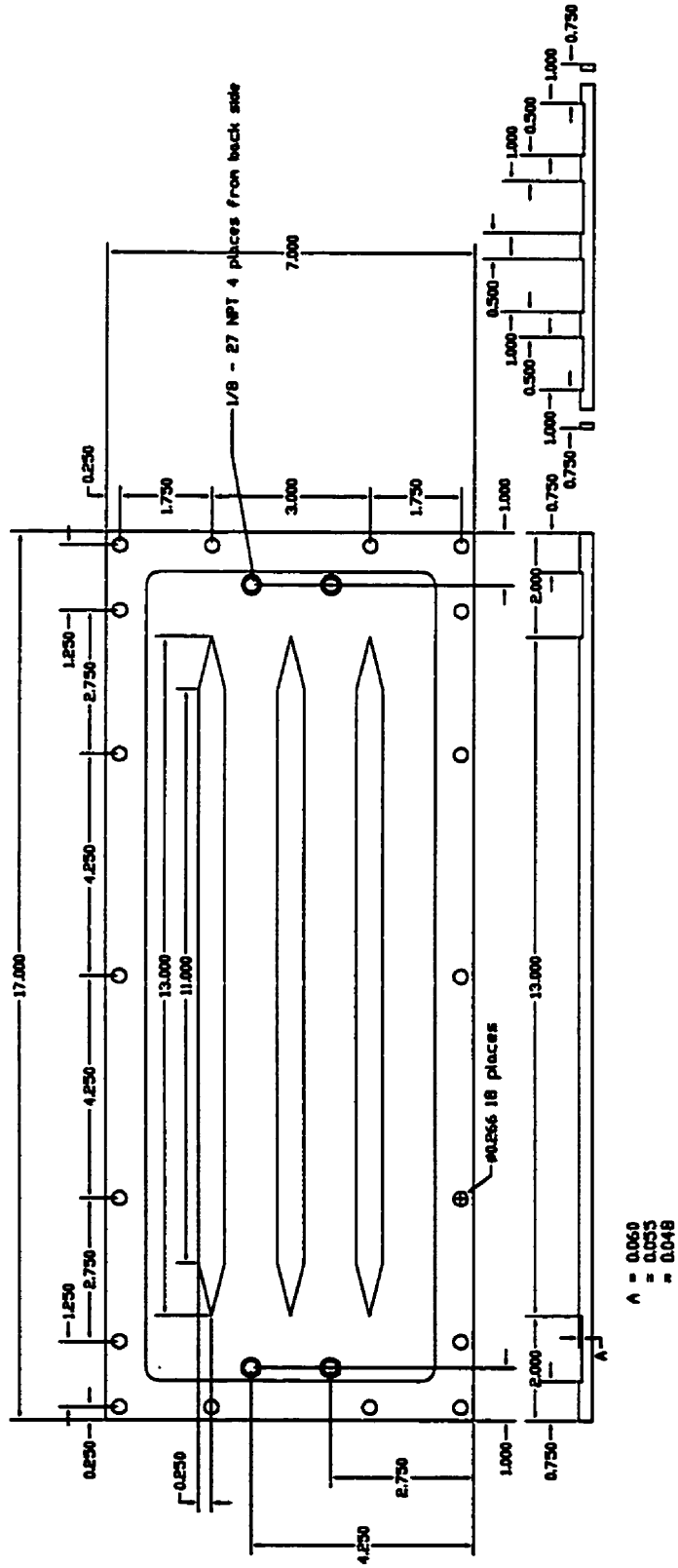

Fig. B.2 - Test Plate B.

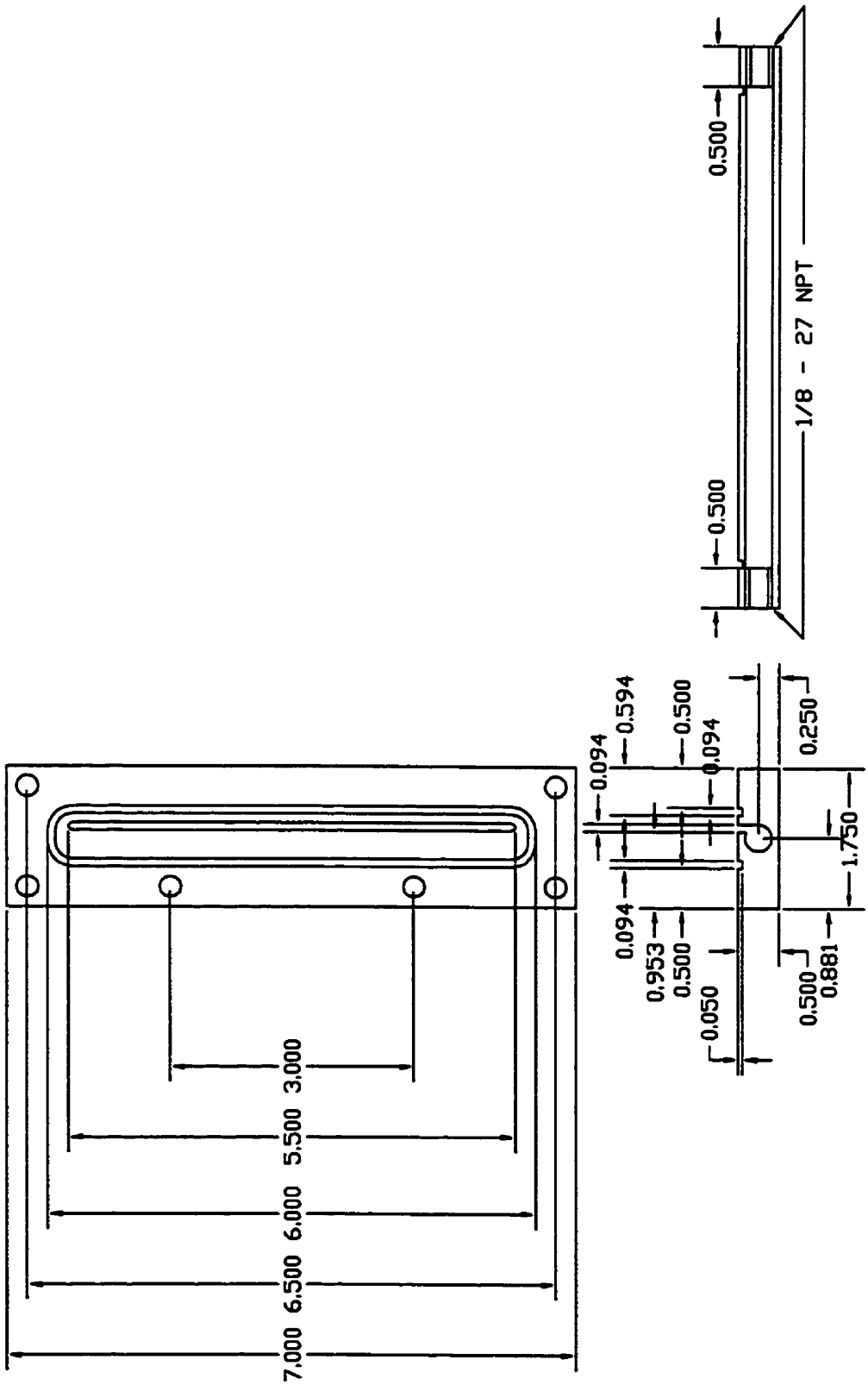

Fig. B.3 - Test Side Inlet/Exit Manifold.

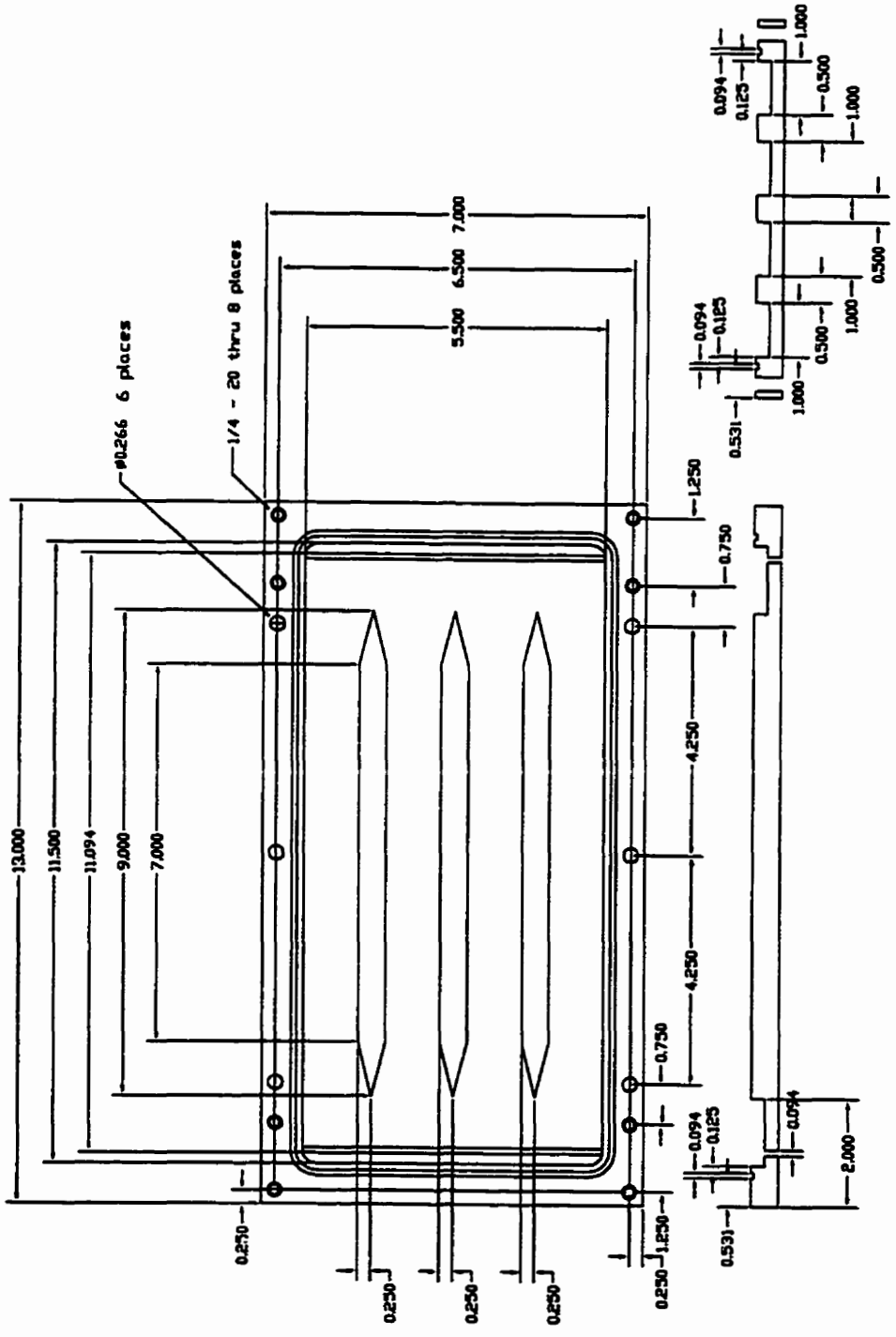

Fig. B.4 - Coolant Jacket.

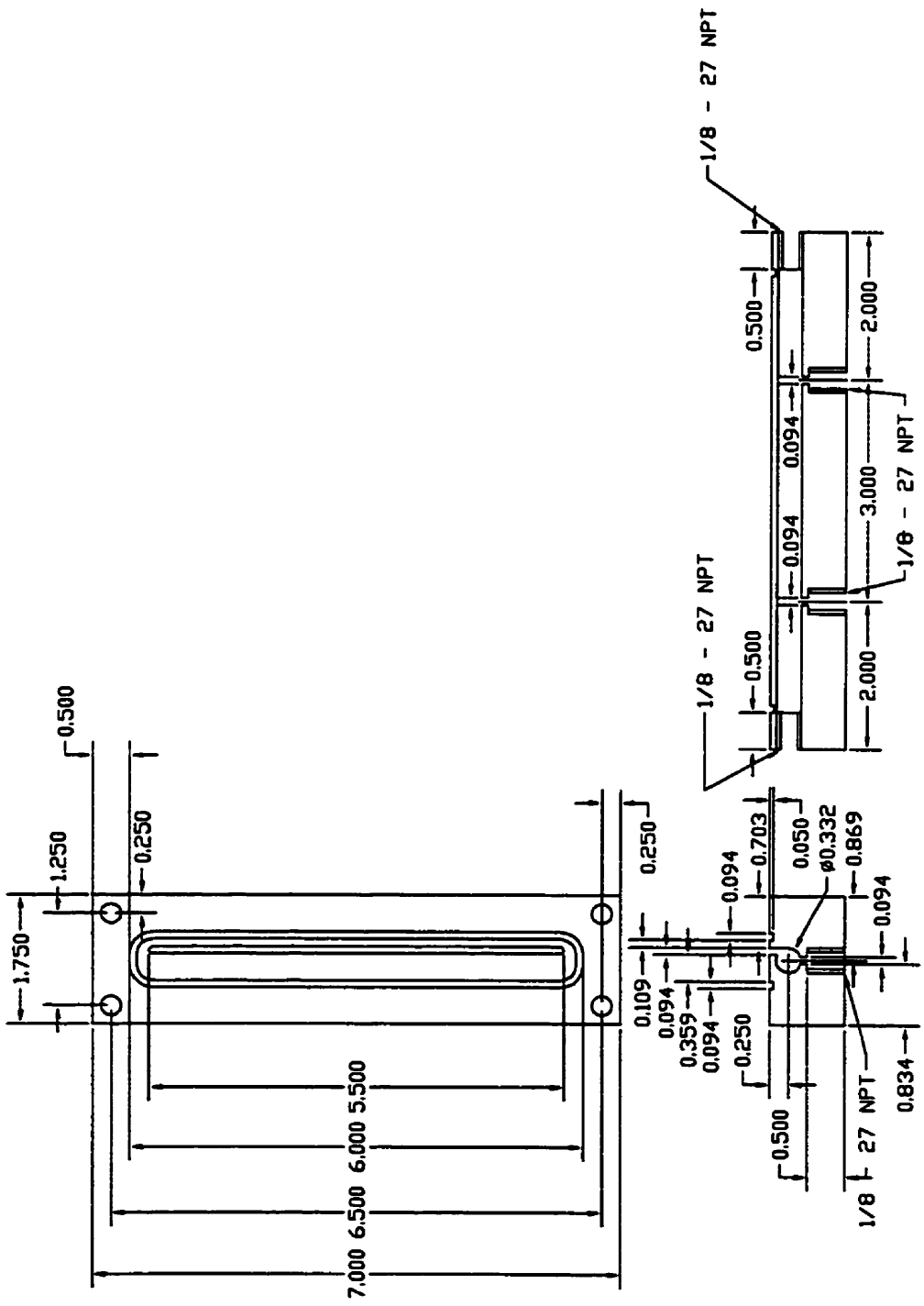

Fig. B.5 - Coolant Side Inlet/Exit Manifold.

Appendix C

Data Reduction Code

Maple V4 Symbolic Programming Language Code

```
> restart;
> with(stats):
> with(plots):

Read Data File

> readlib(readdata):
> rawdata:=readdata('d:/path/filename.txt',10):
> N:=nops(rawdata);

Atmospheric Pressure

> Patm:=Patm/29.92*101325;

Input of Data and Geometry

> ExpData:=array(rawdata):
> OilSide:=[W[oil]=0.0254, L[oil]=0.2794];
> WaterSide:=[H[water]=0.00692, W[water]=0.0254,
  L[water]=0.2794, t[wall]=0.00513, k[wall]=186];
> Dynamic:=[AER=1.7213476, FAR=0.4190602, ERR=0.876948,
> H[oil]=0.002438, A[free]=0.002438*0.0254, k[turb]=186,
  t[turb]=0.0003,FL=0.00225703];
```

```
> d[water]:=subs(WaterSide,4*H[water]*W[water]/
  (2*H[water]+2*W[water]));
> d[oil]:=.002484098;

Define Mean Temperatures for Property Evaluation

> Tmo:=(ExpData[i,1]+ExpData[i,2])/2;
> Tmw:=(ExpData[i,3]+ExpData[i,4])/2;

Define Fluid Properties

> mu[oil]:=[seq(10^(198.598-0.0245473*Tmo^(3/2)
  -29.6011*Tmo^(1/2)+1.46836*Tmo),i=1..N)];
> mu[water]:=[seq((3.23858-0.310287*Tmw^(1/2)+0.00761038*Tmw)^3,i=1..N)];
> rho[oil]:=[seq(1159.7-11.0605*Tmo^(1/2)-0.359005*Tmo,i=1..N)];
> rho[water]:=[seq(1416.3-22.2397*Tmw^(1/2)+0.0703129*Tmw,i=1..N)];
> k[oil]:=[seq(0.178947-0.00267278*Tmo^(1/2)-6.5788e-6*Tmo,i=1..N)];
> k[water]:=[seq(-1.12878+0.151667*Tmw^(1/2)-0.0035556*Tmw,i=1..N)];
> Cp[oil]:=[seq(237.467+66.7114*Tmo^(1/2)+1.73041*Tmo,i=1..N)];
> Cp[water]:=[seq(4302.06-186.873*Tmw^(1/2)+7.45361*Tmw,i=1..N)];

Compute Velocity, Reynolds Number, and Prandtl Number

> V[oil]:=[seq(subs(Dynamic,ExpData[i,9]/
  (4*A[free]*ERR)),i=1..N)];
> V[water]:=[seq(subs(WaterSide,ExpData[i,10]/
  (8*W[water]*H[water])),i=1..N)];
> RE[oil]:=[seq(rho[oil][i]*V[oil][i]*d[oil]/mu[oil][i],i=1..N)];
> RE[water]:=[seq(rho[water][i]*V[water][i]*d[water]/mu[water][i],i=1..N)];
> Pr[oil]:=[seq(mu[oil][i]*Cp[oil][i]/k[oil][i],i=1..N)];
> Pr[water]:=[seq(mu[water][i]*Cp[water][i]/k[water][i],i=1..N)];

Compute Heat Transfer and Overall Heat Balance

> Q[oil]:=[seq(Cp[oil][i]*rho[oil][i]*ExpData[i,9]*
  (ExpData[i,1]-ExpData[i,2]),i=1..N)];
> Q[water]:=[seq(Cp[water][i]*rho[water][i]*ExpData[i,10]*
  (ExpData[i,4]-ExpData[i,3]),i=1..N)];
> difference:=[seq((Q[oil][i]-Q[water][i])/Q[oil][i]*100,i=1..N)];
> Q[avg]:=[seq((Q[oil][i]+Q[water][i])/2,i=1..N)];
```

```
Epsilon - NTU and LMTD Calculations of UA

> Cmin:=[seq(rho[oil][i]*ExpData[i,9]*Cp[oil][i],i=1..N)];
> Cmax:=[seq(rho[water][i]*ExpData[i,10]*Cp[water][i],i=1..N)];
> Cr:=[seq(Cmin[i]/Cmax[i],i=1..N)];
> epsilon:=[seq(Q[avg][i]/(Cmin[i]*(ExpData[i,1]-ExpData[i,3])),i=1..N)];
> NTU:=[seq(1/(Cr[i]-1)*ln((epsilon[i]-1)/(Cr[i]*epsilon[i]-1)),i=1..N)];
> U:=[seq(subs(Dynamic,OilSide,Cmin[i]*NTU[i]),i=1..N)];
> LMTD:=[seq(((ExpData[i,1]-ExpData[i,4])-(ExpData[i,2]-ExpData[i,3]))
  /ln((ExpData[i,1]-ExpData[i,4])/(ExpData[i,2]-ExpData[i,3])),i=1..N)];
> UA:=[seq(subs(Dynamic,OilSide,Q[water][i]/LMTD[i]),i=1..N)];

Compute Coolant Heat Transfer Coefficient

> h[channel]:=[seq(0.37049*RE[water][i]^0.565*Pr[water][i]^(1/3)
  *k[water][i]/d[water],i=1..N)];

Define Fin Efficiency and Surface Efficiency

> eta[f]:=tanh(sqrt(2*ho/k[turb]/t[turb])*FL)/
  (sqrt(2*ho/k[turb]/t[turb])*FL);
> eta[o]:=1-FAR*(1-eta[f]);

Solve For Test Side Heat Transfer Coefficient

> h[oil]:=[seq(fsolve(subs(Dynamic,OilSide,WaterSide,
  1/(UA[i])=(1/(eta[o]*ho*AER*4*2*W[oil]*L[oil])
  +t[wall]/k[wall]/(8*W[oil]*L[oil])+1/(h[channel][i]*
  8*W[oil]*L[oil]))),ho),i=1..N)];

Compute Fin and Surface Efficiencies

> eta_fin:=[seq(evalf(subs(Dynamic,OilSide,
  tanh(sqrt(2*h[oil][i]/k[turb]/t[turb])*FL)/
  (sqrt(2*h[oil][i]/k[turb]/t[turb])*FL))),i=1..N)];
> eta_surface:=[seq(evalf(subs(Dynamic,OilSide,eta[o])),ho=h[oil])];

Compute Nusselt Number and Colburn j Factor

> Nu[oil]:=[seq(h[oil][i]*d[oil]/k[oil][i],i=1..N)];
> Nu_over_Pr:=[seq(Nu[oil][i]/Pr[oil][i]^(1/3),i=1..N)];
```

```
> j:=[seq(Nu[oil][i]/Pr[oil][i]^(1/3)/RE[oil][i],i=1..N)];
> jPlot:=[seq([RE[oil][i],Nu[oil][i]/Pr[oil][i]^(1/3)/
  RE[oil][i]],i=1..N)];

Compute Friction Factor Using Appropriate Pressure Loss Correlation

> q:=[seq(evalf(ExpData[i,9]/(Pi*(3/8*0.0254)^2/4)*
  rho[oil][i]*(3/8*0.0254)/mu[oil][i]),i=1..N)];
> PLFDL := .4533498172e-6*FL^3+.3089373274e-2*FL^2+
  7.622443565*FL+860.8708236;
> DeltaP[losses]:=[seq(PLFDL,FL=q)];
> f:=[seq(subs(OilSide,(((ExpData[i,5]-(ExpData[i,6]-Patm))-
> DeltaP[losses][i])/L[oil])/(1/2*rho[oil][i]*V[oil][i]^2))
  *d[oil]/4,i=1..N)];
> fPlot:=[seq([RE[oil][i],f[i]],i=1..N)];

Plot f and j Data

> loglogplot({jPlot,fPlot},axes=BOXED,style=POINT,symbol=CIRCLE,
  view=[10..1000,0.001..10]);

Output Data to File

> output:=[seq([Pr[oil][i],RE[oil][i],h[oil,regress][i],
  Nu[oil][i],Nu_over_Pr[i],j[i],f[i]],i=1..N)];
> readlib(writedata):
> writedata(`d:/path/filename.dat`,jPlot);
> writedata(`d:/path/filename.dat`,fPlot);
> writedata(`d:/path/filename.dat`,output);
```

Appendix D

Uncertainty Analysis

D.1 Introduction

The uncertainty in the experimental measurements has been determined using the root sum square method, (Holman (1984), Moffat (1988)). The analysis was conducted for both sets of experiments ($T_{oil,in} = 85°C$ and $T_{oil,in} = 115°C$). It was found that uncertainties in the friction factor and Reynolds number were insensitive to the temperature level, however, the uncertainties in the Colburn j factor and Nusselt number were very sensitive to the temperature level. The more accurate values of the j and Nu groups were obtained at the higher inlet temperature due to larger temperature drops being recorded.

D.2 Propagation of Errors

The propagation of errors is computed using the root sum square method. Given a particular result R in which

$$R = R(x_1, x_2, x_3, \ldots, x_n) \tag{D.1}$$

where x_i are independent measured quantities, the uncertainty w_R in the result R is

given by

$$w_R = \left[\left(\frac{\partial R}{\partial x_1} w_1 \right)^2 + \left(\frac{\partial R}{\partial x_2} w_2 \right)^2 + \left(\frac{\partial R}{\partial x_3} w_3 \right)^2 + \ldots \left(\frac{\partial R}{\partial x_n} w_n \right)^2 \right]^{1/2} \qquad \text{(D.2)}$$

where w_i are the uncertainties in the independent variables x_i.

D.3 Uncertainty Due to Measurement Error

The uncertainty in the experimental measurements of temperature, pressure and flow are summarized in Table D1. The uncertainty in these measurements is well within the limits discussed by Shah (1985).

Table D.1

Uncertainty in Measurements

Measurement	Uncertainty
Temperature - T $[C]$	$\pm 0.05C$
Pressure - p $[Pa]$	$\pm$ 1 %
Flow Rate - Θ $[m^3/s]$	$\pm$ 1 %

D.4 Uncertainty Due to Fluid Properties

Uncertainty in the fluid properties contributes the most to the uncertainty in the measurements of j and f. The uncertainty in the fluid properties is due to several contributions, namely, the properties determined by the manufacturers may not be exactly the same as those of the test fluids, the error due to the polynomial correlations, and the error due to errors in temperature measurement. The first of these is the greatest contributor to the uncertainty. For this analysis, it will be assumed that the properties of the test fluids provided in Lemczyk and Molloy (1996) are representative of the fluids used in the experiments. Figure D.1 provides a comparison of the

viscosity of various automotive oils in the range of temperatures that the experiments were conducted. The variation for automatic transmission fluid (ATF) is of the order 5-15 percent. The present experiments were conducted using a Type H ATF oil. The present analysis assumes that the viscosity data of Lemczyk and Molloy (1996) are accurate. Thus, if a five percent uncertainty in oil viscosity is considered, the values for uncertainty computed later will increase. The error due to the polynomial fitting of the data is small, on the order of 0.5 percent or less. Finally, the error due to errors in temperature measurement were determined to less then 0.05 percent. The uncertainty applied to the thermal properties will be assumed to be 0.5 percent assuming that the correlations are valid for the fluids used in the experiment.

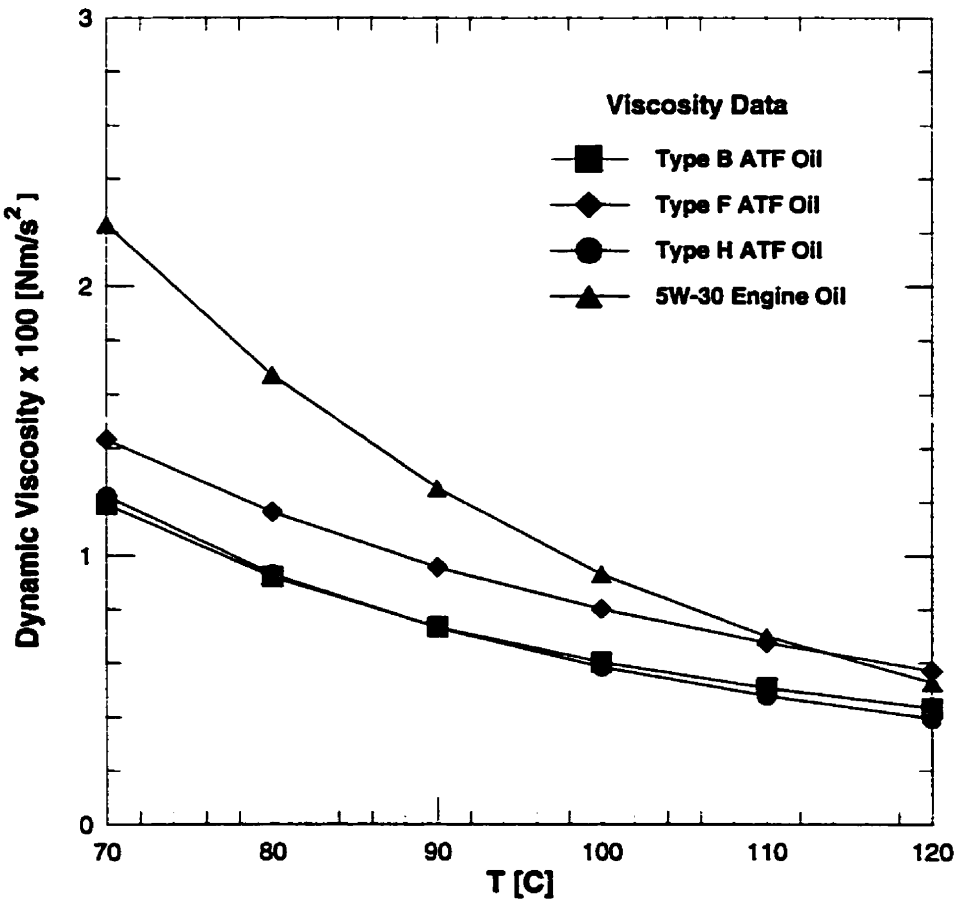

Fig. D.1 - Viscosity of Automotive Oils.

Table D.2

Uncertainty in Fluid Properties

Property	Uncertainty
$\rho\ [kg/m^3]$	0.5 %
$\mu\ [kg/m \cdot s]$	0.5 %
$C_p\ [J/kg \cdot K]$	0.5 %
$k\ [W/m^2 \cdot K]$	0.5 %

D.5 Uncertainty in Q and UA

The uncertainty in heat transfer measurements are determined from

$$\frac{\delta Q}{Q} = \left\{ \left(\frac{\delta \dot{m}}{\dot{m}}\right)^2 + \left(\frac{\delta C_p}{C_p}\right)^2 + \left(\frac{\delta \Delta T}{\Delta T}\right)^2 \right\}^{1/2} \tag{D.3}$$

where

$$\frac{\delta \Delta T}{\Delta T} = \left\{ \left(\frac{\delta T_i}{T_i}\right)^2 + \left(\frac{\delta T_o}{T_o}\right)^2 \right\}^{1/2} \tag{D.4}$$

and

$$\frac{\delta \dot{m}}{\dot{m}} = \left\{ \left(\frac{\delta \rho}{\rho}\right)^2 + \left(\frac{\delta \dot{\Theta}}{\dot{\Theta}}\right)^2 \right\}^{1/2} \tag{D.5}$$

The uncertainty in heat transfer for both fluids and their average values are summarized in Table D.3. As a result of the larger temperature drops obtained on the oilside, the uncertainty in oilside heat transfer is less than that for the coolant side. The uncertainty in the average heat transfer is found to be 4.62-8.79 percent. This is supported by the imbalance in heat transfer rates measured in each fluid which was

recorded between 4-7 percent RMS and observed to vary by ±7.5 percent.

Table D.3

Uncertainty in Heat Transfer

Parameter	Uncertainty
Q_{oil}	2.36/1.59 %
$Q_{coolant}$	8.46/4.34 %
$\overline{Q}$	8.79/4.62 %

The uncertainty in the overall heat transfer coefficient may be determined from the following expression:

$$\frac{\delta UA}{UA} = \left\{ \left(\frac{\delta Q}{Q} \right)^2 + \left(\frac{\delta \Delta T_{LMTD}}{\Delta T_{LMTD}} \right)^2 \right\}^{1/2} \tag{D.6}$$

The uncertainties in the overall heat transfer coefficient based upon the heat transfer rates of each fluid and the arithmetic mean of rates are given in Table D.4.

Table D.4

Uncertainty in Overall Heat Transfer Coefficient

Parameter	Uncertainty
UA_{oil}	8.44/2.86 %
$UA_{coolant}$	11.72/4.95 %
$\overline{UA}$	11.95/5.19 %

D.6 Uncertainty in f, j, and Re

The overall uncertainty in the Reynolds number may be computed from

$$\frac{\delta Re}{Re} = \left\{ \left(\frac{\delta \dot{m}}{\dot{m}}\right)^2 + \left(\frac{\delta D_h}{D_h}\right)^2 + \left(\frac{\delta A}{A}\right)^2 + \left(\frac{\delta \mu}{\mu}\right)^2 \right\}^{1/2} \tag{D.7}$$

The overall uncertainty in the Prandtl number may be computed from

$$\frac{\delta Pr}{Pr} = \left\{ \left(\frac{\delta \mu}{\mu}\right)^2 + \left(\frac{\delta C_p}{C_p}\right)^2 + \left(\frac{\delta k}{k}\right)^2 \right\}^{1/2} \tag{D.8}$$

The overall uncertainty in the Nusselt number may be computed from

$$\frac{\delta Nu}{Nu} = \left\{ \left(\frac{\delta h}{h}\right)^2 + \left(\frac{\delta D_h}{D_h}\right)^2 + \left(\frac{\delta k}{k}\right)^2 \right\}^{1/2} \tag{D.9}$$

where

$$\frac{\delta h}{h} = \left\{ \left(\frac{\delta A}{A}\right)^2 + \left(\frac{\delta UA}{UA}\right)^2 + \left(\frac{\delta (hA)_c}{(hA)_c}\right)^2 \right\}^{1/2} \tag{D.10}$$

The uncertainty in the j factor is computed using the uncertainties in the Nusselt, Reynolds, and Prandtl numbers from

$$\frac{\delta j}{j} = \left\{ \left(\frac{\delta Nu}{Nu}\right)^2 + \left(\frac{\delta Re}{Re}\right)^2 + \left(\frac{1}{3}\frac{\delta Pr}{Pr}\right)^2 \right\}^{1/2} \tag{D.11}$$

Finally, the uncertainty in the friction factor is computed from

$$\frac{\delta f}{f} = \left\{ \left(\frac{\delta \Delta P}{\Delta P}\right)^2 + \left(\frac{\delta D_h}{D_h}\right)^2 + \left(\frac{\delta L}{L}\right)^2 + \left(\frac{\delta \rho}{\rho}\right)^2 + \left(2\frac{\delta \overline{w}}{\overline{w}}\right)^2 \right\}^{1/2} \tag{D.12}$$

where

$$\frac{\delta \Delta P}{\Delta P} = \left\{ \left(\frac{\delta P_i}{P_i} \right)^2 + \left(\frac{\delta P_o}{P_o} \right)^2 \right\}^{1/2} \tag{D.13}$$

The calculated uncertainties in the friction factor f and Colburn j factor, along with uncertainties in the Nusselt, Prandtl, and Reynolds numbers is summarized in Table D.5. Uncertainties in the Colburn j factor and Nusselt number were determined assuming that the experimentally measured coolant side heat transfer coefficient had an uncertainty of 5 percent which is in agreement with theoretical predictions. Since the data were reduced using the average value of the total heat transfer $\overline{Q}$, the uncertainties are higher than those computed using the more accurate oilside measurements, which were found to be 9.89/5.89 percent for the Colburn j factor and 9.83/5.78 percent for the Nusselt number. Finally, the uncertianties for the friction factor and Reynolds number were found to be well within the limits discussed in Shah (1985).

Table D.5

Uncertainty in f, j, and Re

Parameter	Uncertainty
f	3.20 %
j	13.01/7.31 %
Nu	12.96/7.23 %
Re	1.23 %
Pr	0.87 %